Analyse multi-échelle des processus d'érosion hydrique et de transferts sédimentaires en territoire agricole : exemple du bassin versant de la Canche (France)

Edouard Patault

THESE

présentée en vue

d'obtenir le grade de

DOCTEUR

en

Discipline : Sciences de la terre et de l'univers

par

Edouard PATAULT

DOCTORAT DE L'UNIVERSITE DE LILLE
DELIVRE PAR IMT LILLE DOUAI

Titre de la thèse :

Analyse multi-échelle des processus d'érosion hydrique et de transferts sédimentaires en territoire agricole : exemple du bassin versant de la Canche (France)

Soutenue le 16 Novembre 2018 devant le jury d'examen :

Président	Jan NYSSEN	Professeur, Ghent University
Rapporteur	Benoit LAIGNEL	Professeur, Université de Rouen
Rapporteur	Olivier EVRARD	Chargé de recherche, CEA
Examinateur	Jan NYSSEN	Professeur, Ghent University
Examinateur	Sébastien SALVADOR-BLANES	Maître de conférences, Université de Tours
Membre invité	Jean PRYGIEL	Professeur, Université de Lille
Membre invité	Jean-François OUVRY	Directeur, AREAS
Directeur	Nor-Edine ABRIAK	Professeur, IMT Lille-Douai
Co-Directeur	Arnaud GAUTHIER	Professeur, Université de Lille
Encadrante	Claire ALARY	Enseignant-chercheur, IMT Lille-Douai
Co-Encadrante	Christine FRANKE	Enseignant-chercheur, MINES ParisTech

Laboratoires d'accueil : (1) Département Génie Civil et Environnemental de l'IMT Lille Douai, (2) Département Géosciences des MINES ParisTech

Ecole Doctorale SPI 072

Remerciements

Mes plus sincères remerciements sont adressés dans un premier temps à mes deux encadrantes, Claire Alary (enseignante-chercheuse, IMT Lille-Douai) et Christine Franke (Ingénieure de recherche, MINES ParisTech). Elles m'ont donné leur totale confiance et une réelle autonomie dans mon travail dès le début. Elles ont su être à l'écoute des difficultés que je pouvais éprouver et ont toujours répondu présentes lorsque je les réquisitionnais pour aller sur le terrain. De plus, elles m'ont encouragé et poussé à mener à bien les différentes démarches que j'ai pu entreprendre, que ce soit pour aller en conférence à l'étranger, ou bien pour mettre en place des collaborations avec différents partenaires scientifiques (M2C, BRGM). Cette considération qu'elles ont eue à mon égard a été pour moi une réelle source de motivation. Je ne me suis jamais senti comme un étudiant, mais comme un collègue à part entière. J'ai pu m'épanouir pleinement dans mon travail, et pour cela, je vous en remercie.

Je remercie chaleureusement mes directeurs de thèse, Nor-Edine Abriak (Prof. IMT Lille-Douai) et Arnaud Gauthier (Prof. Université de Lille). Tout comme mes encadrantes, ils m'ont fait confiance, m'ont laissé m'épanouir pleinement dans mon travail de recherche et m'ont donné l'autonomie nécessaire. J'espère sincèrement les rendre fiers de ce que nous avons accompli à travers ce manuscrit.

Je remercie sincèrement Benoit Laignel et Olivier Evrard pour avoir accepté d'être rapporteurs de ce manuscrit. Également Sébastien Salvador Blanes et Jan Nyssen pour avoir accepté d'être examinateurs. Et enfin Jean-François Ouvry et Jean Prygiel en qualité de membre invité. C'est un réel honneur pour moi, de vous avoir dans mon jury de thèse. J'espère avoir été à la hauteur de vos attentes et de vos exigences.

Je remercie également l'ensemble des membres du laboratoire (professeurs, enseignants-chercheurs, personnel technique et administratif). Je ne vais malheureusement pas tous les citer, la liste serait trop longue. Mais à travers ces quelques mots, je vous exprime ma sincère gratitude, que ce soit pour l'accueil lors de mon arrivée, pour votre aide sur les analyses de mes échantillons, mais aussi pour ces trois années passées à vos côtés. C'est avec regret que je vais vous quitter pour une nouvelle aventure professionnelle, mais je garderai toujours un excellent souvenir de mon passage au sein du département Génie Civil et Environnemental de l'IMT Lille Douai.

Je tiens à remercier les différents partenaires financiers et techniques qui ont pris part au projet QUASPER : Agence de l'Eau Artois-Picardie, Chambre d'agriculture Nord-Pas-de-Calais, Syndicat Mixte d'Aménagement de la Canche. Et plus particulièrement, Emilie Delattre, Jordan

Délépine, François Derancourt, Jean-Luc Carpentier et Jean-Pierre Lefebvre, d'une part pour leur aide indéfectible sur le terrain mais aussi pour leurs conseils avisés et pour leurs nombreuses invitations au travers de comités, réunions et assises.

Un grand merci également à deux anciens collègues, maintenant amis : Maxime Debret (UMR CNRS 6143 M2C Rouen) et Valentin Landemaine (BRGM) pour leur collaboration tout au long de ce projet. Je n'ai cessé de vous solliciter au travers de ma thèse et vous avez toujours été là pour m'épauler. Ce travail ne serait probablement pas aussi abouti sans votre aide.

Un gigantesque merci à mes parents, Sylvie et Dominique, ma sœur, Julie pour leur soutien de tous les jours et pour m'avoir encouragé à faire cette thèse. Je n'ai pas toujours su très bien vous expliquer en quoi cela consistait, ni ce que cela allait m'apporter, mais vous avez cru en moi, à chaque instant. C'est avec une immense fierté que je vous montrerais les résultats de ces trois années de recherche. Sincèrement, et du fond du cœur, merci !

Et pour finir, le plus beau et le plus grand des mercis, je l'adresse à ma compagne (femme bientôt ?☺), Marion. Soutien inconditionnel de tous les jours, qui aura su m'écouter, me soutenir, m'épauler, tout au long de ces trois années de thèse. Cela n'aura pas toujours été très facile pour nous, les trajets en train quotidiens, la thèse, la maison en construction, l'arrivée de bébé... Mais malgré tout ça, tu n'as jamais fléchi et a toujours été là pour moi. Le 26 mai 2018, tu nous as également offert le plus beau des cadeaux qui puisse exister, notre fils Antoine, et a fait de moi le plus heureux des papas.

Table des matières

Contexte de recherche

L'érosion accélérée des sols et l'export de sédiments fins dans les rivières sont deux grands enjeux environnementaux qui préoccupent de plus en plus les autorités de gestion des terres et de l'eau à travers le monde (Duvert et al., 2010). Les exports de sédiments dans les rivières constituent l'essentiel des transferts de matières de surfaces continentales vers les océans et résultent de processus variés d'érosion, transferts et dépôts au sein des bassins versants (Lal, 2003). Les sols constituent la couche supérieure de la croûte terrestre et ils sont dégradés sous l'action de la pluie, du vent et sous la pression exercée par les activités humaines (agriculture, urbanisme, industrie, transport). Des quantités de sols importantes sont déplacées chaque année sous l'effet de l'érosion hydrique. A l'échelle mondiale, les pertes en terre annuelles à l'origine de l'érosion hydrique sont estimées à 25 milliards de tonnes. Ainsi, l'érosion des sols agricoles conduit à la disparition progressive et à l'appauvrissement des sols qui constituent pourtant une ressource non renouvelable à l'échelle de la vie humaine (Le Bissonnais et al., 2002). Sans une gestion durable des sols, l'érosion pourrait provoquer une réduction drastique des rendements agricoles à l'horizon 2050 (Commission of the European Communities, 2006). Avec une augmentation de la population mondiale en parallèle, les enjeux sont d'autant plus importants que la demande en denrées alimentaires est vouée à augmenter. Le défi est donc double pour les prochaines décennies : garantir la durabilité des sols fertiles et des écosystèmes associés, tout en répondant à la demande croissante en produits alimentaires.

A l'échelle Européenne, l'érosion hydrique affecte 115 millions d'hectares soit 12% du territoire européen (Commission of the European Communities, 2006). La perte en terre est donc estimée à 1,2 t ha^{-1} an^{-1} en Europe. Selon les chiffres édités par le Service de la donnée et des études statistiques (SDeS) en 2013, l'érosion hydrique est estimée en moyenne à 1,5 t ha^{-1} an^{-1} en France et peut dépasser les 10 t ha^{-1} an^{-1} dans les zones de grande culture (Fig.1) (Cerdan et al., 2010). La

région Hauts-de-France est la zone la plus touchée par ces phénomènes et subit la plus forte perte en terres arables.

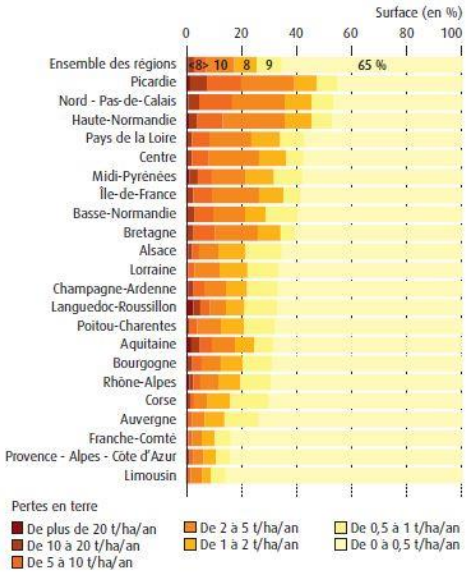

Fig. 1 : Surfaces concernées par l'érosion hydrique des sols en France (Source : BRGM, 2010. D'après Cerdan et al., 2010. Traitements : SDeS, 2013).

Sous l'effet de l'intensification des pratiques agricoles (mécanisation, rotation des cultures, etc…) et des modifications paysagères (remembrement des parcelles, suppression des haies et talus) des dernières décennies, les phénomènes érosifs se sont accélérés et multipliés et on observe une déstabilisation complète de la cascade sédimentaire (Foucher, 2015). La modification de ce continuum hydro-sédimentaire favorise le transfert des particules et des polluants associés, depuis les parcelles agricoles vers les masses d'eau (Landemaine, 2016).

Les transferts sédimentaires peuvent avoir de lourds impacts vers les milieux récepteurs. Ils peuvent être vecteurs d'apports de nutriments (phosphore et carbone organique particulaire), de bactéries, de pesticides, de métaux lourds et de radioéléments vers les masses d'eau de surface et altérer la qualité des eaux (Takken et al., 2001). Ils peuvent aussi être à l'origine d'envasement des réservoirs et des lits fluviaux, ce qui induit une dégradation de la qualité des zones humides et continentales (atterrissement et eutrophisation ; Viel, 2012) avec des dommages importants sur la biodiversité des écosystèmes aquatiques (Young et al., 2001). Ils peuvent également provoquer des

envasements dans les estuaires et les voies navigables, ce qui pose des problèmes de navigabilité et de gestion pour les activités fluviales et portuaires (Fig.2). Les réseaux des voies navigables en Hauts-de-France sont particulièrement touchés par ces phénomènes. Enfin, ils peuvent être à l'origine d'inondations et de coulées boueuses sur les territoires.

Fig. 2 : (A) Envasement d'un canal et création d'îlots à Saint-Omer (62500, France) en 2012, (B) Coulée boueuse à Sebourg (59990, France) en juin 2018, et (C) Coulée boueuse à Valdampierre (60790, France) en septembre 2014.

En France, de 1985 à 2000, 17282 coulées boueuses survenues dans 11415 communes on fait l'objet d'un arrêté de catastrophe naturelle (Heitz, 2009). Ces évènements sont particulièrement préjudiciables et engendrent des coûts matériels et humains particulièrement élevés. En 1997, des coulées boueuses en Normandie sur les communes de Saint-Martin-de-Boscherville et la Vaupallière furent particulièrement dévastatrices, causant le décès de trois personnes, et 1,5 M€ de dommages matériels (Viel, 2012). Par ailleurs, le coût lié aux dommages sur les infrastructures et au nettoyage induit par les coulées boueuses sur le territoire belge est estimé entre 16 à 172 M€ an^{-1} (Evrard et al., 2007). Plus récemment, les orages qui ont touché une majeure partie de la France entre le 25 mai et 14 juin 2018 ont provoqué 214 000 sinistres pour un coût évalué à 430 M€ selon la FFA (fédération française de l'assurance)[1]. Dans ce contexte, garantir la protection des biens, des personnes mais aussi de leur environnement semble essentiel.

Grâce à la prise de conscience, des populations et des pouvoirs publics, des impacts de l'érosion hydrique et du ruissellement, et face à la dégradation des masses d'eau, la Directive Cadre sur l'Eau (DCE) a été adoptée en 2000 par les états membres de l'Union Européenne. Cette politique

[1] https://www.lemonde.fr/planete/article/2018/06/25/le-cout-des-inondations-de-mai-et-de-juin-estime-a-430-millions-d-euros_5320831_3244.html - consulté le 02/07/2018.

globale vise à protéger et gérer durablement les ressources en eau au travers d'un programme ambitieux de restauration pour atteindre le bon état écologique et chimique des masses d'eau à l'horizon 2015. Mais ces objectifs sont loin d'être atteints. A l'échelle Européenne, seulement 53% des masses d'eau présentèrent un bon état écologique en 2016. En France, sur les bassins de Seine-Normandie et Loire-Bretagne, 70 à 90% des masses d'eau sont en mauvais état. Sur le bassin Artois-Picardie, 67% des masses d'eau présentent un mauvais état chimique, et 79% de ces mêmes masses d'eau sont dans un mauvais état écologique (Agence de l'Eau Artois-Picardie 2016). Parmi l'ensemble des dysfonctionnements constatés, le problème de dégradation de la qualité écologique et physico-chimique des eaux de surface par les transferts sédimentaires est clairement identifié.

La lutte contre l'érosion et le ruissellement a été initiée lors du 7ème programme d'intervention de l'Agence de l'Eau Artois-Picardie (1997-2002). Ce programme a permis l'émergence d'ouvrages de rétention dans les bassins versants et d'une réflexion sur l'approche agronomique dans la lutte contre le phénomène érosif. Les actions visaient essentiellement la préservation de la qualité des eaux souterraines en s'appuyant sur des mesures agro-environnementales. Cette période fut propice au développement d'études et diagnostics du phénomène érosif et à une prise de conscience de cette problématique. Pour des raisons budgétaires et de remise en cause des actions entreprises, l'Agence de l'Eau Artois-Picardie s'est retirée du financement des actions de lutte contre l'érosion lors de son 8ème programme (2003-2006). Ce retrait était motivé par une difficulté bien réelle à cerner la problématique et les enjeux liés à l'érosion hydrique. L'introduction de la dimension du bon état écologique des masses d'eaux par la DCE en 2000, l'augmentation de la fréquence des catastrophes naturelles de type coulées boueuses et l'impact du colmatage des habitats aquatiques par les transferts de matières en suspension ont eu pour conséquence le retour des financements de l'Agence de l'Eau Artois-Picardie sur les travaux de lutte contre l'érosion. Les objectifs du 9ème programme (2006-2012) ont visé à diminuer les transferts de matières en suspension dans les masses d'eau, facteur aggravant pour l'atteinte des objectifs fixés par la DCE. Cette nouvelle politique de lutte contre l'érosion s'est poursuivie lors du 10ème programme de l'Agence de l'Eau Artois-

Picardie (2013-2018) et s'est articulée autour de 4 actions complémentaires : (i) une approche agronomique pour favoriser l'infiltration, (ii) l'installation d'ouvrages d'hydraulique douce répondant à des pluies de retour 2-5 ans, (iii) la mise en place d'ouvrages de régulation (fossés, noues) et (iv) la mise en place d'ouvrages structurants (bassins de rétentions, digues de plein champ) (Fig.3). Le 11ème programme de l'Agence de l'Eau Artois-Picardie (2019-2023) devra progressivement réintroduire une approche agronomique pour limiter les phénomènes érosifs.

Fig. 3 : (A) Fascine (source : http://gerihco.engees.unistra.fr/fascines), (B) Noue à redents en limite de parcelle (source : Yves Nédélec, CEMAGREF) et (C) Bassin de rétention à Méteren (Nord de la France) (source : http://www.charentelibre.fr/)

La quantification et la caractérisation des transferts sédimentaires constituent donc des enjeux majeurs pour la gestion des milieux et l'atteinte des objectifs de la DCE. Si une forte réflexion est faite en région Hauts-de-France pour valoriser et réduire les masses de sédiments érodées et transportées jusqu'aux masses d'eau, peu d'études ont cherché à caractériser et quantifier la dynamique des transferts sédimentaires sur le bassin Artois-Picardie. Une meilleure compréhension des processus d'érosion et de leurs variabilités intrinsèques est pourtant indispensable afin d'orienter des programmes de mesures adaptés et de proposer des actions ciblées et efficaces.

Problématique de recherche

Au cours des dernières décennies, des avancées remarquables ont été réalisées par la communauté scientifique pour mieux comprendre et caractériser les processus érosifs dans leur intégralité. Ces travaux suivent une démarche scientifique intégrée, qui s'intéresse principalement mais pas exclusivement, à l'analyse des sources d'apports de sédiments, la quantification des transferts hydro-sédimentaires, l'identification des paramètres forçants et l'évaluation des conditions de transport.

Obtenir des informations sur l'origine des transferts sédimentaires dans les rivières est essentiel pour les gestionnaires de bassins versants, mais c'est une problématique difficilement appréhendable puisque les matières en suspensions proviennent de différentes sources et que leur contribution varie dans le temps et l'espace en conséquence à différents processus d'érosion (Fig.4 ; Haddadchi et al., 2013). Des approches indirectes existent pour identifier les sources de sédiments (observations de terrain, suivi de mesures), mais sont entravées par des problèmes spatiaux et temporels d'échantillonnage (Collins & Walling, 2002). Plus récemment, on note un engouement pour les méthodes directes dites de « *sediment fingerprinting* » ou traçage sédimentaire (Walling & Woodward 1992; Collins et al., 2001; Krein et al., 2003; Motha et al., 2004; Martínez-Carreras et al., 2010; Evrard et al., 2011; Lamba et al., 2015). Ces approches permettent de quantifier les contributions des sources de sédiments de la section de rivière à l'échelle du bassin versant. La procédure consiste à caractériser les potentielles sources de sédiments par un diagnostic de leurs propriétés bio-géo-physico-chimiques, et de les comparer à celles du matériel fluvial transporté. Les propriétés pouvant être utilisées sont nombreuses : couleur du sédiment (Krein et al., 2003; Poulenard et al., 2009; Martínez-Carreras et al., 2010), propriétés magnétiques (Russell et al., 2001; Gruszowski et al., 2003; Motha et al., 2004), composition chimique (Collins et al., 1997; Carter et al., 2003; Collins et al., 2012; Theuring et al., 2015), radionucléides environnementaux (Evrard et al., 2013; Du & Walling, 2016; Le Gall et al., 2016) et taille des particules (Krein et al., 2003). Les auteurs s'accordent à dire que l'utilisation d'une seule propriété n'est pas suffisante, et qu'il faut utiliser une

combinaison de traceurs pour distinguer les sources de sédiments (Walling et al., 1993; Collins & Walling, 2002). Chaque système réagissant différemment, les auteurs étudient un large panel de traceurs et identifient généralement la meilleure combinaison de proxies pour le système étudié avec des analyses statistiques multivariées (Collins et al., 1997; Collins et al., 2012; Palazón et al., 2015; Nosrati et al., 2018). Les données sont ensuite injectées dans un modèle de mélange pour quantifier la contribution de chaque source au sédiment. La littérature décrit différentes formes de modèles mathématiques pour les modèles de mélange (Collins et al., 1997; Motha et al., 2003; Hughes et al., 2009; Collins et al., 2010; Haddadchi et al., 2013).

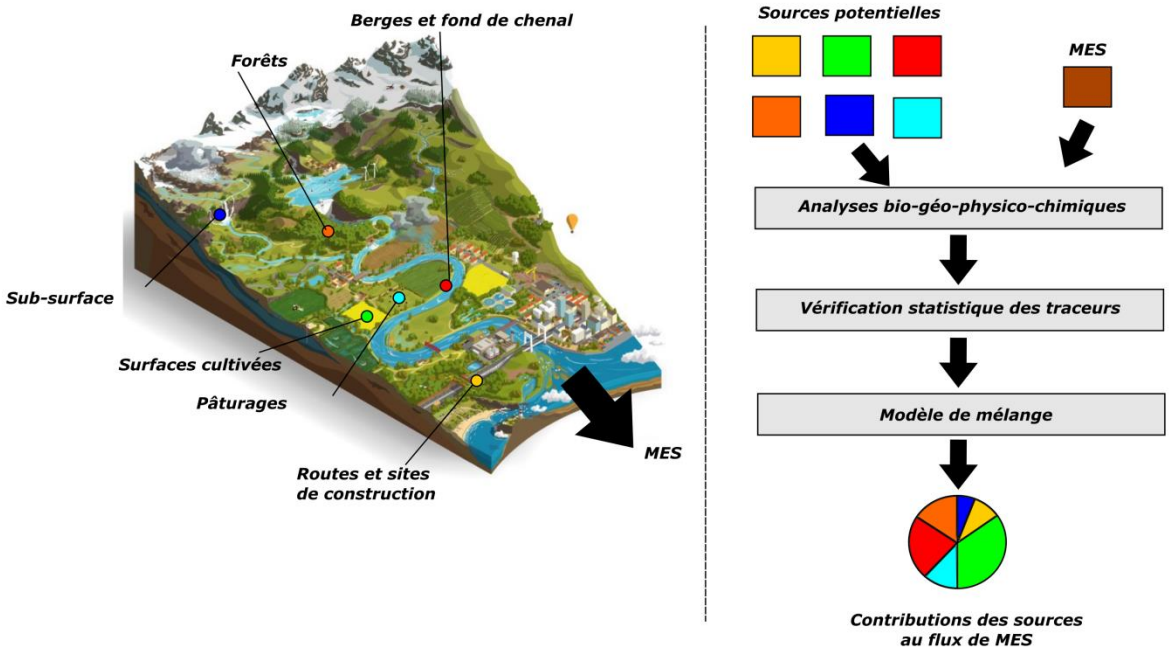

Fig. 4 : Processus requis pour les approches de « sediment fingerprinting » (traçage sédimentaire) dans les systèmes fluviatiles (modifié d'après (Haddadchi et al. 2013). Les différents types de sources notés sur cette figure sont non-exhaustifs et donnés à titre indicatif.

Si l'approche de « sediment fingerprinting » a largement contribué à l'identification de sources d'apports de sédiments pour différents bassins versants à travers le monde, les récentes découvertes montrent certaines limites à cette technique et des verrous scientifiques doivent être levés (Smith et al., 2015). En effet, certains travaux ont montré que la sélection des sources de sédiments sur un bassin pouvait avoir des implications importantes pour l'interprétation des résultats. Des zones très érodables peuvent exercer un effet disproportionné sur la concentration des

traceurs (Wilkinson et al., 2013). Et les sources proches peuvent avoir de plus fortes contributions pour un point donné sur une rivière que les sources lointaines (Haddadchi et al., 2015). Il est également important de pré-identifier les sources contribuant aux matières en suspension (MES), car une source non-échantillonnée peut biaiser les résultats (Smith et al., 2015).

La sélection de traceurs judicieux est un point important pour cette approche. Il a été montré que les incertitudes sur la prédiction des contributions des sources était diminuée en augmentant le nombre de traceurs (Sherriff et al., 2015) et que les contributions prédites pouvaient être différentes selon le choix des traceurs (Pulley et al., 2015). L'aspect conservatif des traceurs peut également introduire des biais dans l'interprétation (Sherriff et al., 2015), pour cela une procédure minutieuse de sélection des traceurs est recommandée (Kraushaar et al., 2015). Le type et la structure du modèle de mélange peuvent aussi affecter les résultats. Il a été montré que l'estimation de la contribution des sources pouvait varier entre les différents modèles jusqu'à 21% (Cooper et al., 2014). Et que les facteurs de correction en fonction de la taille des particules ou de leur contenu en matière organique, initialement utilisés dans les modèles, n'amélioraient pas sensiblement les résultats (Laceby et al., 2015). Face à ces contraintes, on observe l'émergence d'approches dites de « tributary tracing » ou « confluence tracing » (Vale et al., 2016; Nosrati et al., 2018). Le concept consiste à échantillonner des sédiments dans les différents affluents à l'amont et de les considérer comme sources potentielles pour les sédiments collectés à l'aval. Cette approche permet de s'affranchir de l'impact de l'enrichissement potentiel de la taille des particules sur les propriétés du sédiment (Laceby et al., 2017).

Si l'évaluation de la contribution des sources est un élément important pour les gestionnaires de bassin versants, la quantification des flux l'est tout autant et s'avère être une approche complémentaire à la première. Les bassins versant sont de plus en plus nombreux à être instrumentés mais pourtant, la fiabilité des mesures basse-fréquence est remise en cause (Landemaine, 2016) car elles ne sont pas en mesure d'évaluer correctement la variabilité spatio-

temporelle des transferts hydro-sédimentaires. De nombreux auteurs suggèrent l'utilisation de données haute-fréquence pour capturer l'ensemble des variations des processus hydro-sédimentaires. En parallèle, si de nombreux bilans d'exports ont été réalisés à l'échelle des grands bassins versants mondiaux (Walling & Webb, 1996) et aux échelles régionales (Laignel et al., 2006; Landemaine, 2016), peu d'études ont cherché à quantifier les transferts hydro-sédimentaires à l'échelle de petits bassins versants (1-10 km²). Dans le contexte des bassins versants de la ceinture lœssique Nord Européenne, les taux d'érosion spécifiques peuvent atteindre les 180 t km^{-2} an^{-1} (Walling et al., 2002). Des taux d'érosion spécifiques équivalent à 36-70 t km^{-2} an^{-1} ont par ailleurs été mesurés en France (Lefrançois, 2007; Ouvry et al., 2012). Hormis les quantités de sédiments exportées, ce sont les hétérogénéités temporelles de ces phénomènes qui posent question. En effet, certains auteurs ont montré que les quantités de sédiments exportées pouvaient varier du simple au triple suivant les années hydrologiques (Walling et al., 2002; Viel, 2012) et qu'un nombre très restreint d'évènements pouvait être à l'origine du transfert d'une majeure partie du flux sédimentaire annuel (Nu-Fang et al., 2011; Estrany et al., 2009; Lana-Renault & Regüés 2009). Cette sensibilité temporelle peut s'expliquer par de multiples paramètres forçants, comme la durée d'un épisode pluvieux, l'intensité des précipitations, la capacité du sol à infiltrer l'eau, etc… (Le Bissonnais et al., 2002). Ces dernières années, on remarque l'émergence de nouvelles actions sur les parcelles agricoles visant à limiter l'érosion des sols : culture d'hiver, non-labour, ouvrages d'hydraulique douce, ouvrages structurants. Mais à ce jour, peu de retours d'expériences permettent d'évaluer l'efficacité de ces mesures. Par ailleurs, peu d'études à notre connaissance ont été entreprises pour caractériser les transferts hydro-sédimentaires et évaluer les paramètres de contrôle à l'échelle de petits bassins versants (1-100 ha). Les petits bassins versants agricoles sont pourtant parmi les plus gros contributeurs aux flux hydro-sédimentaires (Poesen, 2018). Une connaissance plus approfondie de leur fonctionnement s'avère essentielle pour une éventuelle révision des politiques actuelles en matière de gestion de l'érosion des sols.

Sur le bassin Artois-Picardie, le bassin versant de la Canche (1274 km²) est particulièrement affecté par les transferts sédimentaires. Chaque année, des quantités importantes de sédiments transitent dans la rivière Canche jusqu'à l'exutoire. Le taux d'érosion spécifique à l'exutoire est compris entre 22,5 et 144 t km^{-2} an^{-1} selon les années hydrologiques. Les processus d'érosion diffuse sur les parcelles agricoles, d'érosion concentrée dans les ravines, et de dégradations de berges sont identifiés comme les processus majoritaires à l'origine du transfert sédimentaire. Si le bilan annuel sédimentaire à l'exutoire de la Canche est bien connu, certaines zones d'ombre subsistent sur le fonctionnement sédimentaire interne de ce bassin versant. De plus, l'efficacité des politiques récentes en matière de réduction des flux sédimentaires n'a pas été évaluée. Face à ce constat, les problématiques émergeantes sur ce bassin versant sont les suivantes :

i. Quel est le bilan érosif annuel d'un parcellaire agricole ? Quelle est la variabilité spatio-temporelle des flux sédimentaires ? Et quels sont les paramètres forçants ?
ii. Est-il possible de prédire le flux érosif d'un parcellaire agricole ? Quel est l'efficacité d'un schéma d'aménagement anti-érosion à cette même échelle ?
iii. A l'échelle du bassin versant de la Canche, quelle est la variabilité spatio-temporelle des transferts sédimentaires ? Quelle est l'efficacité des politiques d'aménagement en matière de lutte contre l'érosion ?
iv. Quelles zones, sources de matières, contribuent à ce transfert et selon quelles proportions ?
v. Quels sont les meilleurs traceurs des sédiments de l'érosion dans le contexte du bassin versant de la Canche ?

Orientation du travail de thèse

Ce travail de thèse est donc réalisé sur le bassin versant de la Canche (1274 km², région Hauts-de-France) très largement occupé par l'activité agricole (80% du territoire) et caractérisé par une problématique érosive lourde. Afin d'acquérir une compréhension globale, sur ce bassin versant, de la dynamique des transferts hydro-sédimentaires et de l'origine des sédiments, il est nécessaire d'adopter une démarche systémique à différentes échelles spatio-temporelles. Les processus d'érosion et de transfert des particules depuis les zones sources jusqu'à l'exutoire sont donc abordés à différentes échelles d'observations.

A l'échelle du parcellaire agricole, les transferts hydro-sédimentaires sont observés en continu grâce à l'installation d'une station de mesure haute-fréquence à l'exutoire du bassin versant élémentaire de la Pommeroye (0,54 km²). La variabilité saisonnière des flux est évaluée sur deux années consécutives et les relations entre les flux et les paramètres forçants (hydrologiques et climatiques) sont évaluées par le biais d'analyses statistiques. Une évaluation de la variabilité spatiale des transferts hydro-sédimentaires est alors proposée via un suivi bi-mensuel de l'état de surface des parcelles agricoles et l'injection de ces données dans un nouveau modèle d'érosion. Le choix s'est porté sur le modèle à base expert : *WATERSED* (Landemaine, 2016) qui permet une prédiction spatiale des ruissellements diffus et concentrés pour un évènement de pluie donné en tout point d'un bassin versant. L'efficacité d'un plan d'aménagement anti-érosion est alors évaluée via un module complémentaire du modèle.

A l'échelle du bassin versant de la Canche, la contribution des sources au flux hydro-sédimentaire est évaluée au travers de la méthode de « sediment fingerprinting » avec une approche de « confluence tracing ». Cette méthode de traçage sédimentaire se base sur la comparaison des propriétés physico-chimiques des sédiments des affluents à l'amont et des matières en suspension récupérées à l'aval de l'hydrosystème. Un ensemble d'analyses statistiques est alors utilisé pour vérifier la validité des traceurs et proposer un composé de traceurs optimal qui permet de

différencier les catégories de sources entres elles. L'ensemble est ensuite injecté dans un modèle de mélange et la part contributive de chaque source aux sédiments cible est alors quantifiée. Ces étapes sont réalisées à l'aide du modèle *Sed_Sat-v1.0*, récemment développé par l'USGS (Gorman Sanisaca et al., 2017).

Enfin, il est proposé de tester la pertinence de nouveaux traceurs érosifs. Dans un premier temps, un essai de validation d'utilisation des proxies spectrocolorimétriques est proposé afin d'évaluer les contributions de deux sources de sédiments (terres arables versus berges) à travers une approche de sediment fingerprinting. Dans un second temps, des analyses liées au magnétisme environnemental sont initiées sur du matériel sédimentaire prélevé dans la Canche et ses affluents afin d'évaluer la pertinence de ce traceur alternatif pour caractériser des épisodes érosifs.

1 - Suivi des transferts hydro-sédimentaires (bassin élémentaire)

- Mise en place d'un station haute-fréquence
- Bilan sédimentaire sur deux années
- Analyse de la variabilité temporelle
- Identification des paramètres forçants

2 - Simulation d'épisodes érosifs (bassin élementaire)

- Modélisation numérique: WATERSED
- Suivi des état de surface du sol
- Prédiction spatiale des ruissellements
- Validation des sorties de modèle
- Evaluation d'un schéma d'aménagement "anti-érosion"

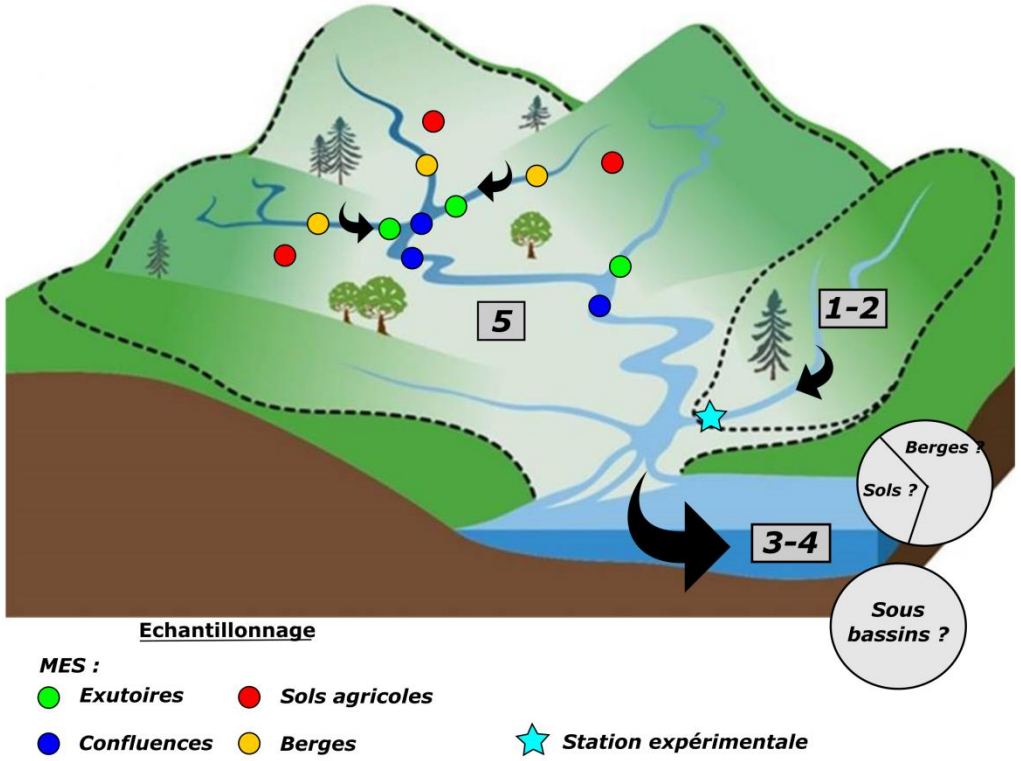

3 - Traçage de sources: Contribution des sous-bassins

- Modélisation numérique: Sed_Sat-v1.0
- Approche "exutoire-confluence"
- Evaluation de l'empreinte digitale sédimentaire : analyses physico-chimiques
- Choix des meilleurs traceurs (analyses statistiques)
- Modèle de mélange

4 - Traçage de sources: Sol vs. Berge

- Modélisation numérique: Sed_Sat-v1.0
- Approche "sol vs. berge"
- Evaluation de l'empreinte digitale sédimentaire
- Utilisation d'un nouveau proxie : couleur du sédiment
- Choix des meilleurs traceurs (analyses statistiques)
- Modèle de mélange

5 - Traçage de sources: Apports du magnétisme environnemental

- Nouveaux proxie : micro-magnétisme environnemental
- Approche spatio-temporelle intégrée : (saisons -> évènements)
- Apports faible coercivité vs. haute coercivité

Fig. 5 : Schéma conceptuel reprenant l'ensemble des orientations/recherches menées dans le cadre des travaux de thèse.

Structuration du manuscrit de thèse

Afin de valoriser l'ensemble des données acquises et le travail de recherche, le manuscrit est organisé sous la forme de 6 chapitres. Le 1er chapitre propose une présentation générale du bassin versant étudié : la Canche. Les chapitres suivants se présentent sous la forme d'articles, publiés, soumis ou en préparation pour soumission dans des journaux scientifiques internationaux de rang A. Chaque article est accompagné d'un résumé étendu en français. La succession des différents chapitres permet de mieux comprendre la dynamique des transferts hydro-sédimentaires sur le bassin versant de la Canche au travers d'une approche systémique globale à différentes échelles spatio-temporelles.

Le chapitre 2 s'attache à quantifier les transferts hydro-sédimentaires à l'échelle du bassin versant expérimental de la Pommeroye (0,54 km²). Ce travail trouve son originalité dans la nature du matériel expérimental utilisé et sa principale contribution est l'évaluation des transferts hydro-sédimentaires à une haute résolution temporelle, ce qui en fait un cas d'étude régional très intéressant. A l'issue de ce chapitre, les variabilités spatiales des flux hydro-sédimentaires n'ont pu être quantifiées. Pour cela, le chapitre 3 propose une évaluation de la variabilité spatiale de ces transferts à travers l'utilisation d'un nouveau modèle d'érosion des sols : *WATERSED*. La nouveauté liée à ce travail est de proposer une validation expérimentale et régionale de ce modèle récemment développé dans la thèse de Landemaine (2016) ainsi que de proposer une évaluation de l'efficacité d'un plan d'aménagement anti-érosion.

Les chapitres suivants proposent de travailler à une plus large échelle, celle du bassin versant de la Canche (1274 km²). Le chapitre 4 se consacre à quantifier les contributions relatives des différents sous-bassins versants de la Canche au flux sédimentaire en transit. Une méthode dite de « confluence tracing » est utilisée, dans lequel les sources de sédiments sont considérées comme étant les exutoires des affluents successifs du bassin versant de la Canche. Cette approche originale utilise un modèle récemment développé par l'USGS : *Sed_Sat-v1.0* (Gorman Sanisaca et al., 2017),

qui n'a jamais été testé auparavant dans le contexte des bassins versants de la ceinture lœssique Nord-Européenne. Le chapitre 5 se consacre, quant à lui, à montrer l'intérêt des traceurs spectrocolorimétriques couplés à ceux de la chimie élémentaire dans les approches de sediment fingerprinting en permettant d'évaluer les contributions respectives des berges et des sols au flux sédimentaire du bassin versant de la Canche. Enfin, le chapitre 6 vise à montrer l'intérêt des proxies émergents (magnétisme environnemental) dans les études de traçage de l'érosion. L'utilisation de ces traceurs est validée selon plusieurs approches spatio-temporelles et montre le fort potentiel de ces méthodes physico-chimiques.

Références

Agence de l'eau Artois-Picardie, 2016. *Schéma Directeur d'Aménagement et de Gestion des Eaux du Bassin Artois-Picardie*, Available at: http://www.eau-artois-picardie.fr/sdage.

Le Bissonnais, Y. et al., 2002. *L'Erosion Hydrique Des Sols En France*, Available at: http://prodinra.inra.fr/?locale=fr#!ConsultNotice:69099.

Carter, J. et al., 2003. Fingerprinting suspended sediment sources in a large urban river system. *The Science of The Total Environment*, 314–316(03), pp.513–534. Available at: http://linkinghub.elsevier.com/retrieve/pii/S0048969703000718.

Cerdan, O. et al., 2010. Rates and spatial variations of soil erosion in Europe: A study based on erosion plot data. *Geomorphology*, 122(1–2), pp.167–177. Available at: http://linkinghub.elsevier.com/retrieve/pii/S0169555X10002813 [Accessed April 29, 2014].

Collins, a. L. et al., 2001. Suspended sediment source fingerprinting in a small tropical catchment and some management implications. *Applied Geography*, 21(4), pp.387–412.

Collins, a. L., Walling, D.E. & Leeks, G.J.L., 1997. Use of the geochemical record preserved in floodplain deposits to reconstruct recent changes in river basin sediment sources. *Geomorphology*, 19, pp.151–167.

Collins, A.L. et al., 2010. Apportioning catchment scale sediment sources using a modified composite fingerprinting technique incorporating property weightings and prior information. *Geoderma*, 155(3–4), pp.249–261. Available at: http://dx.doi.org/10.1016/j.geoderma.2009.12.008.

Collins, A.L. et al., 2012. Sediment source tracing in a lowland agricultural catchment in southern England using a modified procedure combining statistical analysis and numerical modelling. *Science of The Total Environment*, 414, pp.301–317. Available at: http://linkinghub.elsevier.com/retrieve/pii/S0048969711012563.

Collins, A.L. & Walling, D.E., 2002. Selecting fingerprint properties for discriminating potential suspended sediment sources in river basins. *Journal of Hydrology*, 261, pp.218–244.

Commission of the European Communities, 2006. *Impact assessment of the thematic strategy on soil protection*, Available at: http://scholar.google.com/scholar?hl=en&btnG=Search&q=intitle:Thematic+Strategy+for+Soil+Protection#0.

Cooper, R.J. et al., 2014. Sensitivity of fluvial sediment source apportionment to mixing model assumptions: A Bayesian model comparison. *Water Resources Research*, pp.9031–9047.

Du, P. & Walling, D.E., 2016. Fingerprinting surficial sediment sources: Exploring some potential problems associated with the spatial variability of source material properties. *Journal of Environmental Management*, pp.1–12. Available at: http://dx.doi.org/10.1016/j.jenvman.2016.05.066.

Duvert, C. et al., 2010. Drivers of erosion and suspended sediment transport in three headwater catchments of the Mexican Central Highlands. *Geomorphology*, 123(3–4), pp.243–256. Available at: http://linkinghub.elsevier.com/retrieve/pii/S0169555X10003296 [Accessed April 8, 2014].

Estrany, J., Garcia, C. & Batalla, R.J., 2009. Suspended sediment transport in a small Mediterranean agricultural catchment. *Earth Surface Processes and Landforms*, 34(March), pp.155–161. Available at: http://www3.interscience.wiley.com/journal/121517813/abstract.

Evrard, O. et al., 2011. Combining suspended sediment monitoring and fingerprinting to determine the spatial origin of fine sediment in a mountainous river catchment. *Earth Surface Processes and Landforms*, 36(8), pp.1072–1089. Available at: http://doi.wiley.com/10.1002/esp.2133.

Evrard, O. et al., 2007. Effectiveness of erosion mitigation measures to prevent muddy floods: A case study in the Belgian loam belt. *Agriculture, Ecosystems and Environment*, 118(1–4), pp.149–158.

Evrard, O. et al., 2013. Tracing sediment sources in a tropical highland catchment of central Mexico by using conventional and alternative fingerprinting methods. *Hydrological Processes*, 27(6), pp.911–922.

Foucher, A., 2015. *Reconstruction de la cascade sédimentaire en contexte de plaine agricole drainée*. Université François Rabelais de Tours.

Le Gall, M. et al., 2016. Quantifying sediment sources in a lowland agricultural catchment pond using 137Cs activities and radiogenic 87Sr/86Sr ratios. *Science of the Total Environment*, 566–567, pp.968–980. Available at: http://dx.doi.org/10.1016/j.scitotenv.2016.05.093.

Gorman Sanisaca, L.E., Gellis, A.C. & Lorenz, D.L., 2017. Determining the Sources of Fine-Grained Sediment Using the Sediment Source Assessment Tool (Sed _ SAT).

Gruszowski, K.E. et al., 2003. Sediment sources and transport pathways in a rural catchment, Herefordshire, UK. *Hydrological Processes*, 17(13), pp.2665–2681.

Haddadchi, A. et al., 2013. Sediment fingerprinting in fluvial systems: review of tracers, sediment sources and mixing models. *International Journal of Sediment Research*, 28(4), pp.560–578. Available at: http://linkinghub.elsevier.com/retrieve/pii/S1001627914600135.

Haddadchi, A., Olley, J. & Pietsch, T., 2015. Quantifying sources of suspended sediment in three size fractions. *Journal of Soils and Sediments*. Available at: http://link.springer.com/10.1007/s11368-015-1196-1.

Heitz, C., 2009. *La perception du risque de coulées boueuses: analyse sociogéographique et apports à l'économie comportementale*. Université de Strasbourg.

Hughes, A.O. et al., 2009. Sediment source changes over the last 250 years in a dry-tropical catchment, central Queensland, Australia. *Geomorphology*, 104(3–4), pp.262–275. Available at: http://dx.doi.org/10.1016/j.geomorph.2008.09.003.

Kraushaar, S. et al., 2015. Sediment fingerprinting in northern Jordan: element-specific correction factors in a carbonatic setting. *Journal of Soils and Sediments*, pp.2155–2173. Available at: http://link.springer.com/10.1007/s11368-015-1179-2.

Krein, A., Petticrew, E. & Udelhoven, T., 2003. The use of fine sediment fractal dimensions and colour to determine sediment sources in a small watershed. *Catena*, 53, pp.165–179.

Laceby, J.P. et al., 2015. A comparison of geological and statistical approaches to element selection for sediment fingerprinting. *Journal of Soils and Sediments*, 15(10), pp.2117–2131.

Laceby, J.P. et al., 2017. The challenges and opportunities of addressing particle size effects in sediment source fingerprinting: A review. *Earth-Science Reviews*, 169, pp.85–103. Available at: http://linkinghub.elsevier.com/retrieve/pii/S0012825216304548.

Laignel, B. et al., 2006. Erosion balance in the watersheds of the western Paris Basin by high-frequency monitoring of discharge and suspended sediment in surface water. *Comptes Rendus* -

Geoscience, 338(8), pp.556–564.

Lal, R., 2003. Soil erosion and the global carbon budget. *Environment international*, 29(4), pp.437–50. Available at: http://www.ncbi.nlm.nih.gov/pubmed/12705941 [Accessed April 29, 2014].

Lamba, J., Karthikeyan, K.G. & Thompson, A.M., 2015. Apportionment of suspended sediment sources in an agricultural watershed using sediment fingerprinting. *Geoderma*, 239–240, pp.25–33. Available at: http://linkinghub.elsevier.com/retrieve/pii/S0016706114003565.

Lana-Renault, N. & Regüés, D., 2009. Seasonal patterns of suspended sediment transport in an abandoned farmland catchment in the Central Spanish Pyrenees. *Earth Surface Processes and Landforms*, 34(June), pp.155–161. Available at: http://www3.interscience.wiley.com/journal/121517813/abstract.

Landemaine, V., 2016. *Érosion des sols et transferts sédimentaires sur les bassins versants de l'Ouest du Bassin de Paris : analyse, quantification et modélisation à l'échelle pluriannuelle*. Université de Rouen Normandie.

Lefrançois, J., 2007. Dynamiques et origines des matières en suspension sur de petits bassins versants agricoles sur schiste. , p.280.

Martínez-Carreras, N. et al., 2010. The use of sediment colour measured by diffuse reflectance spectrometry to determine sediment sources: Application to the Attert River catchment (Luxembourg). *Journal of Hydrology*, 382(1–4), pp.49–63. Available at: http://dx.doi.org/10.1016/j.jhydrol.2009.12.017.

Motha, J. a. et al., 2004. Unsealed roads as suspended sediment sources in an agricultural catchment in south-eastern Australia. *Journal of Hydrology*, 286(1–4), pp.1–18.

Motha, J.A. et al., 2003. Determining the sources of suspended sediment in a forested catchment in southeastern Australia. *Water Resour. Res.*, 39(3), p.1056. Available at: http://dx.doi.org/10.1029/2001WR000794%5Cnhttp://www.agu.org/pubs/crossref/2003/2001WR000794.shtml.

Nosrati, K., Collins, A.L. & Madankan, M., 2018. Fingerprinting sub-basin spatial sediment sources using different multivariate statistical techniques and the Modified MixSIR model. *Catena*, 164(January), pp.32–43. Available at: https://ac.els-cdn.com/S0341816218300031/1-s2.0-S0341816218300031-main.pdf?_tid=b9e0886c-fc62-11e7-8b31-00000aab0f6b&acdnat=1516288841_9ebb9c2cdc279d7741183743155b1299.

Nu-Fang, F. et al., 2011. Rainfall, runoff, and suspended sediment delivery relationships in a small agricultural watershed of the Three Gorges area, China. *Geomorphology*, 135(1–2), pp.158–166. Available at: http://linkinghub.elsevier.com/retrieve/pii/S0169555X11004119 [Accessed July 10, 2014].

Ouvry, J.F. et al., 2012. Maîtrise du ruissellement et de l'érosion des sols en Haute-Normandie. Expérimentations sur les pratiques culturales 2001-2010. Synthèse des résultats de ruissellement et d'érosion. Groupe Maîtrise du ruissellement par les pratiques culturales. , p.36.

Palazón, L. et al., 2015. Comparing catchment sediment fingerprinting procedures using an auto-evaluation approach with virtual sample mixtures. *Science of The Total Environment*, 532, pp.456–466. Available at: http://www.sciencedirect.com/science/article/pii/S0048969715300619.

Poesen, J., 2018. Soil erosion in the Anthropocene: Research needs. *Earth Surface Processes and*

Landforms, 43(1), pp.64–84.

Poulenard, J. et al., 2009. Infrared spectroscopy tracing of sediment sources in a small rural watershed (French Alps). *Science of the Total Environment*, 407(8), pp.2808–2819. Available at: http://dx.doi.org/10.1016/j.scitotenv.2008.12.049.

Pulley, S., Foster, I. & Antunes, P., 2015. The application of sediment fingerprinting to floodplain and lake sediment cores: assumptions and uncertainties evaluated through case studies in the Nene Basin, UK. *Journal of Soils and Sediments*, pp.1–23. Available at: http://dx.doi.org/10.1007/s11368-015-1136-0.

Russell, M.., Walling, D.. & Hodgkinson, R.., 2001. Suspended sediment sources in two small lowland agricultural catchments in the UK. *Journal of Hydrology*, 252(1–4), pp.1–24.

Sherriff, S.C. et al., 2015. Uncertainty-based assessment of tracer selection, tracer non-conservativeness and multiple solutions in sediment fingerprinting using synthetic and field data. *Journal of Soils and Sediments*. Available at: http://link.springer.com/10.1007/s11368-015-1123-5.

Smith, H.G. et al., 2015. Preface—Addressing challenges to advance sediment fingerprinting research. *Journal of Soils and Sediments*, (OCTOBER). Available at: http://link.springer.com/10.1007/s11368-015-1231-2.

Takken, I. et al., 2001. The effect of tillage-induced roughness on runoff and erosion patterns. *Geomorphology*, 37(1–2), pp.1–14. Available at: http://linkinghub.elsevier.com/retrieve/pii/S0169555X00000593.

Theuring, P., Collins, A.L. & Rode, M., 2015. Source identification of fine-grained suspended sediment in the Kharaa River basin, northern Mongolia. *Science of The Total Environment*, 526(APRIL), pp.77–87. Available at: http://linkinghub.elsevier.com/retrieve/pii/S0048969715004180.

Vale, S.S. et al., 2016. Characterization and quantification of suspended sediment sources to the Manawatu River, New Zealand. *Science of the Total Environment*, 543, pp.171–186. Available at: http://dx.doi.org/10.1016/j.scitotenv.2015.11.003.

Viel, V., 2012. *Analyse spatiale et temporelle des transferts sédimentaires dans les hydrosystèmes normands. Exemple du bassin versant de la Seulles*.

Walling, D.E. et al., 2002. Establishing sediment budgets for two small lowland agricultural catchments in the UK. *Catena*, 47(4), pp.323–353.

Walling, D.E. & Webb, B.W., 1996. Erosion and sediment yield: a global overview. *Erosion and Sediment Yield: Global and Regional Perspectives*, (236), pp.3–19. Available at: http://books.google.com/books?hl=en&lr=&id=bZ-ufVQV5yAC&oi=fnd&pg=PA3&dq=Erosion+and+sediment+yield:+a+global+overview&ots=u-QfIZyy5V&sig=iFyBdzc5dvvd-rF0T35j1jn5EZg.

Walling, D.E. & Woodward, J.C., 1992. Use of radiometric fingerprints to derive information on suspended sediment sources. Erosion and Sediment Transport Monitoring Programmes in River Basins. (Proceedings Oslo Symposium). In *Erosion and sediment transport Programmes in River Basins*. pp. 64–153.

Walling, D.E., Woodward, J.C. & Nicholas, A.P., 1993. A multi-parameter approach to fingerprint suspended-sediment sources. In *Tracers in Hydrology*.

Wilkinson, S.N. et al., 2013. Using sediment tracing to assess processes and spatial patterns of erosion in grazed rangelands, Burdekin River basin, Australia. *Agriculture, Ecosystems and Environment*, 180, pp.90–102. Available at: http://dx.doi.org/10.1016/j.agee.2012.02.002.

Young, W.J. et al., 2001. Relative changes in sediment supply and sediment transport capacity in a bedrock-controlled river. *Water Resources Research*, 37(12), pp.3307–3320.

Chapitre 1

Présentation du territoire d'étude : le bassin versant de la Canche (Hauts-de-France).

Chapitre 1 : Présentation du territoire d'étude : le bassin versant de la Canche (Hauts-de-France).

1. Généralités

Le territoire d'étude se situe dans le Nord de la France, au Nord du Bassin de Paris et dans la partie Ouest du bassin Artois-Picardie (Fig.6). Le périmètre du bassin versant de la Canche concerne 203 communes (15 communautés de communes) correspondant à une population de 105 000 habitants[2] avec une faible concentration au sein des principales villes. La densité de population est assez faible avec 81 habitants km^{-2}. Le secteur littoral avec les communes d'Etaples et le Touquet-Paris-Plage correspond au secteur le plus urbanisé, et connaît des écarts de fréquentation importants liés à son statut de station touristique et balnéaire. Cette attractivité du littoral explique une urbanisation plus dense le long de l'axe Canche par une occupation du lit majeur.

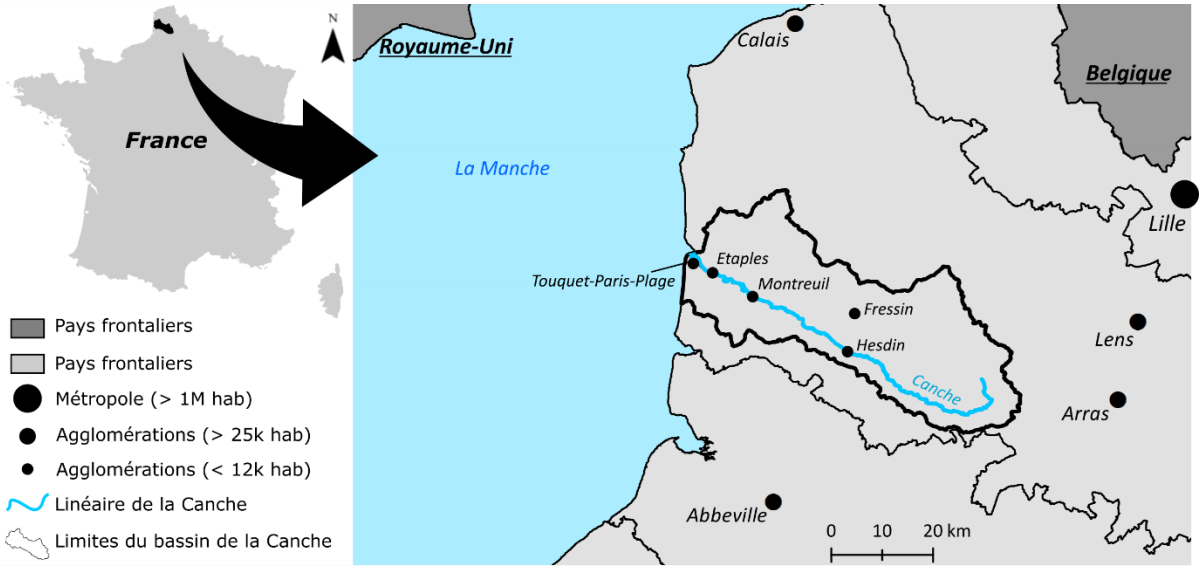

Fig. 6 : Carte de localisation du bassin versant de la Canche

2. Géomorphologie

La Canche est un petit fleuve côtier qui prend sa source à Gouy-en-Ternois et qui débouche dans la Manche entre Etaples et le Touquet-Paris-Plage. C'est le plus important fleuve non-canalisé

[2] http://www.gesteau.fr/sites/default/files/questcequelesagecanche.pdf

de la Région Hauts-de-France. Son bassin versant s'étend sur le haut et le moyen Artois et sa surface est de 1274 km². Le linéaire hydrographique de la Canche mesure 85 km et de nombreux sous-systèmes viennent se greffer au système principal. Le bassin versant de la Canche est parcouru par un réseau hydrographique d'environ 320 km réparti entre la Canche et ses principaux affluents : la Ternoise, la Planquette, la Créquoise, le Bras de Bronne, la Course, la Dordogne, le Huîtrepin (Fig.7). Le bassin versant est caractérisé par des plateaux de faible altitude (< 210 m), entaillés par un réseau de vallées assez étroites, surnommé les *« 7 Vallées »*. Les pentes sont assez douces sur l'ensemble du bassin avec une pente moyenne le long du bassin comprise entre 2 et 3%. Les pentes sont plus marquées sur les talwegs, entre 4 et 6%.

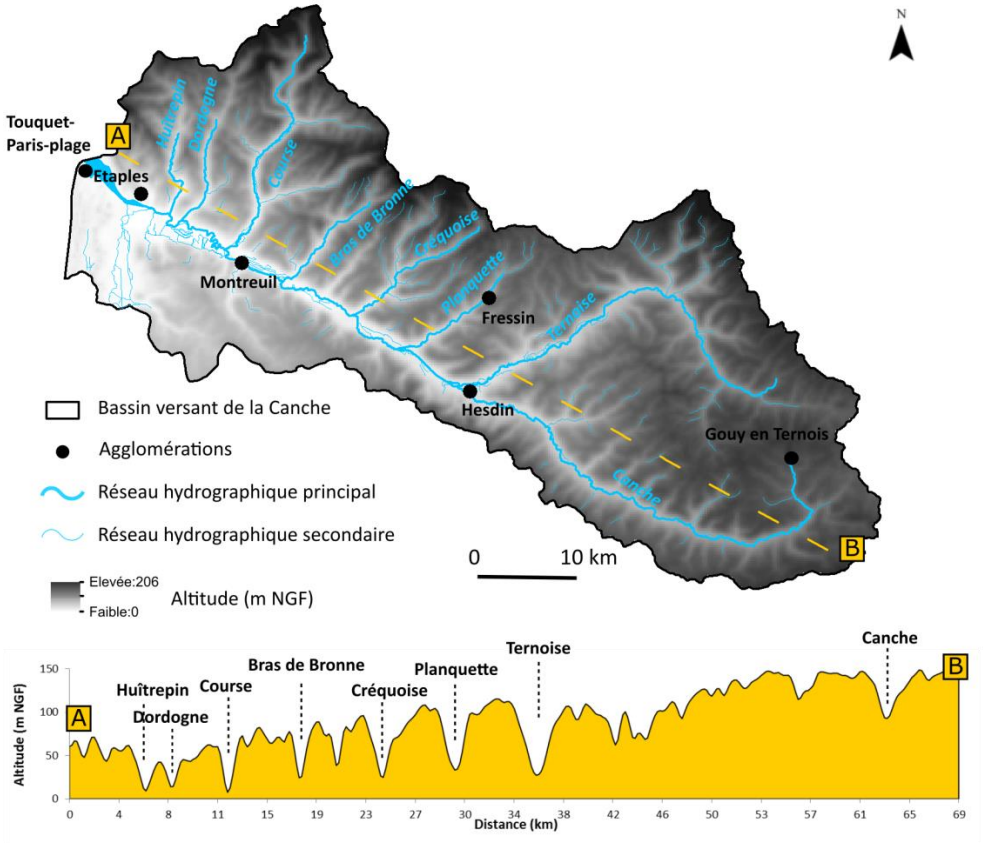

Fig. 7 : Carte et coupe topographique Sud-Sud-Est/Nord-Nord-Ouest du bassin versant de la Canche et réseau hydrographique associé (données IGN 25m).

3. Cadre géologique

La Picardie, insérée dans le sous-bloc de la Somme, est constituée de plaines et de plateaux crayeux. La morphologie est marquée par de longues ondulations et conditionnée par la tectonique

(Sommé, 1988). La région présente des plis Est-Ouest et des failles de direction Nord-Sud localisées dans les charnières. La région d'Etaples est limitée au Nord par le horst Artois-Boulonnais et au Sud par le Marquenterre, partie intégrante de la plaine maritime (Despeyroux, 1985). Le fleuve Canche suit le sens des axes des plis déterminée par des failles parallèles : la faille de Montreuil-Bassurelle à caractère décrochant affectant le Crétacé et la faille de Marguelfe-Wimereux (Auffret & Colbeaux, 1977). La vallée de la Canche correspond à un synclinal d'orientation ESE-ONO qui s'élargit d'est en ouest. Il est limité au Nord comme au sud par une ride anticlinale (Gerin, 1966). Dans sa partie aval, la Canche se trouve à la limite de deux provinces structurales contrastées : au Sud, les couches secondaire et tertiaires sont subhorizontales jusqu'au fleuve Authie et au Nord, elles se relèvent assez fortement à l'approche du Boulonnais.

Les formations géologiques (Fig.8A) sont dominées par la série marno-crayeuse du Crétacé supérieur hormis un secteur à l'Ouest de Montreuil où subsiste une butte témoin du Tertiaire, formée de sables et d'argiles du Landénien. Le paysage de la vallée est dominé par des limons de plateaux du Pléistocène qui reposent sur les terrains crayeux du Crétacé supérieur. Ceux-ci marquent les bordures de vallées. Il arrive fréquemment que ces dernières soient recouvertes en partie par une couche plus ou moins épaisse de colluvions qui adoucissent les versants (Despeyroux, 1985). Le fond des vallées principalement humides est bien occupé par des dépôts alluvionnaires, argilo-sableux et tourbeux. A partir de Montreuil-sur-Mer jusqu'à l'embouchure, la vallée de la Canche est occupée par des sables littoraux quaternaires.

Les plateaux de la Canche sont recouverts majoritairement de limons Pléistocènes (-2,5 Ma à -9600 ans) qui reposent sur les terrains crayeux du Séno-Turonien (-92 à -88 Ma) (Fig.8B). En sous-sol, on trouve une succession de marnes crayeuses du Turonien moyen et inférieur et de craies marneuses du Cénomanien (-96 à -92 Ma) qui reposent sur les grès et schistes du Carbonifère supérieur (-310 à -295 Ma). Enfin les couches profondes sont les grès, schistes et calcaires du

Dévonien supérieur et inférieur (-410 Ma à -355 Ma) puis les schistes Silurien (-435 Ma à -410 Ma). Au niveau de l'estuaire de la Canche, on note la présence en surface de sables littoraux Quaternaires.

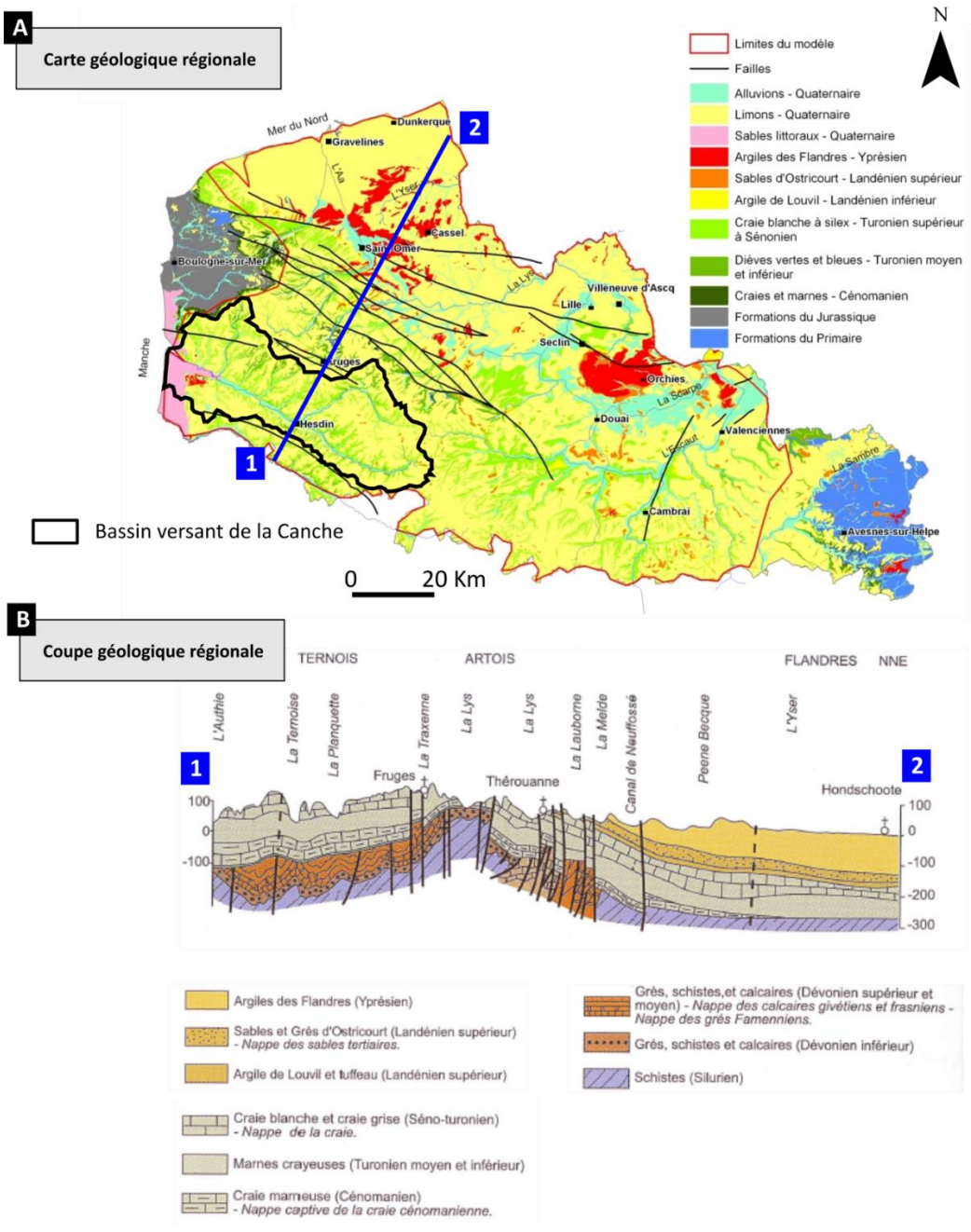

Fig. 8 : (A) Carte géologique régionale du bassin Artois-Picardie (modifiée d'après BRGM : http://sigesnpc.brgm.fr/Geologie-en-Nord-Pas-de-Calais.html) et (B) Coupe géologique régionale du bassin Artois-Picardie (modifiée d'après (Beckelynck, 1981)).

4. Pédologie

L'ensemble du bassin versant de la Canche est occupé par des sols bruns lessivés sur les plateaux, des sols bruns calciques et calcaires sur les fortes pentes, des sols alluviaux fluviatiles dans

le cours d'eau de la Canche et, enfin, des sols peu évolués sableux au niveau de l'estuaire (Fig.9). Cet ensemble pédologique est en lien direct avec le contexte géomorphologique évoqué dans la section 2.

Les sols bruns lessivés de plateaux sont également appelés néoluvisols ou luvisols rédoxiques (Baize & Girard, 2008). Ce sont des sols limoneux en surface, de type limons Eoliens (lœss) qui reposent sur les craies, marnes et argiles à silex de l'Artois. Ces sols sont relativement épais (2-4 m) (Lautridou, 1985) et caractérisés par la présence dans le solum de deux horizons bien distincts. Un premier horizon, en surface, appauvri en argile et en fer, peu coloré, peu structuré et généralement assez perméable. L'horizon plus profond est quant à lui enrichi en argile et en fer, avec une structure bien développée (polyédrique ou primatique), bien coloré et moins perméable. Cette différentiation morphologique résulte des processus de lessivage des argiles (illuviation d'argiles). Ces propriétés de sol sont propices au phénomène de battance : la dégradation structurale du sol entraîne une diminution de la capacité d'infiltration et provoque du ruissellement (Le Bissonnais et al., 1998). Néanmoins, ces sols sont reconnus pour leurs excellentes qualités agronomiques.

Les sols bruns calciques et calcaires sont également appelés rendosols ou calcosols (Baize & Girard, 2008). Ces formations associées principal aux dépôts limoneux se retrouvent principalement sur les versants. Ces sols se caractérisent par des solums peu épais et peu différenciés. En surface, on trouve des limons argileux bruns à la structure grumeleuse grossière assez forte, qui ont la particularité d'avoir une effervescence à l'HCl importante. Cet horizon ne dépasse pas les 30-40 cm. Plus en profondeur, on trouve un horizon minéral où la roche a subi une altération géochimique. L'abondance fréquente d'éléments grossiers en surface rend ces sols difficiles à travailler et non propices à l'agriculture.

Les sols alluviaux fluviatiles ou fluviosols (Baize & Girard, 2008) sont développés dans des matériaux déposés récemment, mis en place par transport, puis sédimentation en milieux aqueux.

Ces matériaux reflètent la diversité des matériaux géologiques et pédologiques situés en amont du bassin versant. Ils constituent les lits mineurs et majeurs des rivières du bassin versant de la Canche.

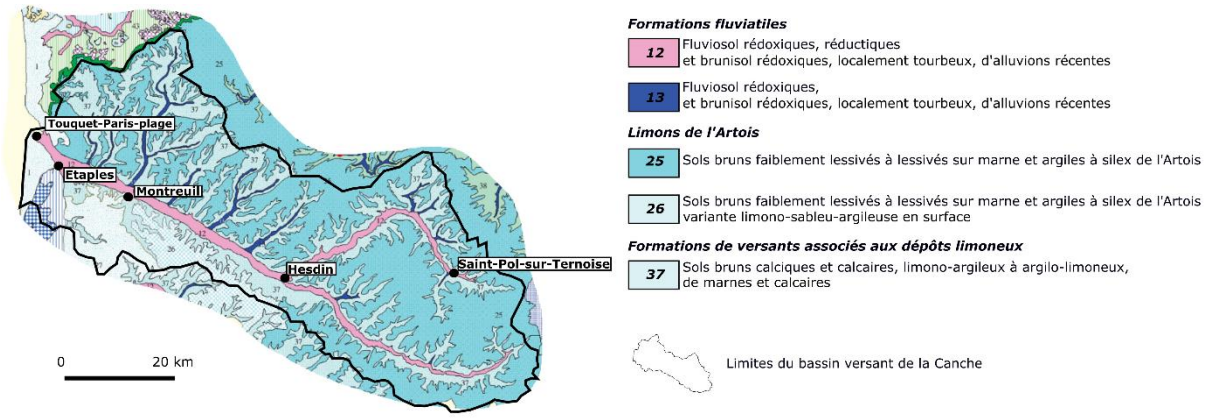

Fig. 9 : Carte pédologique du bassin versant de la Canche (modifiée d'après DRAFF Nord-Pas-de-Calais, 2013[3]).

5. Occupation de sols

La pédologie du bassin versant de la Canche étant majoritairement occupée par des sols bruns lessivés ayant un excellent rôle agronomique, il en résulte une forte occupation des terres arables sur l'ensemble du territoire (< 80%). Le reste du territoire (> 20%) est occupé essentiellement par des territoires artificiels, des forêts et des milieux semi-naturels (Fig.10). Les zones humides et les surfaces en eau occupent une faible part du territoire (< 1%). Les orientations majoritaires des exploitations sont l'association polyculture/polyélevage et la polyculture. Les principales cultures que l'on peut trouver sur le bassin sont les céréales, le blé, les orges d'hiver et de printemps et les plantes sarclées telles que la betterave, le maïs et la pomme de terre (Alexandre, 2015).

La conversion d'une agriculture extensive vers une agriculture intensive au cours du 20ème siècle s'est traduite par une profonde mutation des paysages ruraux avec notamment le remembrement des parcelles agricoles (Foucher, 2015). En France, le remembrement des parcelles a eu pour conséquence l'augmentation de la surface des exploitations. En 2000, la part des exploitations supérieures à 100 ha atteignait 12% et celles inférieures à 20 ha étaient descendues à

[3]http://draaf.hauts-de-france.agriculture.gouv.fr/IMG/pdf/Demarche_IGCS_dans_le_Nord-Pas_de_Calais_v2013-04-06_cle014cb8.pdf

50%[4]. Les conséquences de ces changements, outre une modification paysagère, sont l'aggravation des phénomènes d'érosion, la diminution des rendements agricoles et l'augmentation de la fréquence des coulées boueuses.

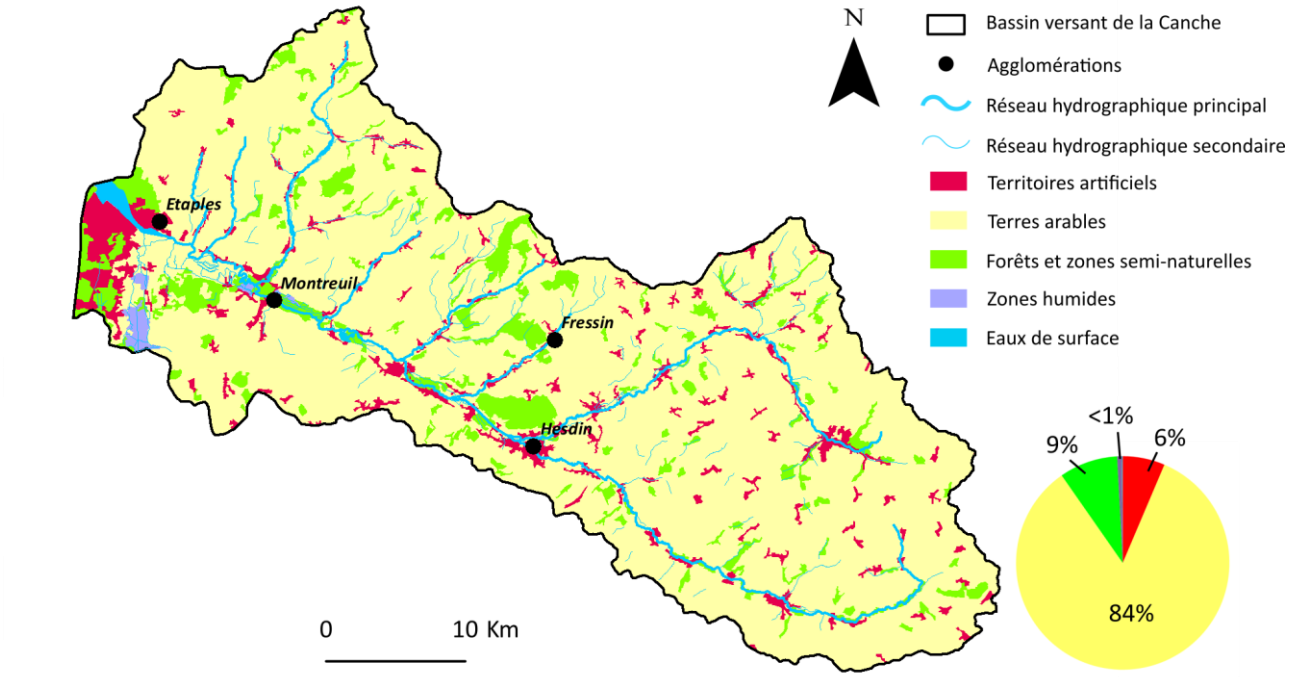

Fig. 10 : Carte d'occupation des sols sur le bassin versant de la Canche (données reclassifiées d'après Corine Land Cover 2012).

6. Climat du bassin versant de la Canche

Le territoire du bassin versant de la Canche, étant donné sa surface et son allongement Nord-Ouest/Sud-Est, connaît des variations climatiques et pluviométriques qui peuvent être très marquées notamment entre la frange littorale et les plateaux. Le climat du bassin versant de la Canche est de type océanique. La moyenne annuelle des températures est de 11°C. Les amplitudes thermiques sont assez faibles, avec des hivers doux et des étés plutôt frais. L'analyse des données du réseau pluviométrique du service de prévision des crues du bassin Artois-Picardie montre que les

[4] http://agreste.agriculture.gouv.fr/

précipitations moyennes annuelles sur la période 2005-2015 sont de 940 ± 170 mm avec une forte variabilité pluriannuelle (Fig.11A). La répartition spatiale des pluies est également très hétérogène sur l'ensemble du bassin Artois-Picardie avec de fortes variations latérales. Selon les données 2015, on observe sur la partie Ouest entre 900 et 1200 mm, alors que sur la partie Est on observe entre 600 et 800 mm de pluie (Fig.11B).

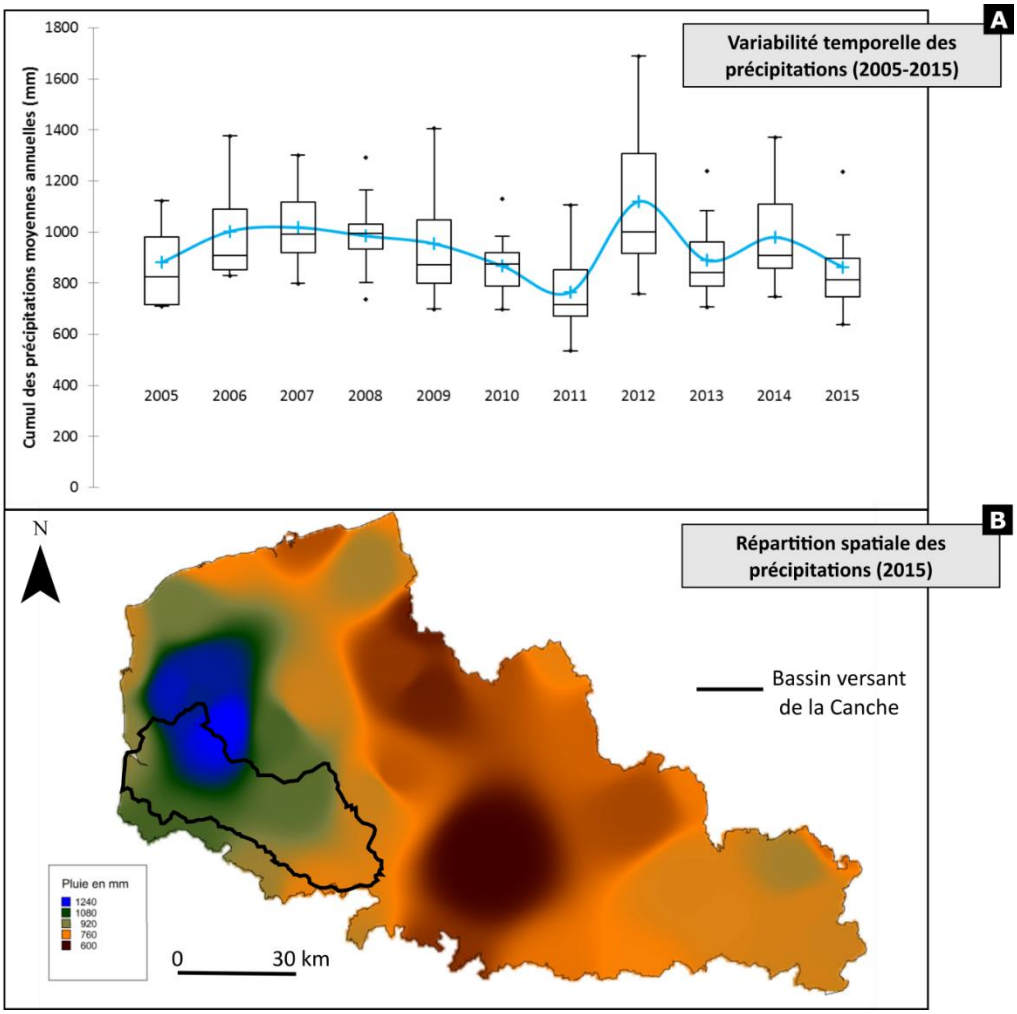

Fig. 11 : (A) Variabilité temporelle des cumuls de précipitations annuelles (mm) sur l'ensemble du bassin Artois-Picardie et (B) Répartition spatiale des précipitations moyennes annuelles pour l'année 2015 sur le bassin Artois-Picardie (données Météo France[5] et DREAL[6]).

[5] http://www.hauts-de-france.developpement-durable.gouv.fr/IMG/pdf/bsh2014.pdf
[6] https://www.hauts-de-france.developpement-durable.gouv.fr/?Reseau-pluviometrique-annuaire-2015

7. Flux hydro-sédimentaires

Le régime hydrologique de la Canche est de type pondéré, contrôlé par le stock d'eau de l'aquifère à craie blanche du Séno-Turonien. Les crues de la Canche sont dues à deux facteurs principaux : d'une part, une forte pluviométrie qui entraîne des ruissellements et d'autre part, une saturation de la plaine alluviale qui s'accompagne d'une remontée de la nappe phréatique. Sur le bassin versant de la Canche, les débits sont mesurés par plusieurs stations hydrologiques hautes et basses fréquences (Fig.12).

Les mesures hautes-fréquences sont prises sur la Canche au niveau de la ville d'Attin. Les débits et la charge en MES sont mesurés en continu à l'aide d'une station de monitoring haute-fréquence gérée par l'Agence de l'Eau Artois-Picardie (débitmètre et sonde à turbidité ; Δt = 15 min). Le débit moyen sur cette portion est estimé à 21 $m^3\ s^{-1}$, mais montre de très fortes variabilités en raison de l'influence de la marée : elle se fait ressentir assez loin puisque l'onde de marée remonte jusqu'à Montreuil-sur-Mer (soit 14 km de cours d'eau ; Fig.13). Le couplage du débitmètre avec le suivi de la concentration en MES permet d'estimer les flux annuels de sédiments qui transitent jusqu'à l'exutoire. Sur la période 1999-2015, les flux annuels varient de 29 à 185 kt ce qui correspond à un taux d'érosion spécifique compris entre 22 et 144 t $km^{-2}\ an^{-1}$ (Agence de l'eau Artois-Picardie, 2016). Ces taux d'érosion sont parmi les plus faibles à l'échelle de la planète mais restent problématiques avec des conséquences directes telles que : forte turbidité des écoulements fluviaux, envasement ou risque accru de coulées boueuses. Ces taux d'érosion sont du même ordre de grandeur que ceux observés sur les sols limoneux de l'Ouest du Bassin de Paris (Laignel et al., 2006; Landemaine, 2016).

Les mesures basse-fréquence sont prises à trois localisations différentes sur le bassin versant de la Canche. D'une part, sur le linéaire principal de la Canche et, d'autre part, sur les deux affluents majeurs : la Ternoise et la Course. Les débits sont mesurés à l'aide d'une échelle limnimétrique (une mesure journalière). Sur la Canche, les mesures sont prises au niveau de la ville de Brimeux. Pour les

affluents, les mesures sont prises dans les villes de Hesdin (Ternoise) et Estrée (Course). Les débits caractéristiques des trois stations basses-fréquence sont résumés dans le Tableau 1.

Tab. 1 : Débits caractéristiques des trois stations basse-fréquence sur le bassin versant de la Canche. Q_{moy} et ΔQ_{moy} représentent le débit moyen et la déviation standard en $m^3 s^{-1}$. $Q_{spéc}$ représente le débit spécifique en $l s^{-1} km^{-2}$. Q_5, Q_{10} et Q_{50} représentent respectivement le débit quinquennal, décennal et cinquantennal en $m^3 s^{-1}$.

Bassin versant	Q_{moy}	ΔQ_{moy}	$Q_{spéc}$	Q_5	Q_{10}	Q_{50}
Canche	12,1	2,8	13,5	26	31	40
Ternoise	4,5	1	13,2	5,5	/	/
Course	2,9	0,7	19,5	6	/	/

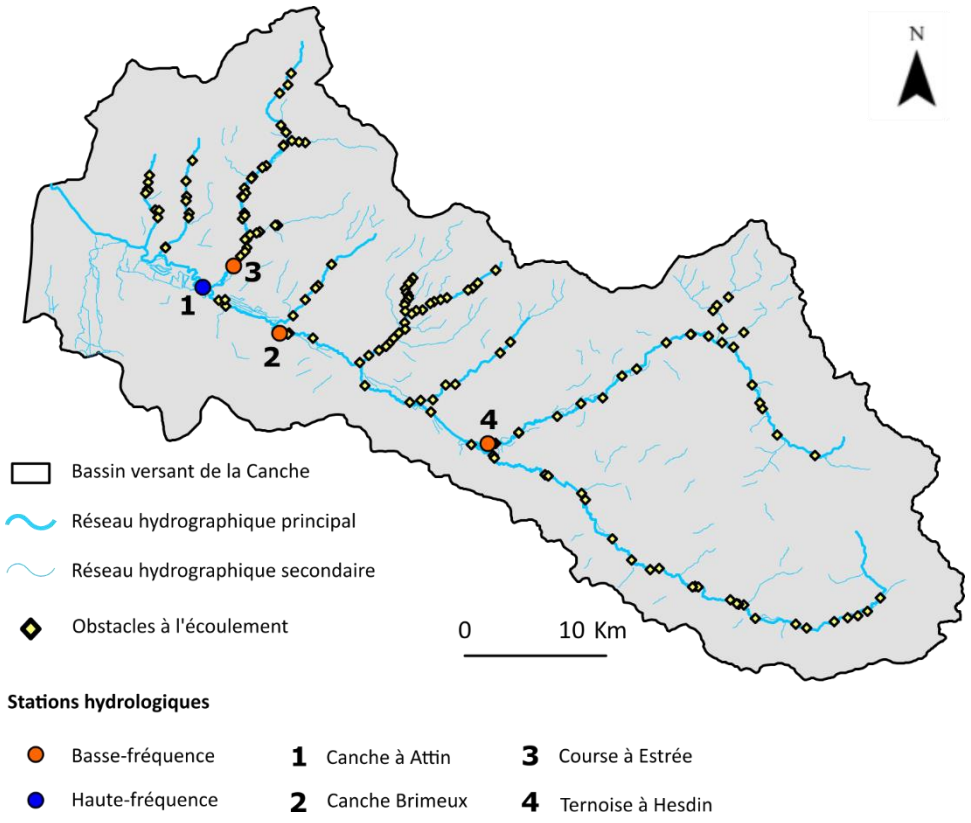

Fig. 12 : Carte de localisation des stations hydrologiques et des obstacles à l'écoulement sur le bassin versant de la Canche (données Agence de l'eau Artois-Picardie, Banque hydro[7] et Référentiel des obstacles à l'écoulement[8]).

[7] http://hydro.eaufrance.fr/
[8] http://carmen.carmencarto.fr/66/ka_roe_current_metropole.map

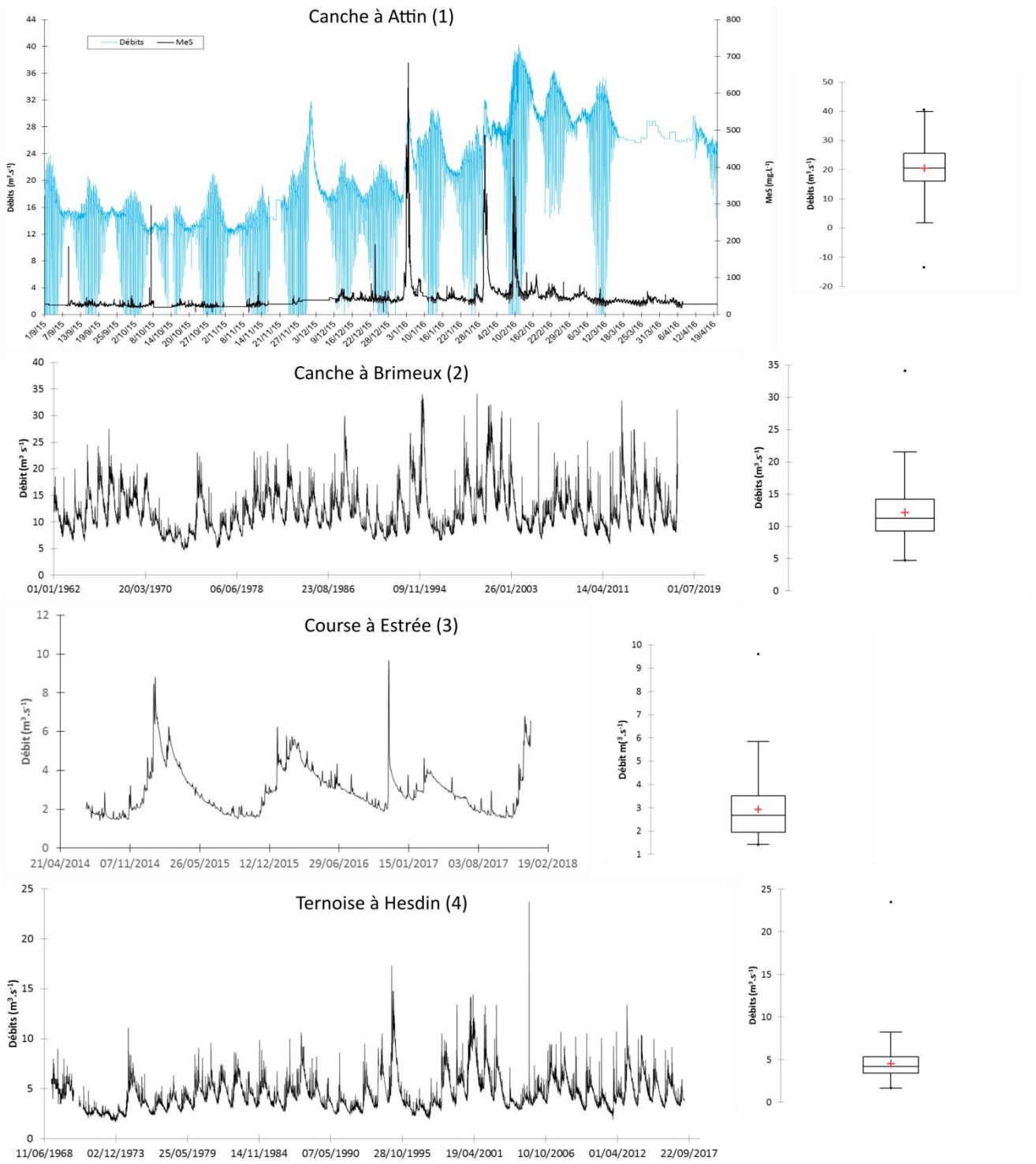

Fig. 13 : Chroniques hydrologiques de la station haute-fréquence de la Canche à Attin et des stations basse fréquence de la Canche, la Course et la Ternoise à Brimeux, Estrée et Hesdin (données Agence de l'eau Artois-Picardie et Banque hydro).

Références

Agence de l'eau Artois-Picardie. (2016). *Schéma Directeur d'Aménagement et de Gestion des Eaux du Bassin Artois-Picardie*. Retrieved from http://www.eau-artois-picardie.fr/sdage

Alexandre, H. (2015). *Quantification de l'efficacité des fascines : diagnostic initial du bassin versant de la Pommeroy et paramétrage d'un modèle de ruissellement/érosion*.

Auffret, J. ., & Colbeaux, J. . (1977). Etude structurale du Boulonnais et de son prolongement sous-marin en Manche orientale. *Bull. Soc. Géol. France*, *19*(5), 1047–1055.

Baize, D., & Girard, M.-C. (2008). *Référentiel pédologique 2008*. *Savoir Faire*.

Beckelynck, J. (1981). *Traitement régionalisé des paramètres contribuant à la gestion des nappes: application à la modélisation de la nappe de la craie dans le bassin de l'Aa et de la moyenne Lys*. Université des Sciences et Techniques de Lille. Retrieved from https://ori-nuxeo.univ-lille1.fr/nuxeo/site/esupversions/1ea8eb07-e140-446e-be38-7383cefdb7fc

Despeyroux, Y. (1985). *Etude hydrosédimentaire de l'estuaire de la Canche (Pas-de-Calais)*. https://doi.org/10.1017/CBO9781107415324.004

Foucher, A. (2015). *Reconstruction de la cascade sédimentaire en contexte de plaine agricole drainée*. Université François Rabelais de Tours.

Gerin, B. (1966). *Contribution à l'étude hydrogéologique du bassin de la Canche*. Université Paris 6.

Laignel, B., Dupuis, E., Durand, A., Dupont, J.-P., Hauchard, E., & Massei, N. (2006). Erosion balance in the watersheds of the western Paris Basin by high-frequency monitoring of discharge and suspended sediment in surface water. *Comptes Rendus Geoscience*, *338*(8), 556–564. https://doi.org/10.1016/j.crte.2006.03.010

Landemaine, V. (2016). *Érosion des sols et transferts sédimentaires sur les bassins versants de l'Ouest du Bassin de Paris : analyse, quantification et modélisation à l'échelle pluriannuelle*. Université de Rouen Normandie.

Lautridou, J. P. (1985). *Le cycle périglaciaire pléistocène en Europe du Nord- Ouest et plus particulièrement en Normandie*. Université de Caen Basse Normandie.

Le Bissonnais, Y., Benkhadra, H., Chaplot, V., Fox, D., King, D., & Daroussin, J. (1998). Crusting, runoff and sheet erosion on silty loamy soils at various scales and upscaling from m2to small catchments. *Soil and Tillage Research*, *46*(1–2), 69–80. https://doi.org/10.1016/S0167-1987(98)80109-8

Sommé, J. (1988). Géomorphologie de la zone terminale du tunnel sous la Manche dans le Nord de la France. *Hommes et Terres Du Nord*, (3), 155–161. https://doi.org/https://doi.org/10.3406/htn.1988.2172

Chapter 2

Assessing temporal variability and controlling factors of the sediment budget of a small agricultural catchment in Northern France (the Pommeroye).

Résumé étendu – Chapitre 2

Contexte

Chaque année, de nombreuses catastrophes naturelles liées à des inondations et des coulées boueuses sont recensées dans le Nord de la France. Ces désastres sont la conséquence d'importants transferts hydro-sédimentaires liés à des phénomènes d'érosion diffuse et/ou concentrée, et une occupation du sol majoritairement dominée par l'agriculture. Actuellement, peu d'études ont cherché à caractériser la variabilité de ces transferts à l'échelle de petits bassins versants agricoles (< 1 km²) reconnus pour être de gros contributeurs. Pourtant, comprendre et quantifier la variabilité spatio-temporelle de ces transferts est essentiel pour pouvoir améliorer la durabilité des sols et réduire les flux de matières exportés. Dans ce contexte, cette étude régionale vise à améliorer notre connaissance de la variabilité intrinsèque des transferts hydro-sédimentaires et leurs facteurs de contrôle. A court-terme, un suivi de l'efficacité des ouvrages d'hydraulique douce est également proposé.

Matériel et Méthodes

Pour quantifier les transferts hydro-sédimentaires, une station de mesure haute-fréquence a été installée à l'exutoire du bassin versant de la Pommeroye (0,54 km²). Cette station est opérationnelle depuis le 31 mars 2016. Elle est composée d'un canal Venturi à section exponentielle en polyester (*ISMA type VII*) qui permet de canaliser les écoulements (Fig.14). Grâce à une relation débit = f(hauteur d'eau) prédéfinie, il est possible d'évaluer les débits selon une période temporelle choisie. Pour cela, un débitmètre à ultrasons a été installé à l'aplomb de ce même canal pour mesurer la hauteur des écoulements. Le débitmètre utilisé est le *LNU 300-X* de chez *IJINUS*. En parallèle, des mesures de turbidité sont effectuées avec une sonde *Odeon* de chez *Aqualabo*. La relation avec la charge en MES est estimée sur des échantillons prélevés avec un échantillonneur automatique (*ISCO 3700*). Toutes les sondes sont couplées à des enregistreurs de données. Les paramètres sont mesurés toutes les six minutes et téléchargés toutes les deux semaines via un ordinateur et le logiciel *Avelour 6.0.4*. Enfin, un pluviomètre à auget (*Précis mécanique ; 0.2 mm*) a

été installé en tête du bassin versant afin d'évaluer les caractéristiques des événements pluvieux. Les paramètres forçants (i.e. durée, quantité de précipitations pendant et 48h avant un épisode, intensité max à 6 min, débit moyen et maximum, concentration en MES moyenne et maximale, flux sédimentaire, et quantité d'eau ruisselée) de l'ensemble des épisodes érosifs enregistrés avec la station de mesures sont analysés, statistiquement, afin d'évaluer leur influence sur les transferts hydro-sédimentaires lors d'épisodes érosifs.

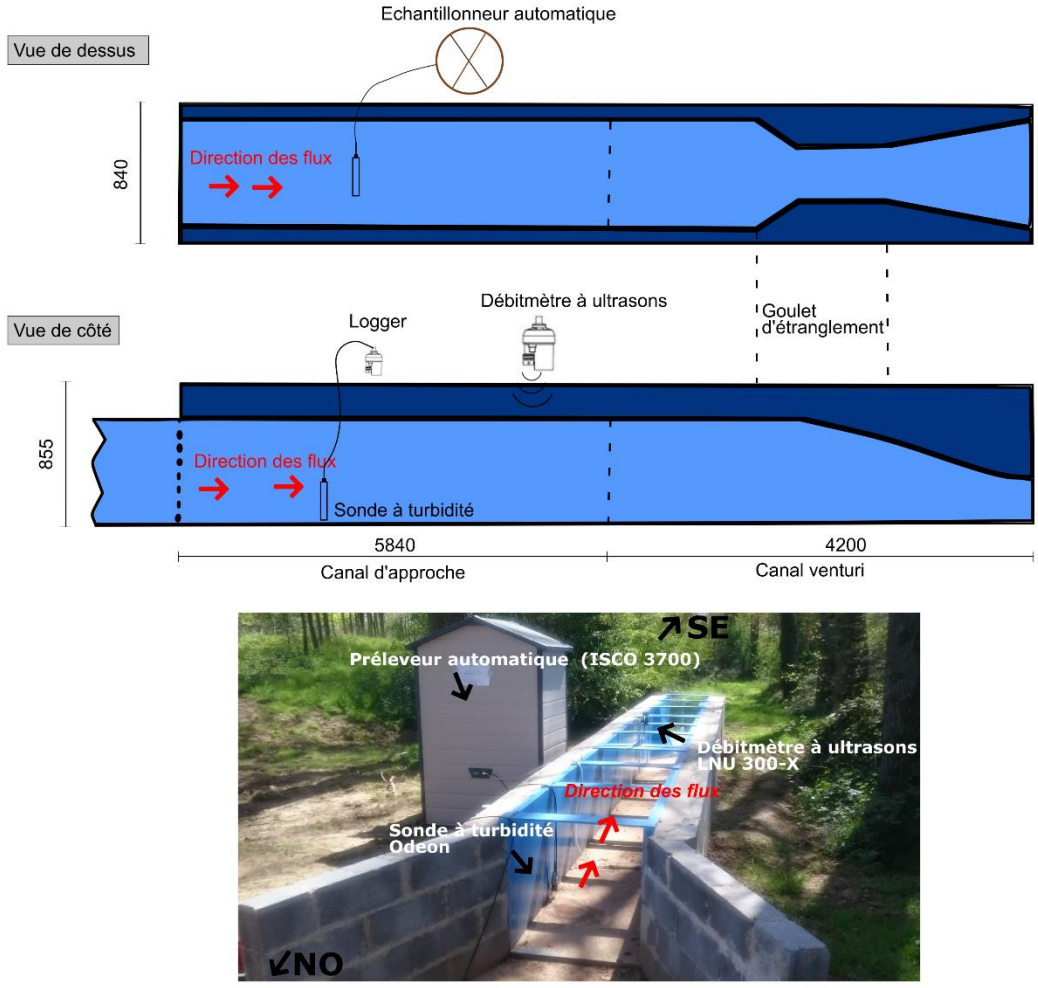

Fig. 14 : ***Détail de l'instrumentation de la station de mesure haute-fréquence située à l'exutoire du bassin versant de la Pommeroye.***

Principaux résultats

Au cours de deux années de mesures consécutives (04/2016 - 04/2018), 48 épisodes érosifs ont été enregistrés (Fig.15). Les transferts hydro-sédimentaires sur ce bassin versant sont évalués entre 29 et 70 t km^{-2} an^{-1}. La variabilité spatio-temporelle liée à ces évènements érosifs est très

importante. Pour un épisode érosif donné, les flux sédimentaires peuvent atteindre 7132 kg et la lame d'eau écoulée 8630 m^3. Les flux sont exportés majoritairement en hiver (55%) et en automne (42%), et sont peu représentés lors des périodes printanières et estivales (3%). Les flux sont également exportés en majorité (40%) sur un faible nombre d'évènements (6%). Les analyses statistiques multivariées ont montré que la quantité de pluie et la durée de l'évènement pluvieux sont les principaux paramètres forçants. Les intensités de pluie et les quantités tombées 48h avant un épisode ne sont quant à elles pas corrélées aux flux hydro-sédimentaires.

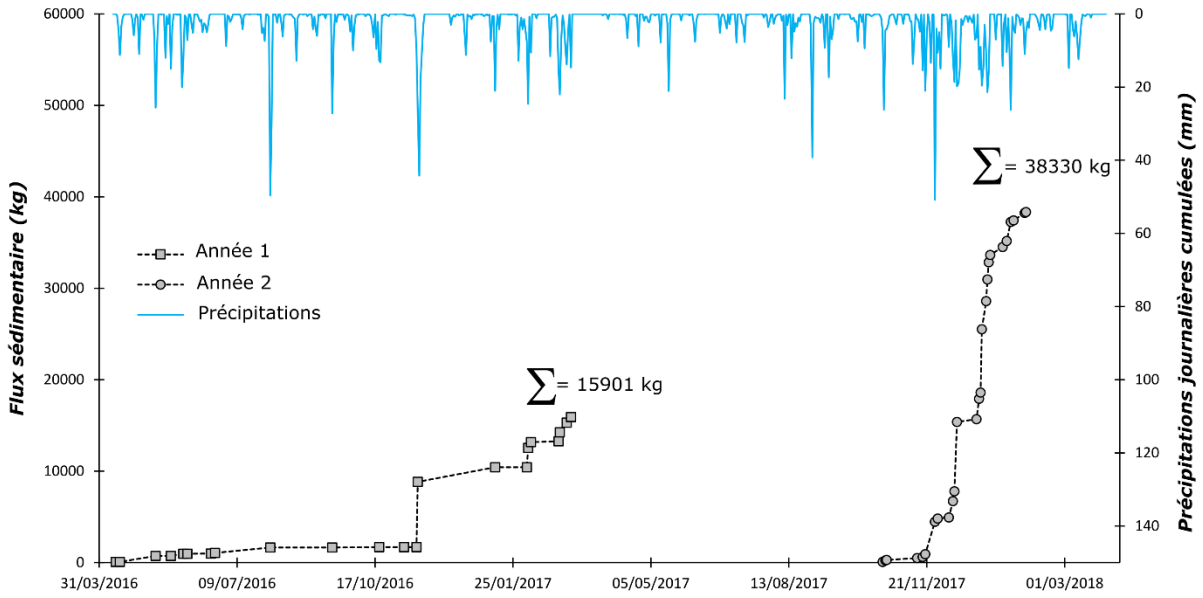

Fig. 15 : ***Flux sédimentaire (kg) et précipitations journalières cumulées (mm) enregistrés à la station de mesure haute-fréquence du bassin versant de la Pommeroye au cours des deux premières années de mesure.***

Conclusions et Perspectives

Les transferts hydro-sédimentaires à l'échelle du petit bassin versant agricole du Nord de la France (la Pommeroye) ont pu être quantifiés et montrent une importante variabilité temporelle intra et interannuelle. Cette variabilité est majoritairement guidée par les cumuls de pluie et la durée des épisodes pluvieux en automne et en hiver. En perspective, l'efficacité des solutions d'hydraulique douce (haies, fascines, bandes enherbées) pour la réduction du transport hydro-sédimentaire pourra être évaluée sur ce bassin versant grâce à l'aménagement d'un futur plan anti-érosion et à la continuité du suivi hydro-sédimentaire.

Chapter 2: Assessing temporal variability and controlling factors of the sediment budget of a small agricultural catchment in Northern France (the Pommeroye).

Edouard Patault[a,b], Claire Alary[a], Christine Franke[b], Arnaud Gauthier[c], Nor-Edine Abriak[a]

[a]IMT Lille Douai, Univ. Lille, EA 4515 - LGCgE - Civil Engineering and Environmental Department, F-59000 Lille, France

[b]MINES ParisTech, PSL Research University, Center of Geosciences, 35 rue Saint-Honoré, 77305 Fontainebleau Cedex, France

[c]Département des sciences de la Terre, Université de Lille 1, Villeneuve d'Ascq, France

This chapter is presented in the form of an article submitted on June 10, 2018 to the journal Heliyon. The article is under review.

Highlights

- The specific sediment yield ranges from 29.4 to 70 t km^{-2} yr^{-1} over two years of monitoring.
- 6% of the erosive events produced 40% of the hydro-sedimentary flux.
- Seasonal production of sediment yield: winter (55%), autumn (42%), spring and summer (3%).
- Rainfall amount and duration of the event control the hydro-sedimentary response.
- Rainfall intensities and 48h-antecedent rainfall are not correlated with the hydro-sedimentary response.

Graphical abstract

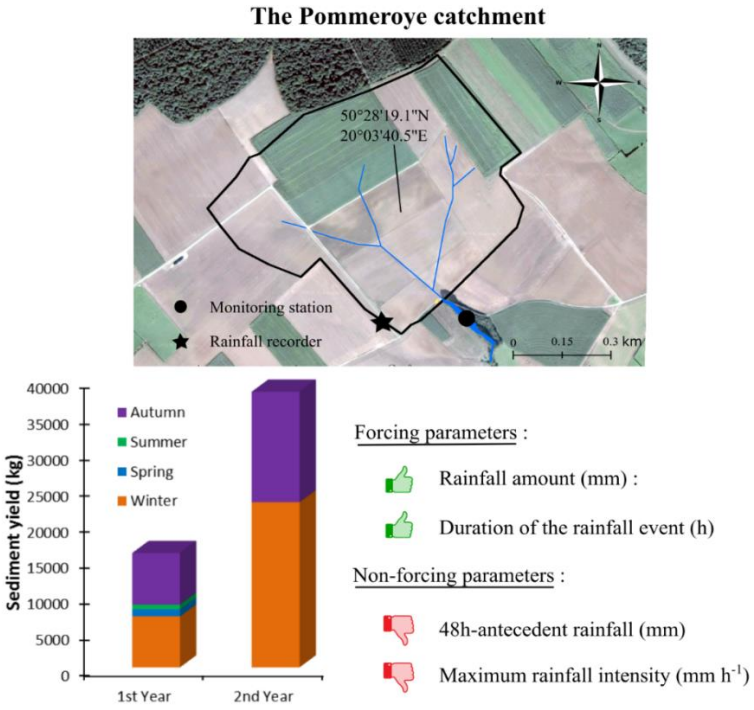

Abstract

A high-frequency monitoring station was implemented at the outlet of the small catchment of the Pommeroye (0.54 km²) in Northern France to study erosion by runoff and hydro-sedimentological responses to heavy rainfall events in the context of Quaternary loess deposits. The aim of this experimental work is to assess the temporal variability of sediment yield and to identify the factors controlling the hydro-sedimentary response. To achieve this goal, statistical and hydro-sedimentary dynamic analyses were performed. During two years of monitoring (04/2016 – 04/2018), 48 flood events were recorded. The specific sediment yield is highly variable and was evaluated to 29.4-70 t km^{-2} yr^{-1} which is conventional for the study region. Most of the sediment yield was produced in winter (55%) and autumn (42%). Only 3% were produced during spring and summer periods. According to our results, only 6% of the erosive events are responsible for the transport of more than 40% of the flux recorded at the outlet. This underlines the temporal variability of the hydro-sedimentary production in small agricultural catchments for which most of the hydro-sedimentary flux is produced during a small number of events. The results of statistical analyses show that the total amount of rainfall and the duration of a rainfall episode are the main controlling factors on the hydro-sedimentary response. Our results also suggest that the rainfall intensities and the 48h-antecedent rainfall are not linked to the hydro-sedimentary response.

Keywords: high-frequency monitoring; soil erosion; sediment yield; temporal variability; hydro-sedimentary response; Northern France

1. Introduction

In the North-western European loess plateau and in particular the North of the Paris Basin, the erosion of agricultural land is a serious environmental issue (Delmas et al., 2012; Evrard et al., 2007). Every year, numerous natural disasters occur due to various erosion processes which result in on-site and off-site problems including the loss of fertile soils, the silting of riverbeds and dams as well as infrastructure and property damage by muddy floods (Capra, 1993).

The most common type of soil erosion pattern observed in these territories are (i) sheet erosion, (ii) rills, (iii) interrills, (iv) classical gullies, and (v) ephemeral gullies (Foster, 1986). So far, the focus was drawn to rill/interrill erosion, but recently a growing interest has focused on ephemeral gullies (Castillo & Gomez, 2016; Nachtergaele et al., 2002; Poesen, 1993; Valentin et al., 2005) since they have been recognized as a major contributor to sediment yield in small agricultural catchments in the European loess belt (Poesen et al., 1996). Classical survey methods to evaluate sediment production on small catchments are aerial photography (Marzolff et al., 2011; Nachtergaele & Poesen, 1999), terrestrial photography (Frankl et al., 2011), terrestrial laser scanning (Li et al., 2017), airborne laser scanning (Goodwin et al., 2017), or direct measurements of channel volumes (Valcárcel et al., 2003). However, these methodologies are not suitable for quantifying the sediment yield at the catchment scale (Vandaele & Poesen, 1995).

Understanding and quantifying the dynamics of suspended sediment transport is essential for controlling soil and implementing effective mitigation practices to reduce stream suspended matter and associated pollutants load. Currently, catchment monitoring was successfully used by several authors (Estrany et al., 2009; Giménez et al., 2012; Nadal-Romero et al., 2008; Nu-Fang et al., 2011) to quantify erosion processes in small agricultural catchments and to assess the relationships between hydro-sedimentological parameters. These studies have reported on sediment transfer that showed high temporal and spatial variabilities, and the fact that only few erosive events are responsible for huge sediment export. They also found complex correlations between rainfall

characteristics and the hydro-sedimentary response. However, few attempts have been made to evaluate the variability of the hydro-sedimentary response in the context of agricultural plains of North-Western Europe. This regional case study aims to further improve our knowledge on the factors that control sediment export and the temporal variability of sediment transfer.

The aim of this study is (i) to develop an innovative and robust methodology for high-frequency monitoring of the sediment load at the outlet of a small agricultural catchment (0.54 km²), (ii) to quantify short-term changes for different runoff events, (iii) to identify the parameters that explain the hydro-sedimentary response, and (iv) to determine the seasonal variability.

2. Study area

The Pommeroye catchment (0.54 km²) is situated in the European loess belt in Northern France (Fig.16A). It is a subcatchment of the Canche River watershed (1274 km²). The dominant climate is oceanic and the average annual temperature in this region is 11°C. The thermal amplitude is low, with soft winters and cool summers. The annual precipitation rate is 1000 ± 150 mm yr^{-1}. The elevation of the study area ranges from 115 to 145 m and the average slope is 4.2%. The soil is constituted of Pleistocene silt which overlays the chalky soil of the Seno-Turonian (Beckelynck, 1981). Analyzes carried out by the regional Chamber of Agriculture resulted in an average composition of fine silt levels of 34%, coarse silt of 48%, and low clay content of 18% (Alexandre, 2015). An ephemeral gully network is well-established and recurrent, resulting from the junction of rills that form a dendritic channel pattern (Fig.16B). The study site is exclusively occupied by arable land, divided into 14 fields. The dominant crops here are cereals, winter and spring barley, rape seed, and mustard.

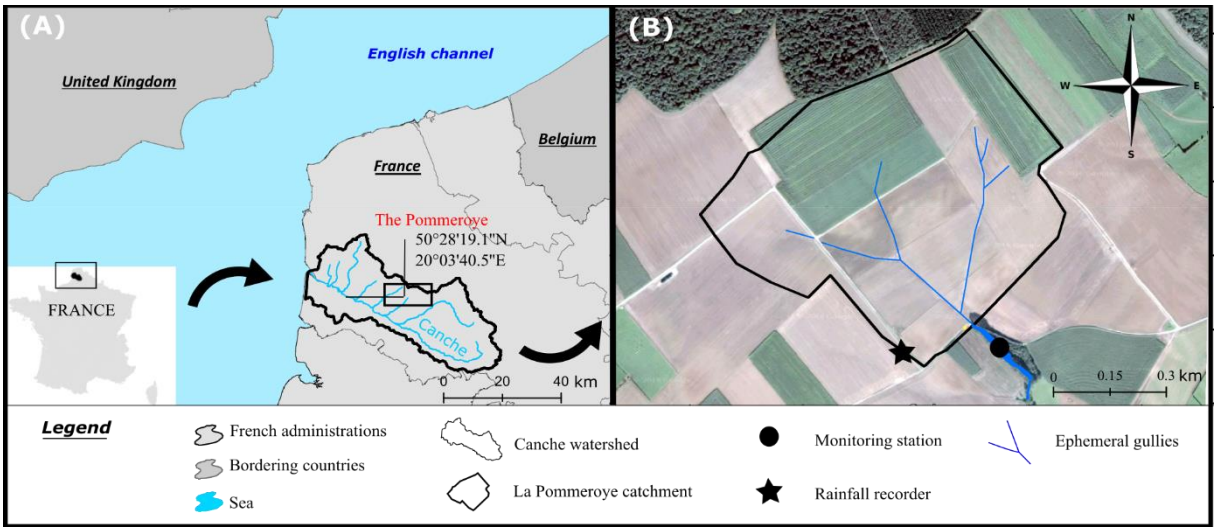

Fig. 16 : (A) Overview on the study region and (B) map of the Pommeroye catchment showing the location of the ephemeral gullies and instruments used in this study.

3. Material & Methods

3.1 The monitoring station

A monitoring station consisting of an exponential Venturi channel has been installed on March 31, 2016 at the outlet of the Pommeroye catchment to record the flow discharge and suspended sediment concentration (SSC; Fig.17). The water height is recorded by an ultrasound water-level logger (*Ijinus LNU 300-X*). Runoff discharge is calculated for each time step in the Venturi channel using the following equation provided by the supplier of the Venturi channel (Eq.1):

$$Q = -7{,}223 \times h + 2873{,}2 \times h^2 - 766 \times h^3 + 770 \times h^4 \quad (1)$$

Where Q is the flow discharge in the Venturi channel ($m^3\ h^{-1}$) and h the water height (m).

The range of the ultrasound water-level is 0 to 792 mm in the channel and the resolution is 2 mm. The SSC is estimated using a turbidity probe (*Odeon/Aqualabo*), its accuracy is lower than 5% FNU. Regular cleaning of the probe head is carried out after each flood event. An automatic water sampler (ISCO 3700; 24 x 1 l) is used to collect water samples during flood events. The sampler is coupled to the water-level sensor and only operates when water flows through the Venturi channel. All sensors are connected to a data logger (*Ijinus Log0500*). The measured parameters are recorded

every 6 min. Information is downloaded every two weeks on a laptop computer (Software Avelour 6.0.4). A tipping-bucket rain gauge (*Précis mécanique; model: 303x*; resolution: 0.2 mm) was also installed in the catchment close to the station (see star symbol in Fig.16B).

To estimate the SSC over time, 100 mL of water samples are filtered in the laboratory using dehydrated cellulose nitrate filters (pore size of 0.45 µm). Subsequently, the filters are dried in an oven at 30°C for 72 hours and weighed. A correlation curve is defined between the turbidity data measured in the field and the SSC obtained in the laboratory (Eq.2):

$$SSC = -5 \times 10^{-8}\, T^2 + 0.001T + 0.0089 \quad (2)$$

With SSC corresponding to the suspended sediment concentration (g L^{-1}) and T the turbidity (FNU). Suspended sediment flux (SSF) is then calculated using Eq.3:

$$SSF = Q \times SSC \times 10^3 \quad (3)$$

With Q the flow discharge in $m^3\ s^{-1}$ and SSF the instant suspended sediment flux in kg s^{-1}. The sediment yield (SY) for each event is evaluated as (Eq.4):

$$SY = \int_{t_0}^{t} SSF\ \Delta t \quad (4)$$

With SY as the sediment yield for each event (kg) and Δt corresponding to the time elapsed between the beginning and the end of an event.

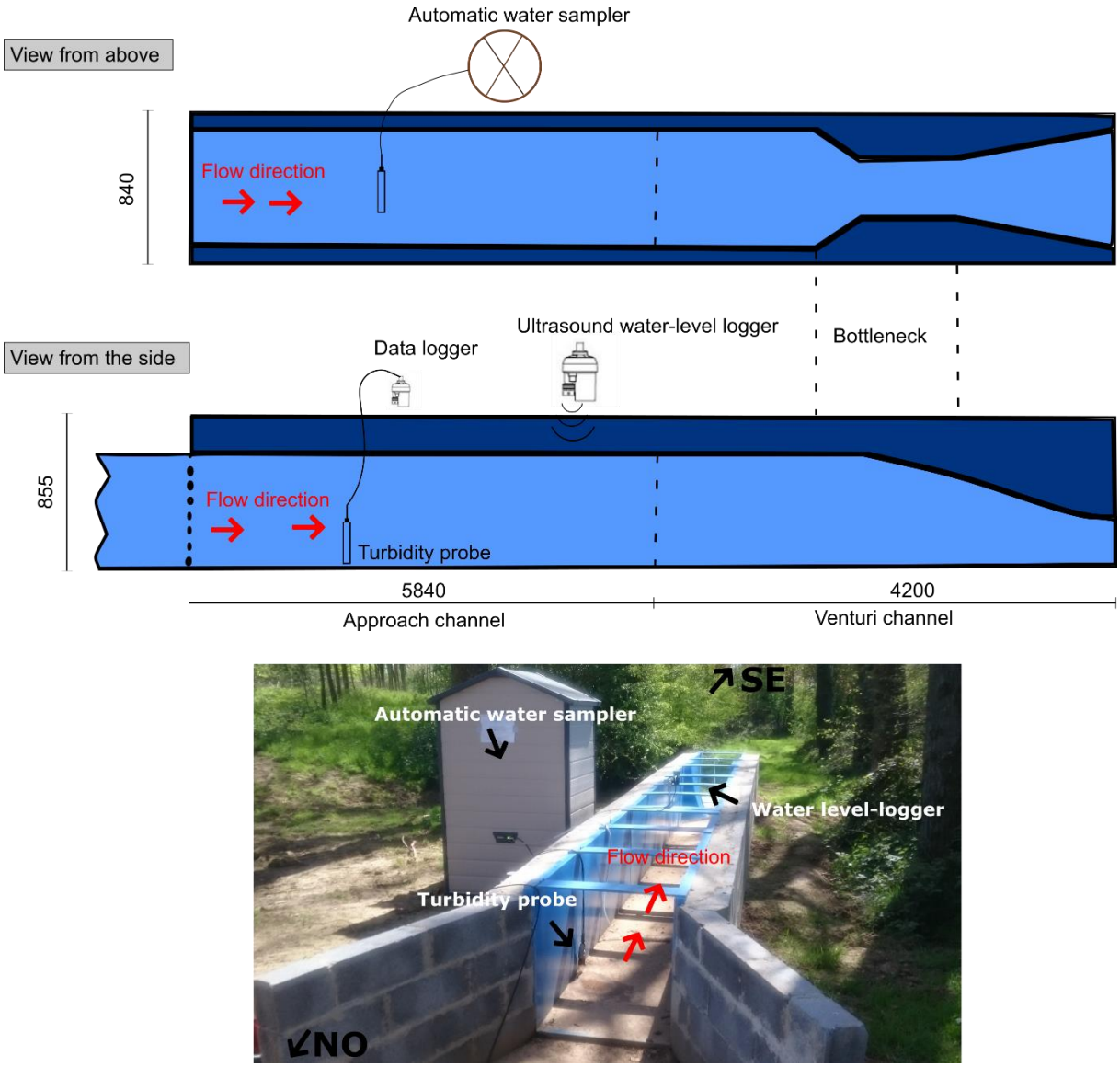

Fig. 17 : Schema and picture of the monitoring station at the outlet of the Pommeroye catchment viewed from different perspectives (the dimensions are given in mm).

3.2 Analysis of variables

During the two years of monitoring (04/2016 - 04/2018), a total of 48 runoff events was recorded. For each event, multiple variables were extracted, related to : (i) duration rainfall event (R_{time}, min), (ii) rainfall amount (Ra, mm), (iii) max 6 min rainfall intensity (Ri_{max}, mm h^{-1}), (iv) rainfall amount 48h before the beginning of the investigated event (Ra_{48}, mm), (v) mean flow and peak flow (Q_{mean}, Q_{max}, m^3 h^{-1}), (vi) mean and maximum SSC concentration (SSC_{mean}, SSC_{max}, g l^{-1}), (viii) sediment yield (SY, kg), and (ix) total runoff (R_{tot}, m^3).

3.3 Pearson correlation matrix and Principal Component Analysis (PCA)

Statistical analyses were performed using the statistical software *R*[9] and the following packages: *FactoMiner*[10] and *Corrplot*[11]. Pearson correlation matrix is used to evaluate the linear dependency between multiple variables simultaneously. The result is given using the Pearson correlation coefficient r which reflects the linear correlation between two variables. The coefficient is calculated using the covariance of two variables divided by the product of their standard deviations (Eq.5):

$$r = \frac{\sum_{i=1}^{n}(x_i - \bar{x})(y_i - \bar{y})}{\sqrt{\sum_{i=1}^{n}(x_i - \bar{x})^2}\sqrt{\sum_{i=1}^{n}(y_i - \bar{y})^2}} \quad (5)$$

Where n is the sample size; x_i and y_i are the values of the sample; $\bar{x}$ and $\bar{y}$ are the mean values of the sample. A value of 1 implies that a linear equation describes the perfect relationship between x_i and y_i, with all data points lying on a line for which y_i increases as x_i increases. A value of −1 implies that all data points lie on a line for which y_i decreases as x_i increases. A value of 0 implies that there is no linear correlation between the variables.

PCA is commonly used in environmental studies (Raux et al., 2011; Viel, 2012). The purpose of PCA is to describe linear relationships between variables of large data sets. It calculates principal dimensions that represent the degree of correlation between all variables. Dimensions that show the percentage of highest variance are chosen to explain the variables and the individual distribution. To run the PCA, all data must be normalized because variables may exhibit different scales and measurement units. Then the PCA calculates a covariance matrix describing the dispersion of all parameters. The correlation matrix is diagonalized allowing the transformation of the correlated

[9] R Core Team (2016). R: A Language and Environment for Statistical Computing. R Foundation for Statistical Computing, Vienna, Austria. URL https://www.R-project.org/.
[10] https://cran.r-project.org/web/packages/FactoMineR/index.html
[11] https://cran.r-project.org/web/packages/corrplot/index.html

variables into orthogonal variables called principal dimensions, which are a linear combination of the initial variables. The closer a coordinate is to 0 on a given axis, the less significant is the variable on the axis.

4. Results

4.1 General characteristics of runoff events

4.1.1 First year of monitoring

Between April 2016 and April 2017, 22 runoff events were recorded: 7 occurred in spring, 3 in summer, 4 in autumn, and 8 in winter. The main characteristics of these events are summarized in Table 2 and are described in detail in the following text:

i. The duration of runoff events ranged from 126 to 7200 min in total with a median value of 534 min. 5 events (22%) showed a duration longer than 1000 min, and 5 events (22%) correspond to shorter period (less than 360 min). One event exceeded 2000 min.

ii. The rainfall amount ranged from 6 to 103.8 mm with a median value of 16.1. 8 events (36%) exceeded 20 mm, and 5 events (22%) had values lower than 10 mm.

iii. The maximum 6-min rainfall intensity ranged from 3 to 76 mm h^{-1}, and 3 events (13%) exceeded 20 mm h^{-1}. The amount of precipitation 48h before the beginning of an event ranged from 0.2 to 25.4 mm. 7 events (32%) showed a rainfall amount 48h before the beginning of an event that was higher than 10 mm.

iv. The peak flow ranged from 0.6 to 378.3 m^3 h^{-1} and the mean flow ranged from 0.11 to 94.5 m^3 h^{-1}. 10 events (45.5%) showed values of a peak flow exceeding 100 m^3 h^{-1}.

v. The maximum SSC ranged from 0.15 to 5 g L^{-1} and the mean SSC ranged from 0.06 to 1.6 g L^{-1}. 11 events (50%) showed values of maximum SSC exceeding 3 g L^{-1}.

vi. The sediment yield values ranged from 0.07 to 7131.9 kg and were extremely variable. 3 events (13.6%) exceeded 1500 kg and one event exceeded 2500 kg. This event represents 44.8% of the total sediment discharge for the first year of monitoring.

vii. The total runoff ranged from 0.57 to 8630.5 m^3. 4 events (18.2%) exceeded 1000 m^3 and one event exceeded 2500 m^3.

Tab. 2 : Main characteristics of the 22 flood events recorded in the Pommeroye catchment between 04/2016 and 04/2017.

Date	R_{time} (min)	Ra (mm)	Ri_{max} (mm h^{-1})	Ra_{48} (mm)	Q_{mean} (m^3 h^{-1})	Q_{max} (m^3 h^{-1})	SSC_{mean} (g L^{-1})	SSC_{max} (g L^{-1})	SY (kg)	R_{tot} (m^3)
12-Apr-16	192	8.1	9	5.8	15	42	1.2	4.1	71.2	31.4
15-Apr-16	366	13.8	12	0.6	5.9	10.8	0.4	2.1	5.8	8.2
11-May-16	288	32.6	76	7.2	22.2	150.8	1.6	5	652.7	186.5
22-May-16	204	9.8	6	2.8	0.25	0.6	0.06	0.15	0.07	0.8
31-May-16	1110	30.6	14	0.2	22.6	147	0.7	3	235.8	106.2
3-Jun-16	126	6	12	1.4	1.91	6.24	0.13	0.8	1.4	4.6
20-Jun-16	372	8.7	3	3.4	3.7	9.14	0.1	0.27	4.3	23.3
23-Jun-16	245	12.9	21	5.3	13.6	60.7	0.5	2.69	80.2	69.3
2-Aug-16	1968	68.6	10	18.4	12.4	108.6	0.32	4.58	590.9	407.5
9-Sep-16	324	27	24	0.2	4.5	6.2	0.5	2.7	6.8	12.2
20-Oct-16	390	16.6	4	11.4	3.08	12.9	1.06	4.03	30.4	20.3
7-Nov-16	1434	17.5	8	0.9	0.11	0.99	0.5	3.02	0.6	0.57
16-Nov-16	540	9.7	3	1.2	0.34	2.54	0.38	1.63	1.86	3.7
17-Nov-16	7200	103.8	18	10.9	75.2	378.3	0.41	4.02	7131.9	8630.5
12-Jan-17	528	22	12	2	55.18	190.9	1.35	4.9	1597.6	772.6
4-Feb-17	432	6.8	6	11.8	1.96	13.7	0.12	0.89	8.99	16.2
5-Feb-17	702	25.2	6	11.8	94.5	235.8	0.74	3.7	2119.7	1767.4
7-Feb-17	804	10.6	8	25.4	34.4	209.8	0.37	3.4	627.3	561.3
27-Feb-17	852	15.6	8	1	3.9	37.5	0.42	3.7	87.9	57.9
28-Feb-17	1002	21.6	8	17	68.4	221.8	0.35	1.59	991.3	1957.1
5-Mar-17	1050	16.8	10	11.4	36.1	227.9	0.35	3.82	1059.5	1274.6
8-Mar-17	894	14.6	4	0.6	50.8	189.5	0.19	1.27	595.1	2031.8
Mean	955.6	22.7	12.8	6.9	23.9	102.9	0.54	2.8	722.8	815.6
Std dev.	1467.2	22.6	15.2	7	28	108.4	0.42	1.5	1544.9	1873.3

4.1.2 Second year of monitoring

Between April 2017 and April 2018, 26 runoff events were recorded: 12 occurred in autumn and 14 in winter. The main characteristics of these events are summarized in Table 3 and are described in detail in the following text:

i. The duration of runoff events ranged from 72 to 4098 min in total with a median value of 522 min. 8 events (30%) showed a duration longer than 1000 min, and 7 events (27%) correspond to shorter flooding (less than 360 min).

ii. The rainfall amount ranged from 2 to 55.2 mm with a median value of 12.2 mm. 8 events (30%) were over 20 mm, and 11 events (42%) were lower than 10 mm.

iii. The maximum 6-min rainfall intensity ranged from 1 to 32 mm h^{-1} and 5 events exceeded 20 mm h^{-1}. 48 h-antecedent rainfalls ranged from 0 to 31.8 mm and 12 events (46%) showed 48 h-antecedent rainfalls higher than 10 mm.

iv. The peak flow ranged from 60.4 to 348.6 m^3 h^{-1} and the mean flow ranged from 14.7 to 110.1 m^3 h^{-1}. 24 events (92%) showed a value of peak flow exceeding 100 m^3 h^{-1}.

v. The maximum SSC range from 0.5 to 5 g L^{-1} and the mean SSC ranged from 0.08 to 1.31 g L^{-1}. 12 events (46%) showed values of maximum SSC exceeding 3 g L^{-1}.

vi. The sediment yield values ranged from 54.8 to 7577.5 kg. 9 events (34%) exceeded 1500 kg and 3 main events (11%) exceeded 3000 kg.

vii. The total runoff ranged from 141 to 5255.5 m^3. 11 events exceeded 1000 m^3 and 2 main events exceeded 2500 m^3.

Tab. 3 : Main characteristics of the 26 flood events recorded in the Pommeroye catchment between 04/2017 and 04/2018.

Date	R_{time} (min)	Ra (mm)	Ri_{max} (mm h^{-1})	Ra_{48} (mm)	Q_{mean} (m^3 h^{-1})	Q_{max} (m^3 h^{-1})	SSC_{mean} (g L^{-1})	SSC_{max} (g L^{-1})	SY (kg)	R_{tot} (m^3)
20-Oct-17	600	4.8	6	1.3	16.9	74.6	0.11	1.3	54.8	211
22-Oct-17	600	28.9	32	7.8	20	170	0.17	2.2	167.1	210
23-Oct-17	966	7.1	1	28.9	14.7	60.4	0.08	0.5	55.7	461
14-Nov-17	2292	5.6	6	0.5	17.7	144.8	0.12	1.8	200.5	670
18-Nov-17	72	15.2	10	0.8	27.5	183.1	0.24	2.4	137.3	184
20-Nov-17	822	23.2	8	19	33.3	140	0.26	2.3	300.9	786
27-Nov-17	2238	54.8	24	0.2	56.5	308.5	0.59	4.1	3529	2234
29-Nov-17	1158	14.6	10	6.8	36	153	0.3	5.0	354.8	659
7-Dec-17	498	8.8	6	0.6	24.8	177.2	0.22	3.2	120.2	141
10-Dec-17	1338	14.4	10	0	46.6	348.6	0.48	4.0	1799	961
11-Dec-17	1218	20.4	6	14.4	28	285	0.23	4.2	1064.2	1186
13-Dec-17	4098	55.2	8	20.6	64.9	325.9	0.67	4.3	7577.5	5255.5
27-Dec-17	372	5.2	4	6	48.1	117.7	0.45	3.4	311.3	442.5
29-Dec-17	420	15	22	3	91.2	321.5	1.03	4.3	2239.8	1177.1
30-Dec-17	366	6.2	4	15.4	54.5	172	0.52	2.2	677.7	807
31-Dec-17	2694	37.2	30	21.4	80.8	335.7	0.89	3.8	6919.7	4245.1
3-Jan-18	192	10.4	10	17.2	110.1	294.4	1.31	3.1	3084.4	1357.3
4-Jan-18	336	21.2	6	13.6	86.9	239.5	0.99	3.2	2353.1	1286.9
5-Jan-18	360	8	20	31.8	73.1	328.3	0.79	4.3	1886.5	1104.8
6-Jan-18	330	7.4	14	29.8	55.8	235.9	0.56	1.9	796.6	725.9
15-Jan-18	546	14	6	0.2	98.7	229	1.11	3	874.7	622.3
18-Jan-18	408	10	4	3	91.1	178.5	0.99	2.9	645.2	573.6
21-Jan-18	1062	26	6	11.4	71.4	258.7	0.77	3.5	2096.7	1435.7
23-Jan-18	408	2	2	4.8	35.5	156.9	0.31	2.8	161.3	230.7

31-Jan-18	306	5.8	8	7.6	72.3	265.4	0.79	2.3	823.8	571.3
1-Feb-18	174	4.2	6	12.4	45.71	91.4	0.39	1.9	99.1	196.5
Mean	918.2	16.3	10.3	10.7	53.9	215.3	0.55	2.99	1474.2	1066.7
Std dev.	944.6	14.2	8.3	9.8	28.1	86.9	0.35	1.08	1970.2	1198.4

4.2 Relationships between variables

To identify the factors that may explain the measured hydro-sedimentological response at the outlet of the catchment, a Pearson correlation matrix was generated from all collected parameters. The results show significant correlations between the rainfall variables and the hydro-sedimentary response of the catchment area (Fig.18). The highest relationship was found between the sediment yield (SY) and the total runoff (R_{tot}) (r = 0.91). Strong correlations were observed between the duration time of the event (R_{time}), rainfall amount (Ra) and sediment yield (r = 0.76; r = 0.68). Reasonable correlations exist between the discharge variables (Q_{mean}, Q_{max}), sediment yield (SY) and total runoff (R_{tot}) (r = 0.72; r = 0.65; r = 0.59; r = 0.5 respectively).

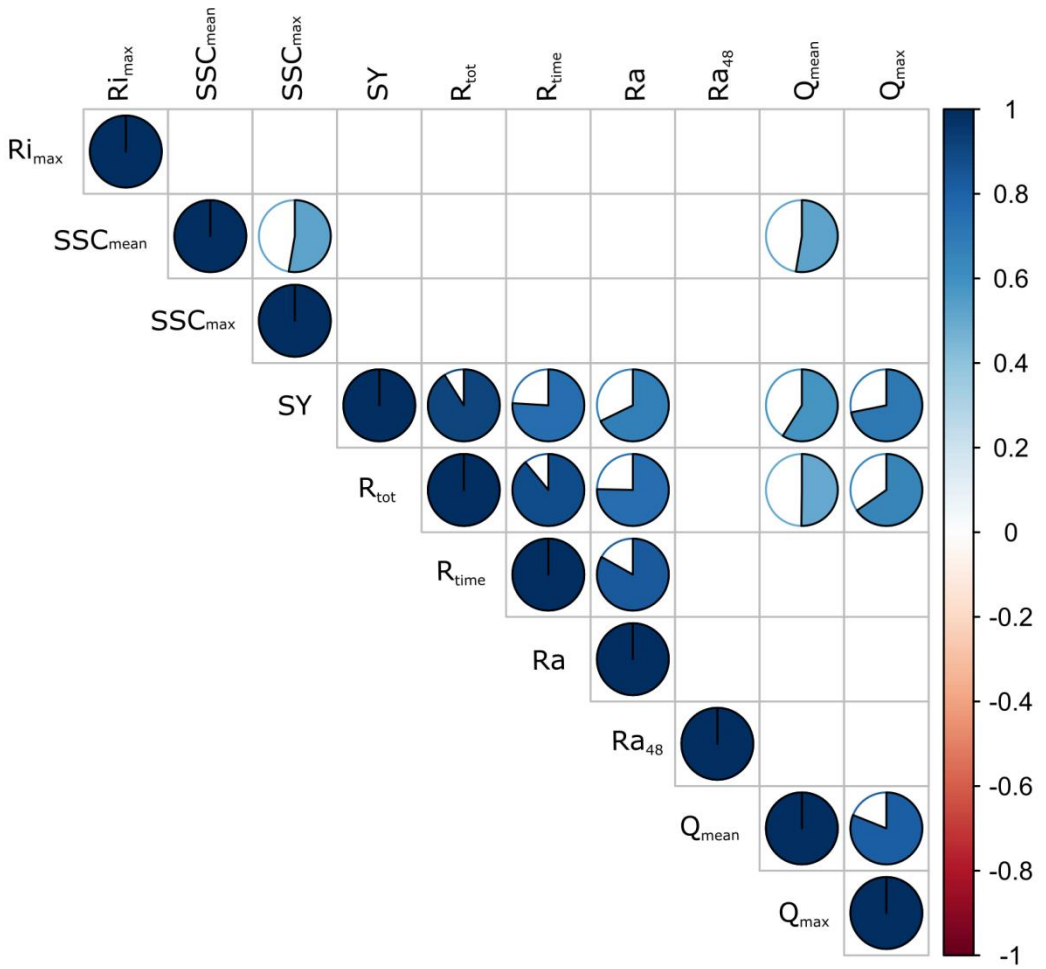

Fig. 18 : Pearson correlation matrix between all variables (n=48 events). Coefficient r is considered significant at p = 0.01.

The relationship between sediment yield and rainfall amount is statistically significant (r = 0.68), although it shows a wide scatter in the data (Fig.19). The maximum sediment yield at the outlet is observed when the rainfall amount exceeds 36 mm, except for one event occurring in summer 2016. Below the threshold of 36 mm, rainfall amount results in a more variable sediment yield at the outlet. For example, a rainfall amount of 15 mm results in a sediment yield varying between 50 and 2300 kg.

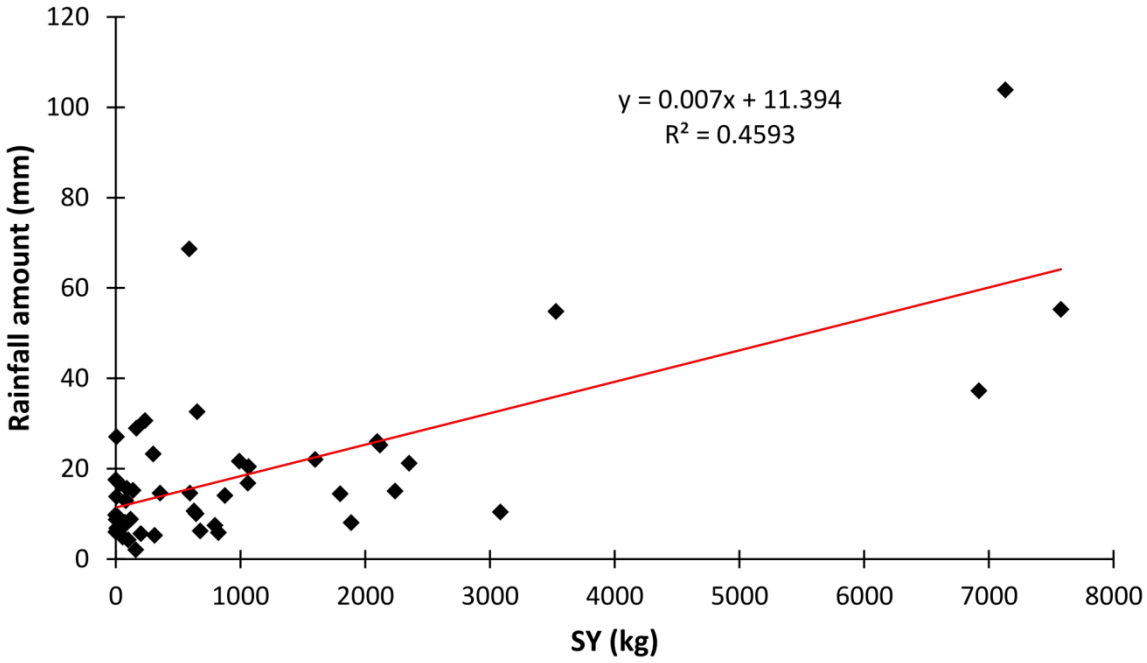

Fig. 19 : Relationship between rainfall amount (mm) and sediment yield (kg) after 2 years of monitoring in the Pommeroye catchment.

The relationship between the peak flow and the maximum suspended sediment concentration was not statistically significant. For a 4 g l^{-1} suspended sediment concentration the resulting peak flow varied between 10 and 380 m^3 h^{-1} suggesting that the relationships between these two variables is more complex (Fig.20). The 48h-antecedent rainfall does not show significant statistical relationships with the hydro-sedimentary response.

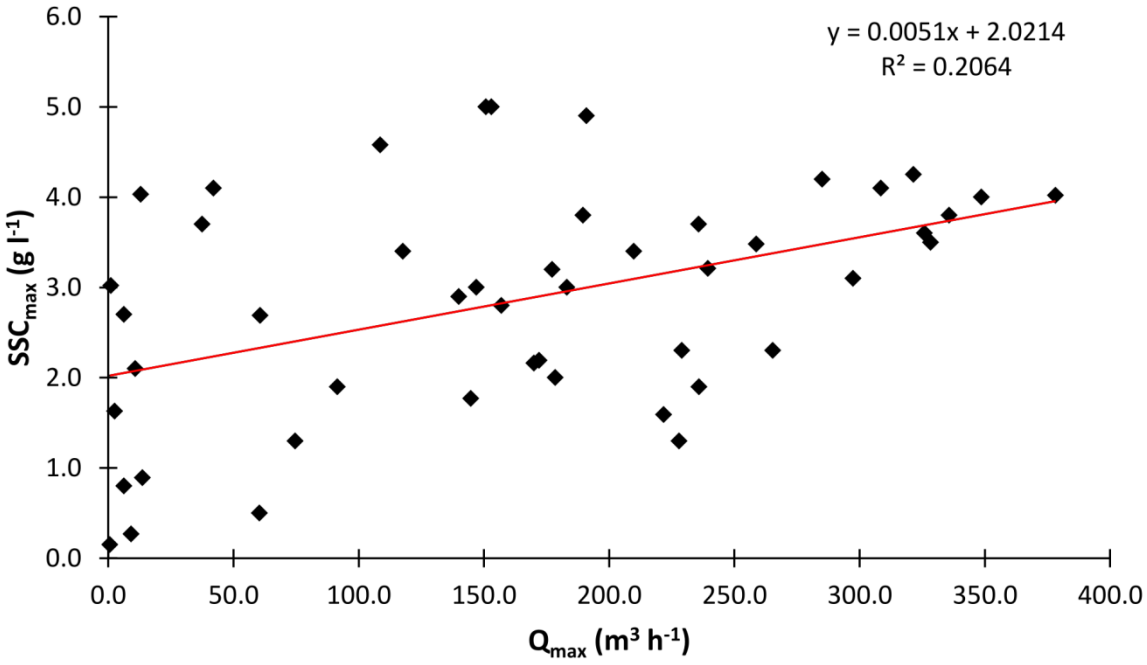

Fig. 20 : Relationship between the maximum suspended sediment concentration (g l^{-1}) and the maximum flow (m^3 h^{-1}) after 2 years of monitoring in the Pommeroye catchment.

4.3 Sediment production variability

4.3.1 First year of monitoring

From 04/2016 to 04/2017, the total SY recorded at the monitoring station reached 15901 kg (Fig.21 and Fig.22). The cumulated rainfall reached 827.1 mm, which is relatively low for the area (mean annual cumulative rainfall = 1000 ± 150 mm yr^{-1}). Normalized to the catchment area (0.54 km^2), the specific sediment yield (SSY) reached 29.4 t km^{-2} yr^{-1}. The sediment yield shows a high heterogeneity between the different seasons. The seasonal SY, compared to annual SY in % is: (i) 971 kg in spring (6.1%), (ii) 678 kg in summer (4.3%), (iii) 7165 kg in autumn (45%), and (iv) 7087 kg in winter (44.6%).

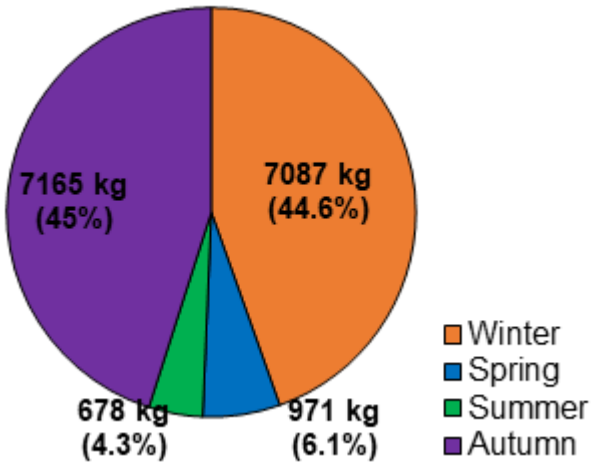

Fig. 21 : Seasonal distribution of the sediment export (%) at the outlet of the Pommeroye catchment for the first year of monitoring (04/2016 – 04/2017).

In spring 2016, 7 events contributed to the SY. Over this period, the total rainfall was 191 mm. The event of May 11, 2016 had the highest impact with a SY of 658 kg following a cumulative rainfall of 32.6 mm. This event contributed to 68% of the seasonal SY for spring. This may be explained by the fact that high rainfall intensities were measured, reaching up to 76 mm h^{-1}. For this event, maximum SSC was observed with a value of 5 g l^{-1}.

In summer 2016, 3 events were recorded. Over this period, the total rainfall was 201.2 mm. On August 02, 2016 a SY of 591 kg and high cumulative rainfall (68.6 mm) was observed. This event contributed to 87% of the seasonal SY for summer. Unlike during the spring season, rainfall intensities observed in summer were much lower. They reached 21 mm h^{-1} for the event on August 02, 2016. This explains why the observed SY is different between these two seasons.

In autumn 2016, 4 events were recorded including a peak event. Over this period, the total rainfall was 195.9 mm. The event of November 17, 2016 was due to a cumulative rainfall of 103.8 mm over 5 days. The SY for this event reached 7132 kg, equivalent to 45% of the total SY for the entire year. The maximum rainfall intensity was relatively high (18 mm h^{-1}) but lower than in the previous seasons.

Winter 2016/2017 was the season with the highest frequency of rainfall events. A total of 8 events were reported. Over this period, the total rainfall was 239 mm. The events of January 15, 2017 and February 02, 2017 contributed to 3717 kg (52.5%) of the total SY for winter season. These two events are the result of cumulative rainfalls of 22 and 25.2 mm, respectively. Four other events contributed to 3273 kg (46%) of the total SY in winter season. These events correspond to cumulative rainfall that ranged from 10.6 to 21.6 mm. During this period, lower heterogeneity between the events was observed, due to an almost equivalent cumulative rainfall for the different events and rainfall intensities which are generally low (between 4 to 12 mm h^{-1}).

Over the entire first year of monitoring, it is noteworthy that during spring period, the highest sediment concentration was observed at the outlet. The autumn and winter seasons contributed equally to the total SY measured but strong heterogeneities between rainfall events was observed.

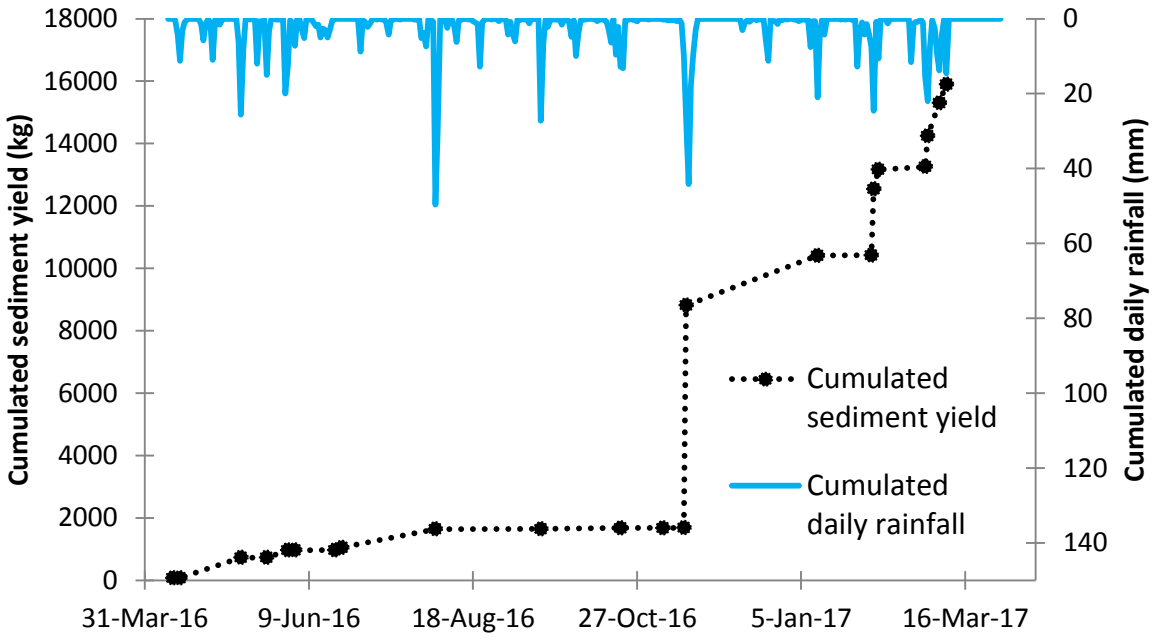

Fig. 22 : Cumulated sediment yield (kg) and cumulative daily rainfall (mm) recorded at the outlet of the Pommeroye catchment during the first year of monitoring.

4.3.2 Second year of monitoring

From 04/2017 to 04/2018, the total SY recorded at the monitoring station reached 38330 kg (Fig.23 and Fig.24). The cumulated rainfall reached 965.8 mm which is higher than previous year. Normalized by the catchment area (0.54 km²), the SSY reached 70 t km^{-2} yr^{-1}. The seasonal SY, compared to annual SY in % is: (i) 15361 kg in autumn (40%) and (ii) 22969 kg in winter (60%). The two other seasons are not represented here as no events were recorded at the monitoring station.

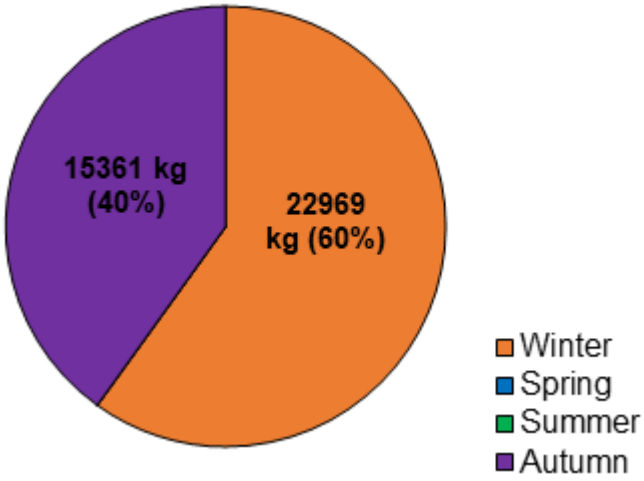

Fig. 23 : Seasonal distribution of the sediment export (%) at the outlet of the Pommeroye catchment for the second year of monitoring (04/2017 – 04/2018).

In autumn 2017, 12 events were recorded for a total rainfall of 367.5 mm. 171.6 mm more than previous year for the same season. Two events contributed to 72% of the seasonal SY for autumn. For the event of November 27, 2017, the measured SY can be explained by a high rainfall amount (54.8 mm) and the highest maximum rainfall intensity recorded for this season (24 mm h^{-1}). For the event of December 13, 2017, the rainfall amount was similar (55.2 mm) but the maximum rainfall intensity was lowest (8 mm h^{-1}). The observed SY can be explained by a long duration of the rainfall event (3 days) and a high amount of 48h-antecedent rainfall (20.6 mm).

In winter 2017/2018, 14 events were recorded for a total rainfall of 323.2 mm. 84.2 mm more than in the previous year for the same season. 74% of the seasonal SY was produced between December 29, 2017 and January 5, 2018. The main event of December 31, 2017 which contributed to

30% showed the longest duration of rainfall event (2694 min). The rainfall amount was 37.2 mm with a high maximum rainfall intensity (30 mm h^{-1}) and a high amount of 48h-antecedent rainfall (21.4 mm). The events following this main event were relatively short with a duration of the rainfall event comprised between 192 and 420 min. The rainfall amount was variable and comprised values between 5.2 and 21.2 mm, just as the maximum rainfall intensity which varied between 4 and 22 mm h^{-1}. 5 events were characterized by a high amount of 48h-antecedent rainfall varying between 13.6 and 29.8 mm. After January 15, 2018, six more events were recorded. They contributed to 20% to the seasonal SY with a rainfall amount ranges from 2 to 26 mm and durations between 174 and 1062 min. Rainfall intensity were relatively low from 2 to 8 mm h^{-1} and 48h-antecedent rainfall ranged from 0.2 to 12.4 mm.

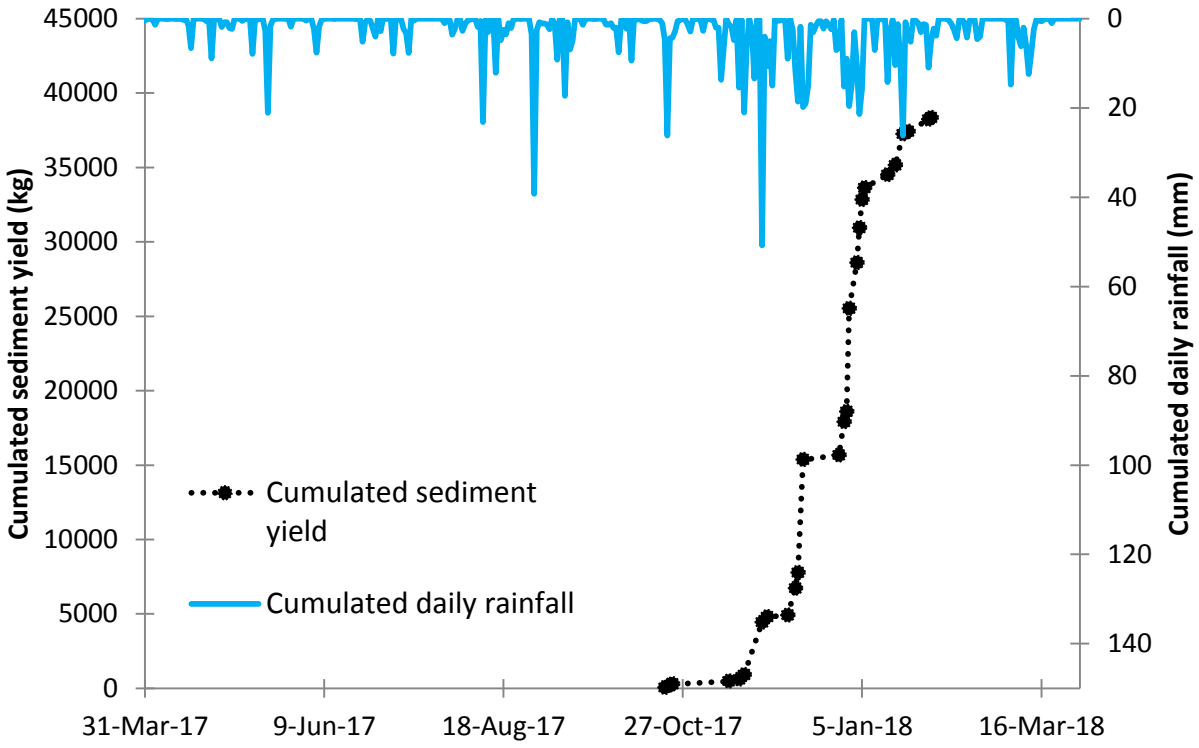

Fig. 24 : Cumulated sediment yield (kg) and cumulative daily rainfall (mm) recorded at the outlet of the Pommeroye catchment during the second year of monitoring.

4.4 Seasonal variability

The eigen-values (Table 4) provide the percentage of the explained variance and the cumulative variance of the principal dimensions. The first three dimensions explain 78.3% of the total

variance: dimension 1 counts for 46.5%, dimension 2 for 17.8% and dimension 3 for 14%. The square cosines of variables indicate the best-described variables on each principal dimension. Dimension 1 is correlated to R_{time} (0.59), Ra (0.59), Q_{mean} (0.43), Q_{max} (0.67), SSC_{max} (0.30), SY (0.86), and R_{tot} (0.82). Dimension 2 is correlated to SSC_{mean} (0.65). Dimension 3 is correlated to Ri_{max} (0.36) and Ra_{48} (0.28). The bi-plot graph allows visualizing the information on both, individual samples and variables (Fig. 25 and Fig.26).

Tab. 4 : Eigen-values, percentages of variance explained, and cumulative variance of principal dimensions for the principal component analysis.

	Eigen-value	Percentage of explained variance (%)	Cumulative percentage of explained variance (%)
Dim 1	4.79	46.5	46.5
Dim 2	1.86	17.8	64.3
Dim 3	1.4	14	78.3
Dim 4	0.83	8.3	86.6
Dim 5	0.55	5.5	92.3
Dim 6	0.39	3.9	96.2
Dim 7	0.18	1.8	98
Dim 8	0.08	0.9	98.9
Dim 9	0.07	0.8	99.7
Dim 10	0.02	0.3	100

In the first space Dim1-Dim2, we observe a classification between the different events (Fig.25). On $Dim1^{+}/Dim2^{+}$, 10 events occurring in winter are represented. They are characterized by high values of the following parameters: Q_{max}, Q_{mean}, SSC_{max}, SSC_{mean}, Ri_{max}. In this space, another event occurring in spring seems to have a high influence on the projection of the PCA due to a high value of the SSC mean. On $Dim1^{+}/Dim2^{-}$, erosive events occurring in autumn are mostly represented. These events are characterized by the highest values of sediment yield and highest values of rainfall characteristics (Ra, R_{tot}, R_{time}). In the two other spaces ($Dim1^{-}/Dim2^{+}$; $Dim1^{-}/Dim2^{-}$), the events occurred mainly in spring, summer and autumn. As there is no discriminating parameter on this side, these events are characterized by the lowest values of the different parameters previously cited.

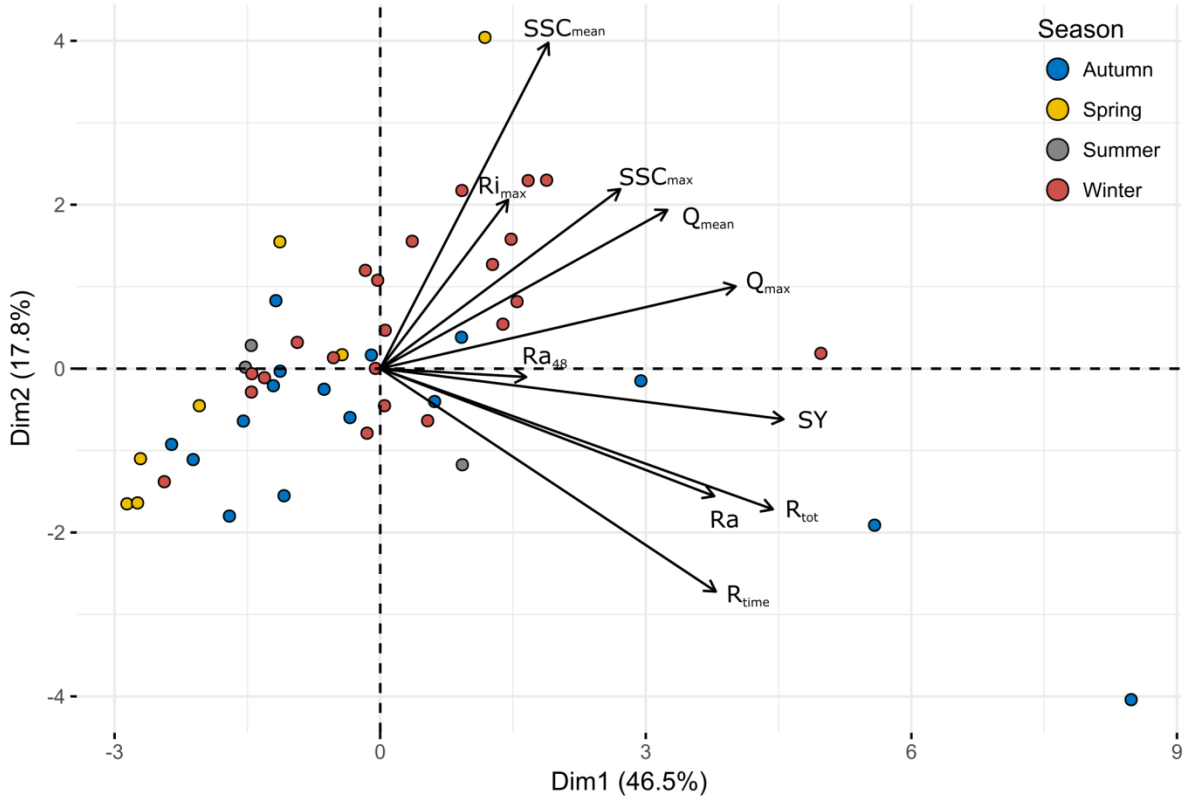

Fig. 25 : Bi-plot of PCA results on dimensions 1-2 for the 48 events and their hydro-sedimentary parameters: (i) duration of the rainfall event (R_{time}, min), (ii) rainfall amount (Ra, mm), (iii) max 6-min rainfall intensity (Ri_{max}, mm h^{-1}), (iv) 48h-antecedent rainfall (Ra_{48}, mm), (v) mean flow and peak flow (Q_{mean}, Q_{max}, m^3 h^{-1}), (vi) mean and maximum SSC concentration (SSC_{mean}, SSC_{max}, g l^{-1}), (viii) sediment yield (SY, kg), and (ix) total runoff (R_{tot}, m^3).

In the second space Dim1/Dim3, the classification of the events shows some similarities with the previous space (Fig.26). A major part of the winter events is represented in the $Dim1^+/Dim3^-$ space and characterized by high values of Q_{mean}, Q_{max}, SY, R_{tot}. A new discriminating parameter appears: Ra_{48}. The minor part of the winter events is represented in the space $Dim1^-/Dim3^-$ and seems to have no discriminating parameters. They can be characterized by the lowest values of the different hydro-sedimentary parameters. In $Dim1^+/Dim3^+$, few events of the season autumn, spring, and summer are represented. They are characterized by the highest values of Ri_{max}, Ra, SSC_{max}, R_{time}. However, most of the events occurring in these three seasons are represented in the space $Dim1^-/Dim3^+$ and are largely influenced by their respective maximum rainfall intensity. The values are low for the other parameters.

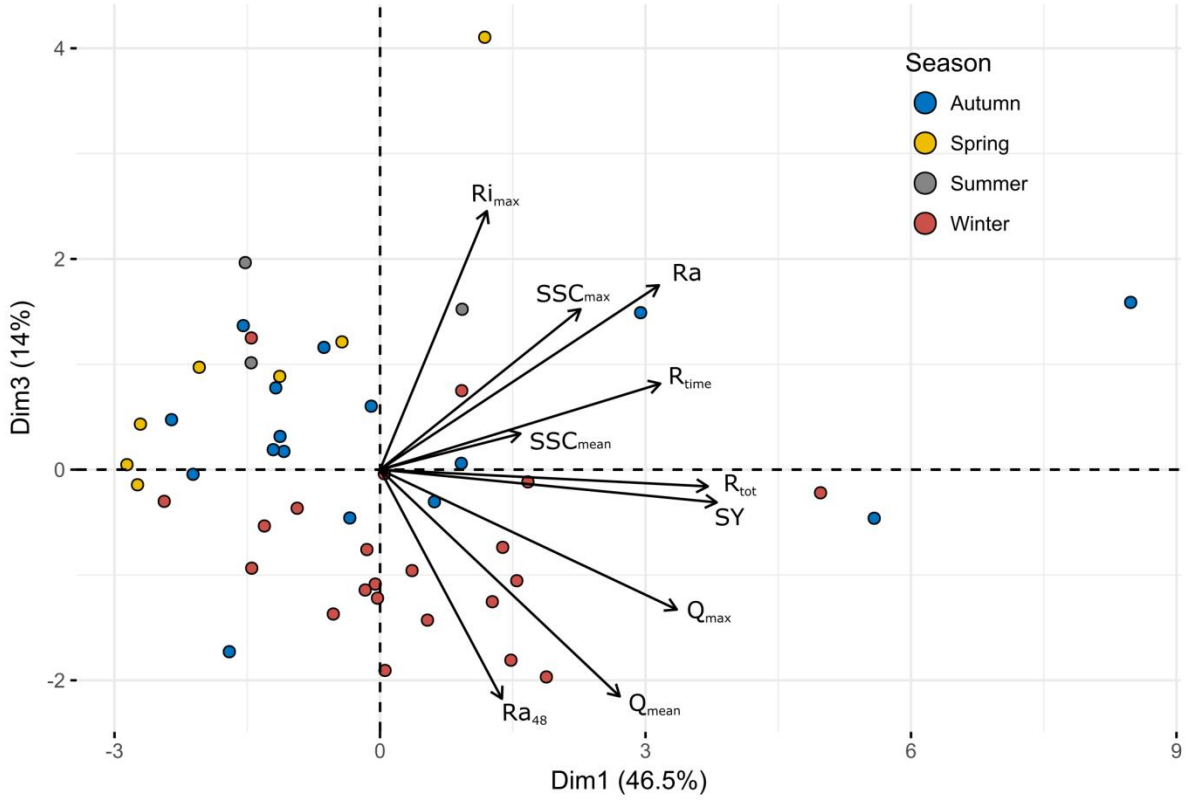

Fig. 26 : Bi-plot of PCA results on dimensions 1-3 for the 48 events and their hydro-sedimentary parameters: (i) duration of the rainfall event (R_{time}, min), (ii) rainfall amount (Ra, mm), (iii) max 6-min rainfall intensity (Ri_{max}, mm h^{-1}), (iv) 48h-antecedent rainfall (Ra_{48}, mm), (v) mean flow and peak flow (Q_{mean}, Q_{max}, m^3 h^{-1}), (vi) mean and maximum SSC concentration (SSC_{mean}, SSC_{max}, g l^{-1}), (viii) sediment yield (SY, kg), and (ix) total runoff (R_{tot}, m^3).

5. Discussion

A high intra-annual variability of the hydro-sedimentary response is observed at the outlet of the Pommeroye catchment. The experimental station measured a specific sediment yield between 29.4 and 70 t km^{-2} yr^{-1} over two years of monitoring while the intra-annual variability of cumulative rainfall is low with a difference of 138.7 mm. The high variability of the hydro-sedimentary response is explained by the 48 erosive events recorded which show a strong heterogeneity. Sediment flux for a single event range from 0.6 to 7131.8 kg with an average of 722.8 kg. The total runoff between discrete events also shows strong variations ranging from 0.57 to 8630.5 m^3. This variability of the hydro-sedimentary response can mainly be explained by different types of rainfall events. Cumulative rainfall for a single event shows a high variability (i.e. from 2 to 103.8 mm) as well as the recorded maximum rainfall intensities (i.e. from 2 to 76 mm h^{-1}).

The amount of exported sediment is consistent with values observed in similar studies areas. The specific sediment yield is higher than those observed (Lefrançois, 2007) in the French catchment of the Moulinet and Violettes (i.e. 25.4 and 36 t km^{-2} yr^{-1}; catchment area = 4.53 and 2.24 km^2 respectively) and those observed by Laignel et al. (2006) and Landemaine (2016) in larger catchments (Austreberthe: 16 t km^{-2} yr^{-1} and Andelle: 21 t km^{-2} yr^{-1}). On the other hand, it is lower than those measured by Walling et al. (2002) in UK catchments (Belmont, Jubilee, and Lower Smisby; catchment area =1.5, 0.3 and 2.6 km^2 respectively) with a specific sediment yield between 70.6 and 181.1 t km^{-2} yr^{-1}.

A strong variability is observed between the two years of measurements at the Pommeroye catchment with a difference of 40.6 t km^{-2} yr^{-1}. Similar observations were made by Walling et al. (2002) for the catchment of Jubilee and New Cliftonthorpe in UK where the specific sediment yield varied from 181.1 to 81.1 t km^{-2} yr^{-1} over two years of monitoring for the Jubilee, and from 0.6 to 122.4 t km^{-2} yr^{-1} for the NC. Similar approaches in Belgium have also shown that hydro-sedimentary responses were highly variable between two distinct hydrologic years (Poesen et al., 1996; Vandaele & Poesen, 1995). Walling et al. (2002) also points out that this variability is not only due to the variability of rainfall amount but also to the temporal variability of the rainfall during the year. This is particularly true in the Pommeroye catchment where rainy events were spread out in time during the first year whereas they mainly grouped over a shorter period during the second year. This succession of rainy events during a short time interval may cause a saturation of the infiltration capacity of the soil and the creation of a slaking crust in loess environments (Le Bissonnais et al., 2002).

Because of the heterogeneity of the rainfall events, only 6% of the erosive events exported 21 tons of sediment, i.e. 40% of the sediment flux transported over the two years. Some authors also observed that a few numbers of erosive episodes were responsible for a large part of the exported sediment. Indeed, Nu-Fang et al. (2011) showed that 90% of the hydro-sedimentary flux could be

produced by only 9 erosive events for a hydrological year in the Wangjiaqiao catchment near the Three Gorges dam in China. Estrany et al. (2009) also observed for the Mediterranean catchment that 90% of the hydro-sedimentary flux was transported during only 0.13% of the time. Similar observations were made by Lana-Renault & Regüés, (2009) in Spain where 75% of the hydro-sedimentary flux were produced by only 15% of the erosive events. These results clearly underline the variability of the hydro-sedimentary production in small agricultural catchments for which most of the hydro-sedimentary fluxes are produced by a small number of events. Strong seasonal variability was identified over the two years of monitoring at the Pommeroye catchment. Most of the hydro-sedimentary transfers were produced in winter (55%) and autumn (42%). Only 3% of the flux is produced during the spring and summer periods whereas the rainfall intensities are the most important. This can be mainly explained by the state of the soil surface, more particularly by a better crop cover on the agricultural plots which plays an important role of protection against the rainfall impact.

Statistical analyses showed very robust correlations between the hydro-sedimentary response, the rainfall amount, and the duration of the rainy episode. The correlation between the amount of rainfall and the sediment yield shows a threshold at 36 mm for which the erosive events are the most important. Below this threshold, a dispersion of the data cloud is observed, which seems to indicate that other forcing parameters must be considered, such as the surface state of the soils. As emphasized by Evrard et al. (2010), the state of the soil surface result from rainfall conditions and the growing system in place. In addition, agricultural operations modify the state of the soil surface and are practiced at different times of the year. Depending on the temporal variability of soil surface conditions in the catchment, it can be assumed that the erosion processes will show significant spatial and temporal variability throughout the year (Cerdan et al., 2002). To better assess the impact of this parameter on the hydro-sedimentary response, it would be recommended to monitor the soil surface conditions over time with an adapted spatio-temporal resolution.

Surprisingly, the amount of 48h-antecedent rainfall is not correlated with the hydro-sedimentary response. Thus, the parameter cannot be considered as an explanatory factor even though this parameter is commonly used in runoff erosion models developed for catchments located on the European loess belt: i.e. *STREAM* and *WATERSED* models (Cerdan et al., 2002; Landemaine, 2016; Souchère et al., 2003). In addition, maximum rainfall intensities are not correlated with the hydro-sedimentary response. These results are contradictory with those published by Nu-Fang et al. (2011) and suggest that the modification of farming practices and the farmer's efforts to get an important crop cover over the plots throughout the year allows a reduction in the impact of the rain splash effect.

The correlation between the maximum sediment concentration and the peak flow was found as not statistically significant, indicating that the relationship is more complex between these two variables. As pointed out by Williams, (1989), hysteresis effects can be observed during erosive episodes and multiple sediment sources can be mobilized. Sources that cause sediment remobilization may include diffuse erosion on plots or concentrated erosion through ephemeral gullies. In the Pommeroye catchment, the hydro-sedimentary response is complex, and it is difficult to identify the exact sediment sources responsible of the sediment transfer via the flood hydrographs. An alternative approach could be to quantify the contribution of these different sources via the use of a GIS model. These approaches have been successfully used by Cerdan et al. (2002) and Stolte et al. (2003). For example, the *STREAM* model (Cerdan et al., 2001; Souchère et al., 2003) and more recently the *WATERSED* model (Landemaine, 2016) allow the prediction of diffuse and concentrated erosion in catchments. These models considered the catchment morphology, the rainfall characteristics, and the soil surface conditions to quantify the hydro-sedimentary response for a specific rainy event and to evaluate the spatial variability of sediment remobilization. We consider this future particularly suitable for the Pommeroye catchment, intending to allow the identification of the spatial variability of the sediment sources during an erosive episode and to quantify their respective contributions.

6. Conclusion

This study reports on a detailed record of the hydro-sedimentary response to rainfall events in the small agricultural catchment of the Pommeroye in Northern France. The research was based on a high-frequency monitoring of rainfall, runoff, and suspended sediment transport over a period of two hydrological years (04/2016 – 04/2018). A high inter-annual variability of the sediment yield has been observed. Over two years, the specific sediment yield ranges from 29.4 to 70 t km^{-2} yr^{-1} suggesting a large heterogeneity of the erosive events. Most of the sediment was transported in winter (55%) and autumn (42%) whereas it was less significant in summer and spring (3%). At the event scale, the results showed high variability in their hydro-sedimentary response. A small number of events (6%) were responsible for a large proportion of the sediment yield (40%). The multivariate statistical analyses showed that the rainfall amount and the duration of an event are the most relevant factors controlling the hydro-sedimentary response, while maximum rainfall intensities and 48h-antecedent rainfall are statistically non-significant. These results confirm the high variability of the hydro-sedimentary response to rainfall events and the complexity of the erosion processes in the European loess belt area.

Acknowledgements

This work was financially supported by the Mines-Telecom Institute of Lille-Douai, with additional funding provided by the Artois-Picardie Water Agency (QUASPER project). We would also like to acknowledge technical support from the SYMCEA and the regional Chamber of Agriculture Nord-Pas-de-Calais, France. The authors are grateful to M.Desmons, the landowner who permitted instrumentation of the catchment.

References

Alexandre, H. (2015). *Quantification de l'efficacité des fascines : diagnostic initial du bassin versant de la Pommeroy et paramétrage d'un modèle de ruissellement/érosion*.

Beckelynck, J. (1981). *Traitement régionalisé des paramètres contribuant à la gestion des nappes: application à la modélisation de la nappe de la craie dans le bassin de l'Aa et de la moyenne Lys*. Université des Sciences et Techniques de Lille. Retrieved from https://ori-nuxeo.univ-

lille1.fr/nuxeo/site/esupversions/1ea8eb07-e140-446e-be38-7383cefdb7fc

Capra, A. (1993). Ephemeral gully and gully erosion in cultivated land: a review. *Drainage Basins and Catchment Management*, 109–141.

Castillo, C., & Gomez, J. A. (2016). A century of gully erosion research: Urgency, complexity and study approaches. *Earth-Science Reviews*, *160*, 300–319. https://doi.org/10.1016/j.earscirev.2016.07.009

Cerdan, O., Le Bissonais, Y., Souchère, V., Martin, P., & Lecomte, V. (2002). Sediment concentration in interill flow: interactions between soil surface conditions, vegetation and rainfall. *Earth Surface Processes*, *205*(27), 193–205. https://doi.org/10.1002/esp.314

Cerdan, O., Souchère, V., Lecomte, V., Couturier, A., & Le Bissonnais, Y. (2001). Incorporating soil surface crusting processes in an expert-based runoff model: Sealing and transfer by runoff and erosion related to agricultural management. *Catena*, *46*(2–3), 189–205. https://doi.org/10.1016/S0341-8162(01)00166-7

Cerdan, O., Souchère, V., Lecomte, V., Couturier, A., & Le Bissonnais, Y. (2002). Incorporating soil surface crusting processes in an expert-based runoff model: Sealing and transfer by runoff and erosion related to agricultural management. *Catena*, *46*(2–3), 189–205. https://doi.org/10.1016/S0341-8162(01)00166-7

Delmas, M., Pak, L. T., Cerdan, O., Souchère, V., Le Bissonnais, Y., Couturier, A., & Sorel, L. (2012). Erosion and sediment budget across scale: A case study in a catchment of the European loess belt. *Journal of Hydrology*, *420–421*, 255–263. https://doi.org/10.1016/j.jhydrol.2011.12.008

Estrany, J., Garcia, C., & Batalla, R. J. (2009). Suspended sediment transport in a small Mediterranean agricultural catchment. *Earth Surface Processes and Landforms*, *34*(March), 155–161. https://doi.org/10.1002/esp

Evrard, O., Bielders, C. L., Vandaele, K., & van Wesemael, B. (2007). Spatial and temporal variation of muddy floods in central Belgium, off-site impacts and potential control measures. *Catena*, *70*(3), 443–454. https://doi.org/10.1016/j.catena.2006.11.011

Evrard, O., Nord, G., Cerdan, O., Souchère, V., Le Bissonnais, Y., & Bonté, P. (2010). Modelling the impact of land use change and rainfall seasonality on sediment export from an agricultural catchment of the northwestern European loess belt. *Agriculture, Ecosystems and Environment*, *138*(1–2), 83–94. https://doi.org/10.1016/j.agee.2010.04.003

Foster, G. R. (1986). Understanding ephemeral gully erosion. In *Soil Conservation vol 2* (Vol. 2, pp. 90–125).

Frankl, A., Nyssen, J., De Dapper, M., Haile, M., Billi, P., Munro, R. N., … Poesen, J. (2011). Linking long-term gully and river channel dynamics to environmental change using repeat photography (Northern Ethiopia). *Geomorphology*, *129*(3–4), 238–251. https://doi.org/10.1016/j.geomorph.2011.02.018

Giménez, R., Casalí, J., Grande, I., Díez, J., Campo, M. a., Álvarez-Mozos, J., & Goñi, M. (2012). Factors controlling sediment export in a small agricultural watershed in Navarre (Spain). *Agricultural Water Management*, *110*, 1–8. https://doi.org/10.1016/j.agwat.2012.03.007

Goodwin, N. R., Armston, J. D., Muir, J., & Stiller, I. (2017). Monitoring gully change: A comparison of airborne and terrestrial laser scanning using a case study from Aratula, Queensland. *Geomorphology*, *282*, 195–208. https://doi.org/10.1016/j.geomorph.2017.01.001

Laignel, B., Dupuis, E., Durand, A., Dupont, J. P., Hauchard, E., & Massei, N. (2006). Erosion balance in the watersheds of the western Paris Basin by high-frequency monitoring of discharge and suspended sediment in surface water. *Comptes Rendus - Geoscience*, *338*(8), 556–564. https://doi.org/10.1016/j.crte.2006.03.010

Lana-Renault, N., & Regüés, D. (2009). Seasonal patterns of suspended sediment transport in an abandoned farmland catchment in the Central Spanish Pyrenees. *Earth Surface Processes and Landforms*, *34*(June), 155–161. https://doi.org/10.1002/esp

Landemaine, V. (2016). *Érosion des sols et transferts sédimentaires sur les bassins versants de l'Ouest du Bassin de Paris : analyse, quantification et modélisation à l'échelle pluriannuelle*. Université de Rouen Normandie.

Le Bissonnais, Y., Thorette, J., Bardet, C., & Daroussin, J. (2002). *L'Erosion Hydrique Des Sols En France*. Retrieved from http://prodinra.inra.fr/?locale=fr#!ConsultNotice:69099

Lefrançois, J. (2007). Dynamiques et origines des matières en suspension sur de petits bassins versants agricoles sur schiste., 280.

Li, Z., Zhang, Y., Zhu, Q., Yang, S., Li, H., & Ma, H. (2017). A gully erosion assessment model for the Chinese Loess Plateau based on changes in gully length and area. *Catena*, *148*, 195–203. https://doi.org/10.1016/j.catena.2016.04.018

Marzolff, I., Ries, J. B., & Poesen, J. (2011). Short-term versus medium-term monitoring for detecting gully-erosion variability in a Mediterranean environment. *Earth Surface Processes and Landforms*, *36*(12), 1604–1623. https://doi.org/10.1002/esp.2172

Nachtergaele, J., & Poesen, J. (1999). Assessment of soil losses by ephemeral gully erosion using high-altitude (stereo) aerial photographs. *Earth Surface Processes and Landforms*, *24*(8), 693–706. https://doi.org/10.1002/(SICI)1096-9837(199908)24:8<693::AID-ESP992>3.0.CO;2-7

Nachtergaele, J., Poesen, J., & Govers, G. (2002). Ephemeral gullies a spatial and temporal analysis of their characteristics, importance and prediction. *Eeen Ruimtelijke En Temporele Analyse van de Karakteristieken, Het Belang En de Voorspelling van Tijdelijke Ravijnen*, (2), 159–182. https://doi.org/10.4000/belgeo.16167

Nadal-Romero, E., Regüés, D., & Latron, J. (2008). Relationships among rainfall, runoff, and suspended sediment in a small catchment with badlands. *Catena*, *74*(2), 127–136. https://doi.org/10.1016/j.catena.2008.03.014

Nu-Fang, F., Zhi-Hua, S., Lu, L., & Cheng, J. (2011). Rainfall, runoff, and suspended sediment delivery relationships in a small agricultural watershed of the Three Gorges area, China. *Geomorphology*, *135*(1–2), 158–166. https://doi.org/10.1016/j.geomorph.2011.08.013

Poesen, J. (1993). Gully typology and gully control measures in the European loess belt. *Farm Land Erosion: In Temperate Plains Environment and Hills*, (June), 221–239. https://doi.org/10.1016/B978-0-444-81466-1.50024-1

Poesen, J. W., Vandaele, K., & Wesemael, B. V. a. N. (1996). Contribution of gully erosion to sediment production on cultivated lands and rangelands. *Erosion and Sediment Yield: Global and Regional Perspectives (Proceedings of the Exeter Symposium July 1996). IAHS Publ.*, *236*(236), 251–266.

Raux, J., Copard, Y., Laignel, B., Fournier, M., & Masseï, N. (2011). Classification of worldwide drainage basins through the multivariate analysis of variables controlling their hydrosedimentary response. *Global and Planetary Change*, *76*(3–4), 117–127.

https://doi.org/10.1016/j.gloplacha.2010.12.005

Souchère, V., Cerdan, O., Ludwig, B., Le Bissonnais, Y., Couturier, A., & Papy, F. (2003). Modelling ephemeral gully erosion in small cultivated catchments. *Catena*, *50*(2–4), 489–505. https://doi.org/10.1016/S0341-8162(02)00124-8

Stolte, J., Liu, B., Ritsema, C. J., Van Den Elsen, H. G. M., & Hessel, R. (2003). Modelling water flow and sediment processes in a small gully system on the Loess Plateau in China. *Catena*, *54*(1–2), 117–130. https://doi.org/10.1016/S0341-8162(03)00060-2

Valcárcel, M., Taboada, M. T., Paz, A., & Dafonte, J. (2003). Ephemeral gully erosion in northwestern Spain. *Catena*, *50*(2–4), 199–216. https://doi.org/10.1016/S0341-8162(02)00139-X

Valentin, C., Poesen, J., & Li, Y. (2005). Gully erosion: Impacts, factors and control. *Catena*, *63*(2–3), 132–153. https://doi.org/10.1016/j.catena.2005.06.001

Vandaele, K., & Poesen, J. (1995). Spatial and temporal patterns of soil erosion rates in an agricultural catchment, central Belgium. *Catena*, *25*(95), 213–226. https://doi.org/10.1016/0341-8162(95)00011-G

Viel, V. (2012). *Analyse spatiale et temporelle des transferts sédimentaires dans les hydrosystèmes normands. Exemple du bassin versant de la Seulles*. *Thèse*.

Walling, D. E., Russell, M. A., Hodgkinson, R. A., & Zhang, Y. (2002). Establishing sediment budgets for two small lowland agricultural catchments in the UK. *Catena*, *47*(4), 323–353. https://doi.org/10.1016/S0341-8162(01)00187-4

Williams, G. P. (1989). Sediment concentration versus water discharge during single hydrologic events in rivers. *Journal of Hydrology*, *111*(1–4), 89–106. https://doi.org/10.1016/0022-1694(89)90254-0

Chapter 3

Simulating erosive event and control measure efficiency in a small agricultural catchment in Northern France (the Pommeroye).

Résumé étendu – Chapitre 3

Contexte

Récemment, les coulées boueuses survenues dans une majeure partie de la France entre Mai et Juin 2018 ont causé 214 000 sinistres dont le coût est estimé à 430 M€. Les gestionnaires de bassins versants font d'importants efforts pour réduire ces coûts en tentant de limiter les transferts hydro-sédimentaires sur les bassins versants. Pour cela, des solutions visant à réduire l'érosion (ex : haies, fascines, etc.) sont implémentées sur les territoires. Cependant, la méconnaissance des voies de transfert sédimentaire peut conduire à des erreurs d'implantation. De plus, l'efficacité réelle de ces ouvrages à l'échelle des bassins versants n'est pas quantifiée. Grâce aux dernières avancées scientifiques, le nouveau modèle d'érosion *WATERSED*, développé par le BRGM, est capable de simuler spatialement les transferts hydro-sédimentaires sur un bassin versant en prenant en compte ces aménagements. L'objectif de cette étude est alors d'évaluer l'opérabilité du modèle dans le contexte d'un petit bassin versant agricole du Nord de la France (La Pommeroye ; 0,54 km²). A travers un module complémentaire, une évaluation de l'efficacité d'un plan d'aménagement de lutte contre l'érosion est également proposée.

Matériel et Méthodes

Pour évaluer la variabilité spatiale des transferts hydro-sédimentaires sur le bassin versant de la Pommeroye et l'efficacité d'un futur plan d'aménagement de lutte contre l'érosion, une approche couplée expérimentation/modélisation est proposée. Dans un premier temps, les transferts hydro-sédimentaires sont quantifiés grâce à l'installation d'une station de mesure haute-fréquence à l'exutoire du bassin (e.g. Patault et al., 2018, *in review – voir chapitre 2*). Dans un deuxième temps, les transferts hydro-sédimentaires sont modélisés (*WATERSED* ; Landemaine, 2016) et confrontés aux résultats expérimentaux (Fig.27). Le modèle *WATERSED* est un modèle non-dynamique distribué prédisant de manière spatialisée les transferts hydro-sédimentaires en tout point d'un bassin versant pour un évènement pluvieux donné.

Pour fonctionner, le modèle nécessite des jeux de données spatialisées relatives aux paramètres forçants de l'érosion :

- La topographie du bassin, dérivée pour notre expérimentation d'un modèle numérique de terrain issu de relevés Lidar (taille du pixel : 50 cm).
- L'état de surface des sols à un instant *t* selon trois paramètres : la rugosité, le couvert végétal et le faciès. Ici, ces paramètres sont obtenus d'après des relevés de terrain bi-mensuels sur les parcelles agricoles qui composent le bassin versant.
- Les caractéristiques d'un évènement pluvieux donné : hauteur de pluie cumulée (mm), durée effective de la pluie (intensités > 2 mm h^{-1}), le cumul de pluie sur les dernières 48h (mm) et enfin l'intensité de pluie maximale à 6 min. Ces paramètres sont obtenus à l'aide d'un pluviomètre à augets basculants installé en tête de bassin versant.

A partir de ces données spatiales, des tables de décision, adaptées au contexte environnemental, sont utilisées pour transformer ces informations en données spatiales utilisables par le modèle. Le modèle nécessite également quatre valeurs de paramètres qui sont calibrées en comparant les flux hydro-sédimentaires observés et ceux prédits par le modèle. Enfin, l'intégration des aménagements d'hydraulique douce se fait à travers un module complémentaire dans lequel différentes caractéristiques des aménagements sont renseignées.

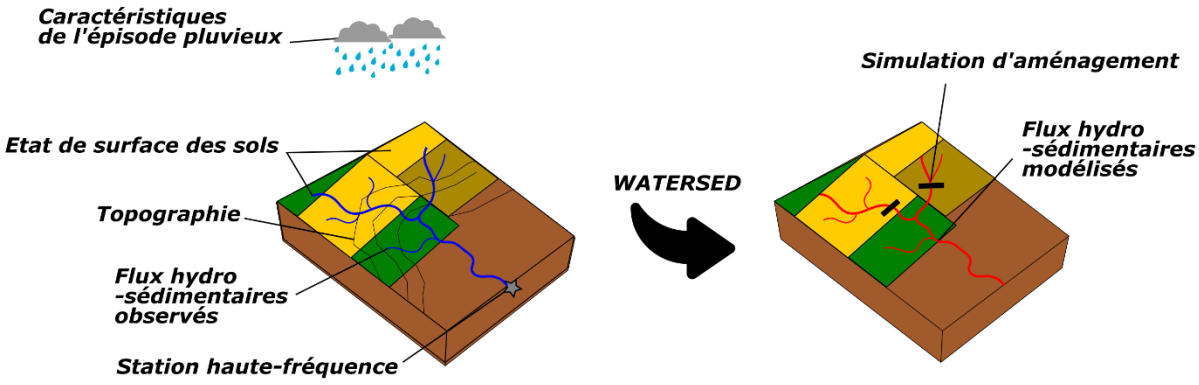

Fig. 27 : Schéma conceptuel reprenant la démarche utilisée pour : (i) comparer les flux hydro-sédimentaires observés/prédits sur le bassin versant de la Pommeroye et (ii) évaluer l'efficacité des aménagements d'hydraulique douce.

Principaux résultats

Trois épisodes érosifs avec une réponse hydrologique simple et dont l'état de surface de sols correspondant était disponible ont été sélectionnés pour calibrer le modèle. Les résultats de modélisation sont concordants avec les flux observés à la station de mesure haute-fréquence à l'exutoire du bassin versant de la Pommeroye (Fig.28). La qualité de prédiction des flux sédimentaires est considérée très bonne, avec un critère de qualité (NSE) égal à 0.92. Les flux hydriques sont globalement cohérents mais légèrement sur estimés sur un épisode pluvieux (NSE = 0.53). La variabilité spatiale des transferts hydro-sédimentaires indique que la majorité des processus d'arrachement des particules ont lieu dans les parties Nord-Ouest et Nord-Est du bassin versant avec des processus d'érosion diffuse en tête de bassin versant et des processus d'érosion concentrée à travers des ravines éphémères dans la partie aval du bassin versant (Fig.29). Les parcelles sont soumises à des taux d'érosion spécifiques relativement élevés pouvant atteindre des valeurs supérieures à 76 t km^{-2} par évènement sur certains points localisés du bassin versant. Enfin, le futur plan d'aménagement pour l'implémentation des solutions d'hydraulique douce semble cohérent. La réduction sur les flux sédimentaires est significative pour 66% des épisodes modélisés et peut atteindre les 84%.

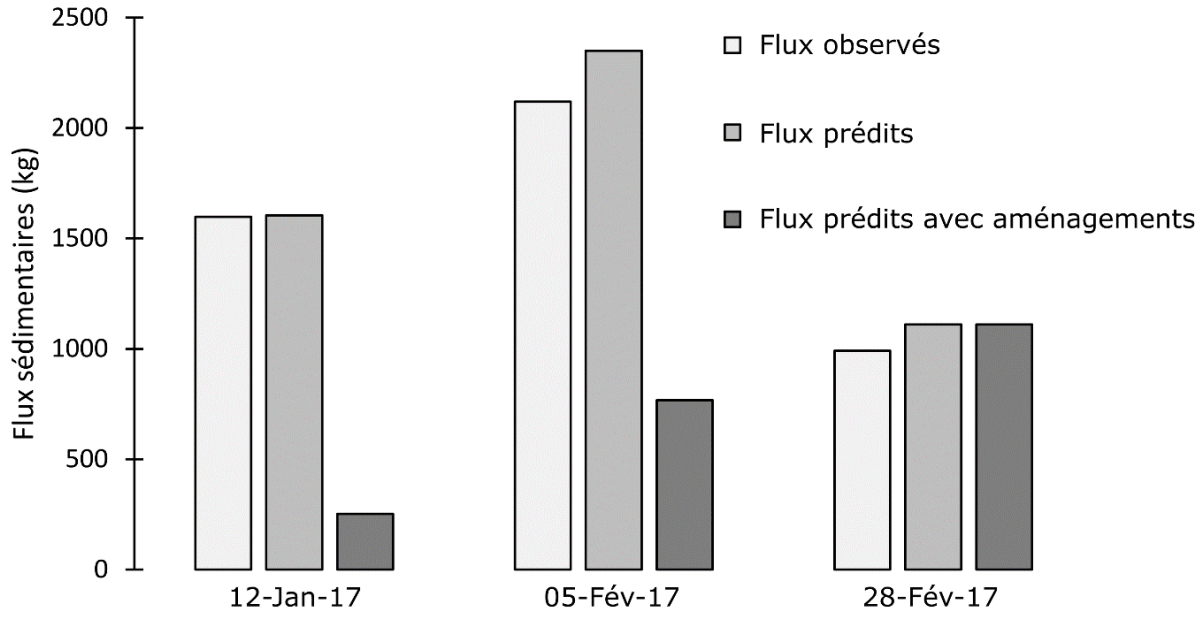

Fig. 28 : Quantités de flux sédimentaires (kg) mesurés et prédits sans/avec aménagements d'hydraulique douce à l'exutoire du bassin versant de la Pommeroye pour trois épisodes érosifs différents.

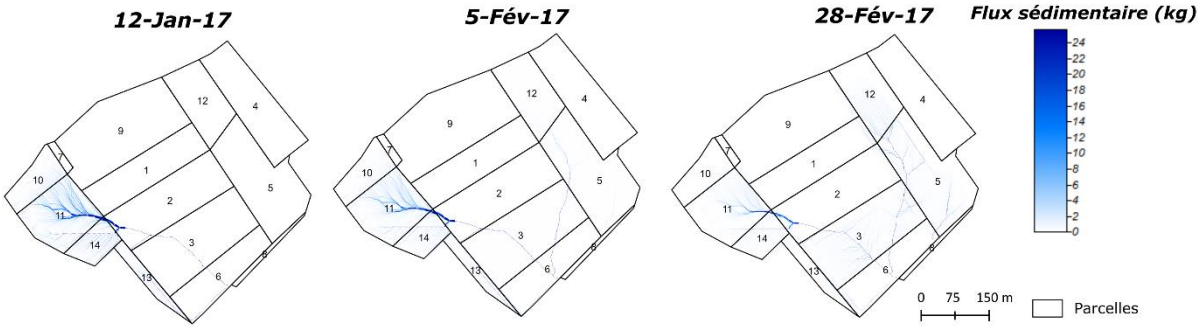

Fig. 29 : Localisation des transferts hydro-sédimentaires pour les trois épisodes érosifs simulés.

Conclusions et perspectives

La variabilité spatio-temporelle des transferts hydro-sédimentaires sur le bassin versant de la Pommeroye a pu être quantifiée grâce à l'outil de modélisation *WATERSED*. Les flux observés sont globalement correctement prédits par le modèle sur les trois épisodes érosifs simples sélectionnés. Des processus d'érosion diffuse et concentrée dans des ravines éphémères sont à l'origine du transfert particulaire et interviennent à différentes localisations sur le bassin versant. La proposition d'aménagement du syndicat local pour l'installation de solutions d'hydraulique est cohérente et les résultats de modélisation montrent une réduction significative des flux sédimentaires pouvant atteindre les 84%. Après l'installation de ces éléments sur le bassin versant (fin 2018), il sera

intéressant de comparer à nouveau les flux observés versus ceux prédits pour quantifier l'efficacité réelle de ces aménagements.

Chapter 3: Simulating erosive event and control measure efficiency in a small agricultural catchment in Northern France (the Pommeroye).

Edouard Patault[a,b], Claire Alary[a], Christine Franke[b], Valentin Landemaine[c], Nor-Edine Abriak[a]

[a]IMT Lille Douai, Univ. Lille, EA 4515 - LGCgE - Civil Engineering and Environmental Department, F-59000 Lille, France

[b]MINES ParisTech, PSL Research University, Center of Geosciences, 35 rue Saint-Honoré, 77305 Fontainebleau Cedex, France

[c]BRGM, 3 avenue Claude Guillemin, BP6009, 45060 Orléans Cedex 2, France

This chapter is presented as an article in preparation for submission to the journal Geomorphology.

Highlights

- Runoff and sediment export were simulated with the *WATERSED* model for multiple erosive events.
- Predicted sediment yield fits perfectly with observed values (model efficiency = 0.92).
- Simulations show spatial variability of erosion processes depending on soil surface characteristics.
- Field-based sediment yield ranges from 0 to 76 t km^{-2} event^{-1}.
- Erosion control measures can potentially store 84% of the sediment flux per event.

Graphical abstract

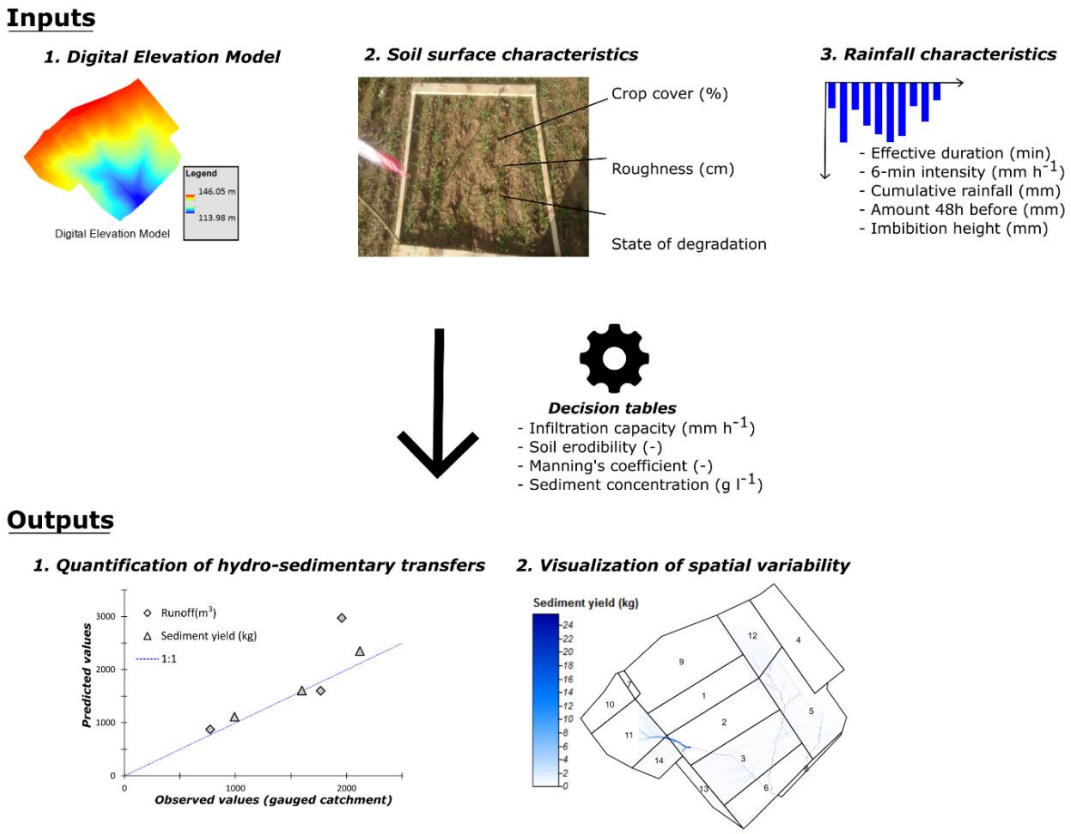

Abstract

Prediction of sediment export and preferential pathways is an ongoing challenge for catchment management to reduce soil loss. The recent development of a novel erosion model by Landemaine (2016) can provide further information with a high level of precision but there is a lack of experimental studies to validate these improvements. This study aims to calibrate the new expert-base erosion model (*WATERSED*) at the outlet of a gauged small catchment situated in Northern France (0.54 km²). Inputs for the model include a digital elevation model (cell size: 50 cm), rainfall event characteristics and soil surface state (crop cover, roughness, and state of degradation). In-field observations and characteristics of three rainfall events providing unique hydrological response were used to calibrate the model. Calibrated values were used for further simulations. The results of the simulations are consistent with hydro-sedimentary transfer measured at the high-frequency monitoring station located at the outlet of the catchment. The coefficient of simulation efficiency of the *WATERSED* model is satisfying: NSE = 0.92 sediment yield (kg) and 0.53 for runoff (m^3). Model simulations showed high spatial variability of the remobilization processes that are impacted by temporal soil surface state modifications. The sediment yield of agricultural parcels was estimated and can reach 76 t km^{-2} $event^{-1}$. Finally, the effectiveness of an existent management plan proposed by the local Water Agency that is meant to reduce erosion (including fascine, hedge, and grass strip) was evaluated via an "erosion control measure" module in the model. Simulations show a significant potential reduction of the hydro-sedimentary transfer ranging up to 84%.

Keywords: soil erosion; erosion control measure; expert-based model; WATERSED model; agricultural catchment; Northern France.

1. Introduction

Areas of intensive agricultural production on the European loess belt are particularly affected by on-site and off-site impact of soil erosion. Accelerated soil erosion results in downstream sediment transfer which induces the silting of riverbeds and reservoirs or the degradation of the physico-chemical water quality. Each year, the cost of off-site soil erosion is estimated between 25 and 75 M€ (Verstraeten et al., 2002). Moreover, during intense rain storm events, soil erosion results in muddy floods that impacts downstream habitations. Northern France is particularly affected by muddy flooding. Between 1983 and 2009, 1100 municipalities were impacted. The cost induce by muddy flooding was estimated in Normandy (France) and Belgium reaching 1.5 M€ $event^{-1}$, respectively 16 to 172 M€ $year^{-1}$ (Evrard et al., 2007; Viel, 2012). More recently, between May 25 and June 16, 2018, muddy floods in a large part of France caused damages at 214,000 locations with costs estimated to 430 M€ according to the French insurance federation. Catchment stakeholders make large efforts to reduce theses costs and try to decrease the off-site impact of soil loss. In fact, erosion control measures (ECM) are being implemented in those affected areas (Evrard et al., 2007; Souchère et al., 2003), but the lack of information on sediment pathways can lead to their mis-implementation (Frankl et al., 2017; Landemaine, 2016; Poesen, 2018). Moreover, most experimental studies that try to control the efficiency of these measures were conducted at the 1D plot scale and there is a rising need for two-dimensional modelling to better understand sediment-trapping efficiency at the event scale and the associated temporal variability (Richet et al., 2017).

In the past, most of the models that have been developed to improve our understanding of sediment dynamics were inappropriate for providing robust information at the catchment scale, and event-based predictions of the sediment load. They suffer from a variety of problems including over-parameterization, unrealistic input requirement, unsuitability of model assumptions or parameter values of local conditions, and inadequate documentation of model testing and resulting performance (Merritt et al., 2003). Expert-based models, such as the *STREAM* model (Cerdan et al., 2001; Souchère et al., 1998) or its updated version : *WATERSED* (Landemaine, 2016) provide a better

compromise focusing on the driving factors of runoff and erosion effects, avoiding over-parameterization and the associated uncertainties derived from increased parameterization. The *WATERSED* model is an effective model because it provides runoff and erosion predictions in regions where Hortonian overland flow dominates (Cerdan et al., 2002; Cerdan et al., 2001; Evrard et al., 2009). Decision rules are derived from expert judgment based on databases of field measurements to convert soil surface characteristics into soil-related input variables. The model was designed on data from Normandy (Pays de Caux) and successfully used to simulate the impact of different agri-environmental scenarios on runoff and erosion. Similar soil characteristics can be observed elsewhere in Northern France where the model can be tested to evaluate its applicability.

The main objective of this study is to calibrate the *WATERSED* model on a well constrained catchment (the Pommeroye; 0.54 km²) to discuss the accuracy of the model predictions compared to the observed results from a high-frequency monitoring station and to evaluate the spatial distribution of the hydro-sedimentary transfers in the catchment. This comparison also aims to evaluate the effectiveness of future ECM installations.

2. Material & Methods

2.1 Study area

The Pommeroye catchment (0.54 km²; Fig.30A) is a sub-basin of the Canche River catchment (1274 km²) situated in the European loess belt in Northern France, under oceanic climate with an average annual temperature of 11°C. The thermal amplitude is low, with soft winters and cool summers. The annual precipitation rate is 1000 ± 150 mm yr^{-1}. The elevation of the study area ranges from 115 to 145 m and the average slope is 4.2%. The soil is constituted of Pleistocene silt which is underlain by chalky soil of the Seno-Turonian (Beckelynck, 1981). Specific sediment yield (SSY) and rainfall were quantified with a monitoring station over 2 years. SSY range from 29.4 to 70 t km^{-2} yr^{-1} (for further details, see Patault et al., 2018 *in review – chapter 2* and Fig.30B). Runoff events mainly occur in winter and autumn. Only few events (6% per year) are responsible for a large proportion of

the sediment yield (40%). The study site is exclusively occupied by arable land, divided into 14 fields (Fig.30C). The dominant crops here are cereals, winter and spring barley, rape seed, and mustard.

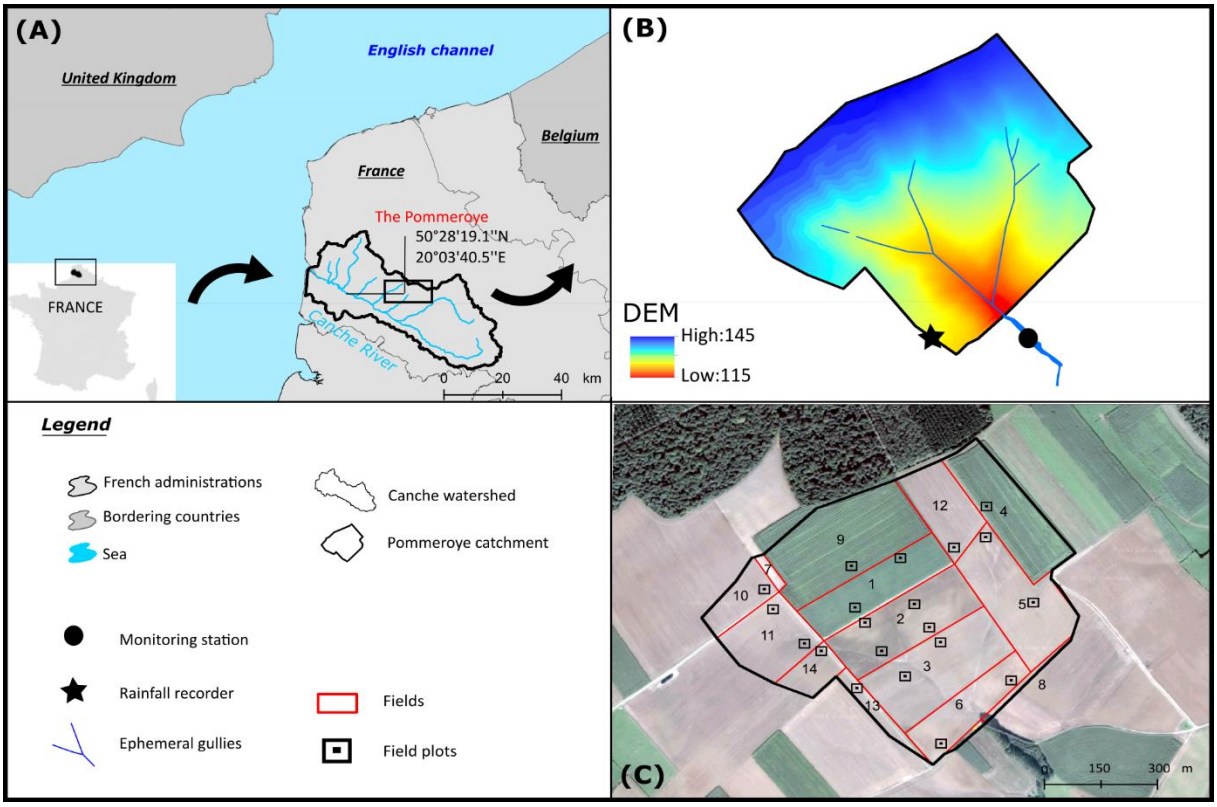

Fig. 30 : (A) Overview of the Canche watershed, (B) Digital elevation model (DEM; cell size = 50 cm) of the Pommeroye catchment and localization of the monitoring station and ephemeral gullies, (C) Parcels and field plots.

Considering that the Pommeroye catchment is affected by major erosive problems, this study site was selected to evaluate the effectiveness of ECM. To our knowledge, no information exists on the effect of ECM over a long investigation period and at the open-field agricultural landscape scale (Landemaine, 2016). The Artois-Picardie Water Agency and Chamber of Agriculture (Northern France) proposed a management plan for ECM to reduce hydro-sedimentary transfer starting at the end of 2018. ECM locations were extracted from the database *RUISSOL*[12], administered by the Chamber of Agriculture. *RUISSOL* is a data governmental management tool for monitoring erosion control of agricultural soils. The future management plan for the Pommeroye catchment consists of the installation of one hedge, three grass strips and ten fascines (Fig.31). Fascines are typical erosion

[12] https://www.ruissol.pro/ - *consulted July 20, 2018*

control measures, largely implemented in Northern France since 2000. Fascines are any type of linear vegetation barrier consisting of living and/or dead vegetation. They differ from hedges in the way that they were especially conceived to reduce velocities and trigger sedimentation. Some studies reported a trapping efficiency of fascines of 47-98% at the field plot scale (~1 m²) (Richet et al., 2017).

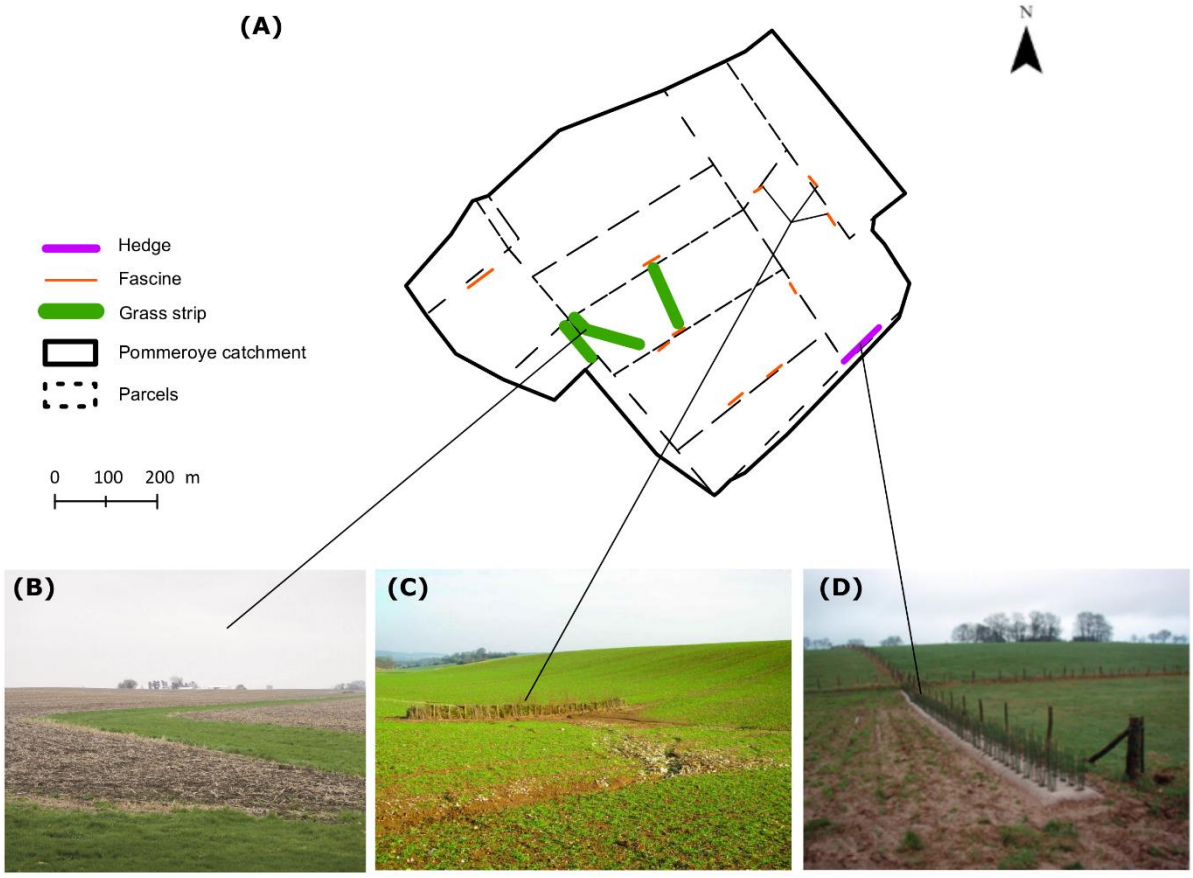

Fig. 31 : Future management plan to reduce erosion in the Pommeroye catchment. (A) Locations of erosion control measures, (B, C, D) Example of erosion control measures implemented in Northern France: respectively grass strip, fascine and young hedge.

2.2 Model description

The *WATERSED* model is a non-dynamic model using a raster-based distributed approach to model the spatial distribution of runoff and soil erosion within a catchment for a given rainfall event. The *WATERSED* model is an upgrade of the *STREAM* model (Cerdan et al., 2001; Souchère et al., 2003; Souchère et al., 1998) which simulates the hydrological processes by conceptualizing each raster grid cell as a reservoir. The properties are calculated at the event-scale, and by routing water

and sediment according to the surface flow network and predefined functions (Couturier et al., 2013). The model assumes that the following surface characteristics are the main determinants of runoff and infiltration at the field scale: soil surface crusting, surface roughness, total cover (crops and residues). These characteristics are set for each field using classification rules developed by Le Bissonnais et al. (2005). Subsequently, a table is used to assign a steady-state infiltration rate value to each combination of these soil surface characteristics (Evrard et al., 2010). The following description is issued from the recent study of Landemaine (2016):

2.2.1 Hydrologic balance

For a given rainfall event, the state of each cell is given by the hydrologic balance:

$$HB_{R_i} = R_i - IR_i - (\theta \times IC_i \times t_{eff_i}) \quad (6)$$

Where R_i is the rainfall amount for the cell i (mm), IR_i is the amount of rainfall needed to reach soil saturation (mm), IC_i is the steady-state infiltration rate (mm h^{-1}), t_{eff_i} is the effective rainfall duration (min), and θ is a dynamic adjustment parameter. Negative values of HB_{R_i} correspond to infiltration and positive values to runoff. The model estimates the continuous abstraction for the runoff duration for each cell. Runoff duration needs the estimation of the velocity and the flow travel time of each grid cell.

2.2.2 Flow velocity and flow travel time

The average excess rainfall intensity e_i (mm h^{-1}) can be derived from the excess rainfall E_{R_i} (mm) as:

$$e_i = \frac{E_{R_i}}{t_{eff_i}} \quad (7)$$

Overland flow travel time in a grid cell is estimated using Manning's formula (Melesse & Graham, 2004). The overland flow velocity V_{H_i} (m s^{-1}) is calculated as:

$$V_{H_i} = \frac{{S_i}^{0.3} {L_i}^{0.4} {e_i}^{0.4}}{{n_i}^{0.6}} \quad (8)$$

Where S_i is the slope of the surface in cell i (m m^{-1}), L_i is the flow length of the cell and n_i is the Manning's roughness coefficient (s m$^{-1/3}$). The channel flow velocity V_{C_i} (m s^{-1}) is estimated by combining Manning's equation and the steady state continuity equation for a wide channel (Muzik, 1996):

$$V_{C_i} = {S_i}^{0.3} \left(\frac{Q_i}{W_i}\right)^{0.4} {n_i}^{-0.6} \quad (9)$$

Where Q_i is the cumulative discharge through the cell obtained by summing upstream flow contributions and the contribution from precipitation excess for that cell i (m^3 s^{-1}), and W_i is the channel width (m). Based on overland and channel flow velocity, the travel time of each cell is computed by dividing travel distance by cell velocity.

2.2.3 Runoff duration and flow routing

The flow through a given cell during the runoff duration can be described with a runoff hydrograph. From this concept, the lag time is calculated for each cell by summing up upslope travel time, weighted by the cumulative discharge. The effective rainfall is assumed to be equally distributed over time and the centroid of the effective rainfall is $\frac{t_{eff_i}}{2}$. The time to peak T_{P_i} (h) is obtained by summing up the lag time, L_i (h), and $\frac{t_{eff_i}}{2}$:

$$T_{P_i} = \frac{t_{eff_i}}{2} + L_i \quad (10)$$

The runoff duration or time of concentration T_{Ci} (h) is derived from the time to peak T_{Pi} and the recession parameter α (-)[13]:

$$T_{Ci} = T_{Pi} + \alpha \times T_{Pi} \quad (11)$$

Finally, using the total runoff volume through the cell V_i (m^3), the runoff duration, and assuming a triangular unit hydrograph for each cell, a runoff peak Q_{Pi} ($m^3\ s^{-1}$) is computed as:

$$Q_{Pi} = \frac{2V_i}{T_{Ci}} \quad (12)$$

2.2.4 Sheet and gully erosion

For interrill erosion, a table is used to assign a potential sediment concentration in the flow SC_i ($g\ l^{-1}$) to each combination of soil surface characteristics and rainfall intensity. The corresponding interrill erosion SE_{S_i} (kg) is calculated as:

$$SE_{S_i} = E_{R_i} \times SC_i \quad (13)$$

Where E_{R_i} (mm) is the excess rainfall. Gully erosion occurs when the peak discharge on a hillslope grid cell exceeds a critical peak discharge Q_{crit} ($m^3\ s^{-1}$). A gully is assumed to be rectangular and unique per cell. The calculation of the cross section requires first the gully width W_{G_i} (m) calculated from an empirical relationship developed by Nachtergaele et al. (2002):

$$W_{G_i} = 2.51 \times {Q_{peak_i}}^{0.412} \quad (14)$$

The flow velocity V_{G_i} ($m\ s^{-1}$) is computed according to the empirical relationship developed by Govers (1992):

$$V_{G_i} = 3.52 \times {Q_{peak_i}}^{0.294} \quad (15)$$

[13] (-) refers to parameters dimensionless.

Then the gully height H_{G_i} (m) is deduced from the gully W_{G_i}, the gully velocity V_{G_i}, and the peak discharge Q_{peak_i}, as:

$$H_{G_i} = \frac{Q_{peak_i}}{W_{G_i} V_{G_i}} \quad (16)$$

The gully cross section A_{G_i} (m²) is finally determined from the gully width W_{G_i} and the gully height H_{G_i}. The gully volume VOL_{H_i} (m^3) is obtained by multiplying this cross section of incision by the grid cell length. The gully volume is weighted by a soil erodibility factor EF_i (-), in the [0-1] matrix computed from the rules adapted from the methodology developed by Souchère et al. (2003) to determine the sensitivity to gully erosion.

$$A_{G_i} = W_{G_i} \times H_{G_i} \quad (17)$$

$$VOL_{H_i} = A_{G_i} \times L_i \times EF_i \quad (18)$$

Finally, the gully erosion SE_{G_i} (kg) is calculated by multiplying the gully volume VOL_{H_i} by the bulk density ρ (kg m^{-3}) as:

$$SE_{G_i} = VOL_{H_i} \times \rho \quad (19)$$

Therefore, the gross erosion SE_i (kg) of a cell corresponds to the sum of the interrill erosion and gully erosion as:

$$SE_i = SE_{S_i} + SE_{G_i} \quad (20)$$

2.2.5 Sediment yield and deposition

At the catchment scale, sediments are transported in proportion to the runoff volume. For each cell i producing runoff, the mass of sediment leaving this cell SY_i (kg) is expressed as:

$$SY_i = SY_\alpha + SE_i \quad (21)$$

Where SY_α (kg) is the mass of sediment coming from upslope cells, and SE_i (kg) is the gross erosion. Sediment deposition occurs in two cases: in the first case, if a cell has the potential to infiltrate a part or the totality of the upslope run-on, the mass of deposited sediment SD_i (kg), corresponds to the product of the infiltrated water volume I_i (m^3) and the mean suspended sediment concentration of the flow $\overline{SC_\iota}$ ($g\ l^{-1}$).

$$SD_i = I_i \times \overline{SC_\iota} \quad (22)$$

$$\overline{SC_\iota} = \frac{SY_\alpha}{Q_\alpha} \quad (23)$$

Thus, the sediment yield becomes:

$$SY_i = SY_\alpha + SD_i \quad (24)$$

In the second case, sediment deposition occurs when the mean suspended sediment concentration of the flow $\overline{SC_\iota}$ exceeds the suspended sediment concentration for the sediment transport capacity, SC_{TC_i} ($g\ l^{-1}$). Here, the sediment yield is calculated as:

$$SY_i = Q_i \times SC_{TC_i} \quad (25)$$

Where Q_i (m^3) is the runoff volume leaving the cell i. The mass of deposited sediment is then deduced as:

$$SD_i = SY_\alpha - SY_i \quad (26)$$

The suspended sediment concentration for the transport capacity SC_{TC_i} is calculated by weighting the mean suspended sediment concentration in the flow $\overline{SC_\iota}$ by a ratio between the

hydraulic resistance of vegetation, expressed by the Manning's roughness coefficient n_i, and the submergence of the cell expressed by the mean water depth h_i (m):

$$SC_{TC_i} = \overline{SC_i} \times e^{\left(-\beta \times \frac{n_i}{h_i}\right)} \quad (27)$$

Where β is a decay parameter (-). The mean water depth h_i is calculated by dividing the runoff volume Q_i with the runoff duration T_C and the contributing area, A_i (m²):

$$h_i = \frac{Q_i}{T_C \times A_i} \quad (28)$$

2.3 Model input requirements – Application on the Pommeroye catchment

The model requires datasets to compute runoff and erosion at any point of the catchment: (i) Digital Elevation Model (DEM) to extract slope and runoff flow network, (ii) soil texture map associating each field of the catchment with the appropriate soil surface characteristic, (iii) decisions tables to associate each soil surface characteristic observed in the field with a steady-state infiltration rate, a Manning's roughness coefficient, a single potential sediment concentration and a soil erodibility value, and (iv) rainfall events extracted from rainfall time series.

2.3.1 Topography of the Pommeroye catchment

The DEM was provided by the Pas-de-Calais departmental territory and sea office for the study site with a 0.5 m resolution and results from a Lidar campaign in 2015. The depressions were filled according the algorithm developed by Wang & Liu (2006) to ensure the continuity of flow through the landscape. Parcel limits on the catchment were defined using Google Maps Images and field surveys.

2.3.2 Soil texture

The soil texture map was provided by the regional Chamber of Agriculture and showed fine silt levels of 34%, coarse silt of 48%, and low clay content of 18% (Alexandre, 2015). The soil texture is considered homogeneous for this small catchment.

2.3.3 Survey of soil surface characteristics

As observed by Le Bissonnais et al. (2005) the strong heterogeneity of the erosive events is principally linked to the following characteristics of the soils: roughness, crop cover, and state of degradation. Indeed, parcels of land with different cropping systems, for different seasons of the year, suggest that soil conditions are also heterogeneous in the catchment (Evrard et al., 2010). To evaluate the impact of the soil surface characteristics evolution on the SY, we studied the degradation of the soil surface at the plot scale (1 m²). 24 plots were installed across the Pommeroye catchment (see black square symbol in Fig.32), considering the crop diversity in the different parcels. In-field observations were done from October 2016, at the beginning of the plowing activity, until March 2017, on 8 non-consecutive days (Fig.32).

Fig. 32 : Survey of soil surface state evolution in the Pommeroye catchment. For each parcel, crop cover, roughness and state of degradation were evaluated at the plot (1m²). (A) Parcel 2 on November 17, 2016 and (B) Parcel 2 on March 3, 2017.

For each individual observation, the state of degradation, the roughness, and the crop cover were reported. These parameters were distinguished into different classes (see Appendices B; Table 20, 21 and 22) as suggested by Cerdan et al. (2002) Cerdan et al. (2001) Souchère et al. (2003).

Parcels n°7 and 8 are not monitored here because the parcel n°7 serves as a manure deposit and the parcel n°8 is situated on a path.

2.3.4 Decision tables

The soil surface characteristics were then transformed into steady-state infiltration based on Table 23 (Appendices B). Combining the maximum 6-min intensity of the considered rainfall event and the corresponding soil surface characteristics, an additional table is used to define the potential sediment flow concentration (Table 24 – Appendices B). Based on the soil surface characteristics, Manning's values were derived from surface roughness and the percentage of the crop cover (Gilley et al., 1991; Table 25 – Appendices B). Soil surface characteristics were also used to define the soil erodibility factor (Table 26 – Appendices B). From this preprocessing, four grids were produced for each rainfall event: infiltration capacity rate, Manning's roughness coefficient, potential sediment concentration, and soil erodibility.

2.3.5 Rainfall time series

Rainfall time series have been collected between March 2016 and March 2018 from a tipping-bucket rain gauge (*Précis mécanique 303x; 0.2 mm*) installed in the Pommeroye catchment (see star symbol in Fig.30). Rainfall is considered generally homogeneous on the catchment due to its small size. For each event, four parameters were calculated: rainfall amount (mm), effective duration (rainfall period with intensity greater than 2 mm h^{-1}), rainfall amount during 48h before the beginning of the event, and maximum 6-min rainfall intensity. These parameters were rasterized at the DEM resolution (0.5 m). For each event, a rainfall imbibition height grid was deduced according to Table 27 (Appendices B) using the runoff sensitivity and the 48h antecedent rainfall height grid (Table 28 – Appendices B).

2.4 Quantification of erosion and runoff export at the outlet of the catchment

Runoff volumes were monitored in a Venturi channel at the outlet of the catchment (Fig.30B; see also Patault et al., 2018 *in review – see chapter 2*). The water height is recorded by an ultrasound

water-level logger (*Ijinus LNU 300-X*). Runoff discharge is calculated at each time step in the Venturi channel using Eq.29:

$$Q = -7{,}223 \times h + 2873{,}2 \times h^2 - 766 \times h^3 + 770 \times h^4 \quad (29)$$

Where Q ($m^3\ h^{-1}$) is the instant flow in the Venturi channel and h (m) the water height. The range of the ultrasound water-level is 0 to 792 mm in the channel and the resolution is 2 mm. The cumulative runoff volume (V) during the i events is calculated using Eq.30:

$$V = \sum_i V_i = \sum_i Q_i \times \Delta t_i \quad (30)$$

Sediment export is measured using a sediment sampler (*ISCO 3700*) and a turbidity probe (*Odeon from Aqualabo*). The sampler is coupled to the water-level sensor and functions only when water runs through the venturi channel. A correlation curve was defined between the turbidity data measured (Δt = 6 min) in the field and the suspended sediment concentration (SSC in $g\ L^{-1}$) measured in the laboratory:

$$SSC = -5 \times 10^{-8}\, T^2 + 0.001T + 0.0089 \quad (31)$$

With T as turbidity, the suspended sediment flux SF ($kg\ s^{-1}$) is calculated using Eq.32:

$$SF = Q \times SSC \times 10^3 \quad (32)$$

Q is the flow discharge in $m^3\ s^{-1}$. The sediment export for each event is evaluated as:

$$SE = \int_{t_0}^{t} SSF\ \Delta t \quad (33)$$

SE (kg) is the sediment export for each event and Δt (s) the time elapsed between the beginning and the end of an event.

2.5 Evaluation of the model results

The *WATERSED* model has been run for those rainfall events for which relevant surveys of soils surface characteristics and erosion data were available. For 8 days of in-field observations, only 3 were usable because of the rainfall variability. The first condition was that the hydro-sedimentological response of the corresponding erosive event at the outlet was not too complex. The second condition was that the associate soil surface states of the rainfall event were available. If two or more rainfall events happened between 2 days of in-field observations, soils surface states were considered as unknown as a possible degradation of the parcels may have occurred. Considering this, three selected rainfall events were used to calibrate the model (Table 5).

Tab. 5 : Characteristics of the three rainfall events recorded on the Pommeroye catchment that was selected for the calibration of the model.

Date	12-Jan-2017	05-Feb-2017	28-Feb-2017
Rainfall amount (mm)	22	25.2	21.6
Max 6-min intensity (mm h^{-1})	12	6	8
Duration (min)	528	702	852
48h-antecedent rainfall (mm)	2	11.8	17

The runoff volume and the sediment export were calculated from the observed values for each distinct runoff event and compared to those predicted by the model. For each simulation, the accuracy of the simulated runoff volume and sediment export has been assessed by calculating two goodness-of-fit indices.

The coefficient of simulation efficiency (Nash & Sutcliffe, 1970) was calculated as:

$$NSE = 1 - \frac{\sum_{i=1}^{n}(Y_{obs} - Y_{sim})^2}{\sum_{i=1}^{n}(Y_{obs} - \overline{Y_{sim}})^2} \quad (34)$$

Where Y_{obs} is the observed value (runoff volume or respectively sediment export) for the considered event, Y_{sim} is the simulated value, $\overline{Y_{sim}}$ is the mean observed value and, n is the number of events considered. NSE values vary between minus infinity (poor model) and 1, with 1 indicating a perfect fit between observed and predicted values.

The root mean square error (RMSE) was calculated to measure the accuracy of the estimation:

$$RMSE = \sqrt{\frac{1}{n}\sum_{i=1}^{n}(Y_{obs} - Y_{sim})^2} \quad (35)$$

2.6 "Erosion control measure" module

ECM were implemented in the model using a supplementary module in the *WATERSED* model. For each type of ECM (e.g. fascine, hedge, grass strip), a width, a transport capacity and an infiltration capacity were defined (Table 6). Transport capacity and infiltration capacity were attributed after experimental field and laboratory studies (Ouvry et al., 2012). Widths were defined using information provided in the *RUISSOL* database.

Tab. 6 : Characteristics of ECM implemented in the *WATERSED* model.

Type of ECM	Width (m)	Infiltration capacity (mm h^{-1})	Transport capacity (g l^{-1})
Fascine	0.5	170	3
Hedge	1	400	3
Grass strip	6	50	0.5

3. Results

3.1 Observed erosive events and associated soil surface states

The three winter events selected (Table 5) used to calibrate the *WATERSED* model showed temporal variability of the hydro-sedimentary responses and spatial variability of the soil surface characteristics. For the event of January 12, 2017, the hydrograph shows several discharge and sediment concentration peaks (Fig.33A). Highest sediment concentrations were recorded at the beginning of the event with a maximum of 4.9 g L^{-1}. The maximum flow discharge was evaluated to 190.9 m^3 h^{-1}. The rainfall amount was evaluated to 22 mm for this event (max 6-min rainfall intensity = 12 mm h^{-1}; duration = 528 min) and the rainfall amount 48-h before the beginning of the event was negligible (2 mm). The observed runoff and sediment yield were calculated to 773 m^3 and 1597 kg respectively. Before this event, crop cover was well developed in the middle part of the catchment and both sides were not well covered (Fig.34). The western part of the catchment was in F2 state of degradation indicating the presence of a slaking crust, whereas the middle part and eastern part of the catchment were in a transition state (F11 and F12 respectively). Roughness ranged from 0-1 cm to 5-10 cm, showing smallest roughness in the degraded parcel (n° 10, 13, and 14). For the event of February 05, 2017, the hydrograph was different from the previous erosive event (Fig33B). Rainfall amount reached 25.2 mm, the duration of the rainfall event was longer (702 min) but 6-min rainfall intensities were low (6 mm h^{-1}). The rainfall amount 48-h before the event was moderate with a value of 11.8 mm suggesting a minor capacity of infiltration for the soils. Maximum flow discharge was higher (235.8 m^3 h^{-1}) as the runoff volume (1767 m^3). Sediment concentrations is lower (mean = 0.74 g L^{-1}) and reaches 3.71 g L^{-1} at the beginning of the event. Sediment yield for the event was evaluated to 2119 kg. For this second event, the crop cover was the same as for the previous event in January. The roughness and the state of surface were degraded in the North-Western part of the catchment. More than 50% of the area of the catchment was in a F12 to F2 state of degradation.

For the last event of February 28, 2017, the maximum flow discharge reached 221.8 m^3 h^{-1}, but sediment concentration was the lowest recorded in comparison to the two previous events (Fig.33C). Maximum sediment concentration reached 1.59 g L^{-1} and the mean concentration was evaluated to 0.35 g L^{-1}, suggesting that less sediment has been remobilized. Rainfall characteristics for this event were evaluated as follows: rainfall amount was 21.6 mm; maximum 6-min rainfall intensity was 8 mm h^{-1}; rainfall amount 48-h before the beginning of the event was 17 mm, and rainfall duration was 1002 min. The observed runoff and sediment yield were evaluated to 1957 m^3 and 991 kg respectively. Crop cover was higher in the catchment, and globally reaching 21-60% on 80% of the catchment area. Parcels surface state was particularly degraded with more than 80% of the catchment in a F12-F2 state and a low roughness (0-1 cm) for 60% of the catchment area.

Considering the soil surface state for the tree selected erosive events and the appropriate decision tables, inputs for the simulations were calculated (Table 7).

Tab. 7 : Inputs for the *WATERSED* model resulting from the in-field observations for the three selected events.

		Parcel													
	Date	1	2	3	4	5	6	7	8	9	10	11	12	13	14
Soil surface characteristics	3-Jan-17	C2-R2-F11	C3-R2-F11	C2-R1-F2	C1-R4-F0	C2-R2-F12	C2-R1-F11	x	x	C3-R3-F11	C1-R1-F2	C1-R1-F2	C2-R1-F12	C1-R1-F2	C1-R2-F2
	1-Feb-17	C2-R2-F11	C3-R2-F12	C2-R1-F2	C1-R3-F11	C2-R1-F2	C2-R1-F12	x	x	C3-R3-F11	C1-R1-F2	C1-R1-F2	C2-R1-F2	C1-R1-F2	C1-R2-F2
	15-Feb-17	C1-R2-F11	C3-R1-F12	C2-R0-F2	C1-R3-F12	C2-R1-F2	C2-R1-F12	x	x	C2-R3-F12	C2-R0-F2	C2-R1-F2	C2-R1-F2	C2-R1-F2	C2-R2-F2
Infiltration rates (IR; mm h^{-1})	3-Jan-17	20	50	5	50	10	20	x	x	50	2	2	10	2	2
	1-Feb-17	20	20	5	20	5	10	x	x	50	2	2	5	2	2
	15-Feb-17	20	10	2	20	2	10	x	x	20	2	2	2	2	2
Potential sediment	3-Jan-17	7.5	7.5	3.5	7.5	0.5	3.5	x	x	12.5	7.5	7.5	3.5	7.5	12.5
concentration (g l^{-1})	1-Feb-17	3.5	0.5	0.5	12.5	0.5	0.5	x	x	7.5	3.5	3.5	0.5	3.5	0.5
	15-Feb-17	0.5	0.5	0.5	7.5	0.5	0.5	x	x	3.5	0.5	0.5	0.5	0.5	0.5
Manning's roughness	3-Jan-17	0.103	0.159	0.099	0.078	0.103	0.099	x	x	0.168	0.043	0.043	0.099	0.043	0.047
coefficient (s $m^{-1/3}$)	1-Feb-17	0.103	0.159	0.099	0.078	0.099	0.099	x	x	0.168	0.043	0.043	0.099	0.043	0.047
	15-Feb-17	0.047	0.155	0.095	0.078	0.099	0.099	x	x	0.112	0.095	0.099	0.099	0.099	0.103
Soil erodibility (-)	3-Jan-17	0.217	0.047	0.217	0.683	0.217	0.217	x	x	0.047	0.683	0.683	0.217	0.683	0.683
	1-Feb-17	0.217	0.047	0.217	0.683	0.217	0.217	x	x	0.047	0.683	0.683	0.217	0.683	0.683
	15-Feb-17	0.683	0.047	0.217	0.683	0.217	0.217	x	x	0.217	0.217	0.217	0.217	0.217	0.217
Runoff sensitivity (-)	3-Jan-17	1	0	3	0	2	1	x	x	0	4	4	2	4	3
	1-Feb-17	1	1	3	1	3	2	x	x	0	4	4	3	4	3
	15-Feb-17	1	2	4	1	3	2	x	x	1	4	3	3	3	3
Imbibition rainfall height (mm)	3-Jan-17	15	20	8	20	12	15	x	x	20	5	5	15	5	8
	1-Feb-17	12	12	5	12	5	8	x	x	15	2	2	5	2	5
	15-Feb-17	8	5	1	8	2	5	x	x	8	1	2	2	2	2

Crop cover classes, C1: 0-20%; C2: 21-60%; C3: 61-100%
Soil surface roughness state, R0: 0-1 cm; R1: 1-2 cm; R2: 2-5 cm; R3: 5-10 cm; R4 > 10 cm
Soil surface crusting stage, F0: initial fragmentary state; F11: altered fragmentary state with initial crusts; F12: local appearance of depositional crusts; F2: continuous state with depositional crusts
x: no observations

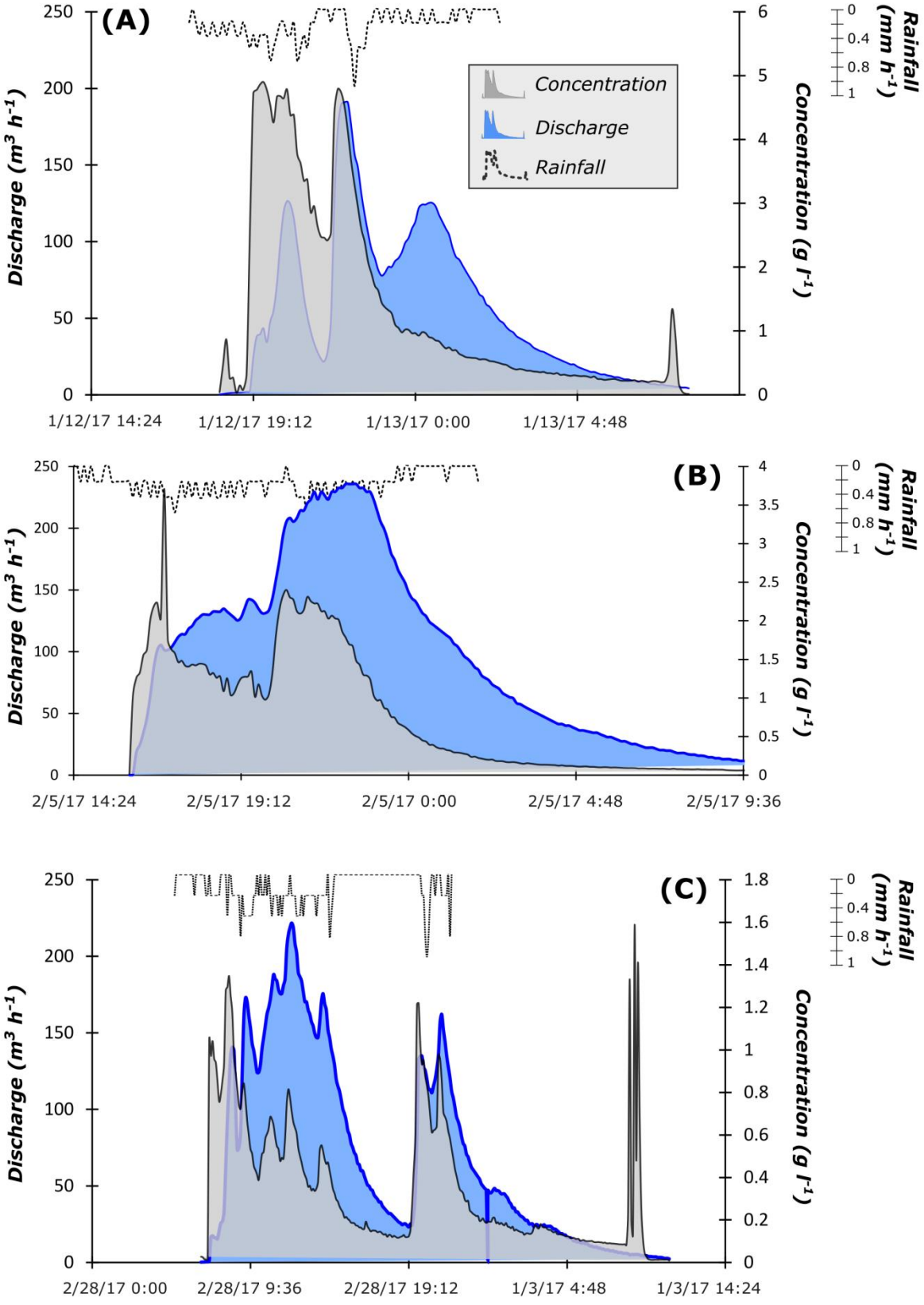

Fig. 33 : Flow discharge (m^3 h^{-1}), sediment concentration (g L^{-1}) and rainfall (mm h^{-1}) for three events recorded at the monitoring station at the outlet of the Pommeroye catchment: (A) January 12, 2017, (B) February 5, 2017, and (C) February 28, 2017.

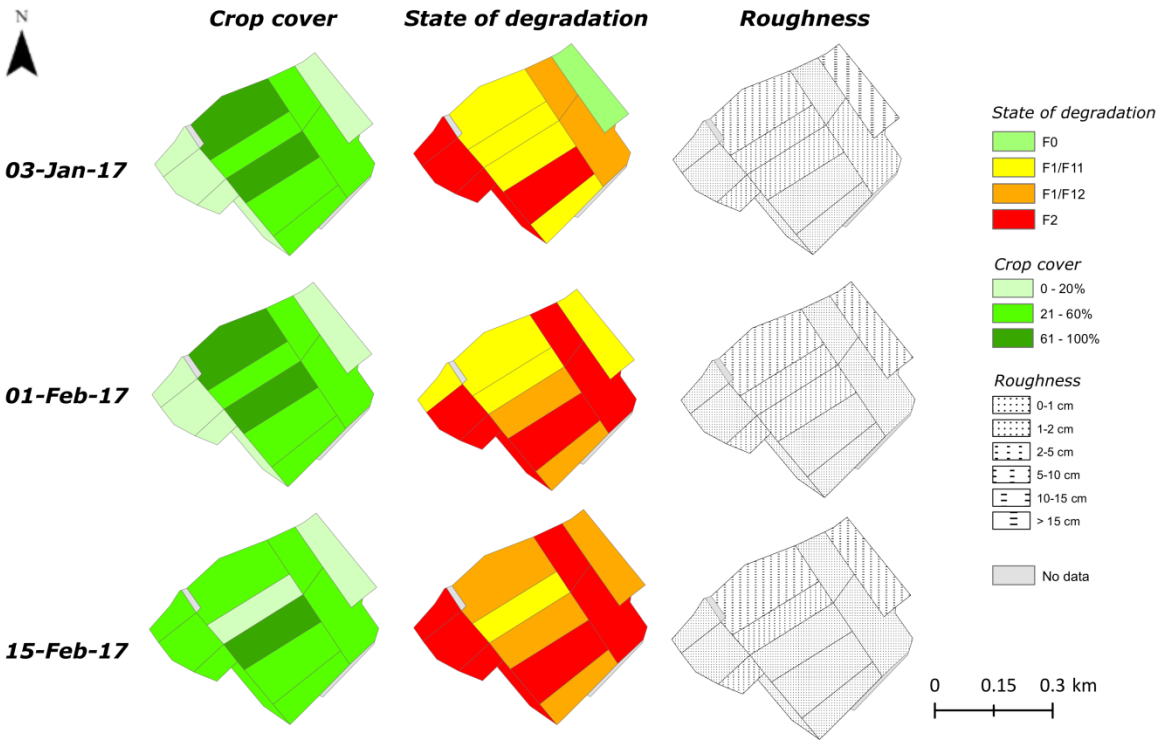

Fig. 34 : Soil surface characteristics (state of degradation, crop cover, and roughness) before the beginning of the three erosive events used to calibrate the *WATERSED* model.

3.2 Calibration of the model

Monitored events and in-field observations were used to calibrate the *WATERSED* model. Over one hundred individual simulations were conducted to calibrate the model and to find the correct value of the sensitive parameters (α, β, θ, and Q_{crit}; Fig.35 and Table 8). The results of the calibration demonstrate that the sediment yield and the runoff simulated values are very sensitive. For the event of January 12, 2017, predicted sediment yield values exhibits high variabilities ranging from 207 to 5892 kg with a median value of 1679 kg. Runoff volumes are less sensitive and range from 473 to 1072 m^3 with a median value of 796 m^3. For the event of February 05, 2017, predicted sediment yield values also exhibit a variability ranging from 1414 to 4349 kg with a median value of 2791 kg. Runoff volumes for this event are less sensitive and values range from 1061 to 2687 m^3. The erosive event of February 28, 2017 exhibits the less variable values for predicted sediment yield. The values range from 786 to 1594 kg with a median value of 1190 kg. The predicted runoff volume ranges from 2250 to 3694 m^3. Globally, the median of predicted values is in the range of the observed values except for the runoff volumes of the last event.

Best calibrated values of the sensitive parameters were evaluated considering the minimization of the root mean square error on the predicted sediment yield and runoff in addition to the maximization of the coefficient of the simulation efficiency. Best combinations of calibrated values are presented in Table 8.

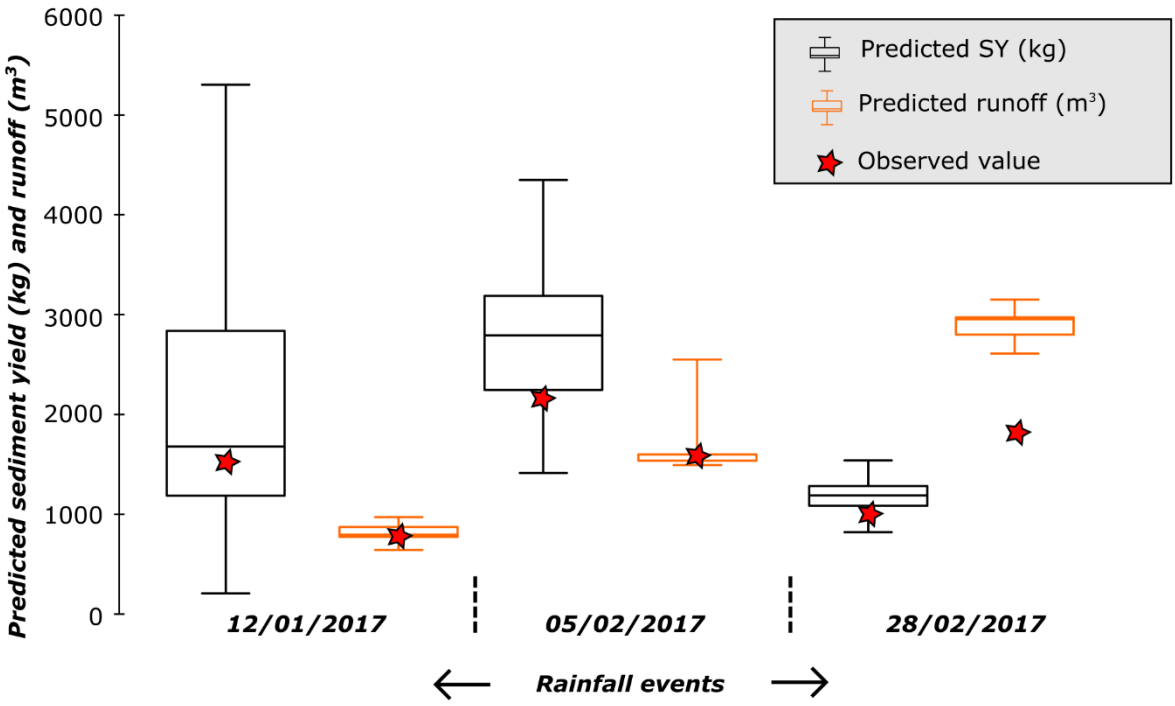

Fig. 35 : Boxplot of the 100 simulations conducted on the sensitive parameters to calibrate the *WATERSED* model.

Tab. 8 : Best optimization of the sensitive parameter for the calibration of the model. (-) refers to parameters dimensionless.

Name	Calibrated value	Sensitive parameter
α	0	Recession time coefficient (-)
β	3.7e-6	Decay parameter (-)
θ	0.4	Coefficient of infiltration rates (-)
Q_{crit}	0.15	Critical runoff peak ($m^3 s^{-1}$)

3.3 Model simulations

The results of the simulations were analyzed after the best calibration test. We previously noticed that the observed runoff volume varied from 773 to 1957 m^3 and the observed sediment yield varied from 991 to 2119 kg (Fig.36). The predicted runoff volume ranges from 873 to 2972 m^3

and the predicted sediment yield ranges from 1110 to 2349 kg. Predictions and observations fit well with the 1:1 curve indicating a good performance of the model. Prediction quality for sediment yield is reasonable with a NSE of 0.92 and a RMSE of 149 kg respectively. Predictions for runoff are less exact with a NSE of 0.53 and RMSE of 590 m^3. Predictions of the runoff volume for the event of February 28, 2017 are over-estimated indicating a possible under-estimation of re-infiltration processes.

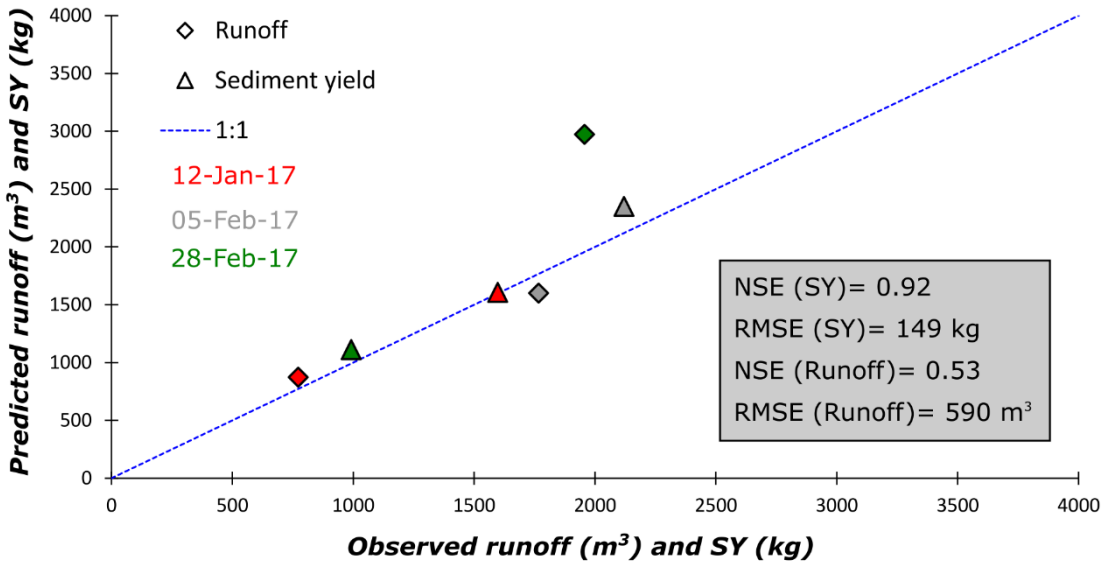

Fig. 36 : Results of the model predictions and comparison to the observed sediment yield (kg) and runoff (m^3). The 1:1 curve indicates that predicted data closed to the dotted line fits closely to the observed data.

3.4 Spatial variability of hydro-sedimentary transfers

The model simulations show evidence of the spatial variability for the three selected erosive events (Fig.37) and the localization of erosion processes is consistent with observations in the field. For the event of January 12, 2017, hydro-sedimentary transfer occurs in the western part of the catchment. Parcels n°10, 11, and 14 are affected by diffuse erosion leading to concentrate erosion in one ephemeral gully crossing parcels n°2, 3, and 6. Diffuse erosion processes occur in the parcels with the lowest crop cover percentage (< 20%) and an advanced state of degradation (F2; see Fig. 3.5). For the event of February 5, 2017, there are residual diffuse processes in the parcels previously cited and thus two ephemeral gullies are active. A new ephemeral gully appears in the North-Eastern

part of the catchment on parcel n°5 because of the degradation of the soil surface state and reduced roughness (0-1 cm). For the event of February 28, 2017 erosion processes occur in the major part of the catchment. Diffuse erosion processes are observed in parcels n°11, 14, 3, and 5. Concentrated erosion is assured by the two ephemeral gullies previously observed. Considering these simulations, parcels with different soil surface characteristics exhibits different protection to soil erosion. This leads to a spatial heterogeneity of the sediment export on the catchment.

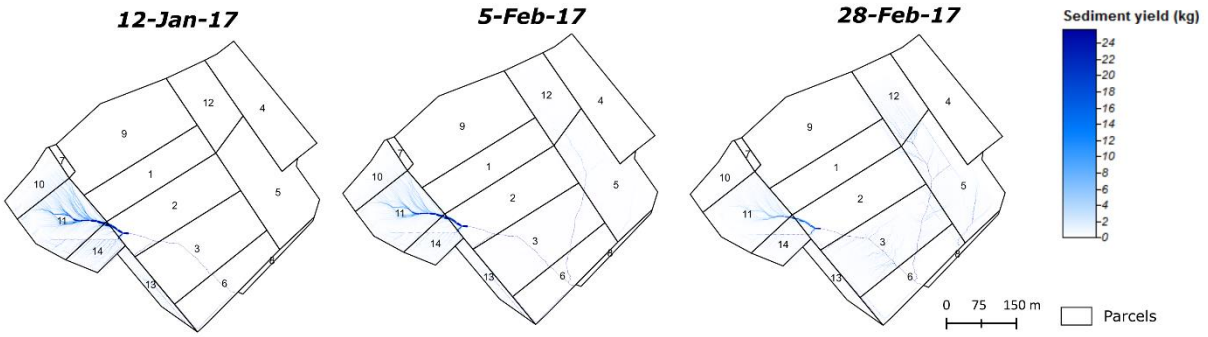

Fig. 37 : Spatially distributed results of the model simulations for the three erosive events showing spatial variability of erosion processes.

3.5 Parcels erodibility

Soil erodibility was evaluated for each event and for each parcel using the predicted SSY. For the event of January 12, 2017, the mean SSY for the entire catchment was predicted to 2.97 t km^{-2} and ranges from 0 to 76 t km^{-2} at the parcel scale. For the event of February 5, 2017, the mean SSY for the entire catchment was predicted to 4.35 t km^{-2} and range from 0 to 11.5 t km^{-2} at the parcel scale, and for the event of February 28, 2017, the mean SSY for the entire catchment was predicted to 2.05 t km^{-2} and ranges from 0 to 6.3 t km^{-2} at the parcel scale. The results show evidence of major spatial variabilities although only a few parcels exhibit a huge erosion capacity. Spatial variabilities of SSY are represented in the catchment in Figure 38. To facilitate the comparison, SSY were distinguished into 3 classes (0-1; 1-6 and > 6 t km^{-2}). The event of January 12, 2017 shows the highest number of parcels with a SSY > 6 t km^{-2}, suggesting a strong and localized remobilization of sediment during this event. The event of February 5, 2017 shows the same characteristics except that the SSY

of parcel n°3 is drastically decreased. A large part of the sediment of this parcel must have been already remobilized during the previous event and the stock of erodible sediment was reduced. Finally, the event of February 28, 2017 showed a decrease of the SSY for parcel n° 11, 14, and 13, probably due to an increase of the crop cover and thus an unavailability of easily mobilizable sediment. Parcel n°3, 12, and 5 show evidence of an increase of the SSY probably due to a higher roughness and soil surface state decrease. The stock of erodible sediment was also probably elevated due to the sediment displacement during the previous runoff event.

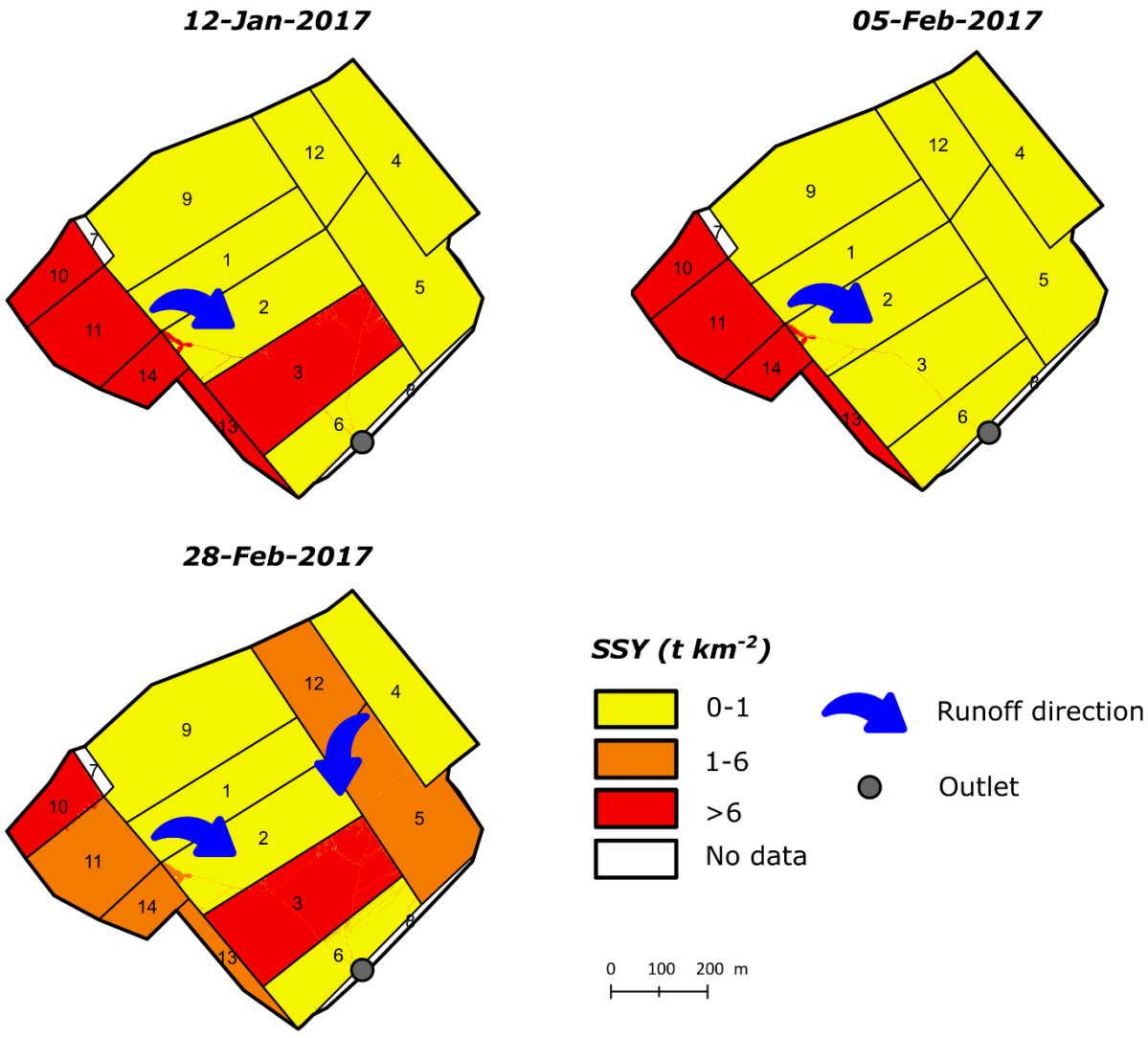

Fig. 38 : Specific sediment yield (t km^{-2}) distinguished into 3 classes on the Pommeroye catchment that allows direct comparison between the different parcels for the three erosive events.

3.6 Evaluation of sediment-trapping efficiency

Efficiency of future ECM on the catchment was simulated using an additional module of the *WATERSED* model. Results show evidence of high trapping efficiency for 2 out of 3 events (Fig.39). For the event of January 12, 2017, the sediment yield was simulated to 1605 kg without ECM and to 253 kg with ECM. Trapping efficiency was particularly high for this event and reached 84%. In February 05, 2017, the sediment yield was first predicted to 2349 kg without ECM and to 767 kg with ECM. Sediment trapping was lower than for the previous event but still efficient and reached 67%. Finally, the last event of February 28, 2017 showed no difference with or without ECM. The predicted sediment yield was the same and evaluated to 1110 kg. Major differences in sediment trapping efficiency could be due to sediment concentration during the runoff event. For the two first events, the sediment concentration was particularly high and reached values > 3 g L^{-1} which correspond to the threshold for transport capacity of ECM. For these two events, runoff water with sediment concentration > 3 g L^{-1} was automatically filtered by the ECM. For the last event, the sediment concentration for runoff water was much lower and did not reach values > 3 g L^{-1}. The principal consequence is that the transport capacity of the runoff water in front and behind ECM is the same. In this case, sediment trapping was unsuccessful.

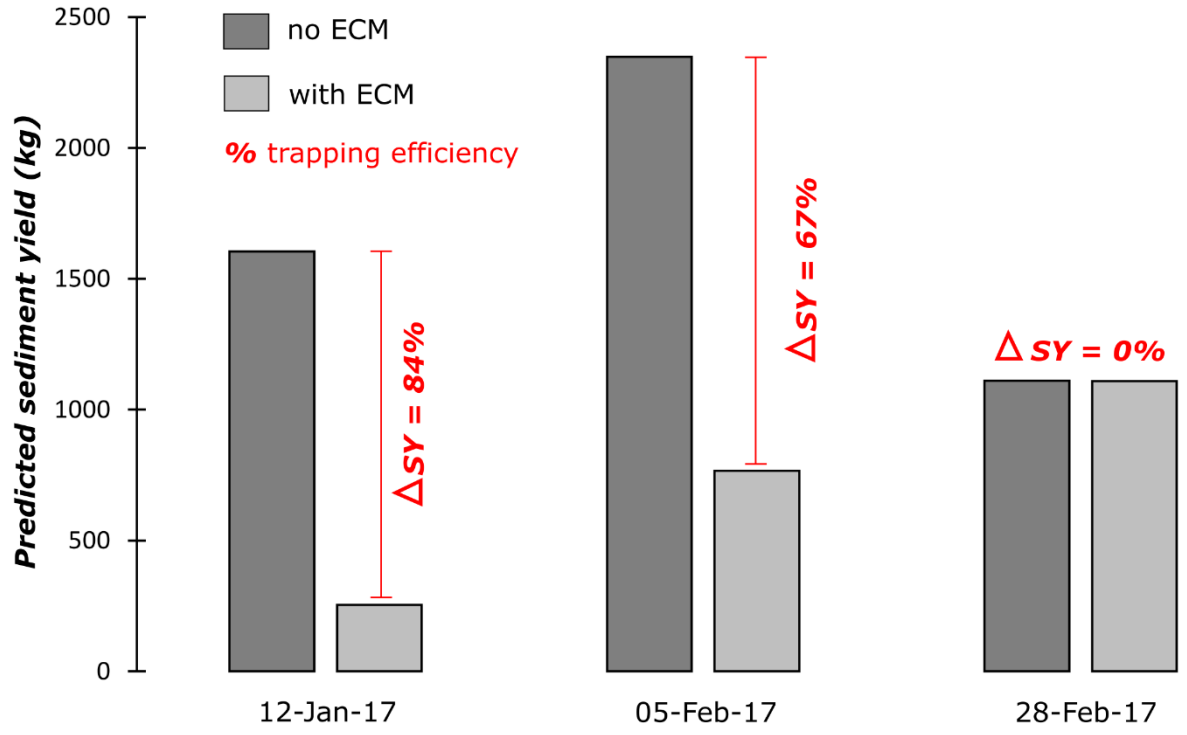

Fig. 39 : Results of the sediment yield model predictions (kg) with/without erosion control measure on the Pommeroye catchment for the three rainfall events.

4. Discussion

Simulations of erosion/runoff and ECM efficiency were done on the agricultural catchment of the Pommeroye using the selected erosive events occurring in 2017. The calibration of the *WATERSED* model was possible on these unique rainfall events. Although the small number of studied events, the use of the *WATERSED* model could be well demonstrated, as a high NSE and low RMSE were observed for the predicted values. Considering that the model is very sensitive and that the calibration is an important step, high quality of input data is needed. Thus, detailed field observations of parcel characteristics were chosen. One main inconvenience of using field observations is that only 3 out of 8 days of observations could have been used, considering that rainfall events usually do not occurred on the entire time frame. But field observations offer high-quality of inputs for the model. The use of field observations differs from other previous studies which use a more general plot calendar (e.g. Evrard et al., 2010). In the latter study, it appears that the use of the employed type of calendar may have some limitations; parcels with the same crop type can show different growth over time. For example, in the Pommeroye catchment, two

comparable parcels with wheat do not evolve in a same way (e.g. parcel 5 and 11; Fig. 3.5). This largely influences the model results since sediment transport parameters are strongly based on the soils characteristics.

Our study considers a soil surface condition over a given period. Yet, farmers are implementing crop rotations. It would be interesting to simulate new erosive events considering another crop rotation. This would allow confirming the *WATERSED* model calibration and help to observe the spatial and temporal variability of hydro-sedimentary transfer. As observed in *Patault et al. (2018 in review)*, the transfer is highly variable and shows a strong heterogeneity between two years of monitoring. The quantity of exported sediment is much larger over the period March 2017-March 2018 and the events occurred in a more limited time frame. Soil degradation must have been faster compared to the previous year. Moreover, diffuse and concentrate erosion may have present at different locations in the catchment. Further simulations could confirm these assumptions.

One main advance of our study is the use of high-resolution DEM. Lidar data at 50 cm resolution were used compared to other studies that mainly used meter resolution data (Ciampalini et al., 2012; Hessel et al., 2006). One main advantage is that the pixel used is adapted to the size of the ECM. If the structure were smaller than the pixel, it would be necessary to interpolate the transport/infiltration capacity between these two elements (Landemaine, 2016).

Moreover, high-resolution data can guarantee a correct location of the ECM. As observed for the event of February 28, 2017, fascine locations were not efficient at some places (Fig.40). The future management plan should be revised to capture most of the hydro-sedimentary transfer. Few ECM were not efficient for the selected erosive event. Further simulations are needed with different land cover to see in which case they could be more efficient.

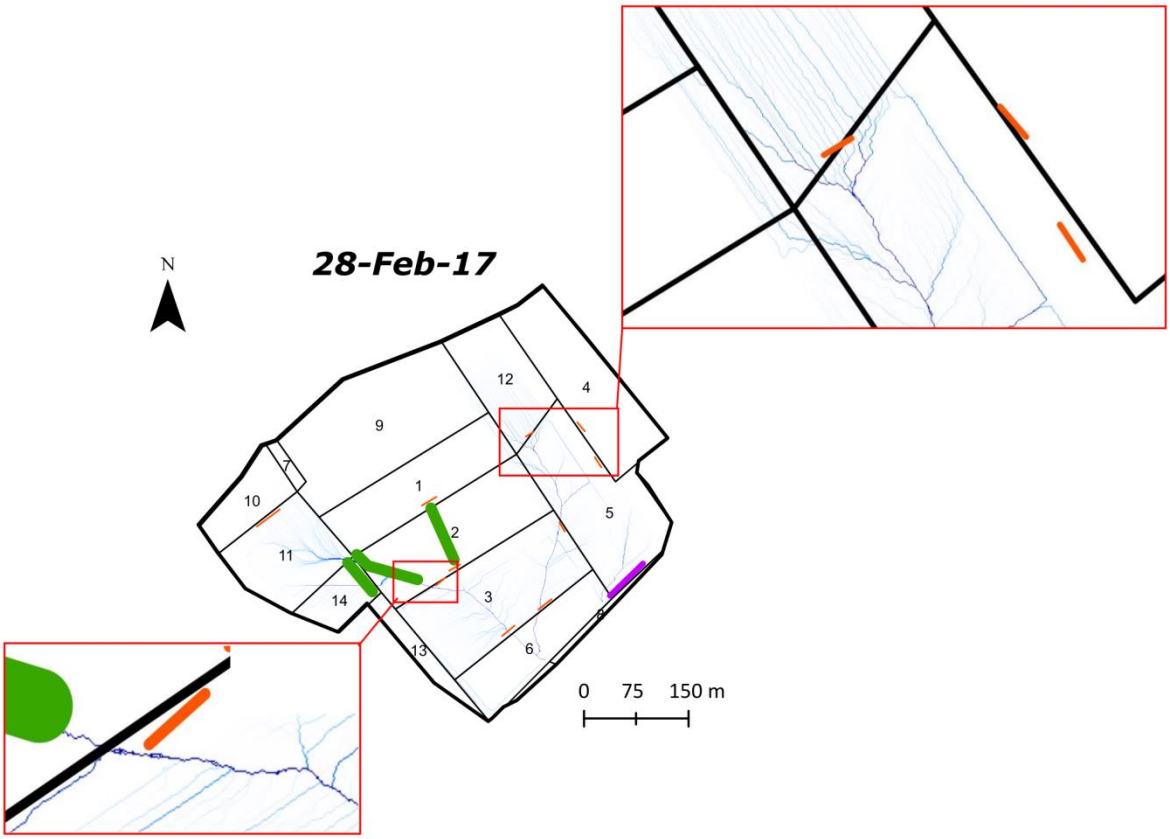

Fig. 40 : Results of predicted hydro-sedimentary transfer for the event of February 28, 2017. Red square allows visualizing that few fascines were misplaced.

The future management plan for ECM appears to be most effective when events are significant and sediment concentrations reach high values. Similar observations were made by Landemaine (2016). The efficiency is in the same range than those observed by the *Association de recherche sur le Ruissellement, l'Erosion et l'Aménagement du Sol (AREAS)* in Normandy (Ouvry et al., 2012; Richet et al., 2017). However, this approach does not consider the quality of the ECM. Indeed, the ECM such as fascines requires special maintenance. Frankl et al. (2017) emphasized on the Aa river catchment in Northern France that fascines badly maintained do not play their role as sediment retainers and their lifespan does rarely exceed 4 years. Richet et al. (2017) observed in Normandy that effectiveness of ECM decreased as sedimentary material is accumulated and notice that a fascine can be filled up during one major event. We suggest that these effects should be considered in the modeling, through a dynamic quality criterion of the ECMs that would impact the transport/infiltration capacity of the ECM.

5. Conclusion

In this study, the non-dynamic raster-based and spatially distributed *WATERSED* model was used to simulate runoff and erosion and to test the efficiency of a future management plan of erosion control measures in the small agricultural catchment of the Pommeroye situated in Northern France. After a calibration phase, the model tends to reasonably reproduce the hydro-sedimentary transfer for the studied erosive events. Comparison to observed data recorded by a monitoring station at the outlet of the studied catchment showed good predictions of the model (NSE = 0.53-0.92; RMSE = 590 m^3 and 149 kg). Moreover, the localization of the sediment transfer provided by the model is concordant with our field observations. Soil erodibility on the parcels was evaluated and ranges from 0 to 76 t km^{-2} $event^{-1}$ which is particularly high. Spatial variabilities of hydro-sedimentary transfers in the catchment were observed due to changes in the soil surface state over time (e.g crop cover, roughness, and state of degradation). Finally, the simulations of the future management plan for erosion control were effective for 66% of the events and reached 84% of sediment trapping efficiency. These results confirm the recent success of land management efforts to reduce soil erosion. In perspective, high-frequency monitoring and follow up simulations are needed after the installation of the ECM to validate experimentally the predictions of the model.

Acknowledgements

This work was financially supported by the Mines-Telecom Institute of Lille-Douai, with additional funding provided by the Water Agency of Artois-Picardie (QUASPER project). We would also like to acknowledge technical support from Emilie Delattre and Jordan Délépine (SYMCEA) and François Derancourt (regional Chamber of Agriculture Nord-Pas-de-Calais, France). Authors are grateful to the Pas-de-Calais departmental territory and sea office (DDTM62) who provided the high-resolution DEM (Lidar).

References

Alexandre, H. (2015). *Quantification de l'efficacité des fascines : diagnostic initial du bassin versant de la Pommeroy et paramétrage d'un modèle de ruissellement/érosion*.

Beckelynck, J. (1981). *Traitement régionalisé des paramètres contribuant à la gestion des nappes: application à la modélisation de la nappe de la craie dans le bassin de l'Aa et de la moyenne Lys*. Université des Sciences et Techniques de Lille. Retrieved from https://ori-nuxeo.univ-lille1.fr/nuxeo/site/esupversions/1ea8eb07-e140-446e-be38-7383cefdb7fc

Cerdan, O., Bissonnais, Y. Le, Couturier, A., & Saby, N. (2002). Modelling interrill erosion in small cultivated catchments, *3226*(June 2001), 3215–3226. https://doi.org/10.1002/hyp.1098

Cerdan, O., Le Bissonnais, Y., Souchère, V., Martin, P., & Lecomte, V. (2002). Sediment concentration in interrill flow: Interactions between soil surface conditions, vegetation and rainfall. *Earth Surface Processes and Landforms*, *27*(2), 193–205. https://doi.org/10.1002/esp.314

Cerdan, O., Souchère, V., Lecomte, V., Couturier, A., & Le Bissonnais, Y. (2001). Incorporating soil surface crusting processes in an expert-based runoff model: Sealing and transfer by runoff and erosion related to agricultural management. *Catena*, *46*(2–3), 189–205. https://doi.org/10.1016/S0341-8162(01)00166-7

Ciampalini, R., Follain, S., & Le Bissonnais, Y. (2012). LandSoil: A model for analysing the impact of erosion on agricultural landscape evolution. *Geomorphology*, *175–176*, 25–37. https://doi.org/10.1016/j.geomorph.2012.06.014

Couturier, A., Daroussin, J., Darboux, F., Souchère, V., Le Bissonnais, Y., Cerdan, O., & King, D. (2013). Improvement of surface flow network prediction for the modeling of erosion processes in agricultural landscapes. *Geomorphology*, *183*, 120–129. https://doi.org/10.1016/j.geomorph.2012.07.025

Evrard, O., Bielders, C. L., Vandaele, K., & van Wesemael, B. (2007). Spatial and temporal variation of muddy floods in central Belgium, off-site impacts and potential control measures. *Catena*, *70*(3), 443–454. https://doi.org/10.1016/j.catena.2006.11.011

Evrard, O., Cerdan, O., van Wesemael, B., Chauvet, M., Le Bissonnais, Y., Raclot, D., … Bielders, C. (2009). Reliability of an expert-based runoff and erosion model: Application of STREAM to different environments. *Catena*, *78*(2), 129–141. https://doi.org/10.1016/j.catena.2009.03.009

Evrard, O., Nord, G., Cerdan, O., Souchère, V., Le Bissonnais, Y., & Bonté, P. (2010). Modelling the impact of land use change and rainfall seasonality on sediment export from an agricultural catchment of the northwestern European loess belt. *Agriculture, Ecosystems and Environment*, *138*(1–2), 83–94. https://doi.org/10.1016/j.agee.2010.04.003

Evrard, O., Persoons, E., Vandaele, K., & Wesemael, B. Van. (2007). Effectiveness of erosion mitigation measures to prevent muddy floods : A case study in the Belgian loam belt, *118*, 149–158. https://doi.org/10.1016/j.agee.2006.02.019

Frankl, A., Prêtre, V., Nyssen, J., & Salvador, P.-G. (2017). The success of recent land management efforts to reduce soil erosion in northern France. *Geomorphology*, *303*, 84–93. https://doi.org/10.1016/j.geomorph.2017.11.018

Gilley, J. E., Kottwitz, E. R., & Wieman, G. a. (1991). Roughness Coefficients for Selected Residue Materials. *Journal of Irrigation and Drainage Engineering*, *117*, 503–514.

https://doi.org/10.1061/(ASCE)0733-9437(1991)117:4(503)

Govers, G. (1992). Relationship between discharge, velocity and flow area for rills eroding loose, non-layered materials. *Earth Surface Processes and Landforms*, *17*(5), 515–528. https://doi.org/10.1002/esp.3290170510

Hessel, R., van den Bosch, R., & Vigiak, O. (2006). Evaluation of the LISEM soil erosion model in two catchments in the East African Highlands. *Earth Surface Processes and Landforms*, *31*(4), 469–486. https://doi.org/10.1002/esp.1280

Landemaine, V. (2016). *Érosion des sols et transferts sédimentaires sur les bassins versants de l'Ouest du Bassin de Paris : analyse, quantification et modélisation à l'échelle pluriannuelle*. Université de Rouen Normandie.

Le Bissonnais, Y., Cerdan, O., Lecomte, V., Benkhadra, H., & Martin, P. (2005). Variability of soil surface characteristics influencing runoff and interrill erosion. *Catena*, *62*, 111–124. https://doi.org/10.1016/j.catena.2005.05.001

Ludwig, B., Boiffin, J., Chaduf, J., & Auzet, A. V. (1995). Hydrological structure and erosion damage caused by concentrated flow in cultivated catchments. *Catena*, *25*(1–4), 227–252. https://doi.org/10.1016/0341-8162(95)00012-H

Melesse, A., & Graham, W. (2004). Storm Runoff Prediction Based on a Spatially Distributed Travel Time Method Utilizing Remote Sensing and Gis1. *Journal of the American Water Resources Association*, *9007*, 863–879. https://doi.org/10.1111/j.1752-1688.2004.tb01051.x

Merritt, W. S., Letcher, R. A., & Jakeman, A. J. (2003). A review of erosion and sediment transport models. *Environmental Modelling and Software*, *18*(8–9), 761–799. https://doi.org/10.1016/S1364-8152(03)00078-1

Muzik, I. (1996). GIS Derived Distributed Unit Hydrograph, a New Tool for Flood Modeling. *Water Resources*, *1*(235), 243–247. https://doi.org/10.4203/ccp.30.10.2

Nachtergaele, J., Poesen, J., & Govers, G. (2002). Ephemeral gullies a spatial and temporal analysis of their characteristics, importance and prediction. *Eeen Ruimtelijke En Temporele Analyse van de Karakteristieken, Het Belang En de Voorspelling van Tijdelijke Ravijnen*, (2), 159–182. https://doi.org/10.4000/belgeo.16167

Nash, J. E., & Sutcliffe, J. V. (1970). River Flow Forecasting Through Conceptual Models Part I-a Discussion of Principles*. *Journal of Hydrology*, *10*, 282–290. https://doi.org/10.1016/0022-1694(70)90255-6

Ouvry, J. F., Coufourier, N., Richet, J. B., Lhériteau, M., Pivain, Y., Martin, P., … Luce, M. (2012). Maîtrise du ruissellement et de l'érosion des sols en Haute-Normandie. Expérimentations sur les pratiques culturales 2001-2010. Synthèse des résultats de ruissellement et d'érosion. Groupe Maîtrise du ruissellement par les pratiques culturales., 36.

Poesen, J. (2018). Soil erosion in the Anthropocene: Research needs. *Earth Surface Processes and Landforms*, *43*(1), 64–84. https://doi.org/10.1002/esp.4250

Richet, J. B., Ouvry, J. F., & Saunier, M. (2017). The role of vegetative barriers such as fascines and dense shrub hedges in catchment management to reduce runoff and erosion effects: Experimental evidence of efficiency, and conditions of use. *Ecological Engineering*, *103*, 455–469. https://doi.org/10.1016/j.ecoleng.2016.08.008

Souchère, V., Cerdan, O., Ludwig, B., Le Bissonnais, Y., Couturier, A., & Papy, F. (2003). Modelling ephemeral gully erosion in small cultivated catchments. *Catena*, *50*(2–4), 489–505. https://doi.org/10.1016/S0341-8162(02)00124-8

Souchere, V., King, D., Daroussin, J., Papy, F., & Capillon, A. (1998). Effects of tillage on runoff directions: Consequences on runoff contributing area within agricultural catchments. *Journal of Hydrology*, *206*(3–4), 256–267. https://doi.org/10.1016/S0022-1694(98)00103-6

van Oost, K., van Rompaey, A., Poesen, J., Govers, G., & Verstraeten, G. (2002). Evaluating an integrated approach to catchment management to reduce soil loss and sediment pollution through modelling. *Soil Use and Management*, *18*(4), 386–394. https://doi.org/10.1079/SUM2002150

Viel, V. (2012). *Analyse spatiale et temporelle des transferts sédimentaires dans les hydrosystèmes normands. Exemple du bassin versant de la Seulles. Geography.* Université de Caen - Basse-Normandie.

Wang, L., & Liu, H. (2006). An efficient method for identifying and filling surface depressions in digital elevation models for hydrologic analysis and modelling. *International Journal of Geographical Information Science*, *20*(2), 193–213. https://doi.org/10.1080/13658810500433453

Chapter 4

Quantification of sub-basin contributions using a confluence-based sediment fingerprinting approach on the Canche river catchment (Northern France).

Résumé étendu – Chapitre 4

Contexte

Connaître l'origine des transferts sédimentaires dans un bassin versant est un élément de réflexion essentiel pour les gestionnaires. Ces informations permettent de localiser et d'appréhender les zones les plus sensibles à l'érosion, et de mettre en place des plans de lutte efficaces. Depuis quelques années, les avancées scientifiques relatives à ce sujet ont permis l'essor de techniques de traçage de sources. Ces approches, communément appelées « sediment fingerprinting » permettent de quantifier les contributions des sources de sédiments au flux sédimentaire, de la section de rivière à l'échelle du bassin versant. Elles consistent à diagnostiquer les signatures géo-physico-chimiques des sources de sédiments et à les comparer à celles du matériel sédimentaire en transit. Via des méthodes d'analyses statistiques multivariées, il est possible d'identifier des traceurs préférentiels qui permettent une distinction des différentes sources entre elles. L'injection de ces traceurs dans un modèle de mélange permet alors de simuler et de quantifier les contributions des différentes sources au flux sédimentaire. Toutefois, la communauté scientifique a soulevé quelques limitations à ces approches. Ces limitations sont liées : (i) au choix des traceurs : il a été démontré que l'utilisation d'un nombre limité de traceurs pouvait conduire à des incertitudes sur les simulations ; (ii) à l'aspect conservatif des traceurs : prérequis pour ce type d'approche et qui nécessite donc une longue procédure pour la sélection des traceurs pertinents et (iii) l'existence d'une « black-box », qui rend compte d'une réelle méconnaissance des processus de dépôt/stockage sédimentaire dans les voies de transfert entre les sources et les matières en transit. Face à ces questions, de nouvelles approches dites de « confluence tracing » émergent. Le concept, similaire à la première approche, consiste à échantillonner les différents exutoires des affluents d'un bassin versant et de les considérer comme des sources potentielles pour les sédiments collectés aux confluences. L'effet escompté étant de s'affranchir des principaux biais liés à la différence de taille des particules. Les objectifs de cette étude sont alors d'évaluer la contribution des différents sous-bassins versants au flux sédimentaire de la Canche à travers une approche dite de « confluence-based sediment fingerprinting » (à savoir

l'étude comparée des cortèges géochimiques de matières en suspension (MES) des affluents avec ceux obtenus à leurs confluences). Cette approche doit nous permettre une meilleure connaissance des affluents les plus productifs en termes de matière érodée et donc *in-fine* d'analyser la pertinence des plans d'action de lutte contre l'érosion déployés ces dernières années sur le territoire de la Canche.

Matériel et Méthodes

Pour répondre aux objectifs de l'étude, plusieurs campagnes d'échantillonnage de MES ont été entreprises sur le bassin versant de la Canche. Les MES ont été récoltées avec des pièges à sédiments sur l'ensemble des exutoires des sous-bassins versant de la Canche et aux différentes confluences pendant cinq périodes d'échantillonnage (prise en compte de la variabilité saisonnière). Les MES ont ensuite été caractérisées (granulométrie, chimie élémentaire : majeurs et traces) et l'ensemble du jeu de données a été injecté dans le modèle *Set_Sat-v1.0*. C'est un modèle de « sediment fingerprinting » récemment développé par l'USGS qui permet de quantifier les contributions relatives des sources au flux sédimentaire. Le modèle se veut intuitif et facile à prendre en main, les calculs sont réalisés avec le logiciel *R* sous une interface *Windows Access*. Au travers d'une procédure d'analyses statistiques robuste (recherche d'éventuels outliers, test de conservativité, analyse factorielle discriminante), le modèle est capable d'identifier un composé optimal (constitué de différents traceurs significatifs) qui permet d'évaluer la contribution des sources aux flux de MES. Les contributions relatives sont alors quantifiées via un modèle de mélange et les potentielles incertitudes associées sont évaluées via des simulations Monte-Carlo. Les contributions relatives permettent alors d'évaluer les flux érosifs annuels des différents sous-bassins versants. Connaissant les quantités de sédiments exportées pour chaque sous-bassin versant et la localisation des dispositifs anti-érosion sur le territoire, il est alors possible d'évaluer la pertinence des actions entreprises ces dernières années.

Principaux résultats

La caractérisation physico-chimique des MES échantillonnées a montré deux points importants : d'une part, il n'existe pas de différence significative en termes de distribution granulométrique entre les affluents et les confluences, ce qui permet une comparaison directe des propriétés des échantillons et, d'autre part, les compositions élémentaires montrent des différences significatives qui rendent pertinente l'utilisation de ces traceurs. Les analyses statistiques ont montré qu'il n'existait pas d'outliers dans le jeu de données, mais que certains traceurs pouvaient être considérés comme non-conservatifs et que cela était dépendant du site d'échantillonnage. La recherche du meilleur composé de traceur par l'analyse factorielle discriminante révèle que les solutions optimales sont dépendantes des sites d'échantillonnage, et qu'entre 53 et 100% des échantillons sont correctement classés dans les groupes auxquels ils appartiennent (Fig.41). Les contributions relatives annuelles ont ainsi pu être quantifiées et montrent une forte influence de la Planquette et de la Créquoise.

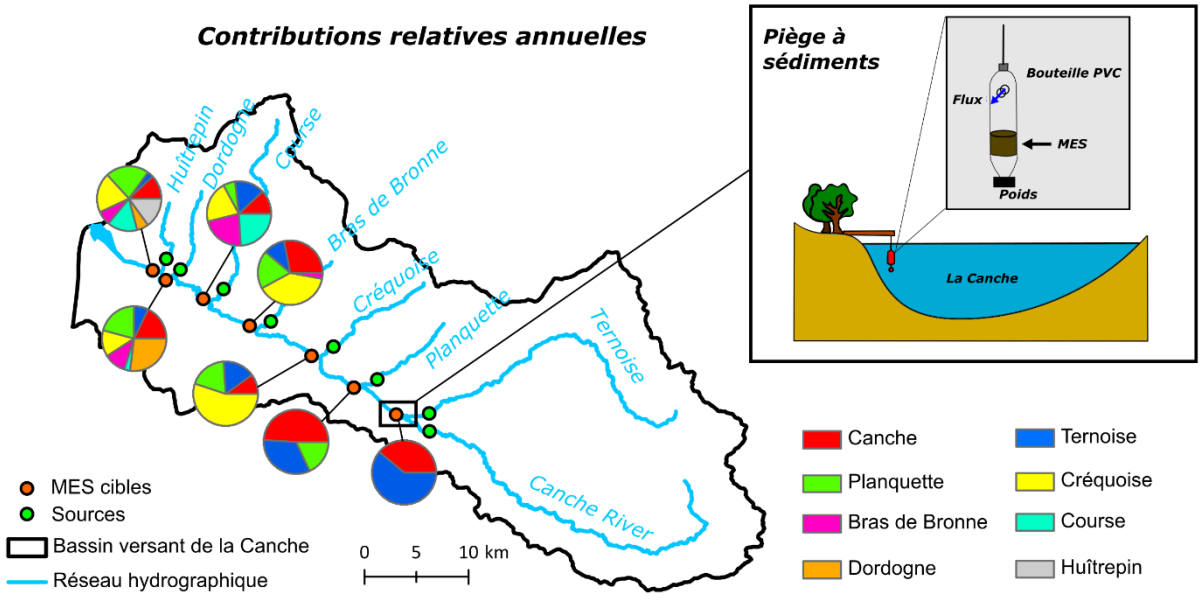

Fig. 41 : Stratégie d'échantillonnage et contributions relatives annuelles au flux sédimentaire calculées par le modèle *Sed_Sat-v1.0* sur le bassin versant de la Canche.

Des effets de dépôt/dilution du signal par les affluents avals sont présents le long du linéaire de la Canche, et de fortes variations temporelles (saisonnières) sont observées avec des fluctuations importantes dans la contribution relative des sources. Considérant le flux sédimentaire annuel de la

Canche depuis les années 2000, les flux sédimentaires des sous-bassins versants sont estimés entre 0,87 et 40,7 kt an^{-1}. La comparaison de ces valeurs avec le nombre d'aménagements anti-érosion par km² montre que les bassins versants les plus aménagés ont les flux sédimentaires moins élevés (Fig.42).

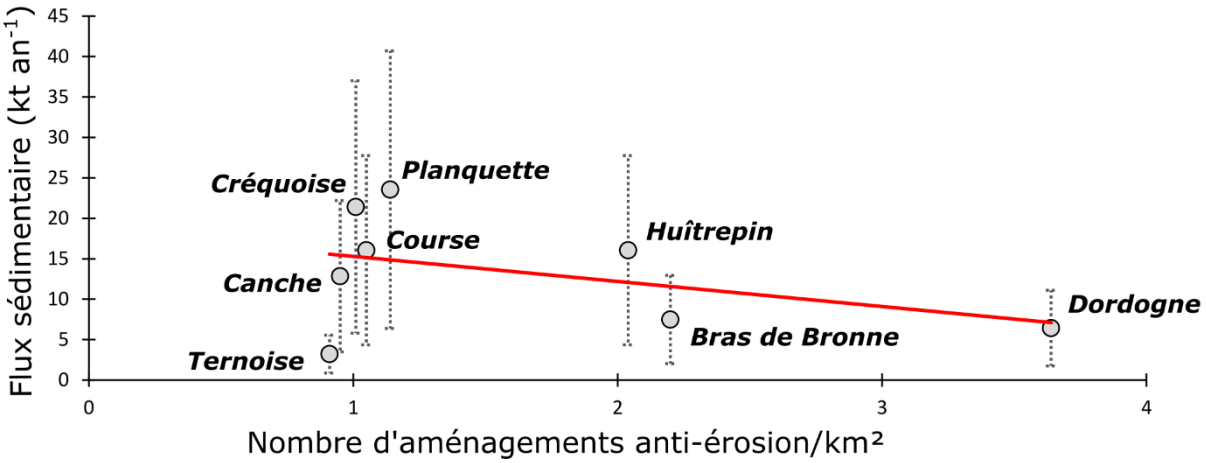

Fig. 42 : Relation entre le flux sédimentaire de chaque sous-bassin versant (kt an^{-1}) et le nombre d'aménagements « anti-érosion » par km². La ligne rouge indique la tendance (R = 0.41).

Conclusions

Les résultats de cette étude montrent qu'il est possible de quantifier les contributions relatives des différents sous-bassins versants de la Canche par une approche « confluence-based sediment fingerprinting » à partir de traceurs physico-chimiques. Cette approche a permis d'identifier des territoires plus enclins aux processus d'érosion où les futurs plans d'actions doivent se concentrer (Créquoise, Planquette). Les résultats semblent traduire également un impact potentiellement positif des politiques d'aménagements passées en matière de lutte contre l'érosion sur le territoire de la Canche.

Chapter 4: Quantification of sub-basin contributions using a confluence-based sediment fingerprinting approach on the Canche river catchment (Northern France).

Edouard Patault[a,b], Claire Alary[a], Christine Franke[b], Nor-Edine Abriak[a]

[a]IMT Lille Douai, Univ. Lille, EA 4515 - LGCgE - Civil Engineering and Environmental Department, F-59000 Lille, France

[b]MINES ParisTech, PSL Research University, Center of Geosciences, 35 rue Saint-Honoré, 77305 Fontainebleau Cedex, France

This chapter is presented as an article in preparation for submission to the journal Science of the Total Environment.

Highlights

- Mass balance mixing model was applied using chemical sediment fingerprint.
- Tributaries contributions of the Canche river were quantified.
- Results confirm the efficiency of erosion control policies in Northern France.

Graphical abstract

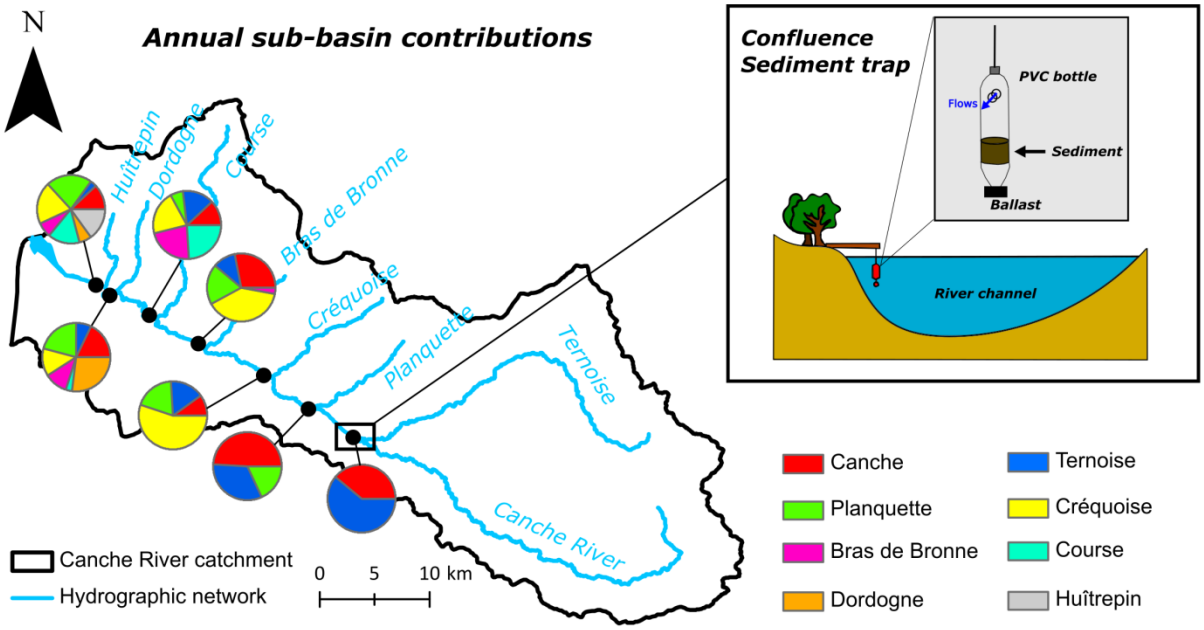

Abstract

Since a few years, land use management aims to reduce and control erosion effects in catchments but there is need for quantitative information on the sources of transported sediment. This information is particularly important because its lack can lead to the mis-implementation of erosion control measures. To address this request, a confluence-based sediment fingerprinting approach was tested on the Canche river catchment (1274 km²; northern France). Suspended sediments were collected during five seasonal sampling campaigns using sediment traps at the outlet of each tributary and at each confluence with the main stream of the Canche river. An optimum composite fingerprint was defined using physico-chemical and statistical analyses. Best tracer parameters for each tributary, were selected using stepwise discriminant function analyses. These parameters were introduced into a mass balance mixing model incorporating Monte-Carlo simulations to represent the uncertainty. Estimates of the overall mean contributions from each sub-basin were quantified at different temporal scales. The annual sediment flux sub-basin contributions ranged from 3 to 22% at the outlet of the Canche river, and annual sediment flux ranged from 0.87 to 40.7 kt yr^{-1}. The Planquette and the Créquoise tributaries appear to be the most erosive areas. On the contrary, sub-basins with the highest number of erosion control on their area, exhibit the lowest values of sediment flux. Our results tend to indicate a positive impact of recent land management policies in the studied watershed.

Keywords: sediment fingerprinting; physico-chemical tracers; sub-basin; sediment trap; unmixing model; Northern France; Canche river catchment

1. Introduction

Providing information on the origin of sediment transfer in river systems is essential for watershed management. This is a complex task considering that suspended material may come from different sources and their contribution may vary over time and space as a consequence of varying erosion processes (Haddadchi et al., 2013). Indirect approaches exist to identify sediment sources (fields surveys, river monitoring) but are complicated by spatial and temporal sampling problems (Collins & Walling, 2002). More recently, there has been a craze for the so-called "sediment fingerprinting" method (e.g. Collins et al., 2001; Evrard et al., 2011; Krein et al., 2003; Lamba et al., 2015; Martínez-Carreras et al., 2010; Motha et al., 2004; Walling & Woodward, 1992). These approaches attempt to quantify the contributions of sediment sources at variable spatial scales: from the river section to the watershed scale. The procedure consists of the characterization of the potential sediment sources by a comparison of their bio-geo-physico-chemical properties to the transported fluvial material. The properties that are suggested are sediment color (e.g. Krein et al., 2003; Martínez-Carreras et al., 2010; Poulenard et al., 2009), magnetic properties (e.g. Motha et al., 2004; Russell et al., 2001), chemical composition (e.g. Carter et al., 2003; Collins et al., 1997; Collins et al., 2012; Theuring et al., 2015), environmental radionuclides (e.g. Du & Walling, 2016; Evrard et al., 2013; Le Gall et al., 2016), and particle size (Krein et al., 2003).

There is a consensus that the use of a single parameter is not sufficient, and that a combination of tracers must be used to identify sediment sources (Collins & Walling, 2002; Walling et al., 1993). Because of the heterogeneity of catchments, the authors generally study a large panel of tracers and use statistical methods to identify the best combination of parameters that discriminates the sediment sources (e.g. Collins et al., 1997; Collins et al., 2012; Nosrati et al., 2018; Palazón et al., 2015). Selected data is injected in a mixing model to quantify the contribution of each source to the target sediment. The literature describes different forms of mathematical models for mixing models (Collins et al., 1997; Collins et al., 2010; Gellis & Walling, 2011; Haddadchi et al., 2013; Motha et al., 2003).

While the sediment fingerprinting method has largely contributed to the quantification of sources of sediment input for different watersheds around the world, recent discoveries showed that some scientific questions still need to be resolved (Smith et al., 2015). Few studies have shown that the selection of sources and sediment targets in a watershed may have important implications for the interpretation of the results. Highly erodible areas may have a disproportionate effect on tracer concentrations (Wilkinson et al., 2013) and nearby sources may have larger contributions for a given point on a river than distant sources (Haddadchi et al., 2015). It is also important to pre-identify the sources contributing to the sediment flux as an un-sampled source can strongly bias the results (Smith et al., 2015). Thus, the selection of tracers is an important point in this approach: uncertainties in the prediction of source contributions decrease by increasing the number of trace parameters (Sherriff et al., 2015). Predicted contributions may be different depending on the choice of tracers (Pulley et al., 2015). The conservative behavior of tracers may also introduce bias in interpretations (Sherriff et al., 2015) therefore a careful tracer selection procedure is recommended (Kraushaar et al., 2015). The type and the structure of the mixing model may also affect the results. Cooper et al. (2014) showed that the estimation of the source contributions varies up to 21% between the different models. (Laceby & Olley, 2015) suggested that correction factors (particle size or organic matter content) did not significantly improve the results.

Hence, the so-called “tributary tracing” or “confluence tracing” approaches were recently developed (Nosrati et al., 2018; Vale et al., 2016). The latter concept consists in the consideration of tributaries upstream sediments as potential sources for downstream sediments. This approach removes a significant proportion of the impact of potential chemical enrichment on sediments due to particle size variations (Laceby et al., 2017). It also reduces the impact of unknown effects of transport on particle signature (Koiter et al., 2013). Observations published by Fryirs et al. (2013) suggest that sedimentary transport pathways cannot be assumed to be directly connected between sources and outlets, but include barriers or buffers that may disrupt the sediment cascade.

In the Canche river catchment in Northern France, most natural hazards are related to mudflows and flooding. Mudflow causes significant damages to infrastructure that induce high economic costs. Since 2000, environmental policies are designed to reduce erosion by runoff in the Canche catchment by implementing hard and soft erosion control measures, such as dams, retention pools, ditches or fascines. However, so far few information is available on the evaluation of the efficiency of theses environmental policies.

The current study proposes to evaluate the contribution of sediment sources in the Canche river catchment in Northern France, using a confluence-based sediment fingerprinting approach. The goal is to quantify the contribution of the different tributaries draining the studied catchment and select the relevant tracers which provide source differentiation at each confluence. This work also tends to evaluate the effect of environmental policies on erosion reduction using the confluence-based sediment fingerprinting approach.

2. Material & Methods

2.1 Context of the Canche river catchment

The Canche river catchment (1274 km²; lat: 50°25'53''N, long: 2°02'24''E; Fig.43A) is in the European loess belt in Northern France and is characterized by oceanic climate conditions. The mean annual temperature is 11°C and the mean annual rainfall is 1000 ± 150 mm. Altitudes range from 0 m at the catchment outlet to 207 m in the upstream areas and catchment slopes are commonly in the range 2-3 % (Fig.43B). The watershed is characterized by a meandriform drainage network dominated by the Canche river (88 km) and seven tributaries. The basin drains Quaternary loess on the chalky grounds of Seno-Turonian. Mean annual discharge for the Canche river is estimated to 21 $m^3 s^{-1}$ with contributions from main sub-catchments: Ternoise (7 $m^3 s^{-1}$), Planquette (1.5 $m^3 s^{-1}$), Créquoise (2 $m^3 s^{-1}$), Bras de Bronne (2 $m^3 s^{-1}$), Course (4 $m^3 s^{-1}$), Dordogne (2.5 $m^3 s^{-1}$), and Huîtrepin (2 $m^3 s^{-1}$). Flow discharge was quantified using low-frequency monitoring station on the Ternoise, Course and Canche. Flow discharge for ungauged catchments was calculated assuming the

occurrence of similar rainfall and hydrological regime across the Canche catchment. Flow discharge was extrapolated from the closest monitoring station by multiplying the value by the appropriate fraction related to the ratio between the closest catchment area and the catchment area at the monitoring station. According to Andréassian et al. (2012), this method can provide interesting results for ungauged catchments. Cross validation with the high-frequency monitoring station on the Canche river evaluated a 17% error associated (*e.g.* Franke et al., 2018*; in review – see chapter 6*). The Canche river catchment is predominantly agricultural consisting of 80% arable lands (Fig.43C). The catchment is mainly affected by mudflows which induce an important economic cost for the local communities. Moreover, the land is affected by soil erosion leading to a highly variable specific sediment yield at the outlet of the river. The annual sediment export is evaluated to 29-185 kt from 1999 to 2016 (Agence de l'eau Artois-Picardie, 2016).

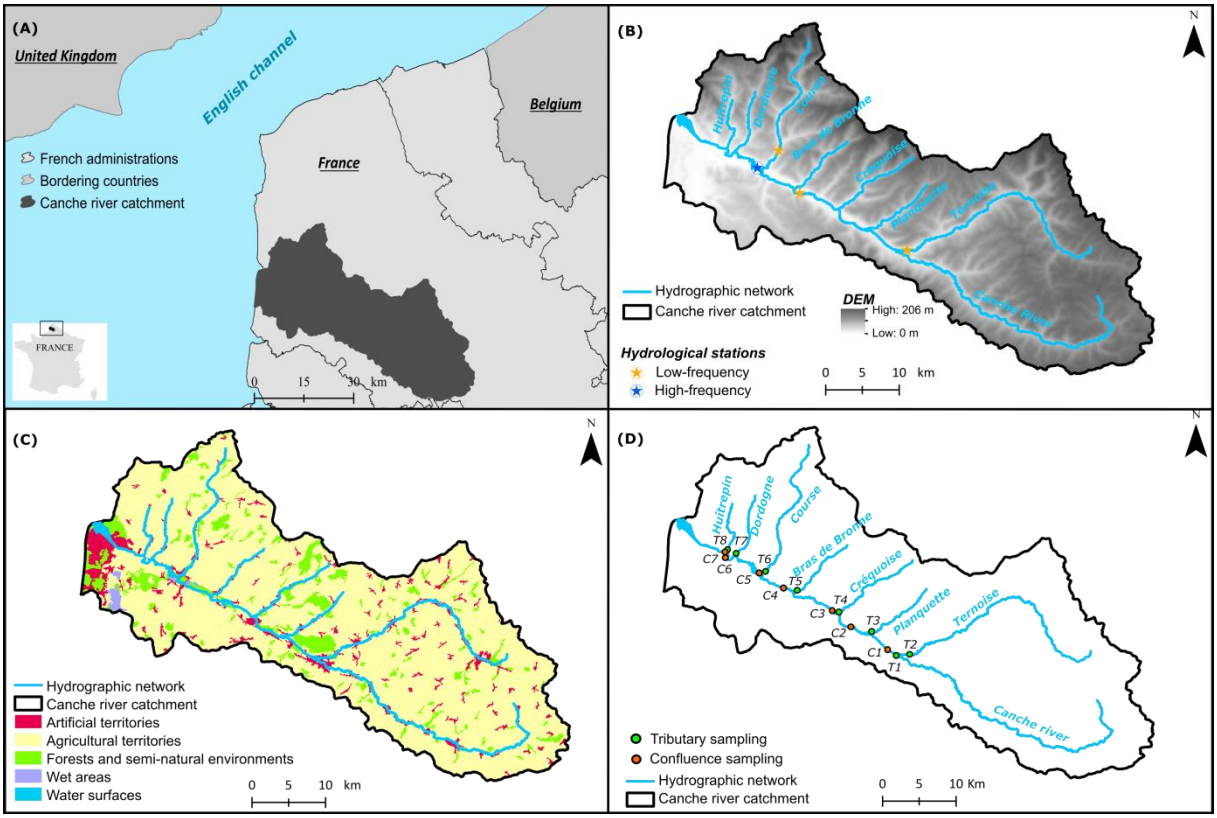

Fig. 43 : (A) Overview of the Canche river catchment, (B) Digital elevation model (DEM; m), hydrographic network and location of monitoring stations, (C) Corine Land Cover 2012 and (D) Location of sediment sampling for the study.

2.2 Sediment sampling

Suspended particulate matter (SPM) was collected using sediment traps installed at each tributary outlet and each confluence (Fig.43D). Sampling campaigns were conducted in winter 2015, winter 2016, spring 2016, summer 2016, and autumn 2016. A total of 65 samples was collected. More details on the sampling devices, exact sampling periods, and site positions are available in Figure 44 and Table 9.

The samples consisted of recently suspended solids transported in the different tributaries. Sediment was sampled using an experimental device adapted from previous studies (e.g. described by Tessier (2003) and Kayvantash et al. (2017)). The sediment traps (Fig.44) consist of 2 l polyethylene bottles, perforated at 5 cm from the top with two opposite bores (diameter 5 cm). The bottle is attached to the river bank with a rope and deposited in the channel. The device is hold in place using either an additional rope or a combination of rope and a wooden beam. The whole device is weighted vertically in the water column using ballast that is adapted to the river flow speed. Traps usually captured between 50 and 100 g of sediments during ~5-7 days water expose. Previous studies observed that there is no significant grain size selection depending on the position of the bottle in the river channel (Kayvantash et al., 2017).

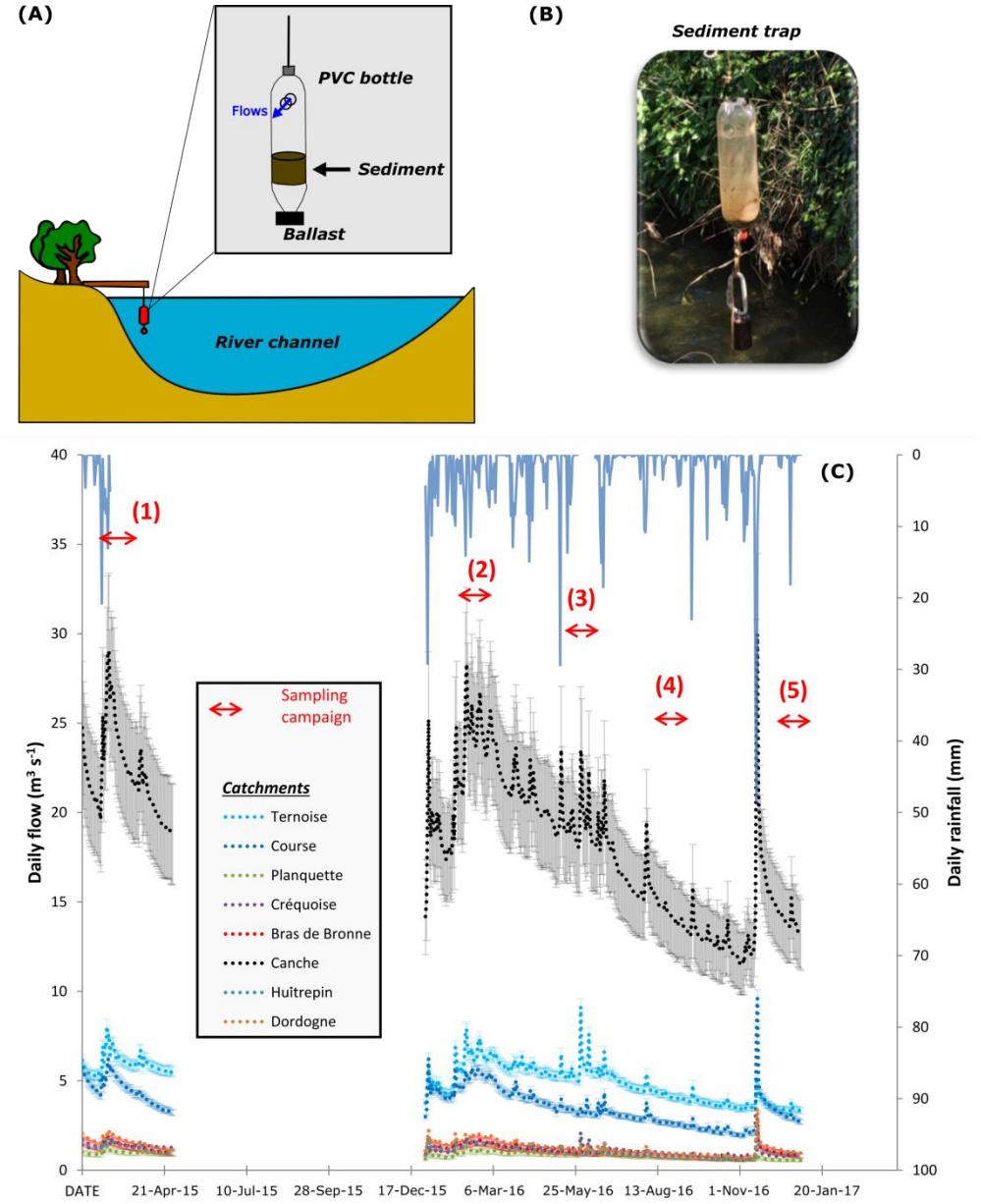

Fig. 44 : (A, B) Protocol and experimental device used to sample suspended particulate matter (SPM) for each tributary and confluence in the study, (C) temporal variability of the flow discharge in the Canche catchment during the five seasonal sampling campaign.

Tab. 9 : Location and sampling periods of the sediment traps.

Sample	Coordinates	Catchment	Sampling periods									
			1		2		3		4		5	
			Drop off	Recovery	Drop off	Recovery	Drop off	Recovery	Drop off	Recovery	Drop off	Recovery
T1	50°22’43.1’’N ; 2°01’03.5’’E	Canche	25-Feb-15	10-Mar-15	15-Feb-16	22-Feb-16	27-Apr-16	03-May-16	11-Jul-16	18-Jul-16	08-Nov-16	14-Nov-16
T2	50°22’47.6’’N ; 2°02’33.7’’E	Ternoise	25-Feb-15	10-Mar-15	22-Feb-16	02-Mar-16	27-Apr-16	03-May-16	11-Jul-16	18-Jul-16	08-Nov-16	14-Nov-16
T3	50°24’26.0’’N ; 1°58’11.0’’E	Planquette	25-Feb-15	10-Mar-15	15-Feb-16	22-Feb-16	27-Apr-16	03-May-16	11-Jul-16	18-Jul-16	08-Nov-16	14-Nov-16
T4	50°25’49.5’’N ; 1°54’23.2’’E	Créquoise	25-Feb-15	10-Mar-15	15-Feb-16	22-Feb-16	27-Apr-16	03-May-16	11-Jul-16	18-Jul-16	08-Nov-16	14-Nov-16
T5	50°27’22.0’’N ; 1°49’32.6’’E	Bras de Bronne	25-Feb-15	10-Mar-15	15-Feb-16	22-Feb-16	27-Apr-16	03-May-16	11-Jul-16	18-Jul-16	08-Nov-16	14-Nov-16
T6	50°28’40.9’’N ; 1°45’48.1’’E	Course	26-Feb-15	10-Mar-15	15-Feb-16	22-Feb-16	27-Apr-16	03-May-16	11-Jul-16	18-Jul-16	08-Nov-16	14-Nov-16
T7	50°30’01.4’’N ; 1°42’28.4’’E	Dordogne	26-Feb-15	10-Mar-15	16-Feb-16	23-Feb-16	27-Apr-16	03-May-16	11-Jul-16	18-Jul-16	08-Nov-16	14-Nov-16
T8	50°30’15.6’’N ; 1°41’30.5’’E	Huîtrepin	26-Feb-15	10-Mar-15	16-Feb-16	23-Feb-16	27-Apr-16	03-May-16	11-Jul-16	18-Jul-16	08-Nov-16	14-Nov-16
C1	50°23’09.0’’N ; 1°59’59.6’’E	Canche	25-Feb-15	10-Mar-15	15-Feb-16	22-Feb-16	03-May-16	09-May-16	18-Jul-16	26-Jul-16	08-Nov-16	14-Nov-16
C2	50°24’45.5’’N ; 1°55’43.3’’E	Canche	25-Feb-15	10-Mar-15	15-Feb-16	22-Feb-16	27-Apr-16	03-May-16	18-Jul-16	26-Jul-16	08-Nov-16	14-Nov-16
C3	50°25’57.2’’N ; 1°53’37.6’’E	Canche	25-Feb-15	10-Mar-15	22-Feb-16	02-Mar-16	27-Apr-16	03-May-16	11-Jul-16	18-Jul-16	08-Nov-16	14-Nov-16
C4	50°27’32.0’’N ; 1°47’58.7’’E	Canche	26-Feb-15	10-Mar-15	15-Feb-16	22-Feb-16	27-Apr-16	03-May-16	11-Jul-16	18-Jul-16	08-Nov-16	14-Nov-16
C5	50°28’41.1’’N ; 1°44’55.9’’E	Canche	26-Feb-15	10-Mar-15	22-Feb-16	02-Mar-16	27-Apr-16	03-May-16	11-Jul-16	18-Jul-16	08-Nov-16	14-Nov-16
C6	50°29’39.5’’N ; 1°41’11.8’’E	Canche	26-Feb-15	10-Mar-15	16-Feb-16	23-Feb-16	28-Apr-16	04-May-16	18-Jul-16	26-Jul-16	09-Nov-16	15-Nov-16
C7	50°30’05.4’’N ; 1°41’11.5’’E	Canche	11-Mar-15	1-Apr-15	16-Feb-16	23-Feb-16	28-Apr-16	04-May-16	12-Jul-16	19-Jul-16	09-Nov-16	15-Nov-16

2.3 Sedimentological and geochemical analysis

All samples were analyzed to obtain particle size distribution and elemental composition. Grain size analyzes were performed using a *Beckman Coulter LS 13320* laser particle sizer. All samples were initially oven-dried at 30°C for 72 h and sieved to 2 mm to remove any coarser debris that could distort further measurement. Two grams of sediment were mixed with 100 mL of ultrapure water and were stirred during 5 min to homogenize the sample. Each solution was analyzed in triplicates to validate the measurement. The analysis of the elemental composition was carried out after acid mineralization in a microwave oven. 22 reactors are used for mineralization. In 18 reactors, 0.250 g of a sample was poured, 2 reactors are used as references with TH2 (reference sediment material) to test the validity of the analysis by comparison with referenced measurements, and 2 blank reactors (without addition of solid material) are used to ensure non-contamination during preparation. For each reactor, 1 ml of nitric acid (HNO_3), 3 ml of hydrochloric acid (HCl), and 0.5 ml of water (H_2O) is added to the sediment. The determination of the major elements in the liquid phase (Al, Si, P, S, Ca, Fe, K, Mg, Na, Mn, Sr, Ti, Zn) was performed using an inductively coupled plasma atomic emission spectrometer (ICP-AES; *ICAP 7400 Thermo Fischer Scientific*). The determination of the trace elements (As, Cd, Co, Cs, Cu, La, Li, Mo, Ni, Pb, Rb, Sb, Se, Sn, Th, Tl, U, Bi, Cr, Sc, V, Ba, Ce) in the samples was carried out using an inductively coupled plasma mass spectrometer (ICP-MS; *PerkinElmer NexION 300x*).

2.4 Sediment fingerprinting procedure

The statistical model *Sed_Sat-v1.0* was developed by the USGS to quantify the relative contributions of sediment sources in a given watershed (Gorman Sanisaca et al., 2017). The model is written using the statistical software *R*[14] and utilizes *Microsoft Access®* as a user interface. The model uses a classical procedure of the sediment fingerprinting approach: (i) identification of outliers, (ii)

[14] R Core Team (2016). R: A Language and Environment for Statistical Computing. R Foundation for Statistical Computing, Vienna, Austria. URL https://www.R-project.org/.

evaluation of conservative behavior, (iii) identification of the tracers with the highest discriminatory potential and (iv) quantification of source contributions with a mixing model and a robust error analysis. The all-procedure is explained in detail in the following.

2.4.1 Test for univariate normal distribution

The first step evaluates the univariate distribution of each tracer in each source group. The Shapiro-Wilk test for normality is used to determine if the raw concentration values are normally distributed within each source group (Shapiro & Wilk, 1965). The p-value for rejecting the null hypothesis that the data is normally distributed is set to p-value > 0.05. If the tracer concentration values are normally distributed, the values are not transformed. If not, the values are transformed using the Tukey Ladder of Powers transformations (Table 4.2) and the respective transformation that yields the maximum Shapiro-Wilk p-value is selected (Tukey, 1977).

Tab. 10 : Tukey Ladder of Powers transformations used in the Sed_Sat-v1.0 model (Tukey, 1977).

Transformations						
x	x^2	$\sqrt[3]{x}$	$\frac{1}{x}$	$\sqrt{x}$	$\frac{1}{\sqrt{x}}$	$\log(x)$

2.4.2 Outlier test

The second step evaluates outliers in the source dataset. Outliers can bias the statistical tests, so the user decides whether to include samples containing outliers according to Eq.36:

$$x_i < \mu_{X_i} \pm N \times \sigma_{X_i} \; or \; x_i > \mu_{X_i} \pm N \times \sigma_{X_i} \tag{36}$$

Here x_i is the tracer value for tracer i in a given source group; X_i represents all tracer values for tracer i in a given source group; N is a multiple of the standard deviation from the mean value that defines an outlier; μ_{X_i} is the mean of X_i ; and σ_{X_i} is the standard deviation of X_i. N=3 is recommended as conservative definition of an outlier (Gellis et al., 2016).

2.4.3 Bracket test

The third step is used to determine if for any given tracer, the target samples lie within the range of the tracer concentration values in the source dataset. A condition for sediment fingerprinting is that the tracer concentration values in the target dataset must be conservative and do not change during transport (Walling et al., 2002). Any tracers that fail to satisfy this condition are considered non-conservative and removed from dataset. The Bracket test does not confirm the complete absence of tracer property transformations but, instead, provides a rudimentary screening for removing tracers undergoing significant changes during transport between upstream sources and downstream sediment sampling sites. To achieve this test, tracers must satisfy Eq.37:

$$\min(Y_i) - p \times \min(Y_i) < x_i < \max(Y_i) + p \times \max(Y_i) \quad (37)$$

Where x_i is the target tracer concentration value for tracer i; Y_i is the vector of all source tracer concentrations for tracer i; and p is the range set at 10%, which is generally within the analytical error of laboratory analyzes.

2.4.4 Stepwise Linear Discriminant Function Analysis (DFA)

The fourth step looks for the linear combination of tracer coefficients that discriminate best the source groups. The DFA is performed using the R-package *klaR* (Weihs et al., 2005). The function starts the tracer selection with the parameter that yields the greatest separation between the source groups and adds tracers using the Wilk's lambda criterion. The closer the Wilk's lambda statistic is to zero, the more significant a tracer's contribution is to the linear discriminant function. In addition, a cross validation procedure using *lda()* and *predict()* functions in the R-package *MASS* (Venables & Ripley, 2002) tests how well the group of tracers selected through the DFA classifies each source sample belonging to the known correct source group. Finally, weighting factors used in the mixing model are generated at this step to reflect the tracer discriminatory power. The tracer with the

lowest percentage of correctly classified source samples will have a weighting factor equal to one. The others are calculated using Eq.38:

$$W_i = \frac{P_i}{P_{opt}} \tag{38}$$

Where P_i is the percentage of correctly classified source samples using tracer i and P_{opt} is the percentage of correctly classified source samples using tracer with the lowest P_i.

2.4.5 Mixing model

The remaining set of tracers selected in the stepwise DFA is incorporated into a mixing model to estimate the relative proportion of sediment source contributions to the target sample. The unmixing model was developed and used by Collins et al. (2010). The model uses a set of linear equations for each composite signature by minimizing the sum of squares of the weighted relative errors according to Eq.39:

$$\sum_{i=1}^{n}\{[C_i - (\sum_{i=1}^{m} P_s S_i)]/C_i\}^2 W_i \tag{39}$$

Where C_i is the concentration of tracer i in the target sample; P_s is the optimized percentage of contribution source type (s); S_i is the mean concentration of tracer i in source s; W_i is the weighting factor for tracer i; n is the number of tracers comprising the optimum composite fingerprint; and m is the number of sediment source types.

The model adheres to two constraints that must be satisfied to produce realistic values, which are: each source group proportion is constrain to a positive value between 0 and 1, and is expressed as:

$$0 \leq P_s \leq 1 \tag{40}$$

And the sum of all source group contributions to be equal to 1, expressed as:

$$\sum_{s=1}^{n} P_s = 1 \tag{41}$$

2.4.7 Monte-Carlo simulations

Various sources of uncertainties need to be recognized when using the sediment fingerprinting approach to be able to quantify sub-basin contributions. Inclusion of these uncertainties in mass balance modelling indicated the possible range of the tributary contributions. Uncertainties were calculated using Monte-Carlo simulations. The set of linear equations representing the composite fingerprint identified for each confluence was solved N = 1000 times to compute ranges in tributary proportions. The mean of the 1000 mixing model result for each confluence sample define the tributary contribution and the standard deviation reflects the source uncertainty.

2.5 Efficiency of erosion control measures

Locations of erosion control measures (runoff retention pools, check dams, fascine, etc.) in the Canche river catchment were provided by the Chamber of Agriculture using the Database *RUISSOL*[15]. For each sub-basin, the number of erosion control measure was extracted. An Erosion Control Index, ECI_i, was calculated using the number of erosion control measures installed on each catchment divided by their respective area:

$$ECI_i = \frac{\sum_1^n ECM_i}{A_i} \tag{42}$$

[15] https://www.ruissol.pro/CGI/DLL.dll?APP=3&MODULE=Ruissol

With ECM_i the number of erosion control measures installed on the catchment i; and A_i the area of the catchment i in km². ECI_i was then compared to the annual sub-basin sediment yield (in kt) calculated using Monte-Carlo simulations.

3. Results

3.1 Sediment analysis

The particles size analysis highlights the absence of significant differences between the D50 (median particle size) of the tributaries (60.3 ± 6.7 µm) in comparison to the sediment sampled at each confluence in the Canche river (67.9 ± 10 µm; Fig.45; Table 29 and 30 – Appendices B). A t-test between the tributaries and the confluences did not show a significant difference between their D50 (p-value = 0.107). For further analyses, no particle size correction was applied considering that no significant particle size effect affects the direct comparison between tributaries and confluences samples.

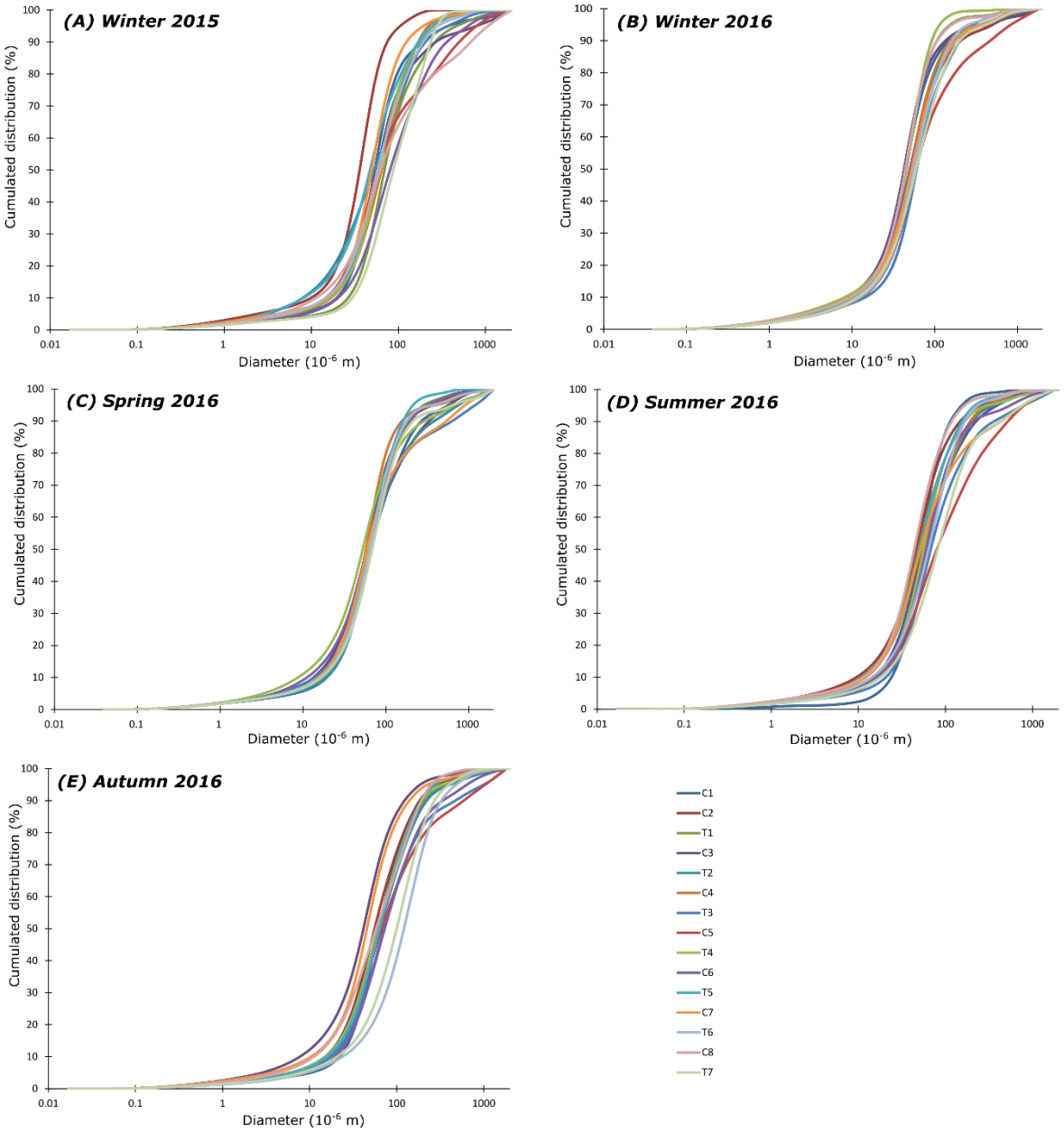

Fig. 45 : Grain size distribution for all samples collected in the Canche river catchment.

The geochemical analysis showed evidence of element concentration heterogeneity for the different sources (Fig.46). The range of element concentrations is particularly high for some major elements (Ca: 22054.9 – 42314 µg g^{-1}; S: 1013.4 – 4723.3 µg g^{-1}) and trace elements (Ce: 29.4 – 55 µg g^{-1}; La 16.6 – 30.7 µg g^{-1}). The element concentrations for the confluences are generally in the range of the values observed for the tributaries. Sometimes the range of the values for confluences is higher than the range for tributaries (Na, Ca, Sr, Cu Bi). Even though the Canche river catchment exhibits a homogeneous geology, major and trace elements seem to have a non-negligible potential

for discriminating sources and quantify their contribution to the suspended sediment sampled at each confluence. Considering this first approach, robust statistical analyses are needed to explore the entire dataset.

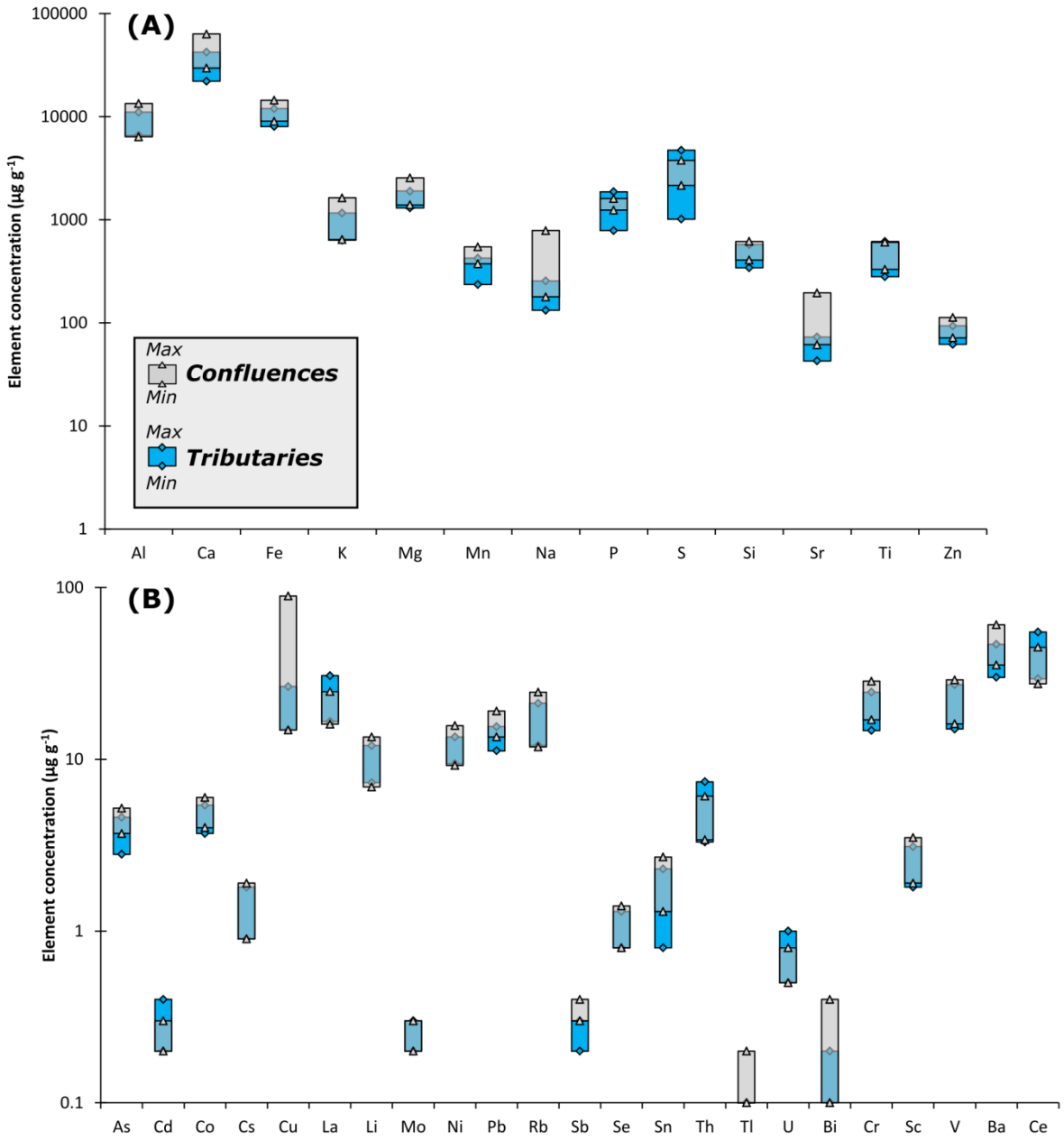

Fig. 46 : Range of concentrations (expressed in µg g^{-1}) of major elements (A) and trace elements (B) in the sediment trap samples during the five seasonal sampling campaigns.

3.2 Optimum composite fingerprint

The first analysis consisted in the identification of outliers in the source dataset. Results showed no outliers for each tributary. All tracers were kept for further analysis. Table 11 presents the

results of the bracket test and show that different elements were considered conservative at each sub-basin outlet (spatial sediment sources). Tracers were considered conservative when, for any given tracer, no significant changes during transport between upstream sources and downstream sediment sampling sites may have occurred according to Eq.37. At this point, conservative tracers were kept for further analysis.

The stepwise DFA produced an optimum composite fingerprint at each confluence which included different chemical elements (Table 12). At the first confluence C1, the solution included four tracers (Co, Ni, Mg, and Ca). The Wilk's lambda criterion was minimized to 0.007 and the optimum composite fingerprint correctly classified 100% of the source samples. At the second confluence C2, the best solution included 6 tracers (La, U, Na, Ti, Cd, and Si) and the Wilk's lambda criterion was minimized to 0.12. This solution correctly classified 53.3% of the source samples. The third solution correctly classified 85% of the source samples at the confluence C3. The optimum composite fingerprint includes the following elements: Bi, Sr, Sb, As, Se and Ti. The Wilk's lambda reached 0.003. At the confluence C4, 7 tracers composed the optimum solution (Ca, Bi, Mn, Si, K, Sb, and Fe) and 69% of the source samples were correctly classified. At the fifth confluence C5, 61.6% of the sources samples were correctly classified with the following elements: Ca, Mn, Mg, Sb, Si, Cs, Rb, Sr, Na, P, As, Ni, Cd and a Wilk's lambda criterion was equal to 0.00006. On the two last confluences (C6 and C7), 53.5 and respectively 55% of the source samples were correctly classified. The optimum composite fingerprint was respectively: (i) Mo, Pb, As, Se, Ni, Fe, Co, P, Mn, Zn, and (ii) Mo, Pb, As, Se, Co, Ni, Fe, Mn, Zn, Cs, Al, V, Sb, Cd, Cr, Ce, Si. The Wilk's lambda criterion was minimized to 0.0011 and respectively 0.00001.

Tab. 11: Results of the Bracket test to determine conservative tracers at each confluence.

Confluence	Conservative tracers
C1	As, Co, La, Mo, Ni, Sn, Th, U, Ce, Al, Ca, Fe, K, Mg, Na, P, S, Sr, Ti, Zn
C2	Cd, La, Sn, Th, U, Ce, Na, Si, Ti
C3	As, Co, Cu, La, Mo, Pb, Sb, Se, Sn, Th, Tl, U, Bi, Cr, V, Ba, Ce, K, Mg, Mn, Na, Si, Sr, Ti, Zn
C4	As, Cd, Co, Cs, La, Li, Pb, Rb, Sb, Sn, Th, Tl, U, Bi, Cr, Sc, V, Ba, Ce, Al, Ca, Fe, K, Mg, Mn, Na, P, S, Si, Sr, Ti, Zn
C5	As, Cd, Co, Cs, Cu, La, Ni, Pb, Rb, Sb, Se, Sn, Th, U, Ba, Ce, Al, Ca, Fe, Mg, Mn, Na, P, S, Si, Sr, Ti, Zn
C6	As, Cd, Co, Cs, Cu, La, Li, Mo, Ni, Pb, Rb, Sb, Se, Sn, Th, Tl, U, Bi, Cr, Sc, V, Ba, Ce, Al, Fe, K, Mn, P, S, Si, Ti, Zn
C7	As, Cd, Co, Cs, La, Li, Mo, Ni, Pb, Rb, Sb, Se, Sn, Th, U, Bi, Cr, V, Ba, Ce, Al, Fe, Mn, P, S, Si, Ti, Zn

Tab. 12 : Results of the stepwise DFA to identify the optimum composite fingerprint at each confluence.

C1			C2			C3			C4			C5			C6			C7		
Tracer	%[a]	TDW[b]	Tracer	%[a]	TDW[b]	Tracer	%[a]	TDW[b]	Tracer	%[a]	TDW[b]	Tracer	%[a]	TDW[b]	Tracer	%[a]	TDW[b]	Tracer	%[a]	TDW[b]
Co	60	1.5	La	47	3.5	Bi	44	2.3	Ca	36	3	Ca	34	8.1	Mo	13	2	Mo	14	2.6
Ni	50	1.3	U	40	3	Sr	20	1.1	Bi	30	2.5	Mn	16	3.7	Pb	26	4	Pb	23	4.1
Mg	60	1.5	Na	13	1	Sb	19	1	Mn	19	1.6	Mg	15	3.5	As	16	2.4	As	9	1.6
Ca	40	1	Ti	20	1.5	As	23	1.2	Si	23	1.9	Sb	13	2.9	Se	7	1.1	Se	6	1.1
Total[c]	**100**		Cd	47	3.5	Se	20	1.1	K	12	1	Si	17	3.9	Ni	6	1	Co	8	1.3
			Si	13	1	Ti	34	1.8	Sb	15	1.3	Cs	13	2.9	Fe	27	4.2	Ni	9	1.6
			Total[c]	**53**		Total[c]	**85**		Fe	24	2	Rb	8	1.9	Co	11	1.7	Fe	21	3.8
									Total[c]	**69**		Sr	14	3.3	P	7	1.1	Mn	12	2.1
												Na	4	1	Mn	14	2.1	Zn	8	1.3
												P	8	1.9	Zn	9	1.3	Cs	9	1.7
												As	12	2.7	Total[c]	**54**		Al	11	1.9
												Ni	8	1.7				Cd	6	1
												Cd	8	1.7				Cr	18	3.1
												Total[c]	**62**					Total[c]	**58**	

[a] % source type samples correctly classified by the tracer.

[b] tracer discriminatory weighting used in the mass balance modelling.

[c] % source type samples classified correctly by the optimum composite fingerprint.

3.3 Monte-Carlo simulations

The results relate to the overall means and uncertainties of the repeated Monte-Carlo simulations. The average Monte Carlo results (Fig.47) were very close to the results predicted by the unmixing model (<10%). The results of the unmixing model results shown at each confluence are considered robust. A large spread of the Monte Carlo results between minimum and maximum values can be observed for only few confluences (C2 - C5) indicating that the final set of tracers may not give reliable results. The increase of sources tends to decrease the uncertainties in the Monte-Carlo simulations.

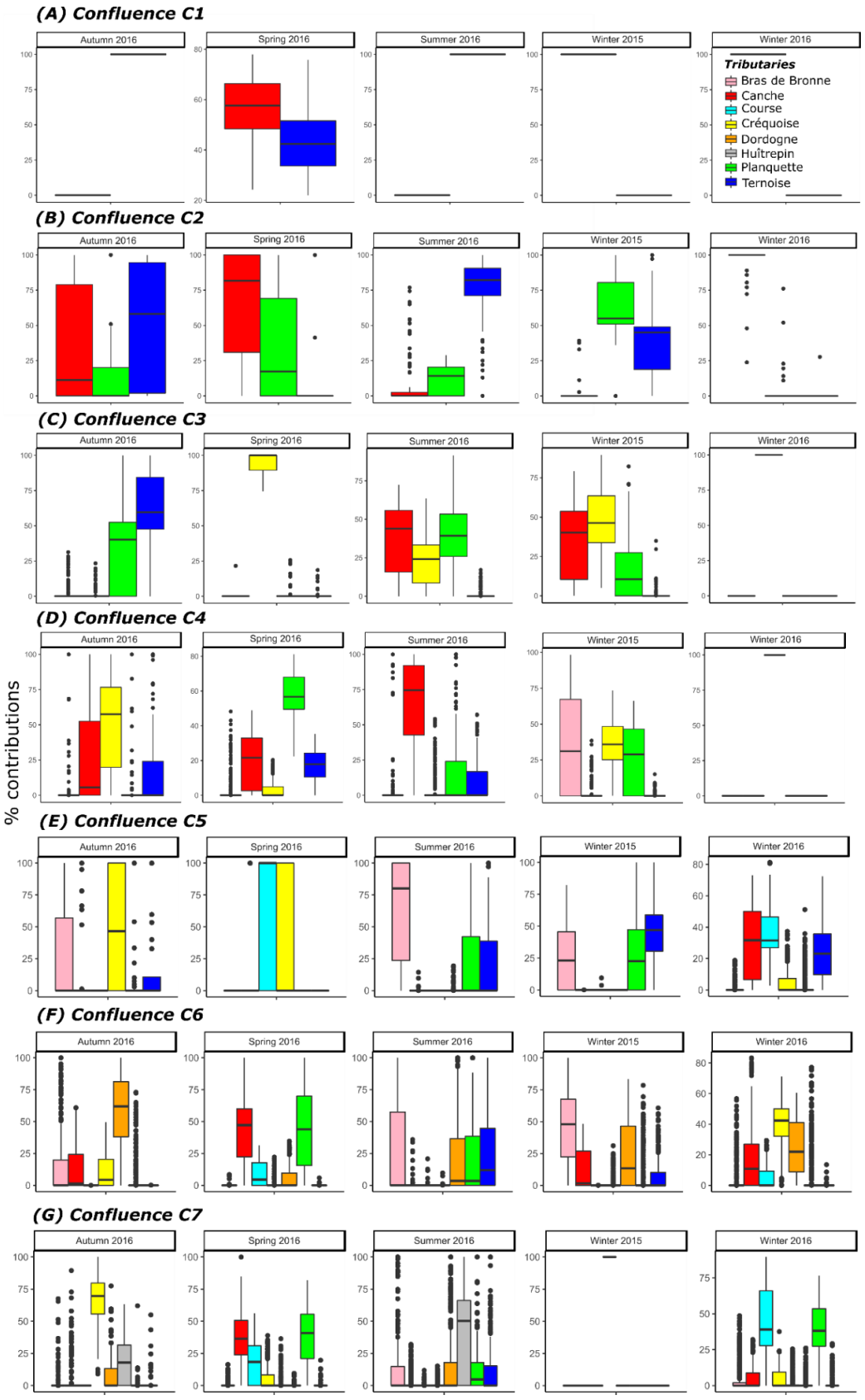

Fig. 47: Results of the Monte-Carlo simulations (N = 1000) for each confluence and each sampling campaign.

3.4 Annual sub-basin contributions.

Annual sub-basin relative contributions could be calculated using the four campaigns performed during the year 2016 (Fig.48). The results show in general a high and persistent relative contribution of the Planquette and the Créquoise along the main channel. The contributions of the Canche river and the Ternoise are particularly high in the upstream areas but tend to decrease as we approach the outlet of the catchment. The relative contribution of the Course seems important in the downstream area except for the point C6 which may have encountered a mis-classification of the source samples. The relative contributions of the downstream tributaries (Dordogne and Huîtrepin) are generally moderate as their outlet is closer to the sampling point. These average results over four sampling campaigns corresponding to the hydrologic year 2016 seem consistent if we consider the relative hydrological contributions of each tributary to the Canche main stream and the length of the main channel. Spatial variations show that along the Canche river catchment, the sedimentary signatures of the upstream tributaries tend to decrease as we approach the downstream indicating a possible effect of storage and/or dilution of the sediment flux.

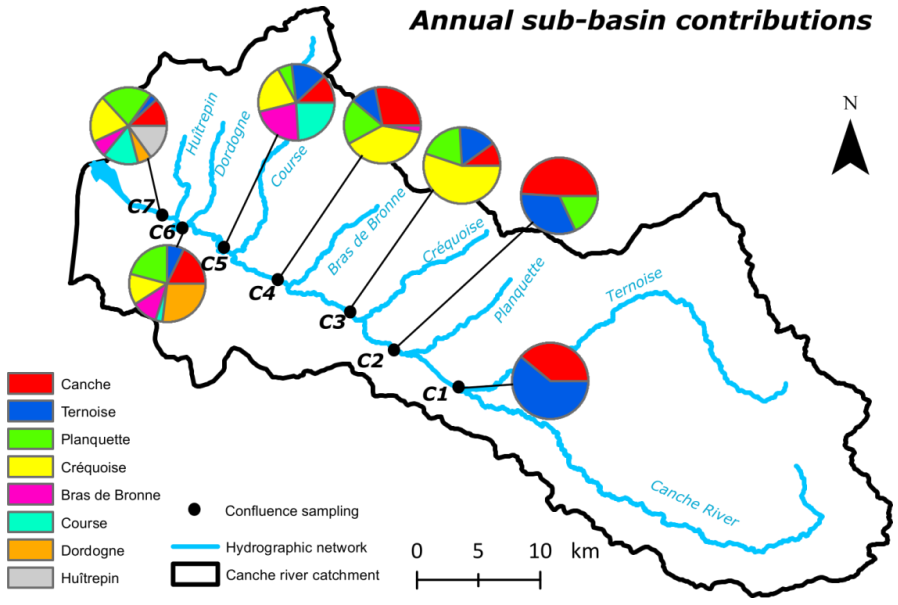

Fig. 48 : Annual sub-basin relative contributions (%) to the sediment yield in the Canche river catchment.

3.5 Sub-basins sediment yield

Considering the information provided by the Artois-Picardie Water Agency, the annual sediment yield of the Canche river catchment ranges from 29 to 185 kt yr^{-1} since 1999. The relative contributions were previously evaluated at the point C7 as follow: Canche 12%, Ternoise 3%, Planquette 22%, Créquoise 20%, Bras de Bronne 7%, Course 15%, Dordogne 6%, and Huîtrepin 15%. Based on the lower and upper boundaries of the annual sediment yield, the range of the sediment yield and specific sediment yield from tributaries to the main stream were calculated (Table 13). The highest sediment yields were calculated for the Créquoise and the Planquette, 5.8 – 37 kt yr^{-1} and respectively 6.38 – 40.7 kt yr^{-1}. The lowest sediment yields were estimated for the Ternoise (0.87 – 5.55 kt yr^{-1}), the Bras de Bronne (2.03 – 12.95 kt yr^{-1}), and the Dordogne (1.74 – 11.1 kt yr^{-1}).

Tab. 13: Estimates of tributaries annual sediment yield (kt yr^{-1}) and specific sediment yield (SSY; t km^{-2} yr^{-1}) to the main stream of the Canche river catchment.

Sediment yield range (1999-2015)		29 - 185 kt		29 - 185 kt	
Tributaries	Area (km^2)	Sediment yield (kt yr^{-1})		SSY (t km^{-2} yr^{-1})	
Canche (upstream area)	350	3.48	22.2	9.9	63.4
Ternoise	346	0.87	5.55	2.5	16
Planquette	57	6.38	40.7	111.9	714
Créquoise	80	5.8	37	72.5	462.5
Bras de Bronne	44	2.03	12.95	46	294
Course	148	4.35	27.75	29.3	187.5
Dordogne	53	1.74	11.1	32.8	209
Huîtrepin	42	4.35	27.75	103.5	660

3.6 Impact of erosion control measures

Considering that catchment stakeholders implemented 1590 erosion control measures in the Canche river catchment since 2000, this study proposes to evaluate their efficiency using an erosion control index (ECI_i) and the sediment yield of each sub-basin previously calculated. Our results show a positive impact of the installation of erosion control measures. Sub-basins with the highest ECI_i (Dordogne, Bras de Bronne, Huîtrepin) exhibit low values of sediment yield. Sub-basin for which few erosion control measures were installed so far (Créquoise, Planquette, Course), high values of sediment yield are observed. The relation between sediment yield and ECI_i decreases as the number

of erosion control measures increases on a catchment (Fig.49). These results are consistent with the environmental policies of the last decades and confirm their benefits.

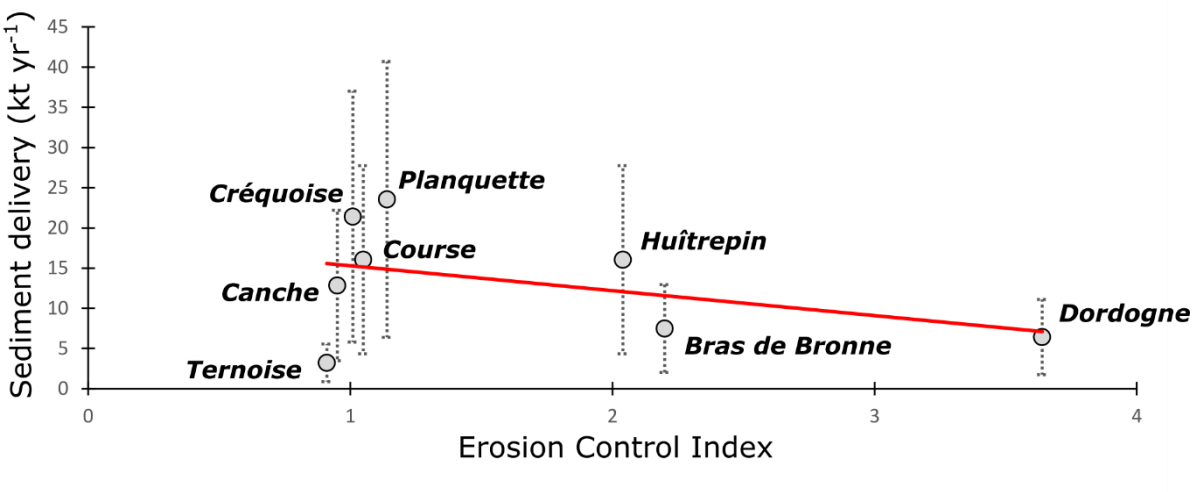

Fig. 49 : Evaluation of each sub-basin sediment flux (kt yr^{-1}) as a function of the Erosion Control Index (number of erosion control measures per km^2). The red line indicates the trend (R = 0.41).

3.7 Seasonal variability of sub-basins contributions

The seasonal contribution of each tributary at each confluence was estimated for the five sampling campaigns (Fig.50). An important seasonal variability can be observed along with major fluctuations in relative source contributions. In general, we can observe an important relative contribution of the upstream sub-basin (Canche, Ternoise, Planquette, Créquoise). The downstream sub-basin (Bras de Bronne, Course, Dordogne, Huîtrepin) exhibits lower contributions to the sediment yield except for the Bras de Bronne in winter 2015 and summer 2015, and for the Course in winter and spring 2016. For the upstream sub-basins, the influence of the Planquette is more effective in dry seasons: summer and spring 2016, the influence of the Créquoise is more effective during wet seasons: winter and autumn 2016. The relative contribution of the Canche is more pronounced during winter and spring 2016 whereas for the Ternoise, the relative contribution is greater in summer and autumn 2016. Effect of storage and/or dilution can be easily observed along the main channel of the Canche river. The relative contributions of the upstream sub-basins generally decrease at the approach of the downstream sections. Moreover, relative contributions of some

downstream sub-basins, such as the Dordogne or the Bras de Bronne, generally decrease near the sampling point (outlet of the respective sub-basin).

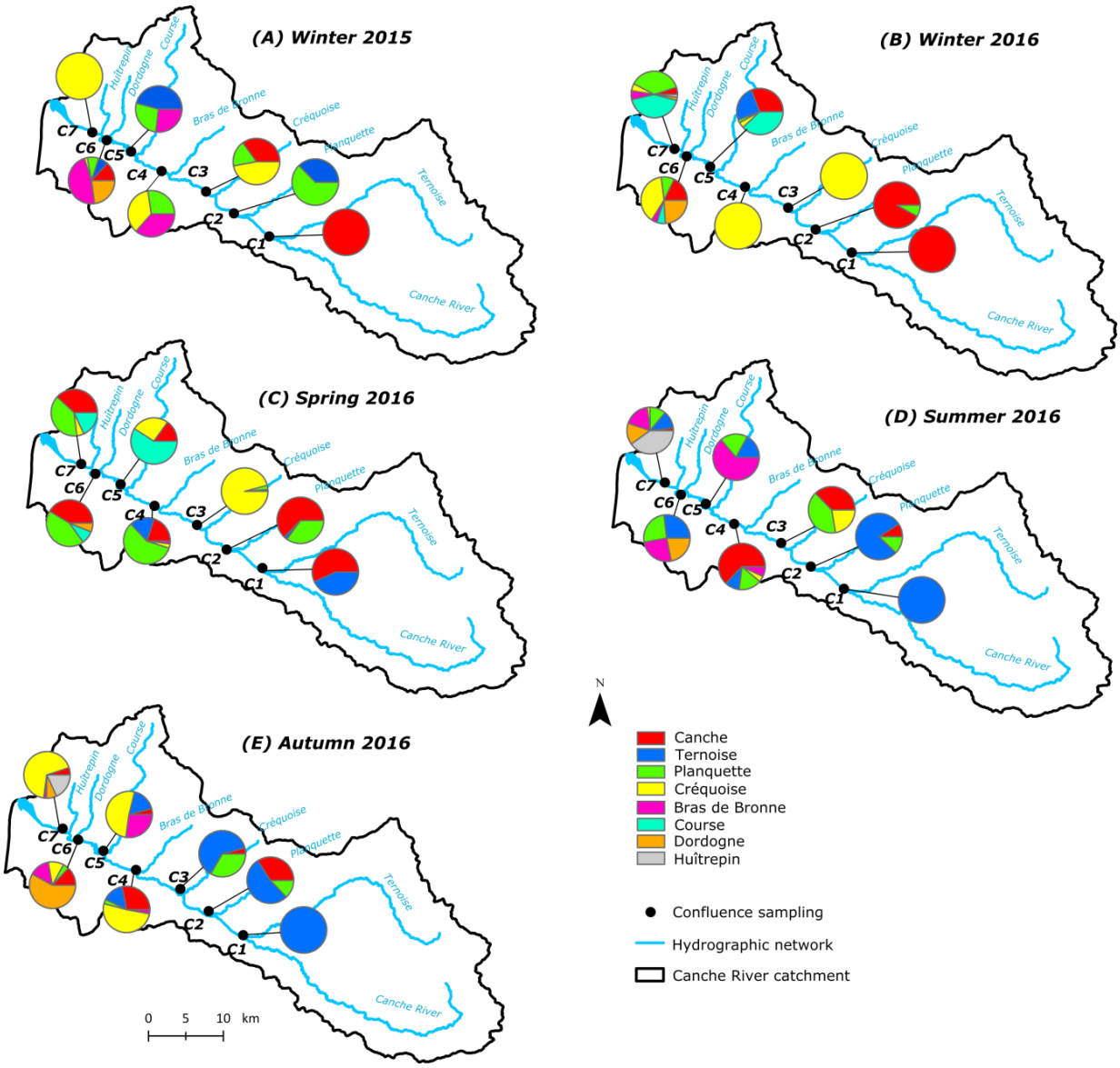

Fig. 50 : Seasonnal sub-basin relative contributions (%) to the sediment yield in the Canche river catchment.

4. Discussion

The quantification of the sub-basin relative contribution using a confluence-based sediment fingerprinting approach was quite conclusive. The sampling strategy deployed was original and spatially representative of the catchment, following the need for sediment fingerprinting approach addressing by several authors (Laceby et al., 2017; Smith et al., 2015). Each tributary and each confluence of the Canche river catchment were sampled using a simple sediment trap. The use of

geochemical tracers was relevant in the Canche river catchment because of significant element composition differences between the different sub-basins. As emphasized by Vale et al. (2016), the short distance between upstream and downstream sediment samples limits the effect that non-conservative behavior has on geochemical signature uncertainty. The results of the simulations showed that sub-basins located in the middle part of the Canche river catchment were the most contributing to the sediment yield and that major fluctuations between the different seasons could be observed. The results of the study also showed that the environmental policies of the last decades in Northern France seem to be potentially effective, confirming the recent observations made by Frankl et al. (2017). Sub-basins with the less erosion control measures installed on their areas, exhibit the highest relative contributions to the sediment yield.

The sub-basin contributions quantified in this study using the confluence-based sediment fingerprinting approach must be interpreted in the context of some limitations and uncertainties. The target river sediment for source apportionment was collected from a single downstream location for each tributary. The estimated sub-basin proportions at each confluence therefore strongly relate to the respective sampling site. Koiter et al. (2013) pointed out that sources estimates are scale-dependent and can differ for sampling locations along a channel network. This limitation, the so-called “black-box”, remains one of the largest limitations of the sediment fingerprinting approach.

Sediment sampling also needs to be temporally representative. Our approach tends to address this question with a seasonal sampling, although our sub-basins estimations are representative of 5 weeks over two years. It is likely that multiple major flood event could have transported a significant proportion of the annual sediment load and may have not been sampled here. Automatic sediment samplers could be deployed on each key location to increase the temporal representability with the big disadvantage that much more sampling logistics would be needed. Considering these limitations, two approaches need to be explored. First, we may suggest the use of other sediment traps, which offer a larger sedimentary storage capacity and that can be dropped at

key locations during a few months. Second, as suggested by Guzmán et al. (2013), we may suggest finding other tracers requiring inexpensive and rapid analysis approach to process quickly a large number of samples. This seems feasible using the spectrocolorimetric or magnetic tracers (Krein et al., 2003; Legout et al., 2013). They allow rapid, non-destructive and quantitative measurements of soil and sediment property.

Although tracer properties were tested for transformation using the range test, this does not confirm the complete absence of tracer property transformation during sediment delivery. As shown by Sherriff et al. (2015), the non-conservative behavior of a single tracer property included in a mass balance mixing model can affect the predicted source contributions. Kraushaar et al. (2015) suggested an expanded procedure including water sample analyses to identify tracers that may be susceptible to dissolution during transport. Using the sediment trap deployed in this study, the experiment could be easily done. Further research in this way must be done.

Particle size effect on element concentration remains one of the biggest uncertainties in sediment fingerprinting approach. Differences between sources and downstream sediments may arise from selective transport (Koiter et al., 2015). Our confluence-based approach, as the work of Vale et al. (2016) and Nosrati et al. (2018), decrease the effect that particle size can exert on predicted source contributions. Our analysis proves that the median particle size (D50) was practically the same for all tributary and confluence samples, and thus no corrections factors were applied. For future research, confluence-based approach should be largely explored.

Results of the Monte-Carlo simulation showed evidence of source prediction uncertainties. As suggested by Pulley et al. (2015), tracer selection must maximize contrasts in tracer concentrations between all sources. In the case of the Canche river catchment, that shows a very homogeneous geology, existing but light differences between the sources tracer concentrations were observed. Considering this, we suggest increasing the number and the type of tracers by addition of parameters related to land use and/or anthropogenic activities.

Sediment yield and Erosion Control Index relations were based on the number of erosion control measures installed on the territory. A positive impact was observed, confirming the success of recent land management to reduce soil erosion in Northern France (Frankl et al., 2017). In the next step research should explore the nature of these control measures. Some sub-basins may be preferentially occupied by hard (dam, pool) versus soft (fascines, hedges, grass strips) erosion control measures. Their effect should be quantified, since the data are available.

Finally, the results of our confluence-based sediment fingerprint approach should be validated using field experiments. High-frequency monitoring of one erosive sub-basin, such as the Créquoise or the Planquette could confirm the sediment yield quantified with these approaches.

5. Conclusion

This study reports on the quantification of sub-basin contributions to sediment yield in the Canche river catchment (Northern France). The study consisted in a confluence-based sediment fingerprinting approach. Sediment was collected at different key points in the catchment using sediment traps and the temporal variability was evaluated with a seasonal sampling strategy. The signature of the sediments was evaluated with physico-chemical analyses. Best tracers able to discriminate the sub-basin were selected using statistical analyses and incorporated into a mass balance mixing model. Annual sub-basin contributions were evaluated and range from 3 to 22% at the outlet of the main stream. Considering information given by the Artois-Picardie Water Agency, the annual sub-basin sediment delivery ranges from 0.87 to 40.7 kt yr^{-1}. The Planquette and the Créquoise were considered as the most erosive tributaries. Sub-basins with the highest number of erosion control measures on the territory exhibit the lowest values of sediment export confirming the generally positive impact of recent land management policies implemented in Northern France.

Acknowledgements

This work was financially supported by the Mines-Telecom Institute of Lille-Douai, with additional funding provided by the Artois-Picardie Water Agency (QUASPER project). We would also like to acknowledge technical support from the SYMCEA and the regional Chamber of Agriculture Nord-Pas-de-Calais, France. The authors are grateful to L. Alleman and B. Malet for the ICP-MS/AES analyses (IMT Lille-Douai – SAGE department). The author thanks A. Gellis and L. Gorman Sanisaca (USGS) who provided the *Sed_Sat-v1.0* model and for their helpful discussions.

References

Agence de l'eau Artois-Picardie. (2016). *Schéma Directeur d'Aménagement et de Gestion des Eaux du Bassin Artois-Picardie*. Retrieved from http://www.eau-artois-picardie.fr/sdage

Carter, J., Owens, P., Walling, D., & Leeks, G. (2003). Fingerprinting suspended sediment sources in a large urban river system. *The Science of The Total Environment*, *314–316*(03), 513–534. https://doi.org/10.1016/S0048-9697(03)00071-8

Collins, a. L., Walling, D. E., & Leeks, G. J. L. (1997). Use of the geochemical record preserved in floodplain deposits to reconstruct recent changes in river basin sediment sources. *Geomorphology*, *19*, 151–167. https://doi.org/10.1016/S0169-555X(96)00044-X

Collins, a. L., Walling, D. E., Sichingabula, H. M., & Leeks, G. J. L. (2001). Suspended sediment source fingerprinting in a small tropical catchment and some management implications. *Applied Geography*, *21*(4), 387–412. https://doi.org/10.1016/S0143-6228(01)00013-3

Collins, A. L., & Walling, D. E. (2002). Selecting fingerprint properties for discriminating potential suspended sediment sources in river basins. *Journal of Hydrology*, *261*, 218–244. https://doi.org/10.1016/S0022-1694(02)00011-2

Collins, A. L., Walling, D. E., Webb, L., & King, P. (2010). Apportioning catchment scale sediment sources using a modified composite fingerprinting technique incorporating property weightings and prior information. *Geoderma*, *155*(3–4), 249–261. https://doi.org/10.1016/j.geoderma.2009.12.008

Collins, A. L., Zhang, Y., McChesney, D., Walling, D. E., Haley, S. M., & Smith, P. (2012). Sediment source tracing in a lowland agricultural catchment in southern England using a modified procedure combining statistical analysis and numerical modelling. *Science of The Total Environment*, *414*, 301–317. https://doi.org/10.1016/j.scitotenv.2011.10.062

Cooper, R. J., Krueger, T., Hiscock, K. M., & Rawlins, B. G. (2014). Sensitivity of fluvial sediment source apportionment to mixing model assumptions: A Bayesian model comparison. *Water Resources Research*, 9031–9047. https://doi.org/doi:10.1002/2014WR016194

Du, P., & Walling, D. E. (2016). Fingerprinting surficial sediment sources: Exploring some potential problems associated with the spatial variability of source material properties. *Journal of Environmental Management*, 1–12. https://doi.org/10.1016/j.jenvman.2016.05.066

Evrard, O., Navratil, O., Ayrault, S., Ahmadi, M., Némery, J., Legout, C., … Esteves, M. (2011). Combining suspended sediment monitoring and fingerprinting to determine the spatial origin of fine sediment in a mountainous river catchment. *Earth Surface Processes and Landforms*, *36*(8), 1072–1089. https://doi.org/10.1002/esp.2133

Evrard, O., Poulenard, J., Némery, J., Ayrault, S., Gratiot, N., Duvert, C., … Esteves, M. (2013). Tracing sediment sources in a tropical highland catchment of central Mexico by using conventional and alternative fingerprinting methods. *Hydrological Processes*, *27*(6), 911–922. https://doi.org/10.1002/hyp.9421

Frankl, A., Prêtre, V., Nyssen, J., & Salvador, P.-G. (2017). The success of recent land management efforts to reduce soil erosion in northern France. *Geomorphology*, *303*, 84–93. https://doi.org/10.1016/j.geomorph.2017.11.018

Fryirs, K., & Gore, D. (2013). Sediment tracing in the upper Hunter catchment using elemental and mineralogical compositions: Implications for catchment-scale suspended sediment

(dis)connectivity and management. *Geomorphology*, *193*, 112–121. https://doi.org/10.1016/j.geomorph.2013.04.010

Gellis, a C., & Walling, D. E. (2011). Sediment Source Fingerprinting (Tracing) and Sediment Budgets as Tools in Targeting River and Watershed Restoration Programs. *Geophysical Monograph Series*, *194*(JANUARY), 263–291. https://doi.org/10.1029/2010GM000960

Gellis, A. C., Fitzpatrick, F., & Schubauer-Berigan, J. (2016). A Manual to Identify Sources of Fluvial Sediment, (September).

Gorman Sanisaca, L. E., Gellis, A. C., & Lorenz, D. L. (2017). Determining the Sources of Fine-Grained Sediment Using the Sediment Source Assessment Tool (Sed _ SAT).

Guzmán, G., Quinton, J. N., Nearing, M. A., Mabit, L., & Gómez, J. A. (2013). Sediment tracers in water erosion studies: current approaches and challenges. *Journal of Soils and Sediments*, *13*(4), 816–833. https://doi.org/10.1007/s11368-013-0659-5

Haddadchi, A., Olley, J., & Pietsch, T. (2015). Quantifying sources of suspended sediment in three size fractions. *Journal of Soils and Sediments*. https://doi.org/10.1007/s11368-015-1196-1

Haddadchi, A., Ryder, D. S., Evrard, O., & Olley, J. (2013). Sediment fingerprinting in fluvial systems: review of tracers, sediment sources and mixing models. *International Journal of Sediment Research*, *28*(4), 560–578. https://doi.org/10.1016/S1001-6279(14)60013-5

Kayvantash, D., Cojan, I., Kissel, C., & Franke, C. (2017). Magnetic fingerprint of the sediment load in a meander bend section of the Seine River (France). *Geomorphology*, *286*, 14–26. https://doi.org/10.1016/j.geomorph.2017.02.020

Koiter, a. J., Owens, P. N., Petticrew, E. L., & Lobb, D. a. (2013). The behavioural characteristics of sediment properties and their implications for sediment fingerprinting as an approach for identifying sediment sources in river basins. *Earth-Science Reviews*, *125*, 24–42. https://doi.org/10.1016/j.earscirev.2013.05.009

Koiter, A. J., Owens, P. N., Petticrew, E. L., & Lobb, D. A. (2015). The role of gravel channel beds on the particle size and organic matter selectivity of transported fine-grained sediment: implications for sediment fingerprinting and biogeochemical flux research. *Journal of Soils and Sediments*, *15*(10), 2174–2188. https://doi.org/10.1007/s11368-015-1203-6

Kraushaar, S., Schumann, T., Ollesch, G., Schubert, M., Vogel, H.-J., & Siebert, C. (2015). Sediment fingerprinting in northern Jordan: element-specific correction factors in a carbonatic setting. *Journal of Soils and Sediments*, 2155–2173. https://doi.org/10.1007/s11368-015-1179-2

Krein, A., Petticrew, E., & Udelhoven, T. (2003). The use of fine sediment fractal dimensions and colour to determine sediment sources in a small watershed. *Catena*, *53*, 165–179. https://doi.org/10.1016/S0341-8162(03)00021-3

Laceby, J. P., Evrard, O., Smith, H. G., Blake, W. H., Olley, J. M., Minella, J. P. G., & Owens, P. N. (2017). The challenges and opportunities of addressing particle size effects in sediment source fingerprinting: A review. *Earth-Science Reviews*, *169*, 85–103. https://doi.org/10.1016/j.earscirev.2017.04.009

Laceby, J. P., & Olley, J. (2015). An examination of geochemical modelling approaches to tracing sediment sources incorporating distribution mixing and elemental correlations. *Hydrological Processes*, *29*(6), 1669–1685. https://doi.org/10.1002/hyp.10287

Lamba, J., Karthikeyan, K. G., & Thompson, A. M. (2015). Apportionment of suspended sediment sources in an agricultural watershed using sediment fingerprinting. *Geoderma*, *239–240*, 25–33. https://doi.org/10.1016/j.geoderma.2014.09.024

Le Gall, M., Evrard, O., Foucher, A., Laceby, J. P., Salvador-Blanes, S., Thil, F., … Ayrault, S. (2016). Quantifying sediment sources in a lowland agricultural catchment pond using 137Cs activities and radiogenic 87Sr/86Sr ratios. *Science of the Total Environment*, *566–567*, 968–980. https://doi.org/10.1016/j.scitotenv.2016.05.093

Legout, C., Poulenard, J., Nemery, J., Navratil, O., Grangeon, T., Evrard, O., & Esteves, M. (2013). Quantifying suspended sediment sources during runoff events in headwater catchments using spectrocolorimetry. *Journal of Soils and Sediments*, *13*, 1478–1492. https://doi.org/10.1007/s11368-013-0728-9

Martínez-Carreras, N., Udelhoven, T., Krein, A., Gallart, F., Iffly, J. F., Ziebel, J., … Walling, D. E. (2010). The use of sediment colour measured by diffuse reflectance spectrometry to determine sediment sources: Application to the Attert River catchment (Luxembourg). *Journal of Hydrology*, *382*(1–4), 49–63. https://doi.org/10.1016/j.jhydrol.2009.12.017

Motha, J. a., Wallbrink, P. J., Hairsine, P. B., & Grayson, R. B. (2004). Unsealed roads as suspended sediment sources in an agricultural catchment in south-eastern Australia. *Journal of Hydrology*, *286*(1–4), 1–18. https://doi.org/10.1016/j.jhydrol.2003.07.006

Motha, J. A., Wallbrink, P. J., Hairsine, P. B., & Grayson, R. B. (2003). Determining the sources of suspended sediment in a forested catchment in southeastern Australia. *Water Resour. Res.*, *39*(3), 1056. https://doi.org/10.1029/2001wr000794

Nosrati, K., Collins, A. L., & Madankan, M. (2018). Fingerprinting sub-basin spatial sediment sources using different multivariate statistical techniques and the Modified MixSIR model. *Catena*, *164*(January), 32–43. https://doi.org/10.1016/j.catena.2018.01.003

Palazón, L., Latorre, B., Gaspar, L., Blake, W. H., Smith, H. G., & Navas, A. (2015). Comparing catchment sediment fingerprinting procedures using an auto-evaluation approach with virtual sample mixtures. *Science of The Total Environment*, *532*, 456–466. https://doi.org/10.1016/j.scitotenv.2015.05.003

Poulenard, J., Perrette, Y., Fanget, B., Quetin, P., Trevisan, D., & Dorioz, J. M. (2009). Infrared spectroscopy tracing of sediment sources in a small rural watershed (French Alps). *Science of the Total Environment*, *407*(8), 2808–2819. https://doi.org/10.1016/j.scitotenv.2008.12.049

Pulley, S., Foster, I., & Antunes, P. (2015). The application of sediment fingerprinting to floodplain and lake sediment cores: assumptions and uncertainties evaluated through case studies in the Nene Basin, UK. *Journal of Soils and Sediments*, 1–23. https://doi.org/10.1007/s11368-015-1136-0

Russell, M. ., Walling, D. ., & Hodgkinson, R. . (2001). Suspended sediment sources in two small lowland agricultural catchments in the UK. *Journal of Hydrology*, *252*(1–4), 1–24. https://doi.org/10.1016/S0022-1694(01)00388-2

Shapiro, S. S., & Wilk, M. B. (1965). An Analysis of Variance Test for Normality (Complete Samples), *52*(3), 591–611. Retrieved from http://www.jstor.org/stable/2333709

Sherriff, S. C., Franks, S. W., Rowan, J. S., Fenton, O., & Ó'hUallacháin, D. (2015). Uncertainty-based assessment of tracer selection, tracer non-conservativeness and multiple solutions in sediment fingerprinting using synthetic and field data. *Journal of Soils and Sediments*.

https://doi.org/10.1007/s11368-015-1123-5

Smith, H. G., Evrard, O., Blake, W. H., & Owens, P. N. (2015). Preface—Addressing challenges to advance sediment fingerprinting research. *Journal of Soils and Sediments*, (OCTOBER). https://doi.org/10.1007/s11368-015-1231-2

Tessier, L. (2003). *Transport et caractérisation des matières en suspension dans le bassin versant de la Seine : identification de signatures naturelles et anthropiques*. Ecole des Ponts ParisTech.

Theuring, P., Collins, A. L., & Rode, M. (2015). Source identification of fine-grained suspended sediment in the Kharaa River basin, northern Mongolia. *Science of The Total Environment*, *526*(APRIL), 77–87. https://doi.org/10.1016/j.scitotenv.2015.03.134

Vale, S. S., Fuller, I. C., Procter, J. N., Basher, L. R., & Smith, I. E. (2016). Application of a confluence-based sediment-fingerprinting approach to a dynamic sedimentary catchment, New Zealand. *Hydrological Processes*, *30*(5), 812–829. https://doi.org/10.1002/hyp.10611

Venables, W. N., & Ripley, B. D. (2002). *Modern Applied Statistics With S*. *Technometrics*. https://doi.org/10.1198/tech.2003.s33

Walling, D. E., Russell, M. A., Hodgkinson, R. A., & Zhang, Y. (2002). Establishing sediment budgets for two small lowland agricultural catchments in the UK. *Catena*, *47*(4), 323–353. https://doi.org/10.1016/S0341-8162(01)00187-4

Walling, D. E., & Woodward, J. C. (1992). Use of radiometric fingerprints to derive information on suspended sediment sources. Erosion and Sediment Transport Monitoring Programmes in River Basins. (Proceedings Oslo Symposium). In *Erosion and sediment transport Programmes in River Basins* (Vol. 210, pp. 64–153).

Walling, D. E., Woodward, J. C., & Nicholas, A. P. (1993). A multi-parameter approach to fingerprint suspended-sediment sources. In *Tracers in Hydrology*.

Weihs, C., Ligges, U., Luebke, K., & Raabe, N. (2005). klaR: analyzing German business cycles. *Data Analysis and Decision Support*, 335–343. https://doi.org/10.1007/3-540-28397-8_36

Wilkinson, S. N., Hancock, G. J., Bartley, R., Hawdon, A. A., & Keen, R. J. (2013). Using sediment tracing to assess processes and spatial patterns of erosion in grazed rangelands, Burdekin River basin, Australia. *Agriculture, Ecosystems and Environment*, *180*, 90–102. https://doi.org/10.1016/j.agee.2012.02.002

Chapter 5

Quantifying input sources in a rural catchment using sediment colour and chemical analyses: case study of the Canche river (France).

Résumé étendu – Chapitre 5

Contexte

Depuis quelques années, les approches de « sediment fingerprinting » ont largement été utilisées par la communauté scientifique pour pouvoir identifier les sources potentielles de sédiments dans un bassin versant et quantifier leurs contributions respectives. Ces approches sont basées sur le postulat que les caractéristiques géo-physico-chimique (traceurs) de différentes sources de sédiment sont comparables à celles du matériel fluvial transporté. Dans le chapitre 4, ces approches se sont révélées performantes pour évaluer la contribution des affluents au flux sédimentaire de la Canche. Considérant que le flux sédimentaire observé sur le bassin versant de la Canche est majoritairement issu de l'érosion des sols et des berges, il peut s'avérer intéressant de quantifier leurs contributions respectives au flux sédimentaire mesuré à l'exutoire. Selon la littérature scientifique, les nouvelles approches basées sur l'utilisation de la couleur sédimentaire (spectrocolorimétrie), couplées à des analyses géochimiques, offrent de nouvelles perspectives en matière de traçage de sources et permettent de discriminer une signature sol/berge dans d'autres contextes environnementaux. Par ailleurs, le caractère non-destructif de ces analyses, leur rapidité d'exécution et leur faible coût d'analyse permet de répondre plus facilement aux besoins matériels des approches de sediment fingerprinting.

Cette étude se propose dès lors de tester la pertinence de ces traceurs spectrocolorimétriques, couplés à des analyses plus classiques (géochimie) afin d'évaluer la contribution des terres arables et des berges dans le bassin versant agricole de la Canche dans le Nord de la France.

Matériel et méthodes

Selon les objectifs initiaux de l'étude, une campagne d'échantillonnage des sources sédimentaires (terres arables et berges ; n = 44) a été entreprise sur le bassin versant de la Canche en Mars 2017. Le matériel fluvial sédimentaire (n = 5) a quant à lui été récolté à l'exutoire du bassin versant de la Canche avec le même dispositif expérimental que celui utilisé dans le chapitre 4, au

cours de 5 campagnes saisonnières. Les échantillons ont ensuite été analysés afin de déterminer leurs empreintes physico-chimiques (variables de chromaticité, spectres de dérivée première, et chimie élémentaire : majeurs et traces). Les meilleurs traceurs potentiels ont été identifiés en suivant la même procédure que pour le chapitre 4 (via le modèle *Set_Sat-v1.0*) et des analyses statistiques robustes ont permis d'identifier la meilleure combinaison de traceurs capable de discriminer la source « berge » de la source « sol » (Fig.51). Via un modèle de mélange, leurs contributions sont quantifiées ainsi que les incertitudes associées. Grâce à une instrumentation haute-fréquence (débitmètre et sonde à turbidité) à l'exutoire du bassin versant de la Canche, il est alors possible d'évaluer les flux sédimentaires inhérents à chaque source sédimentaire au cours de différentes périodes d'échantillonnage.

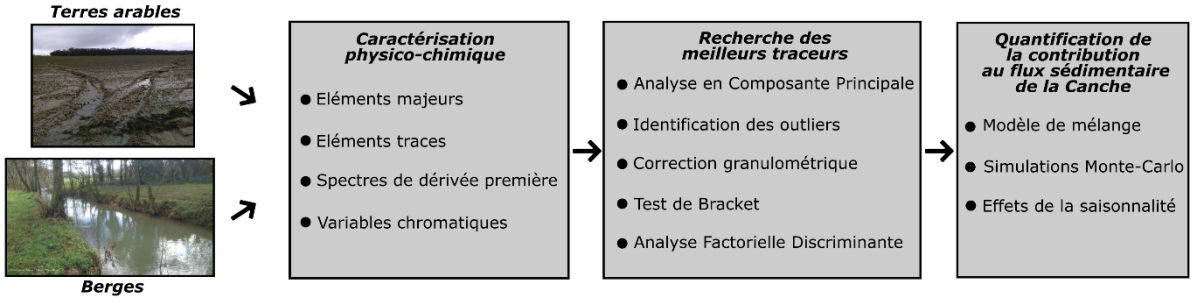

Fig. 51 : Synthèse de la démarche entreprise pour quantifier les contributions des différentes sources au flux sédimentaire de la Canche.

Résultats

Les analyses physico-chimiques sur le matériel sédimentaire ont montré des différences significatives en termes de distribution granulométrique entre les sources et le matériel fluvial transporté. La recherche de la meilleure combinaison de traceurs en utilisant le modèle *Sed_Sat-v1.0* a révélé que les traceurs liés aux caractéristiques colorimétriques de la goethite : le paramètre de chromaticité b* et la dérivée première de la réflectance du spectre visible à la longueur d'onde λ = 530 nm permettent de discriminer les deux sources de matières sédimentaires. Les éléments traces Sr et U ont également été identifiés comme discriminants par le modèle. Les concentrations de ces éléments sont plus élevées dans les terres arables que dans les berges, probablement dû à l'utilisation de fertilisants. A travers le modèle de mélange, les contributions des berges et des terres

arables sont évaluées respectivement à 70 et 30% mais avec de très fortes variabilités temporelles. Les simulations Monte-Carlo confirment que le résultat final du modèle de mélange est robuste, avec de très faibles incertitudes.

Conclusions

Les résultats montrent que les traceurs spectrocolorimétriques, couplés à des traceurs plus classiques de chimie élémentaire offrent d'excellentes opportunités pour évaluer les contributions des terres arables et des berges dans un bassin versant. Les traceurs liés à la couleur des oxy-hydroxides de fer comme la goethite semblent être particulièrement efficaces pour caractériser les processus de transferts des terres arables, tout comme les éléments traces liés aux usages et pratiques agricoles. Les résultats mettent en avant forte contribution significative des berges au cours des différentes périodes d'échantillonnage et soulignent la forte variabilité temporelle des processus d'érosion des terres agricoles sur le bassin versant de la Canche.

Chapter 5: Quantifying input sources in a rural catchment using sediment colour and chemical analyses: case study of the Canche river (Northern France).

Edouard Patault[a, b], Claire Alary[a], Christine Franke[b], Maxime Debret[c], Nor-Edine Abriak[a]

[a]IMT Lille Douai, Univ. Lille, EA 4515 - LGCgE - Civil Engineering and Environmental Department, F-59000 Lille, France

[b]MINES ParisTech, PSL Research University, Center of Geosciences, 35 rue Saint-Honoré, 77305 Fontainebleau Cedex, France

[c]UNIROUEN, UNICAEN, CNRS, M2C, Normandie Univ., 76000 Rouen, France

This chapter is in preparation for submission to the Journal of Soils and Sediments.

Highlights

- Spectral signature of goethite permits source discrimination.
- Sr and U are relevant chemical tracers.
- Channel banks contribution is higher than input from soils over the study period.

Graphical abstract

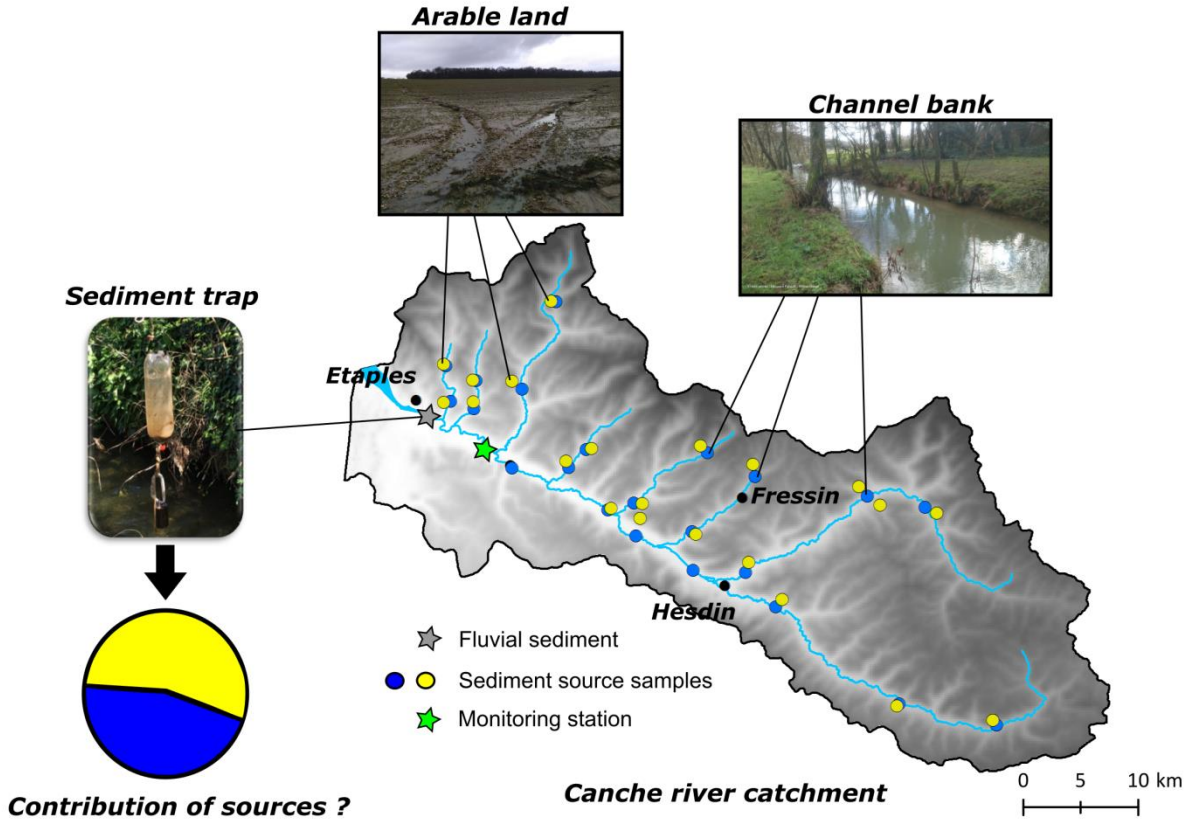

Abstract

In the framework of the efforts taken to understand and manage soil erosion in catchments, sediment fingerprinting approaches are globally applied since several decades. This technique is particularly suitable for quantifying channel banks and topsoil contribution in catchments, but it is recognized that this method could be laborious and expensive. There is need for easy-to-use, low cost and non-destructive analytical techniques in sediment fingerprinting approaches. This study aims to quantify sediment source contributions (soil versus channel bank) in an agricultural catchment in Northern France (Canche river catchment; 1274 km²). Source samples and suspended sediments were collected throughout the entire catchment during five seasonal sampling campaigns between 2016 and 2017. Sediment signatures were defined using classical (chemical composition) and innovating tracers (sediment colour). The Optimum composite fingerprint was identified using *Sed_Sat-v1.0*. The model uses a robust statistical analysis including a stepwise discriminant function analysis and a bracket test. Relative contributions of sources were quantified by including the tracers in a mixing model. The validation of the results was established using the results of Monte-Carlo simulations. Over the studied period, the contribution of channel banks and soils was estimated to 70% and respectively 30%. Our approach reveals the suitability of the spectrocolorimetric tracers in the fingerprinting approach. They have a high potential to trace iron oxy-hydroxides such as goethite. Our results also revealed that studies should focus on the use of trace elements used in fertilizers when working on this type of sediment source.

Keywords: sediment fingerprinting; sediment colour; trace elements; soils; channel banks; northern France

1. Introduction

Since a few years, there is an increasing interest in the understanding of sediment pathways and the identification of suspended sediment sources, to implement effective erosion control strategies in affected catchments. Given the spatial and temporal complexity of sediment mobilization and input, sediment fingerprinting approach has gained increasing attention and has been applied worldwide (see review of Guzmán et al., (2013). The method uses the distinct signature of potential sources to determine their respective relative contribution to the mixed signature in suspended sediment samples. This method is particularly effective for quantifying the contribution of a large variety of suspended sediment sources (e.g. channel banks, crop lands, roads, forests, grasslands, etc.; see review of Haddadchi et al. (2013)). Previous studies have shown the potential of a wide range of tracer parameters for suspended sediment sources from methods such as e.g. : environmental magnetism (e.g. Motha et al., 2004; Russell et al., 2001), radionuclides (e.g. Evrard et al., 2013; Le Gall et al., 2016), chemical composition (e.g. Carter et al., 2003; Collins et al., 2012; Theuring et al., 2015), sediment colour (e.g. Krein et al., 2003; Martínez-Carreras et al., 2010; Poulenard et al., 2009; Legout et al., 2013). However, despite the increasing number of sediment fingerprinting studies, there is no generic guideline for selecting the most useful tracer to discriminate the sources of suspended sediment in river catchments. Consequently, authors generally select a large range of possible tracers and test their ability to discriminate the different sources (Laceby et al., 2017). The sediment fingerprinting approach is known for being long and expensive to undertake. A key-line for research in future might be the further development of inexpensive, non-destructive and rapid to apply tracers that may process large number of samples.

According to Guzmán et al. (2013) this is feasible with colour parameters, and recent developments of analytical methods permit to identify the main components of sediment carrying colour (Balsam et al., 1999; Debret et al., 2011; Sebag et al., 2013). Indeed, the colour can identify specific sedimentary components, for example the range between 470 and 580 nm is indicative for the presence of iron oxides and hydroxides (Deaton & Balsam, 1991), between 400 and 470 nm for

carbonates (Balsam & Beeson, 2003) and between 650 and 700 nm for organic compounds (Wolfe et al., 2006; Debret et al., 2018). Krein et al. (2003) also concluded that the particle colour is a useful parameter for examining variations in suspended particles compositions and that colour differentiation of the material may describe the relative contribution of suspended sediment sources.

More recently, colour tracers were used by a few authors to fingerprint suspended sediment sources in different environments (Legout et al., 2013; Pulley & Rowntree, 2016). For example, Poulenard et al. (2009) were able to quantify the contribution of three different lithological sources (i.e. black marl, marly-limestone, and molasse) during flood events in the Galabre river catchment (France) using spectra obtained by diffuse reflectance. Moreover, Martínez-Carreras et al. (2010 b), studied the Attert River catchment (Luxembourg). They were able to quantify suspended sediment sources using the colour coefficient measured with diffuse reflectance spectrometry. Martínez-Carreras et al. (2010 a) also found that colour could differentiate between top-soil and channel bank material and they offer substantial information that can be integrated into the classical fingerprinting approach. Nevertheless, in their study, the colour-based fingerprinting approach was not able to unequivocally discriminate sediment sources in medium size catchments (i.e > 10^1 km²) and they suggest that parameters drawn from other sediment properties such as geochemistry or radionuclides, would be helpful to improve sediment source discrimination.

Considering these previous studies, colour tracers seems to have a high potential for sediment source discrimination. In the context of our study area in northern France, the Canche river catchment, the main sediment suppliers are arable land and channel bank because grasslands and forests erosion rates are negligible according to Cerdan et al. (2010). The main purposes of this study were: (i) to investigate the discrimination of these two potential suspended sediment source types according to their respective colour and chemical composition, (ii) to reveal the suitability of a

colour-based fingerprinting approach, and (iii) to determine the chemical-colour best model suited for suspended sediment source description.

2. Material and methods

2.1 Study area

The Canche river catchment (1274 km²) is a sub catchment of the Artois-Picardie basin in France (Fig.52). It is located in the northern France loess belt. The climate is oceanic with a mean annual rainfall of 1000 ± 150 mm and a mean annual temperature of 11°C. The catchment is characterized by a meandriform drainage network dominated by the main channel of the Canche river (88 km) and seven tributaries (Ternoise, Planquette, Créquoise, Bras de Bronne, Course, Dordogne, and Huîtrepin). The study area is characterized by Pleistocene silts which rest on the chalky grounds of Séno-Turonian. These soil series are known for being at risk of water runoff erosion (Lautridou et al., 1986; Laignel, 2003; Landemaine, 2016). The catchment is mainly occupied by arable lands (> 80% of the catchment). The rest of the catchment is occupied by urban areas (8%) with a minority of woodlands and grasslands. The Canche river has a history of high suspended sediment concentrations and a reputation for sudden mud floods. Suspended sediment load has been estimated, over several years, using high-frequency monitoring station at Attin near the outlet of the catchment (Fig.53; more information about instruments in Franke et al. (2018), *in prep – see chapter 6*). The range of the annual suspended sediment load (1999 - 2016) is 29 - 185 kt yr^{-1}, resulting in an annual sediment yield of 22.4 – 142.9 t km^{-2} yr^{-1} for the 1274 km² of the Canche river catchment. In this context, high concentrations of suspended sediment in the Canche river are mainly caused by diffuse and/or concentrated erosion processes of the soil surfaces and channel bank degradation.

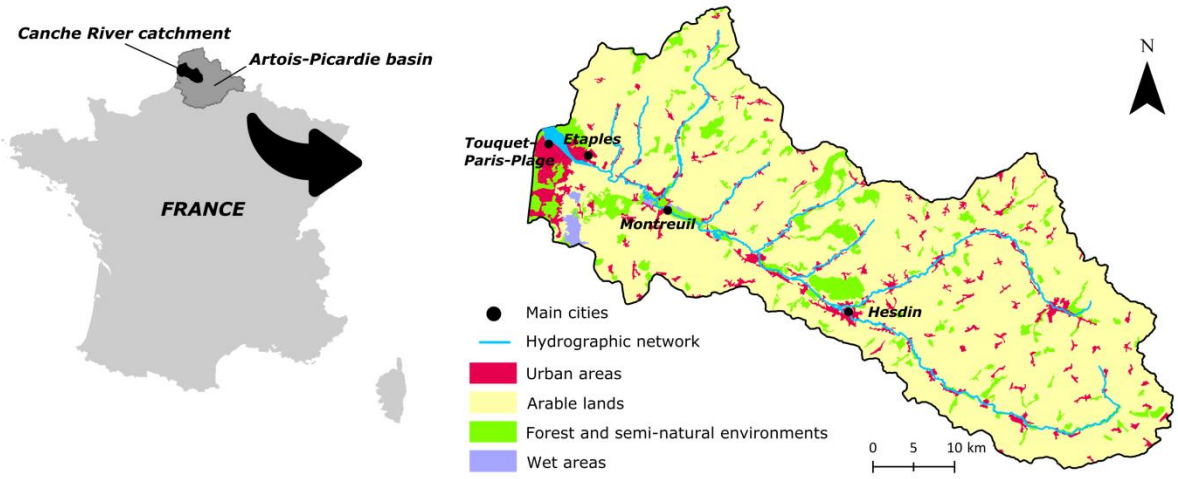

Fig. 52 : Location and land use of the Canche river catchment (Data: Corine Land Cover 2012).

2.2 Sediment sampling

2.2.1 Soils

Arable lands are the main land use in the Canche catchment (> 80%). The surface soil of these areas was sampled at multiple positions throughout the catchment, along the main river channel and the main tributaries. Sampling was concentrated in sediment source areas connected to the river and potentially sensitive to sediment transport (i.e. areas with evidence for erosion). At each location, five sub-samples of surface material were collected from the top 0-2 cm layer in a 5 m² square and homogenized to provide a representative sample. In total, 22 top soil samples were collected during March 2017 (Fig.53).

2.2.1 Channel bank

Channel bank sediments were collected on logistically easy accessible positions of the Canche main river channel and the main tributaries. Samples were collected on channel banks showing evidence of erosion processes, using a nonmetallic trowel to avoid sample contamination. Three sub-samples were collected and mixed at each location to provide a composite sample representative of the respective channel bank. In total, 22 channel bank samples were collected during March 2017 (Fig.53).

2.2.3 Suspended sediments

Suspended sediments were collected during 5 seasonal field campaign using 2-l polyethylene bottles perforated by two opposite holes (diameter 0.05 m). Sediment traps were deposited at the outlet of the main channel of the Canche river and upstream of tributaries, following the method of Tessier (2003) and Kayvantash et al., (2017) (more details on experimental devices and sampling periods in Patault et al., 2018 c and Franke et al., 2018; *both in prep – see chapter 4 and 6*).

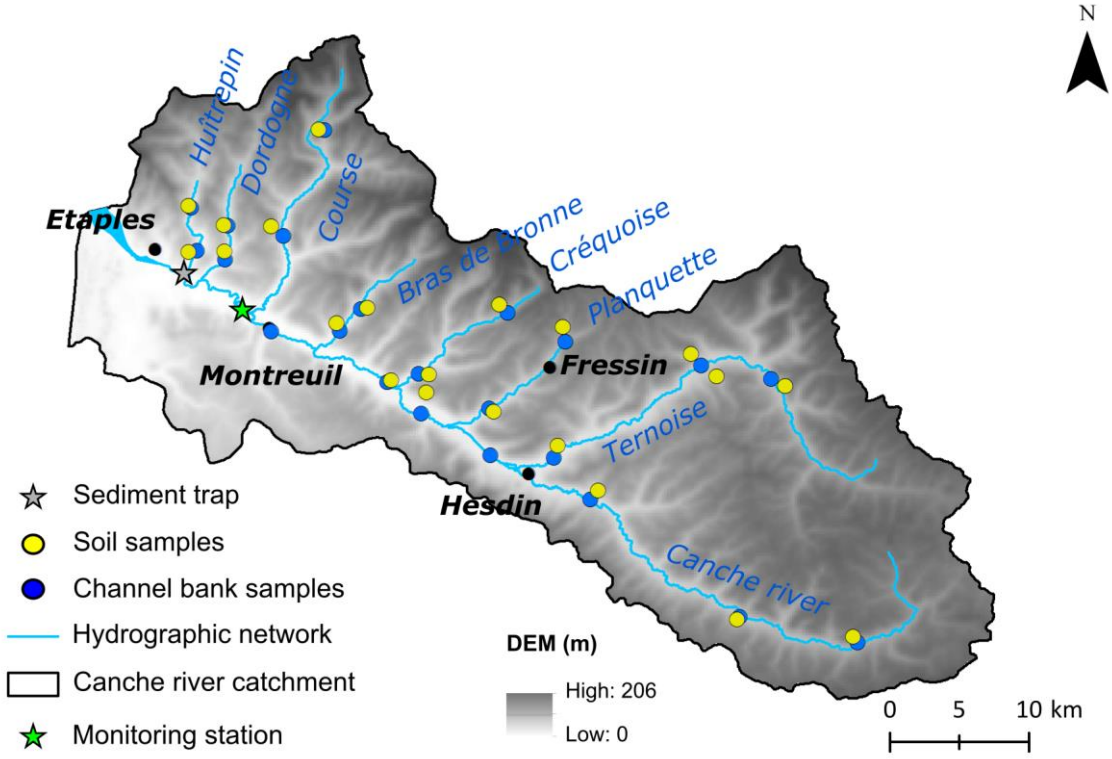

Fig. 53 : Topography of the Canche river catchment and location of source/suspended matter samples and sediment fluxes monitoring station.

2.3 Source and suspended sediment analysis

2.3.1 Grain size distribution

Laser diffraction technique was used to analyze the grain size distribution of the two different sources and the suspended sediments. All samples were initially oven-dried at 30°C for 72 h and sieved to 2000 µm to remove any plant debris that could distort the measurement. Analyzes were performed using a *Beckman Coulter LS 13320* laser particle size by mixing 2 g of sediment with

100 mL of ultrapure water. The solution was stirred to homogenize the sample and each solution was analyzed in triplicate to validate the measurements.

2.3.2 Geochemistry

The analysis of the elemental composition was carried out after acid mineralization in a microwave oven. 22 reactors are used for this mineralization. In 18 reactors, 0.250 g of sediment are poured, 2 reactors are used as references with TH2 (reference sediment material) to test the validity of the analysis by comparison with referenced measurements, and 2 blank reactors (without addition of solid material) are used to ensure non-contamination during preparation. For each reactor, 1 ml of nitric acid (HNO_3), 3 ml of hydrochloric acid (HCl), and 0.5 ml of water (H_2O) are added to the sediment. The determination of the major elements in the liquid phase (Al, Si, P, S, Ca, Fe, K, Mg, Na, Mn, Sr, Ti, Zn) was performed using an inductively coupled plasma atomic emission spectrometer (ICP-AES; *ICAP 7400 Thermo Fischer Scientific*). The determination of trace elements (As, Cd, Co, Cs, Cu, La, Li, Mo, Ni, Pb, Rb, Sb, Se, Sn, Th, Tl, U, Bi, Cr, Sc, V, Ba, Ce) in the samples was carried out using an inductively coupled plasma mass spectrometer (ICP-MS; *PerkinElmer NexION 300x*).

2.3.3 Sediment colour

Measurements were taken using a portable reflectance spectrophotometer (*Konica Minolta CM2600d*). During the measurement, the device emits an arc of light (Xenon) and measures the ratio between the light reflected by the sample and that of a calibrated white standard (barium sulfate: $BaSO_4$). The reflectance spectra are measured between 360 and 740 nm with a pitch of 10 nm. The illuminant used is the D65, a colorimetric standard corresponding to daylight at a colour temperature of 6504 K. The measurement is carried out in specular excluded (specular reflection rejection “mirror effect”). The collected data are the standard chromatic parameters L*, a* and b* (*CIELab System*), and the percentages of the spectrum reflectance for the 39 classes of wavelength. All samples were manually disaggregated using an agate pestle and mortar. 5 g of sediment were spread on a white sheet assuring a minimum thickness of the sample of 1 cm. Measurement were made by simply

placing the device directly on the sediment. Between each measurement, the camera lens was cleaned with demineralized water and dried, and a new white sheet was taken. To take into account the possible heterogeneity of the sample, 5 subsequent measurements were taken for each sample. First Derivative Spectra (FDS) values are deduced from the percentages of the raw data spectrum reflectance and calculated using Eq.43:

$$f'(x_i) = \frac{y_{i+1} - y_{i-1}}{x_{i+1} - x_{i-1}} \quad (43)$$

With f' the FDS value at x_i nm; x_{i+1} and x_{i-1} the pitch of 10 nm; y_{i+1} and y_{i-1} the reflectance spectra measured at each wavelength value.

2.4 Principal Component Analysis (PCA)

The first step of the PCA tries to identify the colour parameters showing the highest potential to differentiate between sediment sources, using a multivariate statistical analysis. PCA is commonly used in environmental studies (Raux et al., 2011; Viel, 2012). The purpose of PCA is to describe linear relationships between variables of large data sets. It calculates principal dimensions that represent the degree of correlation between all variables. Dimensions that show the highest percentage of variance are chosen to explain the variables and their individual distribution. Statistical analyses were performed using the statistical software *R*[16] and the following packages: *FactoMiner*[17] and *Corrplot*[18]. All data were normalized for direct comparison.

[16] R Core Team (2016). R: A Language and Environment for Statistical Computing. R Foundation for Statistical Computing, Vienna, Austria. URL https://www.R-project.org/.

[17] https://cran.r-project.org/web/packages/FactoMineR/index.html

[18] https://cran.r-project.org/web/packages/corrplot/index.html

2.5 Set_Sat-v1.0 model

2.5.1 Data distribution

The second data processing step aimed to identify normality and potential outliers using the model *Sed_Sat-v1.0* (see Patault et al., 2018 c, *in prep – see chapter 4*). Each tracer for each source group was tested to determine if the raw concentration values are normally distributed using the Shapiro-Wilk test (Shapiro & Wilk, 1965). All variables that were not normally distributed were transformed using the Tukey Ladder of Powers transformations (log, power, square root, etc. functions; Tukey, 1977). Then, the average and standard deviation within each source type was determined. If the tracer value for a specific source exceeded three times the standard deviation of the average value, the entire sample was defined as an outlier and removed from the dataset.

2.5.2 Correcting source tracers for sediment size

To assure that tracers of sources samples are comparable to tracers in suspended sediment samples, a regression analysis was performed to determine if a tracer's property in each source groups is related to grain size (D50). The methodology was developed by Gellis & Noe (2013).

If the regression model of a source group's tracer versus D50 was found significant, a correction factor was applied to the tracer (Eq.44):

$$C_n = \{Ti_{i(n)} - [(S_j - CF) * m]\}^{\wedge} \quad (44)$$

Where C_n is the tracer after size correction; $Ti_{i(n)}$ is the original value of tracer (i) in source group (n); S_j is the D50 of the source sample (j); CF is the mean D50 in target samples; m is the slope of regression line; and ^ mean that if transform was applied the Tukey Ladder Power of transformations, the tracer is then untransformed.

2.5.3 Bracket test

The bracket test was used to determine if for a given tracer, the suspended matter samples were within the range of the equivalent values obtained for the potential sediment sources. This test is an important prerequisite and tracer that did not satisfy this constraint within measurement error (Δ = 10% of each suspended matter sample's tracer value) were considered non-conservative and were not taken into further consideration.

2.5.4 Stepwise discriminant function analysis

To find the optimum composite fingerprint that differentiate soils and channel banks, a stepwise discriminant function analysis (DFA) was used. The stepwise DFA incrementally identifies which tracers significantly contribute to correctly differentiating the sediment sources and rejects variables that do not contribute based on the minimization of the computed value of the variable Wilk's lambda. A λ close to 1.0 indicates that the means of all tracers chosen are equal and cannot be distinguished among groups. On the contrary, a λ close to 0 indicates that two groups are well separated (Gorman Sanisaca et al., 2017). At this step, the tracer discriminatory weighting value W_i is calculated. W_i is a weighting used to reflect tracer discriminatory power (Collins et al., 2010) and based on the relative discriminatory power of each individual tracer provided by the results of the DFA. The weighting ensures that tracers with greater discriminatory power are optimized in the unmixing model solutions. For each tracer, W_i is calculated as follows:

$$W_i = \frac{P_i}{P_{opt}} \tag{45}$$

Where P_i is the percentage of source type samples classified correctly using tracer i, and P_{opt} is the tracer that has the lowest percentage of sample classified correctly.

2.5.5 Mixing model

The percentage contribution of each significant source of sediment was defined using a mixing model, developed by Collins et al. (2010), and following Eq.46, 47, and 48:

$$\sum_{i=1}^{n}\{[C_i - (\sum_{i=1}^{m} P_s S_{si})]/C_i\}^2 W_i \quad (46)$$

$$0 \leq P_s \leq 1 \quad (47)$$

$$\sum_{s=1}^{n} P_s = 1 \quad (48)$$

Where C_i is the concentration of tracer i in the suspended matter sample; P_s is the optimized percentage of contribution source type (s); S_{si} is the mean concentration of tracer i in source s after size correction factors were applied; W_i is the weighting factor for tracer i; n is the number of tracers comprising the optimum composite fingerprint; and m is the number of sediment source types.

The model adheres to two constraints: each source group proportion is constrained to a positive value between 0 and 1, and the sum of all source group contributions has to be equal to 1. The unmixing model iteratively tests for the lowest error value using all possible source percentage combinations. A P_s step of 0.01 is used in the source computations. Sediment apportioned to channel banks and soils was determined for each suspended matter sample.

2.5.6 Uncertainties in the sediment fingerprinting approach

Various sources of uncertainties need to be recognized when using the sediment fingerprinting approach to be able to quantify sub-basin contributions. Inclusion of these uncertainties in mass balance modelling indicates the possible range of the different source contributions. Uncertainties were calculated using Monte-Carlo simulations. The Monte-Carlo simulation randomly removes one sample from each of the two source type groups (arable lands and

channel banks) and the unmixing model is run subsequently without these samples. The set of linear equations representing the composite fingerprint identified for each confluence was solved N = 5000 times to compute ranges in source proportions. For each of the 5000 iterations, the average, the minimum, and the maximum sediment source percentage for each source are determined. The difference between the final unmixing model of the sediment source percentage results and the average of the Monte-Carlo simulations are used to assess the robustness of the final set of source samples and tracers.

3. Results & Discussion

3.1 Inclusion of relevant sediment colour parameters

A first selection of colour tracer parameters was executed using PCA to evaluate their respective potential. 91% of the total variance is explained by the first three dimensions of the PCA. Thus, the following other dimensions were not considered significant (<10% of the total variance). On the bi-plot of Dim1/Dim2 (Fig.54A), samples originating from soil are mainly located on the positive quadrant of the axes (Dim1+/Dim2+). The position of the soil samples is explained by the value of their FDS in the range of 515-645 nm, the ratio 700/400 nm, and the chromatic variables a*, b*. The value of the FDS in the range of 365-505 nm and the chromatic variable L* are located in the quadrant Dim1+/Dim2- and can be considered as non-discriminant for both source types. There is no influence of FDS in the range of 655-735 nm in the first space. In the second space, Dim1/Dim3 (Fig.54B), the position of some channel bank samples can be attributed to the value of the FDS in the range of 675-735 nm. The location of the soil samples on these two dimensions are mainly caused by the chromatic variable L*, and the value of the FDS in the range of 505-555 nm and 605-625 nm. As a result of this first analysis, some colour parameters seam to potentially discriminate the two distinct sources. The following colour parameters were kept for further analyses: a*, b*, ratio 700/400 nm, the FDS value in the range of 515-735 nm.

As stated in literature, the expression of the FDS value can express different sediment compositions (e.g. Deaton & Balsam, 1991; Debret et al., 2011; Wolfe et al., 2006). Figure 55 shows the entire range of the FDS value of the source samples. It seems that FDS values in the range of 515-645 nm may discriminate a soil signature and that FDS values in the range of 675-735 nm are preferentially attributed to a channel bank signal. The spectral range of 525-535 nm is typically the expression of the iron oxy-hydroxides such as goethite (αFeOOH). The signature of the iron oxides such as hematite (αFe_2O_3) is mainly attributed to the peak in the range of 545-575 nm. According to Debret et al. (2011) a high increase of the FDS value in the range 655-685 nm could be the expression of fresh organic matter. In Figure 55, this is characteristic of the channel bank whereas the FDS value of the soil in the range 655-685 nm is more stable and could refer to altered organic deposits pattern.

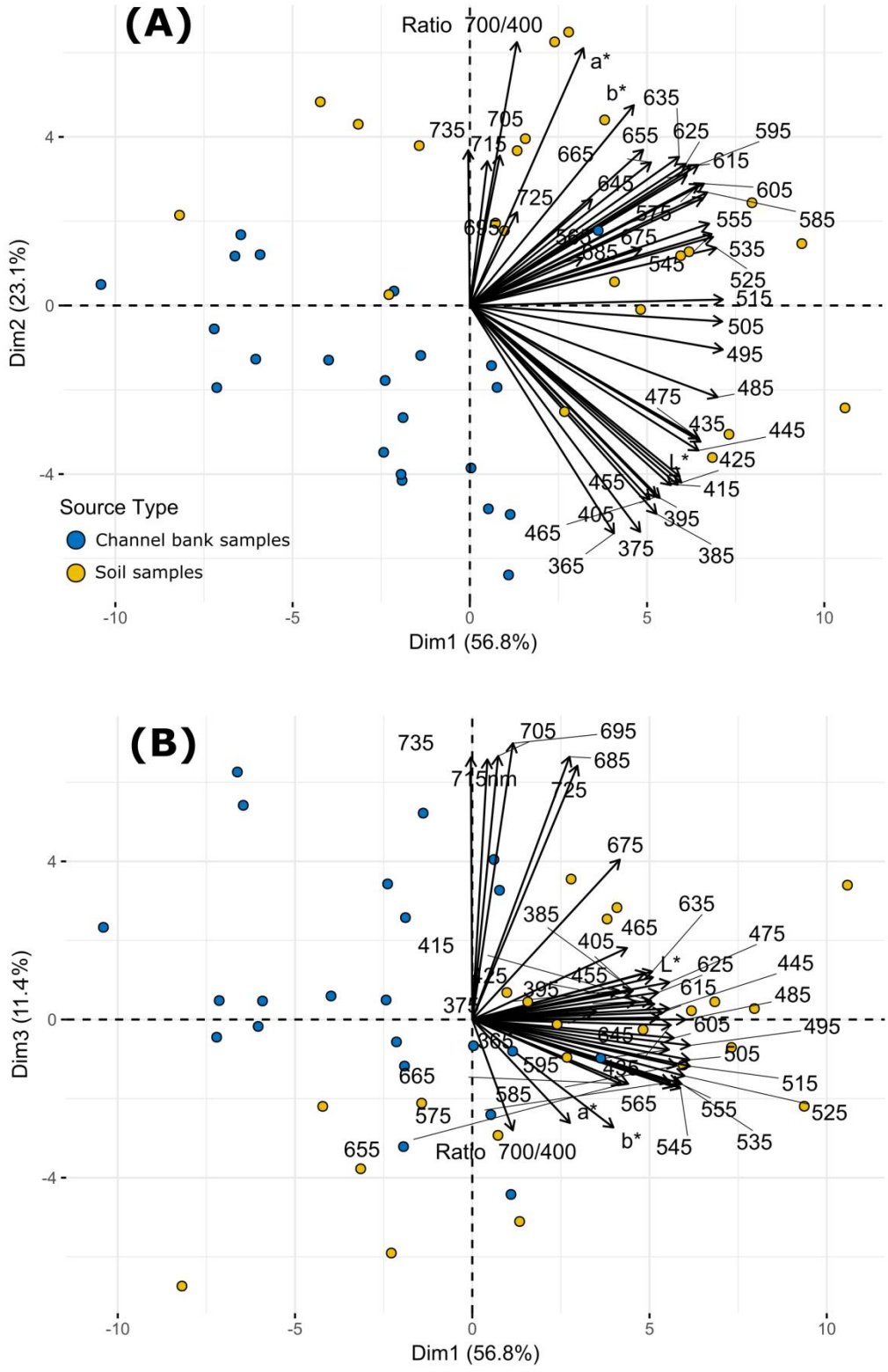

Fig. 54 : Bi-plot of PCA results for the spectrocolorimetric parameters of soil and channel bank samples on the first two spaces Dim1/Dim2 (A) and Dim1/Dim3 (B).

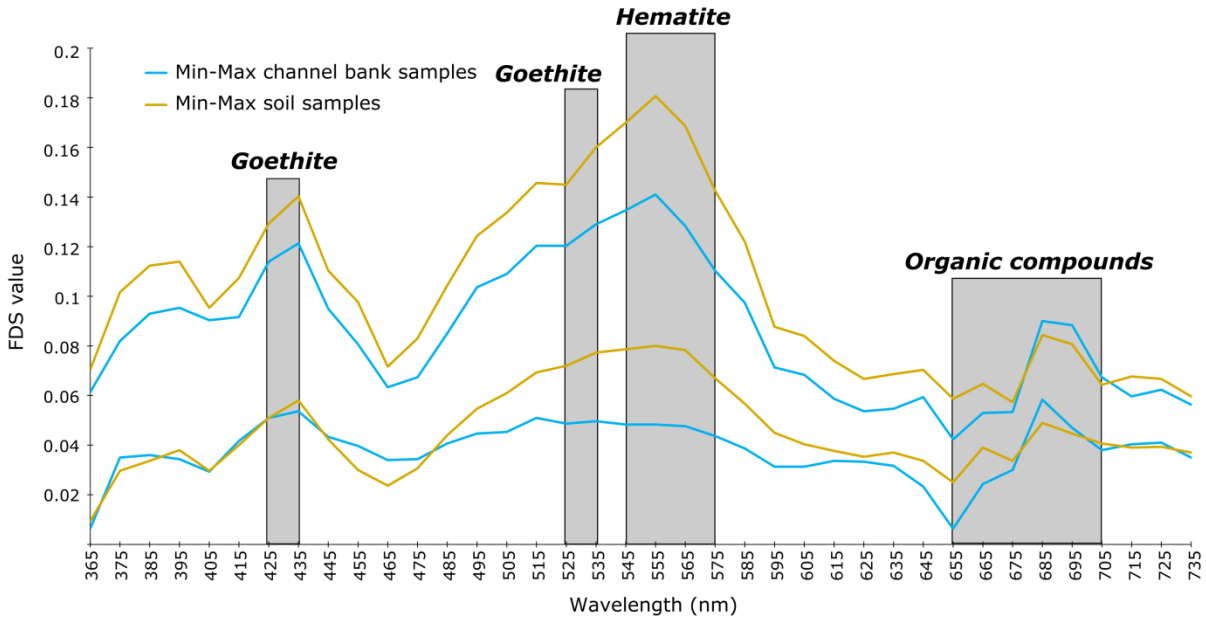

Fig. 55 : Range of the First Derivative Spectra value in all source samples. Sediment components positions on the graph were attributed based on the work of Deaton & Balsam (1991) and Debret et al. (2011).

3.2 Correcting source tracers for sediment particle size

In Fig.56, the particle size analysis highlights significant differences between the D50 (median particle size) of the soil samples (36.6 ± 8.2 µm) and the channel bank samples (63.5 ± 11.8 µm) in comparison to the suspended matter sampled at the outlet of the Canche river catchment (85.8 ± 18.8 µm). A t-test between the soil samples and the suspended matter show a significant difference between their D50 (p-value < 0.001). The same test was applied to the channel bank samples and the suspended matter and show a significant difference between their D50 (p-value = 0.005). Considering these differences in particle size distribution, a potential particle size effect could affect the direct comparison between the source samples (soils and channel banks) and the suspended matter. For further analyses, a regression analysis was performed to evaluate the correlation between a tracer value and the mean grain size. If a correlation was found significant, a particle size correction based on the value of the D50 was applied.

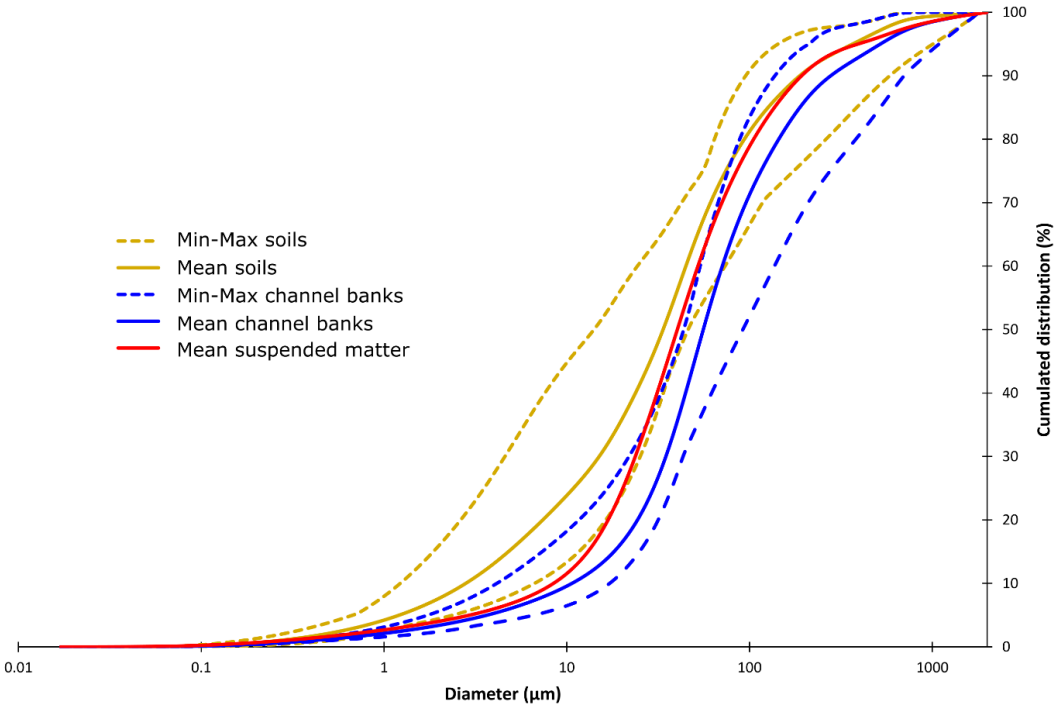

Fig. 56 : Grain size distribution of the sources samples (soil and channel bank) and the suspended matter collected in the Canche river catchment.

Plots of grain size (D50) and tracer concentration indicate a significant relation for Ce, La, Th, Ti, and U in the channel banks (Fig.57). The concentration of these elements decreases as the D50 values increase. This result might be linked to the fact that finer grain sizes have a larger adsorption potential of constituents and thus they show a higher concentration of trace elements (Gellis & Noe, 2013). Considering these effects, a correction factor was applied to these tracers (see section 2.5.2).

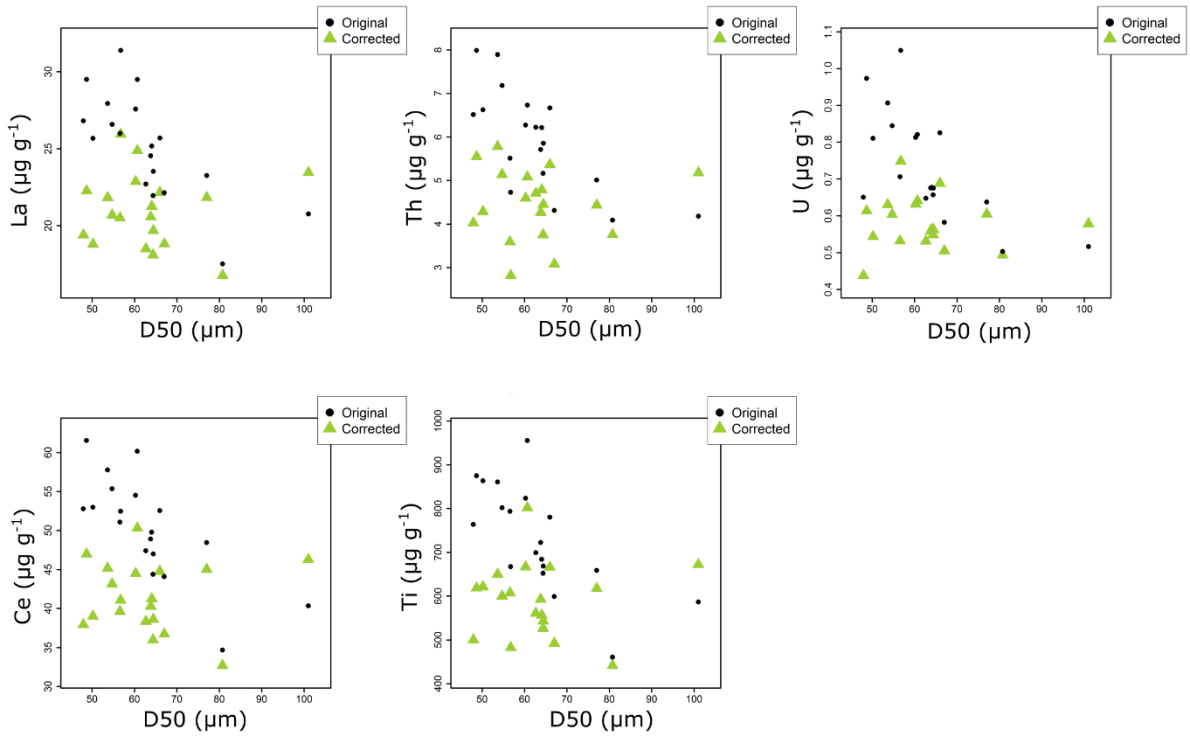

Fig. 57 : Plot of original and grain size corrected data of trace elements concentration (µg g^{-1}) versus D50 (µm).

3.3 Best tracer selection

The identification of outliers indicates that three channel bank samples and one soil sample could be considered as outliers in the dataset. For further analysis, the outlier samples were removed. The results of the bracket test showed that different tracer parameters, relative to the chemical composition and colour of the sediment, were considered conservative at the outlet of the Canche river catchment. 43 tracer parameters were kept for the stepwise DFA (As, Cd, Co, Li, Mo, Ni, Pb, Rb, Se, Sn, Th, U, Bi, Cr, Sc, V, Al, Ca, Fe, Mg, Mn, Sr, Zn, b*, 515 – 645 nm, 675 – 705 nm, and 725 nm). Stepwise DFA was applied to the transformed set of tracers for both source types and showed that four parameters compose an optimum composite fingerprint: U, b*, 535 nm, Sr (see Table 14). The Wilk's lambda criterion was minimized to 0.06. The stepwise DFA using these four parameters successfully classified 100% of the source samples to their correct source category. Tracer discriminatory weightings were applied to the four parameters and the unmixing model was run for each individual SPM sample.

Tab. 14 : Results of the stepwise DFA.

Tracer	Source type samples classified correctly by tracer (%)	Cumulative source type correctly classified by tracer (%)	Wilk's lambda	Tracer discriminatory weighting
U	97.5	97.5	0.17	1.5
b*	89.9	97.5	0.14	1.4
Sr	64.9	100	0.07	1
535 nm	87.2	100	0.06	1.3

The optimum composite fingerprint used by the unmixing model is a combination of spectrocolorimetric and chemical composition parameters that includes U, Sr, b*, and 535 nm. The chromaticity variable b* refers to the content of pigmenting substances and is characteristic of the yellowness/blueness of a given sediment sample. As stated in section 3.1, a peak in the FDS value at 535 nm is typical of the expression of the iron oxy-hydroxides such as goethite (αFeOOH). The two parameters b* and 535 nm exhibit the highest values in the soil samples. The b* is ranging from 17 to 25 and the FDS at 535 nm is ranging from 0.08 to 0.16 (Fig.58A). The low dispersion of the data indicates that the b* variability is mainly carried by the 535 nm wavelength. The selection of these two tracers in the composite fingerprint is likely due to the yellowish-brown colour of the goethite (Vodyanitskii & Savichev, 2017) which seems to be more representative of the soil signature. The results suggest that the chromaticity variable b* and the FDS value at 535 nm are linked to the iron oxy-hydroxides (i.e. goethite) which can be used as an arable land tracer in this study. Other studies using magnetic tracers confirm that the characteristics of goethite are viable tracers when working on soil erosion in rural catchment (Franke et al., 2018, *in prep – see chapter 6*).

The two chemical elements which compose the optimum composite fingerprint are U and Sr. In the channel banks, U and Sr exhibit value between 0.4 and 0.75 µg g^{-1} and respectively 45 and 145 µg g^{-1} (Fig.58B). In the soil samples, U is ranging from 0.75 to 1.28 µg g^{-1} and Sr values are ranging from 40 to 350 µg g^{-1}. The expression of these two elements in the optimum composite fingerprint could be due to the use of fertilizer on arable lands. The value of Sr reaching 350 µg g^{-1} is typical of fertilizers of sedimentary origin (Smidt, 2011). The U value is relatively high, typical values for soils

are lower, for example Du & Walling (2016) found a value of 0.96 µg g^{-1} in soil samples in England at Butsford Barton. The value is higher in soils than in channel banks and can be explained by the fact that iron oxy-hydroxides are well known for their potential to adsorb other elements, such as U that has a high binding capacity and retention potential in soils (Smidt, 2011).

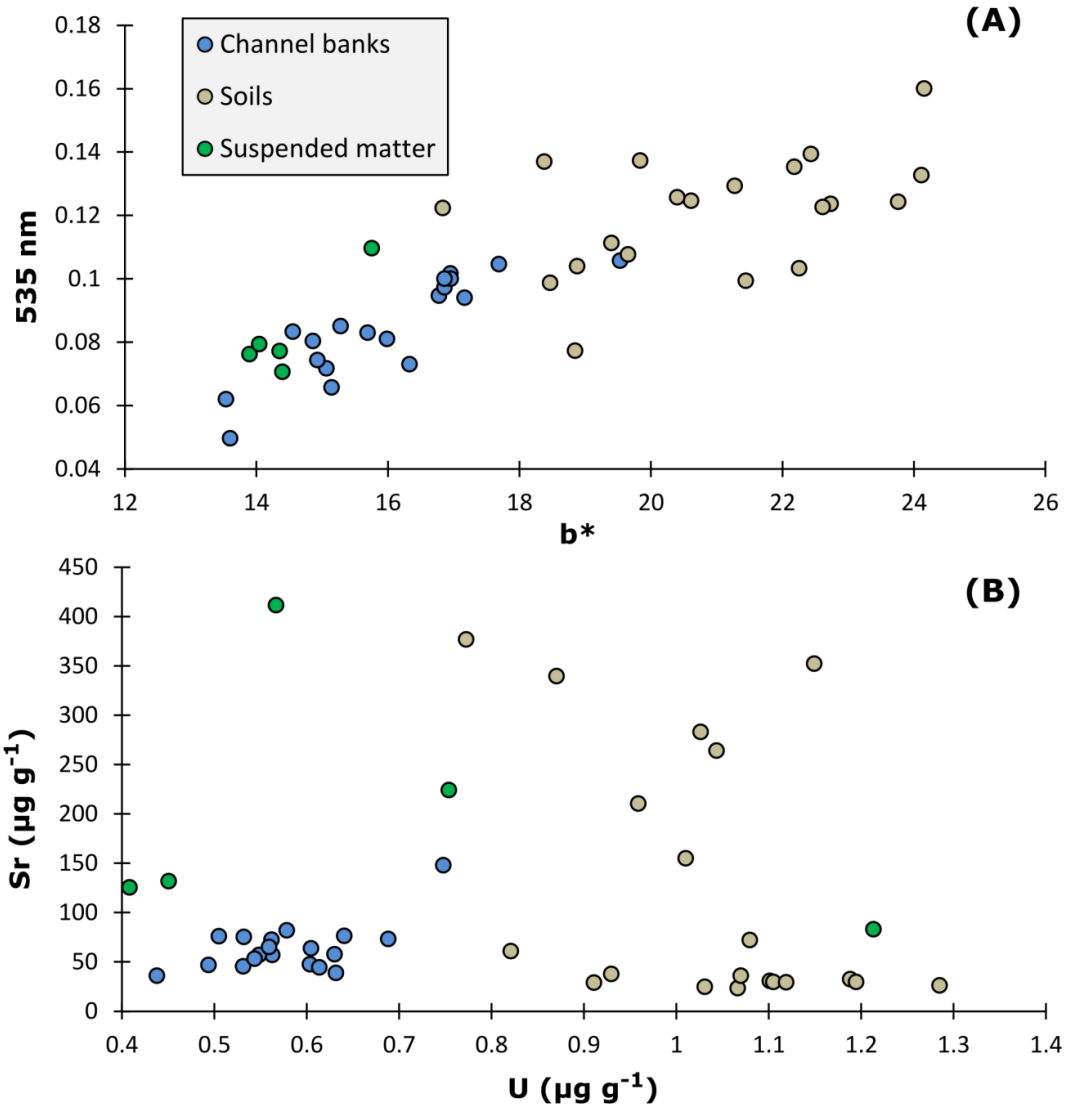

Fig. 58 : Relationship between b* and 535 nm (A) and, U and Sr (B) in sediment samples.

3.4 Relative contributions

The results of the unmixing model and the Monte-Carlo simulations (Fig.59) indicate similar average source percentages for suspended matter (< 2% confidence interval). For soils, the range of all Monte-Carlo results is < 10% higher and lower than the Monte-Carlo average value. For channel

banks, the range of Monte-Carlo results is < 12% higher and lower than the Monte-Carlo average value. The Monte-Carlo analysis is very close to the results of the unmixing model, indicating that the final set of tracer parameters may be considered as robust. The minimum and maximum differences around the average Monte-Carlo source apportionment are for most of the samples <5% with respect to the final fingerprinting results and this narrow range of values confirms that the final composite fingerprint leads to reliable results.

The total suspended sediment transported during the studied periods (5 seasonal campaigns corresponding to 6 weeks) was evaluated to 5288 t at the high-frequency monitoring station of Attin. Main sediment input was observed during the winter periods in 2015 and 2016 (2571 and 1275 t; Fig.59A-B). The sediment input was lower during the three other sampling periods (spring, summer, autumn 2016 respectively 445, 596 and 264 t; Fig.59C-D-E). The corresponding relative source contributions exhibit high temporal variabilities. Soils were the main sediment supplier during the sampling campaign of winter 2015 (56%). Channel banks were the only sediment supplier during three sampling periods (winter 2016, spring 2016, and autumn 2016). Finally, relative source contributions for the soils and the channel banks were respectively of 23 and 77% during a monitored erosive event in summer 2016. Considering the sediment flux and the relative source contributions during these five seasonal campaigns, the contribution of the soils was evaluated to 1578 t (30%) and 3710 t for channel bank sediments (70%). These results are consistent with those found by Nosrati et al. (2014) who have shown that subsurface sources (mainly channel banks) could contribute from 68 to 75% to the suspended sediment transferred downstream in a river channel in Iran. Results of Smith & Dragovich (2008) in south-eastern Australia reported on a contribution of 25% for surface sediment (soils) and 75% for sub-surface sediments (mainly channel banks). In the UK, channel banks can contribute to 50% of fluvial sediment load according to Walling (2005) and arable lands can make up 64% (Collins & Walling, 2007). Comparing these results with our own findings highlight the fact that sediment mobilization is strongly depending on local conditions.

However, the temporal approach used in this study focused on several weeks of sampling. Thus, some major erosive events on the Canche river may have not been included. As observed by Patault et al. (2018, *in review – see chapter 2*), hydro-sedimentary transfer in this context is a sudden process and leads to heavy muddy floods: more than 40% of the sediment export is linked to only 6% of the erosive events during a hydrologic year. The temporal variability of soils versus channel bank contribution is an important factor in this study. As emphasized by Gellis & Noe (2013), the exact moment of the year is an important factor in the determination of specific sediment sources.

Significant differences are observed between the seasonal campaigns. The major contribution of soil to the sediment flux is observed during the sampling campaign in winter 2015. The mean flow discharge was high (26 m^3 s^{-1}) and stable throughout the sampling period. The suspended matter concentration started to increase drastically 7 days before the removal of the trap and reached 110 mg l^{-1} indicating an erosive event in the catchment and a transfer of surface particles. The relative decrease in soil contribution in winter 2016 samples can be explained by the fact that for the erosive event occurring in February 18, 2016, the surface particles did not reach the river and goes in storage. The increase in contribution from channel bank with respect to a higher mean flow discharge (30 m^3 s^{-1}) indicates that the banks of the stream may have been eroded during this sampling period. The low contribution of soil samples in the spring 2016 sampling campaign might be linked to the full cover by the vegetation occurring in the study area preventing soil from degradation. After tillage in early summer, bare ground on arable lands can trigger sediment transfer which seems to be the case in the sampling campaign in summer 2016 that shows an increase of soil contributions. Finally, soil samples were non-contributive in autumn 2016, mean flow discharge and suspended matter concentrations were particularly low indicating that no major erosive events may have occurred.

As observed in winter 2016, channel banks can be an important supplier of sediment. One of the main causes could be the freeze-thaw action on channel bank. Gellis & Noe (2013) emphasized that it might be an important process in the erosion of channel banks during winter months.

Moreover, the important contribution of channel banks can be largely explained by the sediment delivery ratio (SDR). In fact, a large percentage of sediment eroded from upland surface (i.e. arable lands) is not delivered directly to the channel but goes in storage. According to Gellis et al. (2009), the SDR is equal to 0.2 for croplands and 1 for channel banks, considering that there are directly eroded in the river channel. Compared to upland-derived sediment (agriculture and forest), stream bank-derived sediment may have a greater potential to be eroded and delivered during an event due to fewer potential storage locations in transit, and it is likely that the sediment fingerprinting results for sediment derived from stream banks will show a significant relation to flow and seasonal conditions.

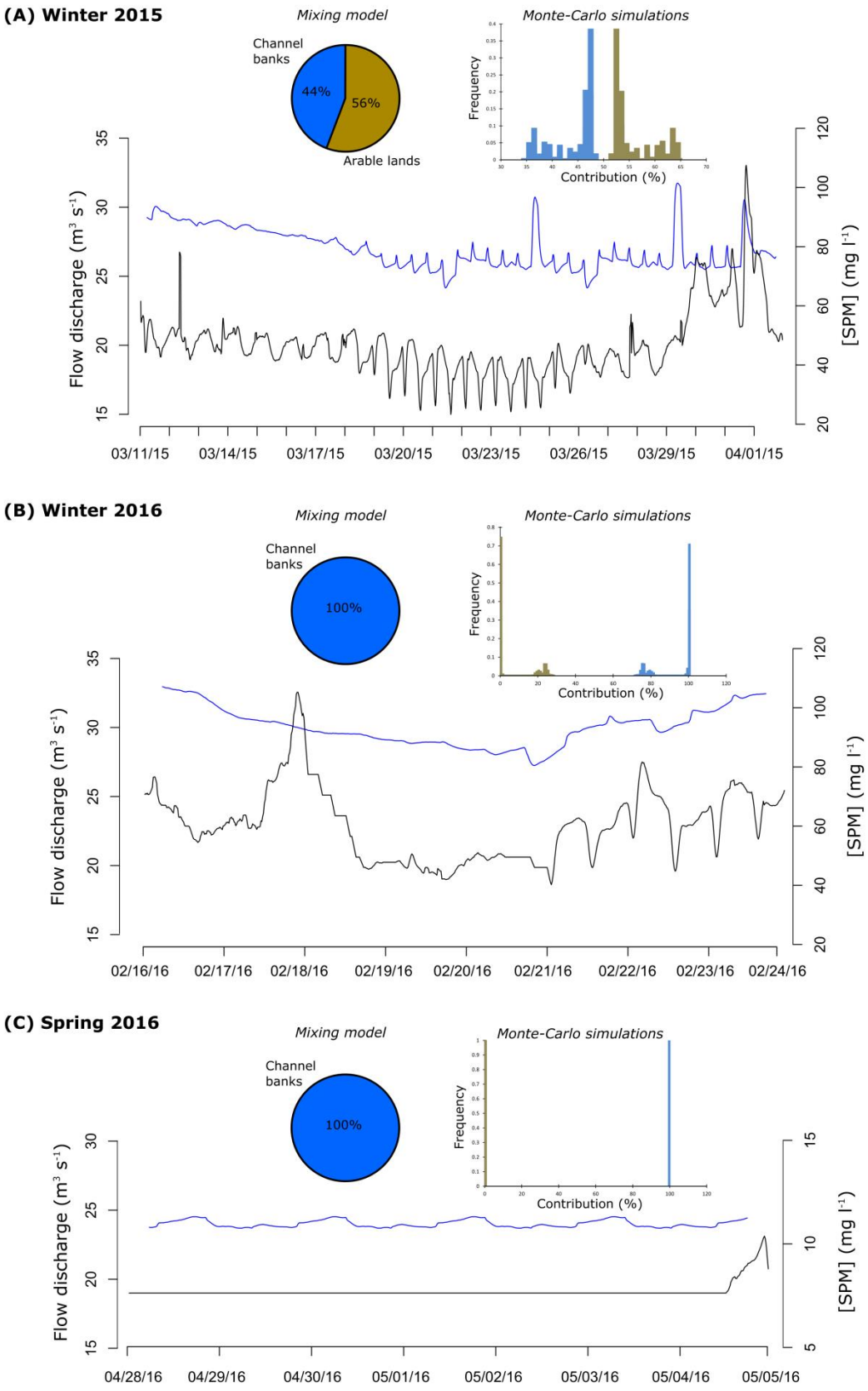

Fig. 59 : Synthesis of the hydro-sedimentary transfer recorded at the monitoring station, and results of the unmixing model and Monte-Carlo simulations for the five sampling campaigns.

(D) Summer 2016

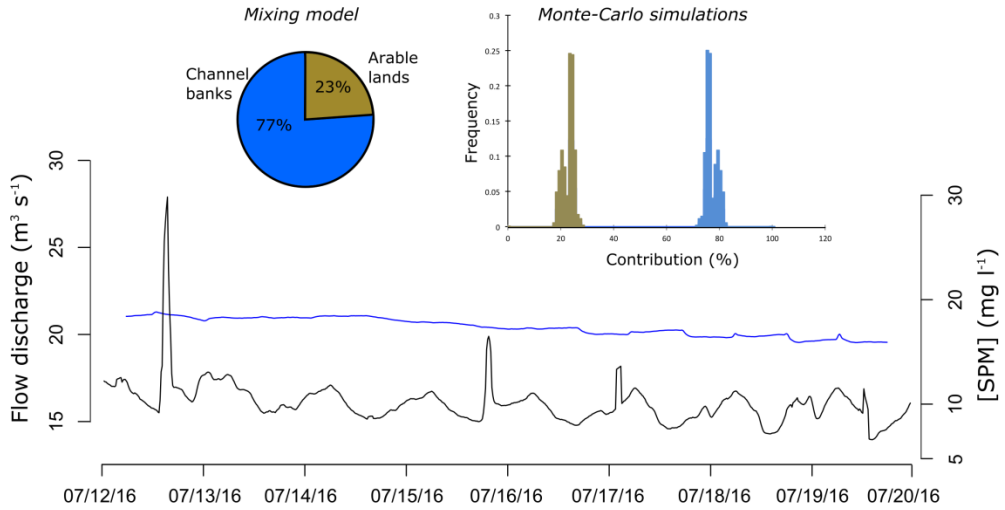

(E) Autumn 2016

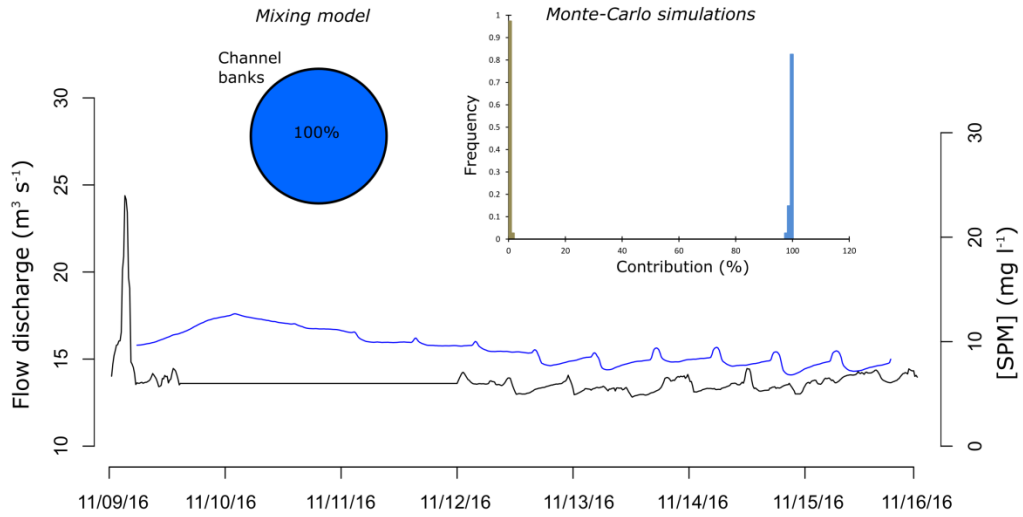

Fig. 59 (continued) : Synthesis of the hydro-sedimentary transfer recorded at the monitoring station, and results of the unmixing model and Monte-Carlo simulations for the five sampling campaigns.

4. Conclusion

Approach using tracer parameters from chemical composition and sediment colour used in this study was successful to understand the partitioning of the sediment source contribution in the studied catchment. Sources (i.e. channel banks and arable lands) were collected all along the catchment and the fluvial sediment transiting at the outlet of the catchment was collected using sediment trap. The temporal variability of the sedimentary flux was evaluated regarding five

different seasons. The signature of the sediment was evaluated using chemical composition and colour characteristics and run through a robust statistical analysis to find an optimum composite fingerprint. Sources contributions were quantified using these best tracers in a mixing model and Monte-Carlo simulations to evaluate the uncertainties. Channel banks and arable lands contributions are evaluated to 70%, and respectively 30% over the studied periods. The sediment fingerprinting approach used in this study reveals that the use of the spectrocolorimetric parameters of the iron oxy-hydroxides, such as goethite, is an interesting straightforward and easy to apply tracer for arable lands in the context of erosion. The study also showed that trace elements, as U and Sr, are particularly suitable for the studied agricultural catchment of the Canche, as they potentially mark the use of sedimentary origin fertilizers.

Acknowledgements

This work was financially supported by the Mines-Telecom Institute of Lille-Douai, with additional funding provided by the Artois-Picardie Water Agency (QUASPER project). We would also like to acknowledge technical support from the SYMCEA and the regional Chamber of Agriculture Nord-Pas-de-Calais, France. The authors are grateful to M. Alleman for the ICP-MS/AES analyses (IMT Lille-Douai – SAGE department). Spectrocolorimetric analyses were realized at the UMR 6143 M2C Rouen.

References

Balsam, W. L., & Beeson, J. P. (2003). Sea-floor sediment distribution in the Gulf of Mexico. *Deep Sea Research Part I: Oceanographic Research Papers*, *50*(12), 1421–1444. https://doi.org/10.1016/j.dsr.2003.06.001

Balsam, W. L., Deaton, B. C., & Damuth, J. E. (1999). Evaluating optical lightness as a proxy for carbonate content in marine sediment cores. *Marine Geology*, *161*, 141–153. https://doi.org/10.1016/S0025-3227(99)00037-7

Carter, J., Owens, P., Walling, D., & Leeks, G. (2003). Fingerprinting suspended sediment sources in a large urban river system. *The Science of The Total Environment*, *314–316*(03), 513–534. https://doi.org/10.1016/S0048-9697(03)00071-8

Cerdan, O., Govers, G., Le Bissonnais, Y., Van Oost, K., Poesen, J., Saby, N., … Dostal, T. (2010). Rates and spatial variations of soil erosion in Europe: A study based on erosion plot data. *Geomorphology*, *122*(1–2), 167–177. https://doi.org/10.1016/j.geomorph.2010.06.011

Collins, a. L., Walling, D. E., & Leeks, G. J. L. (1997). Use of the geochemical record preserved in floodplain deposits to reconstruct recent changes in river basin sediment sources. *Geomorphology*, *19*, 151–167. https://doi.org/10.1016/S0169-555X(96)00044-X

Collins, A. L., & Walling, D. E. (2007). Sources of fine sediment recovered from the channel bed of lowland groundwater-fed catchments in the UK. *Geomorphology*, *88*(1–2), 120–138. https://doi.org/10.1016/j.geomorph.2006.10.018

Collins, A. L., Walling, D. E., Webb, L., & King, P. (2010). Apportioning catchment scale sediment sources using a modified composite fingerprinting technique incorporating property weightings and prior information. *Geoderma*, *155*(3–4), 249–261. https://doi.org/10.1016/j.geoderma.2009.12.008

Collins, A. L., Zhang, Y., McChesney, D., Walling, D. E., Haley, S. M., & Smith, P. (2012). Sediment source tracing in a lowland agricultural catchment in southern England using a modified procedure combining statistical analysis and numerical modelling. *Science of The Total Environment*, *414*, 301–317. https://doi.org/10.1016/j.scitotenv.2011.10.062

Deaton, B. C., & Balsam, W. L. (1991). Visible spectroscopy - A rapid method for determining hematite and goethite concentration in geological materials. *Journal of Sedimentary Research*, *61*(4), 628–632.

Debret, M., Sebag, D., Desmet, M., Balsam, W., Copard, Y., Mourier, B., … Winiarski, T. (2011). Spectrocolorimetric interpretation of sedimentary dynamics: The new "Q7/4 diagram." *Earth-Science Reviews*, *109*, 1–19. https://doi.org/10.1016/j.earscirev.2011.07.002

Debret, M., Copard, Y., Van Exam, A., Bessereau, G., Haeseler, F., Rouzaud, J-N. (2018). The color of refractory organic carbon. BSGF - Earth Sciences Bulletin. 189(9). https://doi.org/10.1051/bgsf/201808

Du, P., & Walling, D. E. (2016). Fingerprinting surficial sediment sources: Exploring some potential problems associated with the spatial variability of source material properties. *Journal of Environmental Management*, 1–12. https://doi.org/10.1016/j.jenvman.2016.05.066

Evrard, O., Poulenard, J., Némery, J., Ayrault, S., Gratiot, N., Duvert, C., … Esteves, M. (2013). Tracing sediment sources in a tropical highland catchment of central Mexico by using conventional and alternative fingerprinting methods. *Hydrological Processes*, *27*(6), 911–922. https://doi.org/10.1002/hyp.9421

Gellis, A. C., Hupp, C., Pavich, M., Landwehr, J., Banks, W. S. L., Hubbard, B., … Reuter, J. (2009). *Sources, Transport, and Storage of Sediment at Selected Sites in the Chesapeake Bay Watershed*. *USGS Scientific Investigations Report* (Vol. 2008–5186). Retrieved from http://pubs.usgs.gov/sir/2008/5186/pdf/sir2008-5186rev1142011.pdf

Gellis, A. C., & Noe, G. B. (2013). Sediment source analysis in the Linganore Creek watershed, Maryland, USA, using the sediment fingerprinting approach: 2008 to 2010. *Journal of Soils and Sediments*, *13*(10), 1735–1753. https://doi.org/10.1007/s11368-013-0771-6

Gorman Sanisaca, L. E., Gellis, A. C., & Lorenz, D. L. (2017). Determining the Sources of Fine-Grained Sediment Using the Sediment Source Assessment Tool (Sed _ SAT).

Guzmán, G., Quinton, J. N., Nearing, M. A., Mabit, L., & Gómez, J. A. (2013). Sediment tracers in water erosion studies: current approaches and challenges. *Journal of Soils and Sediments*, *13*(4), 816–833. https://doi.org/10.1007/s11368-013-0659-5

Haddadchi, A., Ryder, D. S., Evrard, O., & Olley, J. (2013). Sediment fingerprinting in fluvial systems: review of tracers, sediment sources and mixing models. *International Journal of Sediment Research*, *28*(4), 560–578. https://doi.org/10.1016/S1001-6279(14)60013-5

Kayvantash, D., Cojan, I., Kissel, C., & Franke, C. (2017). Magnetic fingerprint of the sediment load in a meander bend section of the Seine River (France). *Geomorphology*, *286*, 14–26. https://doi.org/10.1016/j.geomorph.2017.02.020

Krein, A., Petticrew, E., & Udelhoven, T. (2003). The use of fine sediment fractal dimensions and colour to determine sediment sources in a small watershed. *Catena*, *53*, 165–179. https://doi.org/10.1016/S0341-8162(03)00021-3

Laceby, J. P., Evrard, O., Smith, H. G., Blake, W. H., Olley, J. M., Minella, J. P. G., & Owens, P. N. (2017). The challenges and opportunities of addressing particle size effects in sediment source fingerprinting: A review. *Earth-Science Reviews*, *169*, 85–103. https://doi.org/10.1016/j.earscirev.2017.04.009

Laignel, B. (2003). Mémoire d ' Habilitation à Diriger des Recherches Benoit LAIGNEL Livret I : Axes et Développement de la Recherche.

Landemaine, V. (2016). *Érosion des sols et transferts sédimentaires sur les bassins versants de l'Ouest du Bassin de Paris : analyse, quantification et modélisation à l'échelle pluriannuelle*. Université de Rouen Normandie.

Lautridou, J. P., Monnier, J. L., Morzadec, M. T., Somme, J., Tuffreau, A. (1986). *The Pleistocene of Northern France. Quaternary Science Review*, 5, 387-393.

Le Gall, M., Evrard, O., Foucher, A., Laceby, J. P., Salvador-Blanes, S., Thil, F., … Ayrault, S. (2016). Quantifying sediment sources in a lowland agricultural catchment pond using 137Cs activities and radiogenic 87Sr/86Sr ratios. *Science of the Total Environment*, *566–567*, 968–980. https://doi.org/10.1016/j.scitotenv.2016.05.093

Legout, C., Poulenard, J., Nemery, J., Navratil, O., Grangeon, T., Evrard, O., & Esteves, M. (2013). Quantifying suspended sediment sources during runoff events in headwater catchments using spectrocolorimetry. *Journal of Soils and Sediments*, *13*, 1478–1492. https://doi.org/10.1007/s11368-013-0728-9

Martínez-Carreras, N., Krein, A., Gallart, F., Iffly, J. F., Pfister, L., Hoffmann, L., & Owens, P. N. (2010). Assessment of different colour parameters for discriminating potential suspended sediment sources and provenance: A multi-scale study in Luxembourg. *Geomorphology*, *118*(1–2), 118–129. https://doi.org/10.1016/j.geomorph.2009.12.013

Martínez-Carreras, N., Udelhoven, T., Krein, A., Gallart, F., Iffly, J. F., Ziebel, J., … Walling, D. E. (2010). The use of sediment colour measured by diffuse reflectance spectrometry to determine sediment sources: Application to the Attert River catchment (Luxembourg). *Journal of Hydrology*, *382*(1–4), 49–63. https://doi.org/10.1016/j.jhydrol.2009.12.017

Motha, J. a., Wallbrink, P. J., Hairsine, P. B., & Grayson, R. B. (2004). Unsealed roads as suspended sediment sources in an agricultural catchment in south-eastern Australia. *Journal of Hydrology*, *286*(1–4), 1–18. https://doi.org/10.1016/j.jhydrol.2003.07.006

Nosrati, K., Govers, G., Semmens, B. X., & Ward, E. J. (2014). A mixing model to incorporate uncertainty in sediment fingerprinting. *Geoderma*, *217–218*, 173–180. https://doi.org/10.1016/j.geoderma.2013.12.002

Poulenard, J., Perrette, Y., Fanget, B., Quetin, P., Trevisan, D., & Dorioz, J. M. (2009). Infrared spectroscopy tracing of sediment sources in a small rural watershed (French Alps). *Science of the Total Environment*, *407*(8), 2808–2819. https://doi.org/10.1016/j.scitotenv.2008.12.049

Pulley, S., & Rowntree, K. (2016). The use of an ordinary colour scanner to fingerprint sediment sources in the South African Karoo. *Journal of Environmental Management*, *165*, 253–262. https://doi.org/10.1016/j.jenvman.2015.09.037

Raux, J., Copard, Y., Laignel, B., Fournier, M., & Masseï, N. (2011). Classification of worldwide drainage basins through the multivariate analysis of variables controlling their hydrosedimentary response. *Global and Planetary Change*, *76*(3–4), 117–127. https://doi.org/10.1016/j.gloplacha.2010.12.005

Russell, M. ., Walling, D. ., & Hodgkinson, R. . (2001). Suspended sediment sources in two small lowland agricultural catchments in the UK. *Journal of Hydrology*, *252*(1–4), 1–24. https://doi.org/10.1016/S0022-1694(01)00388-2

Sebag, D., Debret, M., M'voubou, M., Obame, R. M., Ngomanda, a., Oslisly, R., … Giresse, P. (2013). Coupled Rock-Eval pyrolysis and spectrophotometry for lacustrine sedimentary dynamics: Application for West Central African rainforests (Kamalete and Nguene lakes, Gabon). *The Holocene*, *23*, 1173–1183. https://doi.org/10.1177/0959683613483622

Shapiro, S. S., & Wilk, M. B. (1965). An Analysis of Variance Test for Normality (Complete Samples), *52*(3), 591–611. Retrieved from http://www.jstor.org/stable/2333709

Smidt, G. (2011). *Mobility of fertiliser-derived uranium in arable soils and its contribution to uranium concentrations in groundwater and tap water*. Jacobs University.

Smith, H. G., & Dragovich, D. (2008). Improving precision in sediment source and erosion process distinction in an upland catchment, south-eastern Australia. *Catena*, *72*(1), 191–203. https://doi.org/10.1016/j.catena.2007.05.013

Tessier, L. (2003). *Transport et caractérisation des matières en suspension dans le bassin versant de la Seine : identification de signatures naturelles et anthropiques*. Ecole des Ponts ParisTech.

Theuring, P., Collins, A. L., & Rode, M. (2015). Source identification of fine-grained suspended sediment in the Kharaa River basin, northern Mongolia. *Science of The Total Environment*, *526*(APRIL), 77–87. https://doi.org/10.1016/j.scitotenv.2015.03.134

Viel, V. (2012). *Analyse spatiale et temporelle des transferts sédimentaires dans les hydrosystèmes normands. Exemple du bassin versant de la Seulles*. *Thèse*.

Vodyanitskii, Y. N., & Savichev, A. T. (2017). The influence of organic matter on soil color using the regression equations of optical parameters in the system CIE- L*a*b*. *Annals of Agrarian Science*, *15*(3), 380–385. https://doi.org/10.1016/j.aasci.2017.05.023

Walling, D. E. (2005). Tracing suspended sediment sources in catchments and river systems. *Science of the Total Environment*, *344*(1–3 SPEC. ISS.), 159–184. https://doi.org/10.1016/j.scitotenv.2005.02.011

Wolfe, A. P., Vinebrooke, R. D., Michelutti, N., Rivard, B., & Das, B. (2006). Experimental calibration of lake-sediment spectral reflectance to chlorophyll a concentrations: Methodology and paleolimnological validation. *Journal of Paleolimnology*, *36*(1), 91–100. https://doi.org/10.1007/s10933-006-0006-6

Chapter 6

Magnetic fingerprinting of fluvial suspended particles in the context of fertile soil erosion: example of the Canche river watershed (Northern France).

Résumé étendu - Chapitre 6

Contexte

Certains bassins versants sont soumis à des processus d'érosion particulièrement importants, qui peuvent conduire à des catastrophes naturelles (ex. coulées boueuses). La gestion de ces transferts sédimentaires sur les territoires concernés est indispensable et nécessite d'identifier les voies de transferts et les sources à l'origine de ces apports. Ces dernières années, de nombreuses études ont été entreprises à travers le monde pour identifier et quantifier les contributions des sources de sédiments au flux dans les bassins versants. Ces études se basent sur l'utilisation de traceurs des zones sources de l'érosion. Ces dernières peuvent être de différentes natures : minéralogique, géochimique, radionucléides, etc). Si l'efficacité de ces approches est reconnue, elles affichent quelques limites et peuvent se révéler très difficiles à mettre en œuvre pour des gestionnaires de bassin versant. En plus, elles peuvent s'avérer coûteuses en termes de temps et de budget. Dès lors, il est utile de développer de nouveaux traceurs pour pouvoir modéliser, rapidement et efficacement, le transport sédimentaire dans un bassin versant. Dans ce contexte, les méthodes issues du magnétisme environnemental offrent des avantages certains : rapidité d'analyse, non destructif, forte sensibilité, faible coût ; et permettent d'identifier et d'estimer la fraction ferrugineuse du matériel sédimentaire (par spéciation de la magnéto-minéralogie). Cette typologie magnéto-minéralogique est spécifique des différentes zones sources de matière. Plusieurs travaux (Evans & Heller, 2003 ; Maher, 2007) ont montré que la spéciation de la magnéto-minéralogie permet notamment de discriminer une signature sédimentaire liée à de l'érosion de surface et une signature sédimentaire liée à un bruit de fond de l'hydrosystème. L'objectif principal de cette étude est alors de tester la pertinence et la validité des paramètres magnétiques comme traceurs de l'érosion des sols dans le contexte du bassin versant de la Canche, soumis à d'important processus de transferts sédimentaires.

Matériel et méthodes

Pour répondre à l'objectif de l'étude, des matières en suspensions (MES) et trois sources sédimentaires : coulées boueuses issues de l'érosion de sols de surface, berges et fond de chenal, ont été échantillonnées selon plusieurs modalités spatio-temporelles (Tableau 15) dans le bassin versant de la Canche. La fraction ferrugineuse a été caractérisée au travers d'analyses magnétiques sur les échantillons secs entiers.

Tab. 15 : ***Ensemble des échantillons prélevés dans le cadre de l'étude.***

Nature de l'échantillon	Mode de prélèvement	Nombre d'échantillon	Temporalité
MES	Piège à sédiment	n = 75	Hiver 2015 + Hiver-Printemps-Eté-Automne 2016
MES	Préleveur automatique	n = 24	Episode érosif (8 juin 2016)
Coulées boueuses	Piège à sédiment	n = 2	Episode érosif (3 fév 2017)
Berges	Tube PVC	n = 6	Episode érosif (3 fév 2017)
Fond de chenal	Grappin	n = 3	Episode érosif (3 fév 2017)
MES	Piège à sédiment	n = 9	Episode érosif (3 fév 2017)

Les paramètres magnétiques (aimantation à saturation : M_s ; aimantation rémanente : M_r ; aimantation rémanente à saturation : M_{rs} ; force coercitive : H_c ; force coercitive rémanente :H_{cr}) ont été obtenues d'après l'analyse des courbes d'hystérésis à 0,3 et 1 T à température ambiante avec un magnétomètre à gradient de force alternée (*AGFM 2900*). Ces paramètres permettent de discuter de la concentration « magnétique » de l'échantillon. Le ratio entre l'aimantation rémanente à 0,3 T et 1 T (S-ratio) est ensuite calculé et permet ensuite une estimation de la contribution des minéraux de haute coercivité (goethite/hématite) par rapport aux minéraux de basse coercivité (magnétite) dans un échantillon. Pour mieux identifier les composants magnétiques présents (geothite, hématite, magnétite) dans les échantillons, le protocole de Lagroix & Guyodo (2017) a été appliqué sur quatre échantillons en particulier et consiste à effectuer des mesures d'aimantation rémanente isothermique à saturation en température basse avec un système de mesure des propriétés magnétiques (*MPMS Quantum Design XL-5 Ever Cool*). Les contributions des fractions magnétiques de haute et basse coercivité ont ensuite été définies par la déconvolution des composantes des

courbes d'acquisition de l'aimantation rémanente isotherme (M_{rs}) selon le modèle développé par Kruiver et al. (2001).

Résultats

Pour montrer le potentiel des analyses magnétiques comme traceur d'érosion des sols, un premier focus a été entrepris sur un point particulier de la Canche (point C2, confluence Planquette-Canche). En s'appuyant sur les travaux de Kayvantash (2016), on montre que les valeurs de M_s et M_{rs} (à 0,3 et 1T) obtenues dans les MES sont caractéristiques d'un signal érosif en milieu rural. La différence d'aimantation rémanente à saturation entre les deux champs appliqués, caractérisée par le paramètre S-ratio, indique que le signal magnétique est porté par deux groupes de magnéti-minéralogie distinctes. Une première composante de haute coercivité et une seconde de basse coercivité. Pour donner suite à ces premiers résultats, les analyses selon le protocole de Lagroix & Guyodo (2017) ont été effectuées et ont donné plus d'informations sur les composantes de haute coercivité (hématite/goethite) présentes dans les échantillons. A partir des courbes d'acquisition de l'aimantation rémanente isotherme, les contributions respectives des composés de haute et basse coercivité du matériel sédimentaire ont pu être quantifiées sur les MES au cours de différents épisodes érosifs et sur les sources potentielles de matières : coulées boueuses, berges, fond de chenal. Les résultats soulignent que la fraction de haute coercivité (goethite et hématite) est majoritairement présente dans les échantillons de type coulées boueuse et dans les MES récoltées lors d'épisodes érosifs. Le suivi d'un épisode érosif simple, a ensuite été réalisé à l'exutoire de la Canche. Une excellente corrélation a pu être observée entre le S-ratio et la concentration en MES/turbidité. Une augmentation du S-ratio, signataire d'une augmentation de la minéralogie de basse coercivité, est observée dans les échantillons lorsque la turbidité et concentration en MES diminue. Elle conforte l'hypothèse selon laquelle la fraction de haute-coercivité (goethite et hématite) porte une signature des sols de surface et tend à considérer le S-ratio comme traceur d'érosion des terres arables (Fig.60). A une plus large échelle, le bassin versant de la Canche, les analyses des MES selon cinq temporalités différentes montrent que les affluents ont généralement

une plus forte contribution de la fraction magnétique de haute coercivité mais que cela est dépendant des conditions hydrodynamiques.

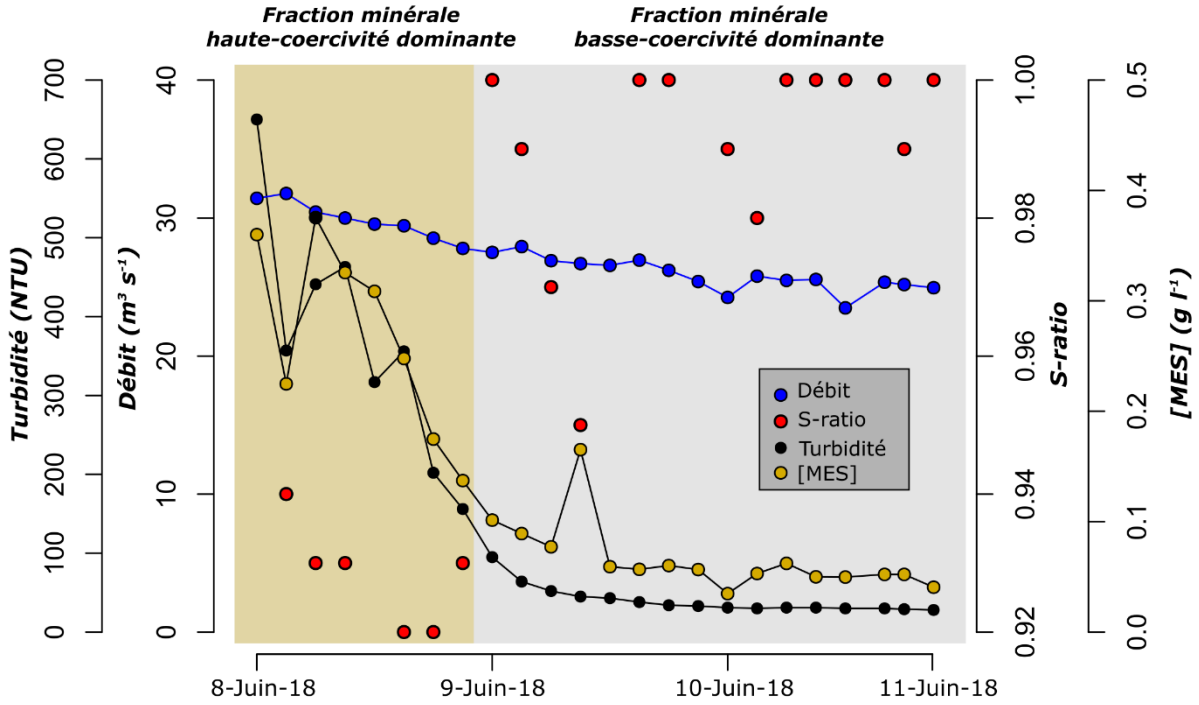

Fig. 60 : ***Variations du S-ratio dans les matières en suspensions de la Canche au cours d'un épisode érosif en juin 2018.***

Conclusions

Les proxies du magnétisme environnemental montrent un réel intérêt pour tracer les processus d'érosion. Leur habilité à distinguer les composants de faible et haute coercivité dans la fraction ferrugineuse permet de révéler que les sédiments en transit lors d'épisode érosifs ont une signature type goethite/hématite et qu'à contrario lors des périodes de faible transfert sédimentaire le signal tend vers une signature dominée par la magnétite. Leurs contributions respectives aux cours de différents évènements/périodes d'échantillonnage est variable et représentative des conditions hydrodynamiques. L'utilisation de ces méthodes se veut relativement rapide à mettre en œuvre, non destructive et peu coûteuses. Elles offrent de nouvelles opportunités en termes de traçage de sources et semblent tout à fait appropriées pour être incorporées dans des analyses/modélisations de type sediment fingerprinting.

Chapter 6: Magnetic fingerprinting of fluvial suspended particles in the context of fertile soil erosion: example of the Canche River watershed (Northern France).

Christine Franke[a], Edouard Patault[a, b], Claire Alary[b], Nor-Edine Abriak[b], France Lagroix[c]

[a]MINES ParisTech, PSL Research University, Center of Geosciences, 35 rue Saint-Honoré, 77305 Fontainebleau Cedex, France

[b]IMT Lille Douai, Univ. Lille, EA 4515 - LGCgE - Civil Engineering and Environmental Department, F-59000 Lille, France

[c]IPGP, Équipe de Paléomagnétisme, 1 rue Jussieu, 75238 Paris Cedex 05, France

This chapter is in preparation for submission to the journal Frontiers in Earth Science.

Highlights

- Deployment of rapid and easy to apply proxy parameters from environmental magnetism
- Characterization of soil erosion vs bed load river signal
- IRM component analysis model serves as spatio-temporal sediment flux parameter
- S-ratio parameter gives reliable "pictures" on the spatio-temporal runoff conditions

Graphical abstract

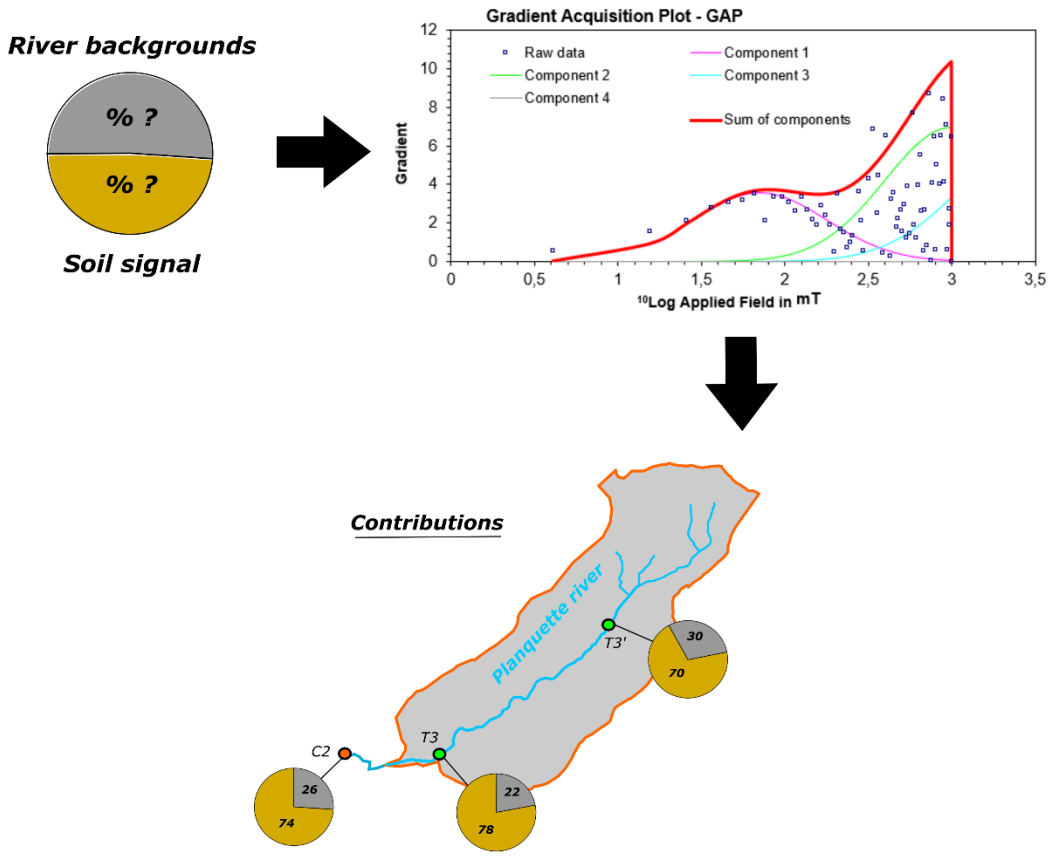

Abstract

In the North of France, land use is mainly dominated by agricultural activity. Erosion by water runoff results in heavy loss of fertile soil and can be responsible for the input of nutrients, pesticides or heavy metals into surface water. There is a need for straightforward tools to trace the sediment flux within a given catchment. This study highlights the potential of environmental magnetism techniques (room temperature hysteresis parameters, low-temperature remanence cycles) to provide additional rapid and non-destructive fingerprint parameters to characterize the spatio-temporal runoff versus bed load signal conditions in the Canche river watershed. Between 2015 and 2017, several spatio-temporal sampling campaigns of suspended particulate matter (SPM) and two distinct "snap shot campaigns" of flood events were conducted at key positions along the Canche river and its tributaries using bottle sediment traps. Room temperature hysteresis curves of the recovered dry bulk SPM were obtained. Magnetic concentration of the SPM evaluated by M_{rs} or M_s values are typical of values for agricultural soils in the region. S-ratio data indicate that during low flow conditions ("natural fluvial background signal") the Canche river SPM is dominated by a soft ferromagnetic mineral assemblage while during high water stages (local rain events) the magnetic mineral assemblage is enriched in high coercivity phases. Increased soil erosion, especially via water runoff, is expected during rain events. The observed temporal (seasonal) variations in the magnetic mineral assemblage would be expected if the agricultural soils were enriched in goethite and/or hematite with respect to ferromagnetic pedogenic minerals. Additional low-temperature remanence experiments on selected samples provide greater insight into the mineralogy of the magnetic phases of the SPM and confirm the room temperature results. Thus, IRM component analysis of the room temperature results may be employed to quantify the relative input of high coercivity versus low coercivity components focused on a given confluence site. Additionally, the results from the snap shot sampling campaigns highlight the link between the enhanced runoff input of high-coercivity particles during flood events and therefore show that the S-ratio parameter is an effective tool to trace erosion by water runoff in fingerprinting models.

Key words: Magnetic fingerprinting; Environmental magnetism; S-ratio; Suspended particulate matter; Canche river watershed; Soil erosion

1. Introduction

In the context of efficient land use management and the rising demand on sediment control strategies, numerous studies on the complex aspects of sediment flux in fluvial systems have been undertaken (e.g. review of Haddadchi et al., 2013). Many of these investigations discuss the different tracers (geochemistry (Carter et al., 2003; Theuring et al., 2015; Vale et al., 2016), radionuclides (e.g. Le Gall et al., 2016; Evrard et al., 2010), sediment color (Poulenard et al., 2009; Martínez-Carreras et al., 2010) which may be used to estimate and model the transported sediment yield and identify the various diffuse or point sources over time and space.

There is a clear need for rapid and easy to interpret proxy parameters (Guzmán et al., 2013) and through the last decades there has been a remarkable diversification of available environmental magnetic fingerprinting techniques applied to fluvial catchment studies (e.g. Walling et al., 1979; Oldfield et al., 1979; Caitcheon, 1993; Slattery et al., 1995; Dearing, 1987; Russell et al., 2001; Motha et al., 2004; Maher et al., 2009).

Environmental magnetism is one of these techniques, which present the advantage of tracing the iron-bearing mineral fraction of the sediment. The ubiquity of iron in the environment leads to iron-bearing minerals, being involved in many of the processes occurring in the fluvial system (runoff, sediment flux, accumulation, diagenesis/oxydo-reduction, etc; e.g. Evans & Heller, 2003; Maher, 2007). The most important challenge for magnetism-based proxies is determining the correct interpretation of the magnetic proxy parameters with respect to sampling process, sediment type, magnetic mineral phase assemblages and range of particle size.

This study aims to develop a straightforward magnetic proxy parameter to trace the erosion of fertile soil at the scale of a catchment to model quantitatively sediment flux spatially and temporally. We take advantage of the fact that fertile soil particles have been found to carry a distinct mineral signature (e.g. Maher, 2007) compared to the average bed load of rivers. This is particularly where lithologies are relatively homogeneous across the drainage areas as is the case for the Canche river catchment in Northern France.

2. Study area and sampling strategy

2.1 Context of the Canche river

The Canche river watershed (1274 km²; latitude: 50°25'53''N, longitude: 2°02'24''E; Fig.61A) is located in the European loess belt in Northern France. This region is characterized by oceanic climate conditions, the mean annual temperature is 11°C and the mean annual rainfall is 1000 ± 100 mm. Daily cumulative rainfall is recorded at two strategic points in the catchment: Touquet-Paris-Plage, and Radinghem (Fig.61B). Altitudes range from 0 m at the catchment outlet to 207 m in upstream areas and slopes in the landscape are commonly in the range of 2-3%. The basin drains Pleistocene silts sitting on top of Seno-Turonian chalks. The land use is dominated by arable lands (> 80%; Fig.61B).

The watershed is characterized by a meandriform drainage network dominated by the Canche river (88 km length) and seven main tributaries: the Ternoise, the Planquette, the Créquoise, the Bras de Bronne, the Course, the Dordogne, and the Huîtrepin (Fig.61C). The flow discharge at each sampling site was quantified using the low-frequency monitoring station on the Ternoise, the Course and the Canche. Flow discharge for the ungauged catchment $Q_{ungauged}$ was calculated assuming similar rainfall and hydrological regimes in the entire Canche catchment. Values were extrapolated from the closest monitoring station by multiplying the value Q_{gauged} with the appropriate fraction related to the ratio between the closest catchment area ($A_{ungauged}$) and the catchment area at the monitoring station A_{gauged} :

$$Q_{ungauged} = Q_{gauged} \times \frac{A_{ungauged}}{A_{gauged}} \quad (49)$$

with Q representing the discharge in $m^3\ s^{-1}$ and A as the area of the catchment in km².

According to Andréassian et al. (2012), this method provides meaningful estimations for ungauged catchments. Cross validation with the high-frequency monitoring station on the Canche

river at Attin evaluates that the flow discharge temporal variability is preserved, and the associated error was quantified to 17%. Mean annual discharge for the Canche river is estimated at 21 $m^3 s^{-1}$ with contributions from main sub-catchments: Ternoise (7 $m^3 s^{-1}$), Planquette (1.5 $m^3 s^{-1}$), Créquoise (2 $m^3 s^{-1}$), Bras de Bronne (2 $m^3 s^{-1}$), Course (4 $m^3 s^{-1}$), Dordogne (2.5 $m^3 s^{-1}$), and Huîtrepin (2 $m^3 s^{-1}$). According to information from the Artois-Picardie Water Agency, the annual sediment export since 1999 at the outlet of the Canche watershed range from 29 to 185 kt. The high amount of sediment flux in this territory is a direct consequence of soil erosion and mudflow, which cause infrastructure damages and an important economic cost for the local communities.

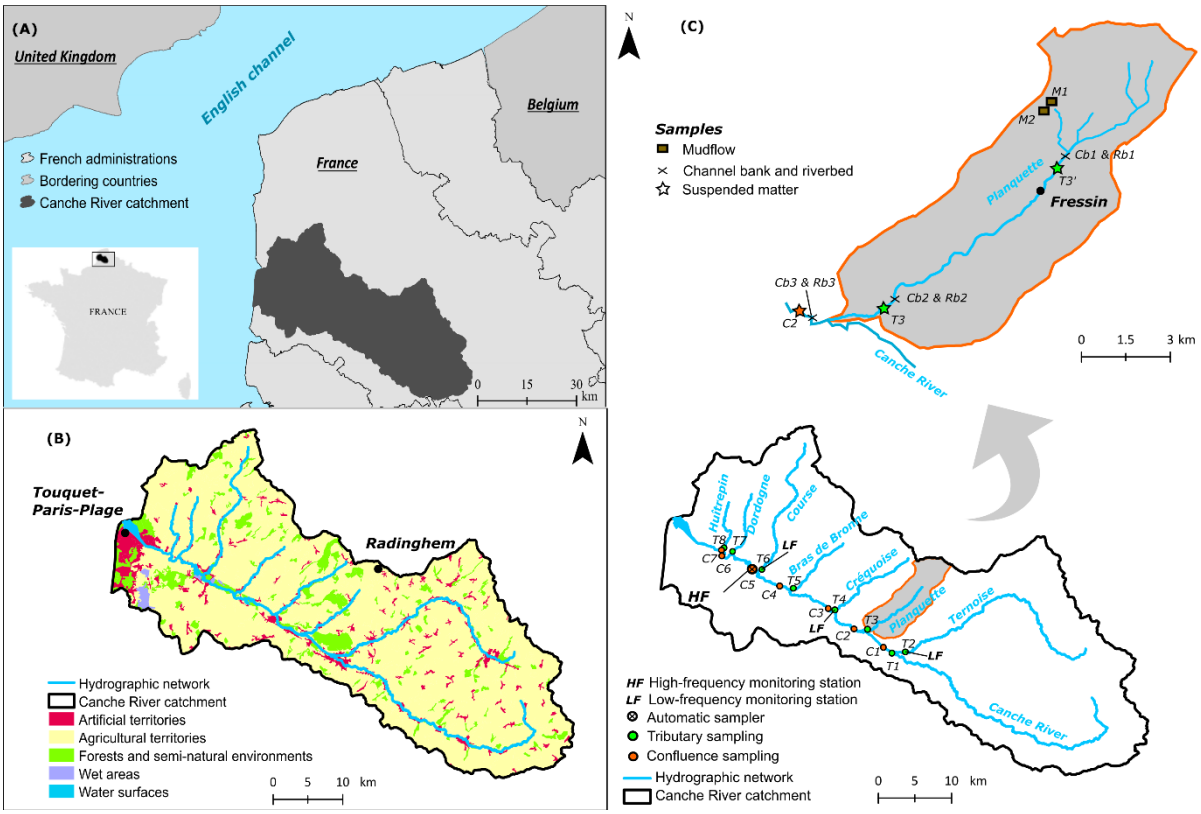

Fig. 61 : (A) Overview of the study area, (B) land cover of the Canche watershed (source: Corine Land Cover 2012) and (C) location of sediment sampling sites in the Canche river watershed and in the Planquette river catchment.

2.2 Sediment sampling

Suspended particulate matter (SPM) was collected using sediment traps installed at each tributary outlet, and confluence as well as upstream of the Planquette river (Fig.61C). Sampling campaigns were conducted in winter 2015, winter 2016, spring 2016, summer 2016, autumn 2016

and one specific flood event on 03-February 2017. Additionally, for one specific flood event on 08-June 2016, SPM were collected using a fix automatic sampler (*Aquamax 2*) at the site of Attin. A total of 119 samples are considered in this study. More details on the sampling devices, exact sampling periods, and site positions are available in Figure 61-62-63-64 and Table 16-17.

83 of 119 samples are suspended solid particles transported in the different streams of the Canche river catchment. Sediments were sampled using an experimental device adapted from previous studies described by Tessier (2003) and Kayvantash et al. (2017). The sediment traps (Fig.62) consist of 2 l polyethylene bottles, perforated at 5 cm from the top with two opposite bores (diameter 5 cm). The bottle is attached to the river bank with a rope and deposited in the channel. The device is held in place using either an additional rope or a combination of rope and a wooden beam. The whole device is weighted vertically in the water column using ballast that is adapted to the river flow speed. Traps usually captured between 50 and 100 g of sediment during ~5-7 days collection period. Previous studies observed that there is no significant grain size selection dependent on the position of the bottle in the river channel (Kayvantash et al., 2017).

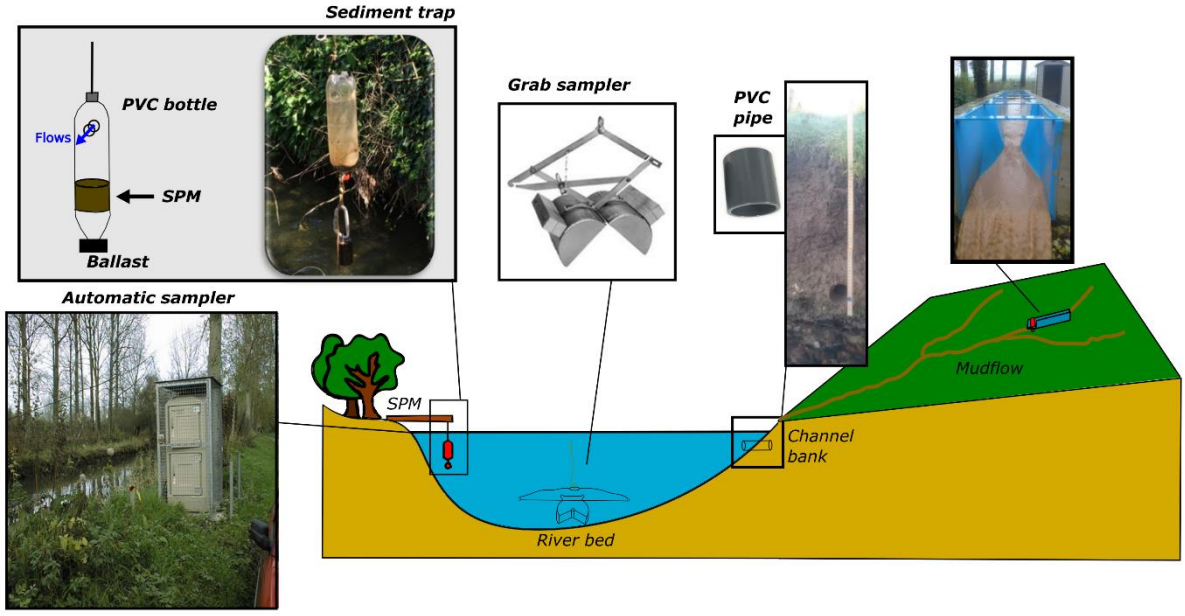

Fig. 62 : Experimental devices used to sample the different sediments of this study.

During the flood event in winter 2017, two distinct mudflow samples were collected using sediment traps in the upstream part of the Planquette river catchment (Fig.61C and 62A). Sediment traps were hooked to an existing Venturi channel designed to monitor hydro-sedimentary transfer in the small Pommeroye agricultural catchment (Fig.62; see also Patault et al., 2018, *in review – see chapter 2*). Here, sediment traps were deployed one day before the start of an erosive event (03-February 2017) and were recovered at the end of the event (06-February, 2017). Each trap recovered 50-100 mg of sediment.

Six distinct channel bank sediments were collected by pushing 5-cm diameter PVC pipes about 10 cm deep into the channel bank (Fig.62). Channel bank sediments were collected at two positions on the Planquette catchment and at one position on the Canche river catchment (Fig.60C). Three distinct river bed sediments were collected using a benthic grab sampler in zinc-plated heavy steel with a sample volume of 2.4 dm^3 (Fig.62). Sediments were sampled launching the benthic grab in the middle-bottom channel at three different sampling points (Fig. 61C). To ensure that the sediment recovered by the grab sampler was representative of the river bed section, three throws were done. Each throw can recover between 100-300 g of sediment. Sampling of channel banks and river bed sediment was done one day before the beginning of a flood event in winter 2017.

Fig. 63 : (A) Mudflow in the upstream part of the Planquette catchment, picture was taken during a typical flood event, (B) the Planquette river at site T3 and (C) the Canche river at site C2; photos B and C were taken during intermediate water conditions.

The sampled suspended sediment was passed through a flow-through centrifuge to separate water from the suspended particulate matter. Collected suspended matter from the centrifuge and all other sediment samples were sieved to 2 mm to remove coarse debris. All sieved samples were

carefully dried in an oven at 30°C during 72 h to avoid potential alteration of minerals such as goethite, magnetite, and clays which may begin to alter at temperatures as low as 40°C.

Tab. 16 : Coordinates and periods of SPM sampling at each confluence and tributary of the Canche river catchment for the five seasonal sampling campaigns.

Sample	Coordinates	Catchment	Device	Sampling periods									
				1		2		3		4		5	
				Drop off	Recovery	Drop off	Recovery	Drop off	Recovery	Drop off	Recovery	Drop off	Recovery
T1	50°22’43.1’’N; 2°01’03.5’’E	Canche	Sediment trap	25-Feb-15	10-Mar-15	15-Feb-16	22-Feb-16	27-Apr-16	03-May-16	11-Jul-16	18-Jul-16	08-Nov-16	14-Nov-16
T2	50°22’47.6’’N; 2°02’33.7’’E	Ternoise	Sediment trap	25-Feb-15	10-Mar-15	22-Feb-16	02-Mar-16	27-Apr-16	03-May-16	11-Jul-16	18-Jul-16	08-Nov-16	14-Nov-16
T3	50°24’26.0’’N; 1°58’11.0’’E	Planquette	Sediment trap	25-Feb-15	10-Mar-15	15-Feb-16	22-Feb-16	27-Apr-16	03-May-16	11-Jul-16	18-Jul-16	08-Nov-16	14-Nov-16
T4	50°25’49.5’’N; 1°54’23.2’’E	Créquoise	Sediment trap	25-Feb-15	10-Mar-15	15-Feb-16	22-Feb-16	27-Apr-16	03-May-16	11-Jul-16	18-Jul-16	08-Nov-16	14-Nov-16
T5	50°27’22.0’’N; 1°49’32.6’’E	Bras de Bronne	Sediment trap	25-Feb-15	10-Mar-15	15-Feb-16	22-Feb-16	27-Apr-16	03-May-16	11-Jul-16	18-Jul-16	08-Nov-16	14-Nov-16
T6	50°28’40.9’’N; 1°45’48.1’’E	Course	Sediment trap	26-Feb-15	10-Mar-15	15-Feb-16	22-Feb-16	27-Apr-16	03-May-16	11-Jul-16	18-Jul-16	08-Nov-16	14-Nov-16
T7	50°30’01.4’’N; 1°42’28.4’’E	Dordogne	Sediment trap	26-Feb-15	10-Mar-15	16-Feb-16	23-Feb-16	27-Apr-16	03-May-16	11-Jul-16	18-Jul-16	08-Nov-16	14-Nov-16
T8	50°30’15.6’’N; 1°41’30.5’’E	Huîtrepin	Sediment trap	26-Feb-15	10-Mar-15	16-Feb-16	23-Feb-16	27-Apr-16	03-May-16	11-Jul-16	18-Jul-16	08-Nov-16	14-Nov-16
C1	50°23’09.0’’N; 1°59’59.6’’E	Canche	Sediment trap	25-Feb-15	10-Mar-15	15-Feb-16	22-Feb-16	03-May-16	09-May-16	18-Jul-16	26-Jul-16	08-Nov-16	14-Nov-16
C2	50°24’45.5’’N; 1°55’43.3’’E	Canche	Sediment trap	25-Feb-15	10-Mar-15	15-Feb-16	22-Feb-16	27-Apr-16	03-May-16	18-Jul-16	26-Jul-16	08-Nov-16	14-Nov-16
C3	50°25’57.2’’N; 1°53’37.6’’E	Canche	Sediment trap	25-Feb-15	10-Mar-15	22-Feb-16	02-Mar-16	27-Apr-16	03-May-16	11-Jul-16	18-Jul-16	08-Nov-16	14-Nov-16
C4	50°27’32.0’’N; 1°47’58.7’’E	Canche	Sediment trap	26-Feb-15	10-Mar-15	15-Feb-16	22-Feb-16	27-Apr-16	03-May-16	11-Jul-16	18-Jul-16	08-Nov-16	14-Nov-16
C5	50°28’41.1’’N; 1°44’55.9’’E	Canche	Sediment trap	26-Feb-15	10-Mar-15	22-Feb-16	02-Mar-16	27-Apr-16	03-May-16	11-Jul-16	18-Jul-16	08-Nov-16	14-Nov-16
C6	50°29’39.5’’N; 1°41’11.8’’E	Canche	Sediment trap	26-Feb-15	10-Mar-15	16-Feb-16	23-Feb-16	28-Apr-16	04-May-16	18-Jul-16	26-Jul-16	09-Nov-16	15-Nov-16
C7	50°30’05.4’’N; 1°41’11.5’’E	Canche	Sediment trap	11-Mar-15	1-Feb-15	16-Feb-16	23-Feb-16	28-Apr-16	04-May-16	12-Jul-16	19-Jul-16	09-Nov-16	15-Nov-16

Tab. 17 : Coordinates and periods of mudflow, channel bank, river bed and SPM sampling in the Canche river catchment during two flood events.

Sample	Coordinates	Catchment	Nature	Device	Date of sampling	Drop off	Recovery
M1	50°28’12.6’’N; 2°03’44.5’’E	Planquette	Mudflow	Sediment trap	03-Feb-17		
M2	50°28’12.6’’N; 2°03’44.5’’E	Planquette	Mudflow	Sediment trap	03-Feb-17		
Cb1a-b	50°25’56.3’’N; 2°02’05.0’’E	Planquette	Channel bank	PVC pipe	03-Feb-17		
Cb2a-b	50°24’26.0’’N; 1°58’11.0’’E	Planquette	Channel bank	PVC pipe	03-Feb-17		
Cb3a-b	50°24’45.5’’N; 1°55’43.3’’E	Canche	Channel bank	PVC pipe	03-Feb-17		
Rb1	50°25’56.3’’N; 2°02’05.0’’E	Planquette	Riverbed	Grab sampler	03-Feb-17		
Rb2	50°24’26.0’’N; 1°58’11.0’’E	Planquette	Riverbed	Grab sampler	03-Feb-17		
Rb3	50°24’45.5’’N; 1°55’43.3’’E	Canche	Riverbed	Grab sampler	03-Feb-17		
C2	50°24’45.5’’N; 1°55’43.3’’E	Canche	Suspended matter	Sediment trap		03-Feb-17	06-Feb-17
T3a-b-c-d	50°24’26.0’’N; 1°58’11.0’’E	Planquette	Suspended matter	Sediment trap		03-Feb-17	06-Feb-17
T3’a-b-c-d	50°25’56.3’’N; 2°02’05.0’’E	Planquette	Suspended matter	Sediment trap		03-Feb-17	06-Feb-17
1-24	50°28’43.7’’N; 1°44’54.3’’E	Canche	Suspended matter	Automatic sampler		08-Jun-16 19 :30	11-Jun-16 16 :30

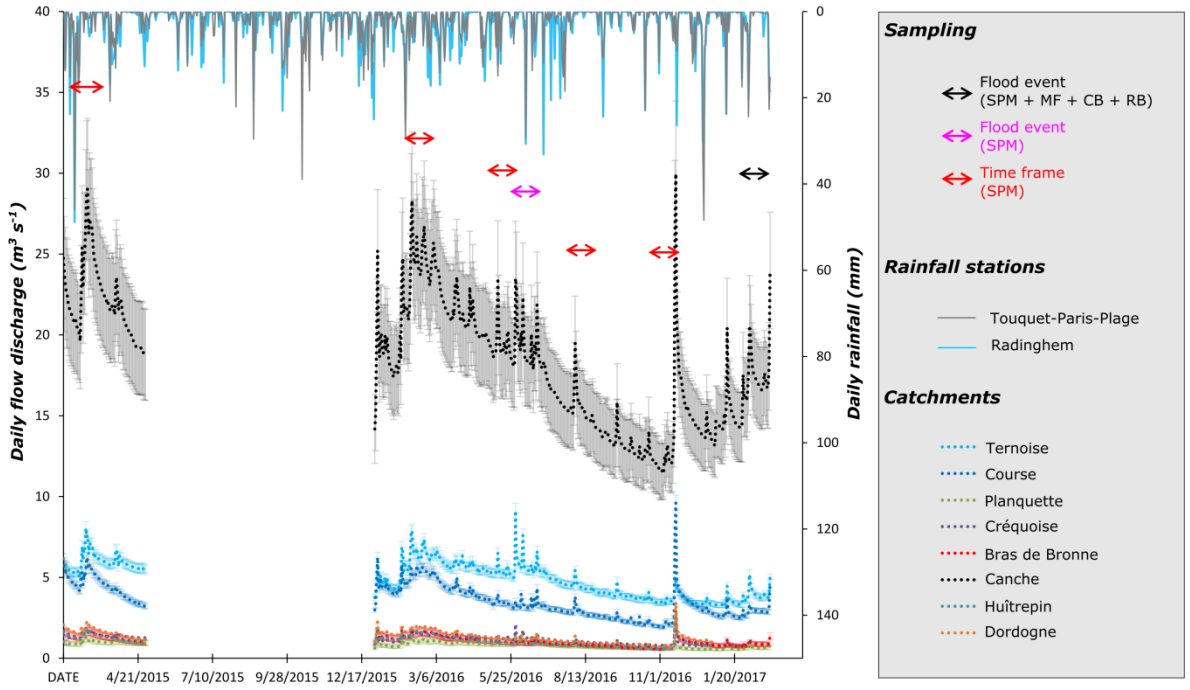

Fig. 64 : Daily flow discharge (m^3 s^{-1}) and daily rainfall (mm) in the Canche river catchment and its tributaries during the different sampling campaign. (Acronyms: Suspended particulate matter (SPM); Mudflows (MF); Channel bank (CB); Riverbed (RB)).

Weather conditions showed temporal variability between the different sampling campaigns (for detailed dates please see Table 16). For the first campaign in winter 2015, rainfall amount was evaluated at 24.5 mm at Radinghem and 17.2 mm at Touquet-Paris-Plage. The mean discharge of the Canche River was 26 m^3 s^{-1}. For the second campaign in winter 2016, rainfall amount was evaluated at 6.8 and 12.3 mm at the same reference stations and a mean flow discharge of 25 m^3 s^{-1} for the Canche river. During this campaign, three trap samples were vandalized and re-sampled during the following week. Weather conditions of these two consecutive weeks were different showing a rainfall amount of 61 and 42.2 mm at Radinghem and Touquet-Paris-Plage. For the third campaign in spring 2016, the amount of rainfall was relatively high (33.7 and 23.8 mm respectively). The mean discharge in the Canche river was lower (19 m^3 s^{-1}), one trap was re-sampled due to vandalism (site C1). The week after, the rainfall amount was evaluated to 15.1 and 7.8 mm at Radinghem and Touquet-Paris-Plage. During the fourth campaign in summer 2016, the rainfall amount was significantly different between the two stations (43.3 mm at Radinghem and 6 mm at Touquet-Paris-Plage) due to very localized precipitations. Three traps were re-sampled the following week (C1, C2,

and C6) and during which rainfall amounts were evaluated at 50 mm at both rainfall stations. For the last sampling period in autumn 2016, the rainfall amount was evaluated to 30 mm at the two rainfall reference stations and the flow discharge was relatively low (14 $m^3 s^{-1}$). For the two specific flood events, the rainfall amount was quantified at 36 mm between June 08-11, 2016, and at 30 mm between February 03-06, 2017.

3. Methods

3.1 Room temperature magnetic measurements (magnetic hysteresis loops)

Magnetic properties are obtained from hysteresis curves using an alternating gradient force magnetometer (*AGFM 2900*) at the Laboratoire des Sciences du Climat et de l'Environnement (LSCE). Hysteresis loops are measured on dry bulk sediments (2 to 25 mg) and on the grain size fraction < 2 mm at room temperature twice by cycling the field to maximum applied field of ± 0.3 T (first low-field loop) and then ± 1 T (high-field loop). Depending on the mass of SPM available for each trap, one to three subsamples are analyzed.

Magnetic parameters derived from the high-field (1 T) slope corrected hysteresis loop data are: saturation magnetization (M_s), saturation remanent magnetization (M_{rs}), and coercitive force ($H_{c;}$ Fig.65). In a separate experiment, a stepwise increasing backfield is applied to M_{rs} to determine the remanent coercive force (H_{cr}).

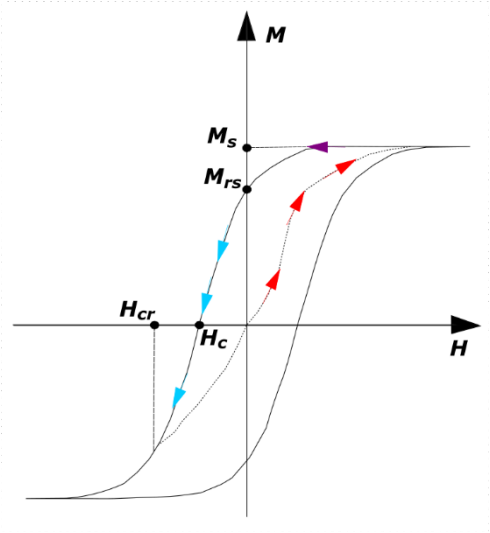

Fig. 65 : Schematic view of a magnetic hysteresis cycle (adapted from Evans & Heller, 2003).

M_s and M_{rs} values are normalized to the sample mass. The so-called "S-ratio" is calculated according to the equation proposed by King & Channell (1991):

$$Sratio = {}^{-IRM_{0.3T}}/_{HIRM_{1T}} \quad (50)$$

The alternating gradient magnetometer is known to be very sensitive to the mass of the sample (Shah et al., 2013). To ensure that there is no major bias in our magnetic hysteresis data and that our samples are representative of the respective SPM obtained in the traps, we compared the results of four samples from site C2 obtained on the alternating gradient force magnetometer *AGFM 2900* at the LSCE to the magnetic hysteresis parameters obtained using a Vibrating Sample Magnetometer (VSM) at the Institut de Physique du Globe de Paris (IPGP), which has a maximum field applied of 1.8 T, dictated by the pole spacing. The latter method is much less affected by the mass and size of the analyzed sample (which is about 200 to 350 mg). The comparison between AGFM and VSM analyses are satisfying for our test samples.

3.2 Decomposition of IRM components

Magnetic properties can be defined with the analysis of isothermal remanent magnetization (IRM) acquisition curves based on Cumulative Log Gaussian (CLG) analysis. This method was first proposed by Robertson & France (1994) to discriminate remanence-carrying minerals in mixtures Kruiver et al. (2001) have shown that magnetic coercivity distributions could be determined based on the CLG appearance of isothermal remanent magnetization (IRM) acquisition curves even if it is far from being saturated. The IRM curve is decomposed into several CLG curves, which can be individually characterized by (i) their saturated isothermal remanent magnetization (SIRM), (ii) the mean coercivity ($H_{1/2}$) and (iii) the dispersion parameter (DP). The CLG analysis is realized with the model used by Kruiver et al. (2001) in an Excel worksheet[19]. Three different representations from the IRM acquisition curve can be plotted (see Fig.66). Initial values for SIRM, $H_{1/2}$ and DP are estimated from the Linear Acquisition Plot (LAP), the Gradient of Acquisition Plot (GAP), and the Standardized Acquisition Plot (SAP). LAP referred to the analysis of IRM curves on a linear ordinate scale, GAP as the gradient curve, and SAP as the probability scale.

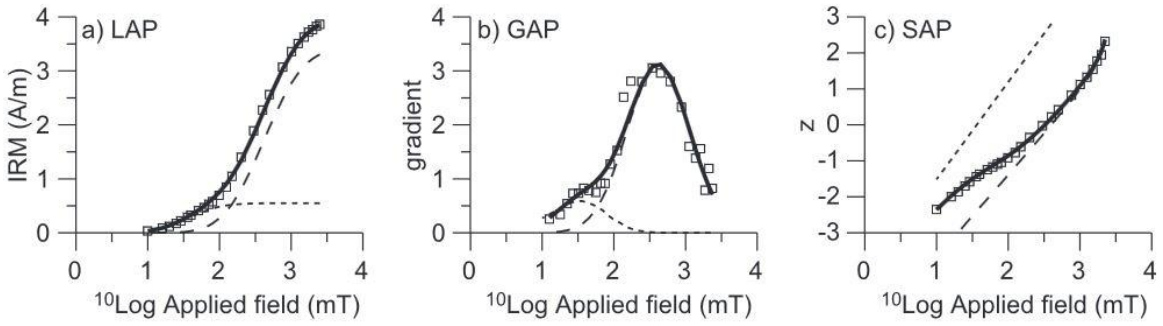

Fig. 66 : (a) Linear Acquisition Plot (LAP), (b) the Gradient of Acquisition Plot (GAP), and (c) the Standardized Acquisition Plot (SAP) for a data example from Kruiver et al. (2001).

3.3 Thermomagnetic measurements

Room temperature saturation isothermal remanent magnetization (RT-SIRM) experiments were performed on dry bulk sediments using the *Quantum Design XL-5 Ever Cool* Magnetic

[19] (http://www.geo.uu.nl/~forth/)

Properties Measurement System (MPMS; noise level ~10−11 Am^2) housed at the IPGP. A 2.5 T field was applied at RT, subsequently the sample was cycled from 300 to 10 K (cooling) and back to 300 K (warming) at a 5 K min^{-1} sweep rate in zero-field, and the remanent magnetization monitored at 5 K increments.

Subsequently, low-temperature zero-field cooled (ZFC) and field-cooled (FC) SIRM were acquired at 10 K. For the ZFC measurements, the 2.5 T field was applied at 10 K and switched off before warming back to 300 K, whereas for the FC measurements, the field was applied at 300 K throughout cooling and switched off before warming back to 300K. Low-temperature warming curves (10–300 K) were acquired at a 5 K min^{-1} sweep rate and by monitored the remanent magnetization at a 5 K increments.

To obtain further knowledge on the individual magnetic components present in the natural mixture of the SPM and sediment samples, a recently proposed experimental protocol (Lagroix & Guyodo, 2017), was applied on four selected samples from sample site C2. This MPMS sequence is available as open access in the supplementary material of the cited reference. It begins with a classic RT-SIRM experiment (i.e., a 2.5 T IRM acquired at 300 K is monitored while cycling the temperature from 300 K to 10 K and back to 300K). A 2.5 T field is then applied as the sample is warmed to 400 K and cooled back to 300 K resulting in an “enhanced” RT-SIRM. Lagroix & Guyodo (2017) state that if any goethite is present in the sample, the “enhanced” RT-SIRM pre-treatment will result in goethite acquiring a thermo-remanent magnetization (TRM) as it cools in the presence of a magnetic field through its Néel temperature of 393 K for stochiometric goethite (Ozdemir & Dunlop, 1996).

The enhanced RT-SIRM is monitored while cycling the temperature from 300 to 10 K and back to 300 K. Subsequently, the cycled “enhanced” RT-SIRM is partially demagnetized by exposing the sample to a decreasing oscillating field from a peak field of 0.3 T to zero. Low coercivity remanences removed, the remaining remanent magnetization is monitored while cycling temperatures from 300 to 10 K and back to 400 K. Finally, the remaining remanent magnetization is

cycled one last time from 400 to 10 K and back to 300 K. Throughout, temperature sweep rate is kept constant at 5 K min^{-1} and measurement interval constant at 5 K.

4. Results

4.1 RT magnetic hysteresis results - zoom on the Canche-Planquette river confluence

To highlight the potential of the employed rock magnetic methods in this environmental context, we would first like to focus on a restricted area of the Canche river catchment, to explain the principle of the idea on our dry bulk sample data and to test some assumptions before going further with our interpretations on the entire Canche river watershed.

Figure 66 presents the results from the RT magnetic hysteresis analyses performed on the SPM samples collected downstream the confluence of the Planquette and the Canche river (sample site C2; see also map Figure 1). Part A of Figure 67 shows the results for the magnetic concentration parameter M_s for the low-field (0.3 T) and high-field (1 T) experiment and part B represents the respective remanent magnetization M_{rs} values. In Figure 66C the magnetic mineralogy parameter S-ratio is shown.

Looking at the magnetic concentration values (Ms) at the Canche site (C2) through the five sampled seasons (Fig.67 – Panel A), we generally detect values between ~ 5-10 nAm^2 mg^{-1}, that are comparable to those published for the upstream River (Franke et al., 2009; Kayvantash, 2016), that is of similar land use and lithology (agricultural rural area, Jurassic chalk or marls). For the samples from winter 2015, summer 2016, and winter 2017 the values of M_s at low-field 0.3 T and high-field loops 1 T are very similar (ΔM_s < 2 nAm^2 mg^{-1}). The sample from winter 2016 presents intermediate ΔM_s of ~ 5 nAm^2 mg^{-1}, whereas the samples from spring 2016 and autumn 2016 show much larger M_s differences between the two respective values (ΔM_s > 5 nAm^2 mg^{-1}).

The differences between the low-field and high-field values are smaller for the remanent magnetization parameter M_{rs}, which is exclusively carried by magnetic particles that are above a

critical domain size range that varies for the different magnetic mineral phases. Below this specific threshold, the magnetic particles may not carry any stable remanence and thus show a superparamagnetic in-field behavior that is responsible for part of the difference between the M_s and M_{rs} values (Butler & Banerjee, 1975; Dunlop et Özdemir, 1997). Despite that, the ΔM_{rs} of the samples from winter 2016, summer 2016, and autumn 2016 are significant.

As already mentioned in the methods section, the S-ratio is equal or close to one for a mono-magnetic mineralogy, carried by low coercive magnetite. As the S-ratio decreases significantly from one, the relative proportion of high coercitive minerals, for example hematite or goethite, increases. These minerals do not reach total saturation in an applied field of 0.3 T (nor in 1 T for goethite), thus the remanent magnetization M_{rs} acquired at 0.3 T and at 1 T shows a significant difference indicative of the presence of high coercivity magnetic minerals in the sample.

All samples show S-ratios that indicate a relative significant off-set from one that corresponds to the contribution of high coercivity minerals. Given the dominant presence of agricultural fields in the watershed this result is to be expected. Agricultural soils are well oxidized and are a major source for the SPM transported by runoff surface waters to the rivers. For the two seasons of spring 2016 and autumn 2016, which show the largest ΔM_{rs}, the S-ratio values show lower values (0.95 respectively 0.89; Fig.67 – panel C), that are comparable to mean values stated in Kayvantash (2016) for the upstream segment of the Seine river (~ 0.92).

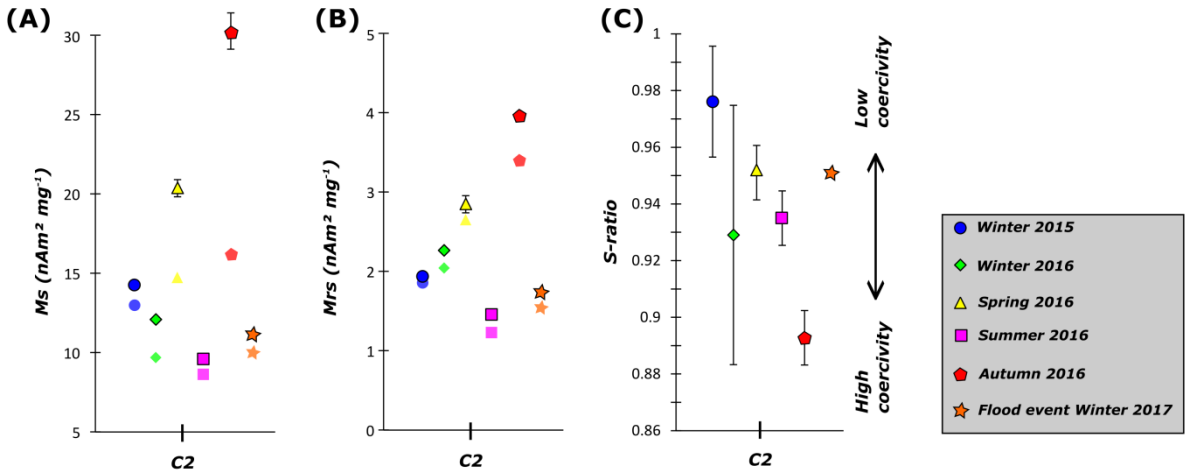

Fig. 67 : Results from rock magnetic analyses for sample site C2 in the Canche river for the sampled seasons between 2015 and 2017. C2 is located just downstream from the Canche-Planquette confluence.

4.2. Low-temperature magnetic behaviour (MPMS experiments)

RT magnetic methods are powerful tools at the first order, but they do have some limitations regarding the dominance of magnetite with respect to other mineral phases that either magnetically order below room-temperature or do need stronger applied fields to saturate. RT magnetic hysteresis measurements have the advantage to be easily applicable on a large variety of sample types, such as SPM that is normally sampled in small quantity and serves for a multitude of analyses. Assumptions drawn to interpret RT magnetic data can, in certain cases, be validated through complementary analyses such as the Lagroix & Guyodo (2017) protocol detailed in the methods section. Figure 68-panels A to D (first column) show the RT-SIRM results for C2 site in the Canche river for all sampled seasons in 2016. The RT-SIRM curves show characteristic low-temperature curves for magnetite (Kosterov, 2003; Lagroix et al., 2004; Özdemir et al., 2002). All curves show a continuous increase with decreasing temperature throughout the entire measurement range. This behaviour is attributed to the presence of goethite (Lowrie & Heller, 1982; Dekkers, 1989). The cooling and warming cycles are reversible in the temperature and range between 10 and 100 K (with exception for the autumn 2016 sample). Relative changes of the remanence loss during the cooling-warming-cycle are only subtle.

Low-temperature warming curves of ZFC and FC remanence (Figure 68-panels E to H; second column) show a distinct steep slope between 10 and 5 K corresponding to the presence of ultra-fine-grained superparamagnetic phase (Özdemir et al., 1993; Smirnov & Tarduno, 2000). The Verwey transition at ~110 K indicates the presence of slightly oxidized magnetite (Kosterov, 2003; Özdemir et al., 2002). The discrepancy between the ZFC and FC curves persisting at temperature above the Verwey transition is interpreted as the presence of goethite is clearly developed.

Comparison of the classic RT-SIRM cycles (Fig.68 – panels A to D, first column) with the enhanced and demagnetized RT-SIRM (Fig.68 – panels I to L; third column) show the successful elimination of the (dominant) magnetite component using the protocol proposed by Lagroix & Guyodo (2017). This is particularly helpful for the identification of the presumed remaining high coercivity carriers, such as goethite and hematite. The resulting 1st cooling-warming cycle (between 300 to 10 back to 400 K) of the enhanced and 0.3 T demagnetized RT-SIRM clearly shows a steadily increasing goethite-dominated signal that is reversible in the summer and autumn 2016 samples and shows a slight irreversibility above 100 K in the winter and spring 2016 sample. The slight irreversible behavior is likely due to partially oxidized magnetite, which was not demagnetized by the 0.3 T peak oscillating field. The remanence loss on heating to 400 K results from the thermal demagnetization of goethite as it is heated above its Néel temperature (393 K). The enhanced RT-SIRM curves show a slight remanence loss at 250-300 K that is likely an indication for the Morin transition of hematite (Lagroix & Guyodo, 2017).

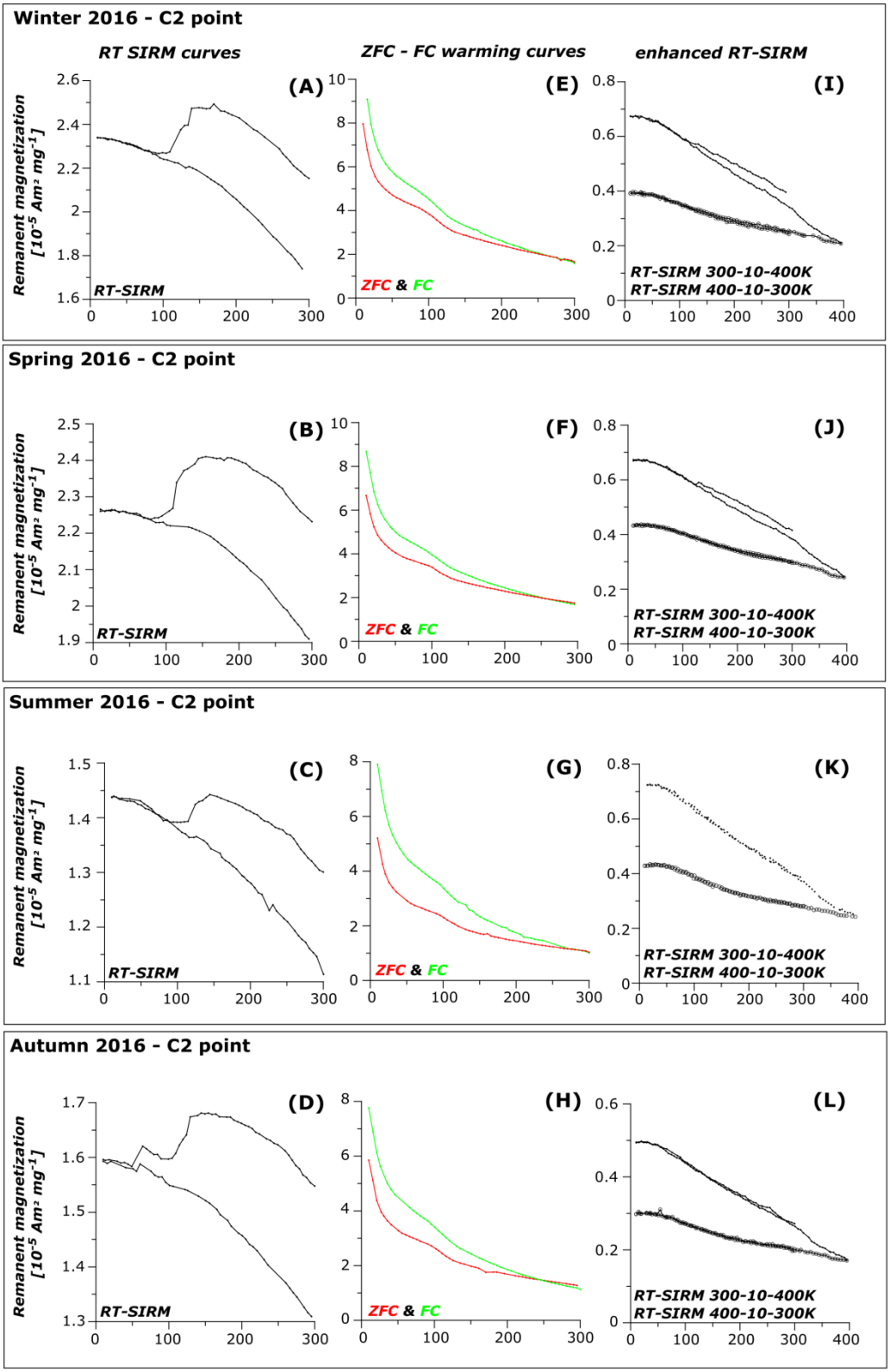

Fig. 68 : Results from MPMS thermomagnetic analyses for four selected seasonal SPM samples from site C2 (Canche river downstream confluence Planquette river). First column: low-temperature zero-field cycles of RT-SIRM (applied field 2.5T); second column: low-temperature ZFC (red) and FC (green) remanence warming curves monitored between 10and 300 K at 5 K intervals acquired at 10 K in an applied field of 2.5 T; third column: enhanced and demagnetized RT-SIRM curves according to the measurement protocol following Lagroix & Guyodo (2017). All curves are normalized to their respective sample mass.

4.3. IRM component analysis of RT hysteresis results

Since the tests on the four selected samples form site C2 confirmed the presence of magnetite as the dominant low-coercivity component and two distinct high coercivity components, goethite and hematite, these results can be use to unmix the components contributing to IRM acquisition curves. The method proposed by Kruiver et al., (2001) has the advantage to be straight forward on an important data set, which is typical for environmental studies.

The IRM unmixing results for the five seasonal sampling campaigns are shown in Figure 69. We observe that the high coercivity (HC) fraction is more important in spring 2016, summer 2016, and autumn 2016 than in winters 2015 and 2016 for the sampled periods. For example, at point T3, the winter 2015 Planquette river sample (T3) shows that 68% of the signal is carried by a HC component and 32% by the LC component. In autumn 2016, at the same site (T3), 85% of the signal is carried by HC and 15% by LC. We observed that the HC component at the outlet of the Planquette (T3) is generally higher than in the Canche river, except for summer 2016 where the two values are ~ equal. We also observe that the HC fraction is generally higher in the downstream part of the Canche (C2) indicating mixing of the signal between the upstream part of the Canche (C1) and the Planquette (T3). For the specific flood event of winter 2017, results showed that the HC component is highest in mudflows (>76%) compared to channel banks and riverbeds (48–73%). For this event, SPM samples also show a high contribution of the HC fraction (>70%) indicating the transfer of soil surface particles in the stream water suspended load. This result supports the hypothesis that the HC component traces soil erosion.

To enter further into the detail of the IRM unmixing results of high-coercivity (HC) and low coercivity (LC) fraction within the SPM and to be able to use this information as a tracer of the sediment flux that occurs during erosive rainfall events, we also need to check on the magnetic mineral composition of the adjacent channel bank and river bed samples in the Planquette catchment. They are potential sediment sources for the SPM material in the river's water column.

For that, we took advantage of the sample set that was recovered during the specific flood event in winter 2017 (03-06 February 2017). IRM unmixing results (Fig. 70A) showed that the HC component is highest in mudflows samples (> 76%) compared to channel banks and river bed values (48-73%). When looking at the magnetic concentration M_s and magnetic mineralogy S-ratio (Fig.70B-C) of these different sample types, it become obvious, that the mudflow samples present the lowest values of magnetic concentration M_s but also the lowest S-ratios. This may be interpreted as a high proportion of goethite and hematite in the mudflow material compared to the channel bank and riverbed samples. This is coherent with the fact that mudflow samples are recovered in the Venturi channel at the outlet of the Pommeroye catchment during the actual flood event and thus represent the direct runoff of the drained agricultural fields just upstream the Venturi channel.

The channel bank samples and river bed samples (Cb 1-3 and Rb 1-3) all show higher M_s and S-ratio values, indicating a stronger contribution of the magnetite component. This generally fits with the fact that channel bank and river bed deposits are less oxic sediments compared to surface soil and usually contain a higher proportion of more reduced iron oxide phases, such as magnetite.

The SPM samples at point T3', T3, and C2 present the suspended particles from winter 2017 flood event from the upstream to downstream Planquette river and after the confluence with the Canche river. On first sight they show similar values of M_s and S-ratio compared to the channel bank and river bed samples, but when looking at the IRM unmixing results, there is a slightly higher proportion of the HC component, thus the SPM samples are clearly carrying a mixed signature (~ 70% HC and 30% LC) between the runoff material (mudflows) and the deposited material (channel banks and river bed).

The quantification of the high coercivity (HC) and low coercivity (LC) fraction within the SPM samples (Figure 69) may now serve as a tracer of the sediments flux that occurs during erosive rainfall events, when runoff transports soil particles towards the surface water (rivers). The correlation of weather conditions (detailed in methods section) to the five seasonal sampling

campaigns is consistent with results shown in Fig.68 and indicates that a high relative contribution of HC minerals occurs during rainfall events, resulting from runoff transport of soil surface particles.

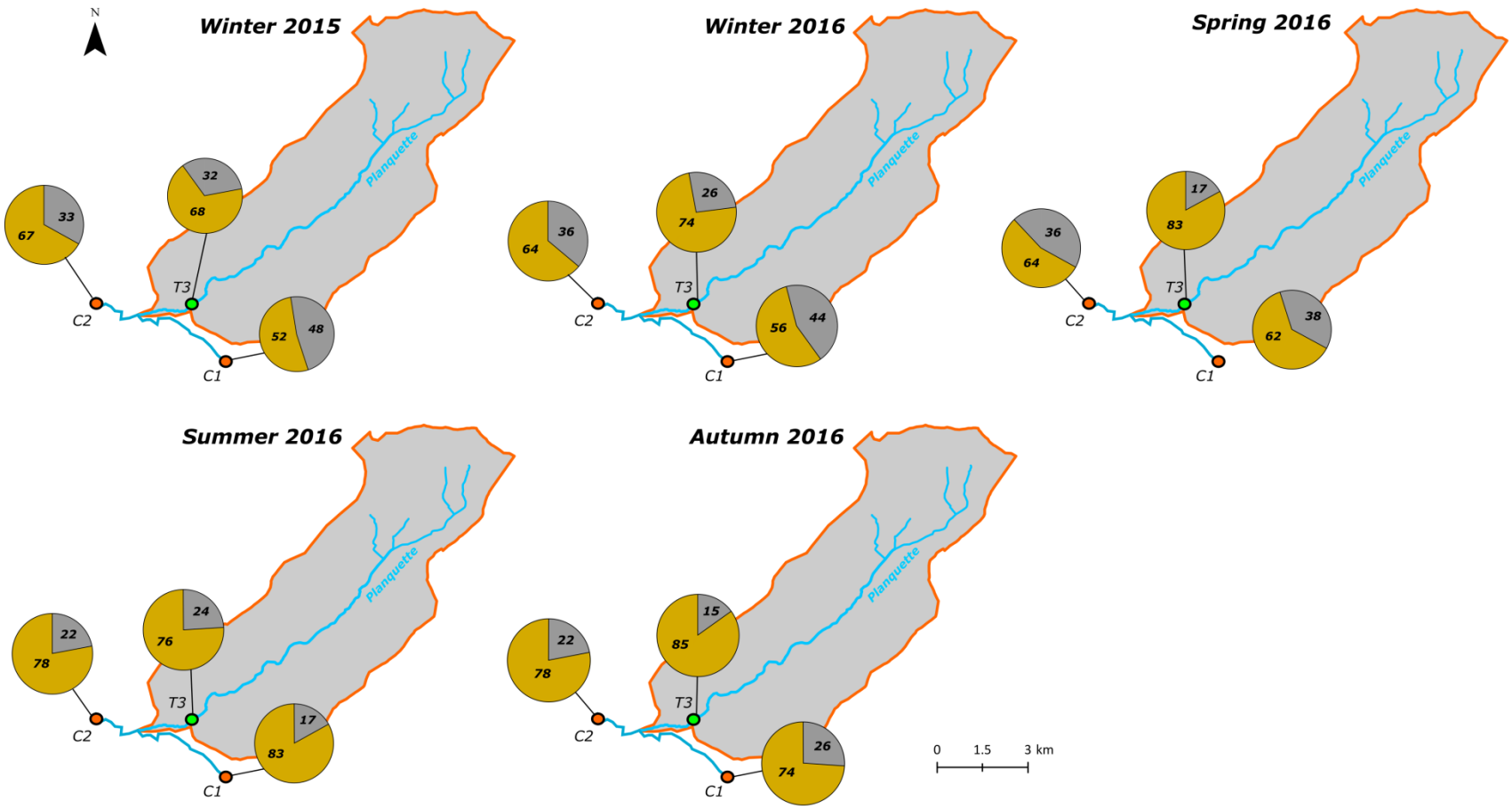

Fig. 69 : Results of the component analysis of IRM acquisition curves for the 5 different seasons between 2015 and 2016. Signification of colors: brownish = High Coercivity; grey = Low Coercivity. Sample site C1 is located upstream of the Canche-Planquette confluence. Sample site T3 is in the lower part of the Planquette catchment. Sample site C2 is located downstream of the Canche-Planquette confluence.

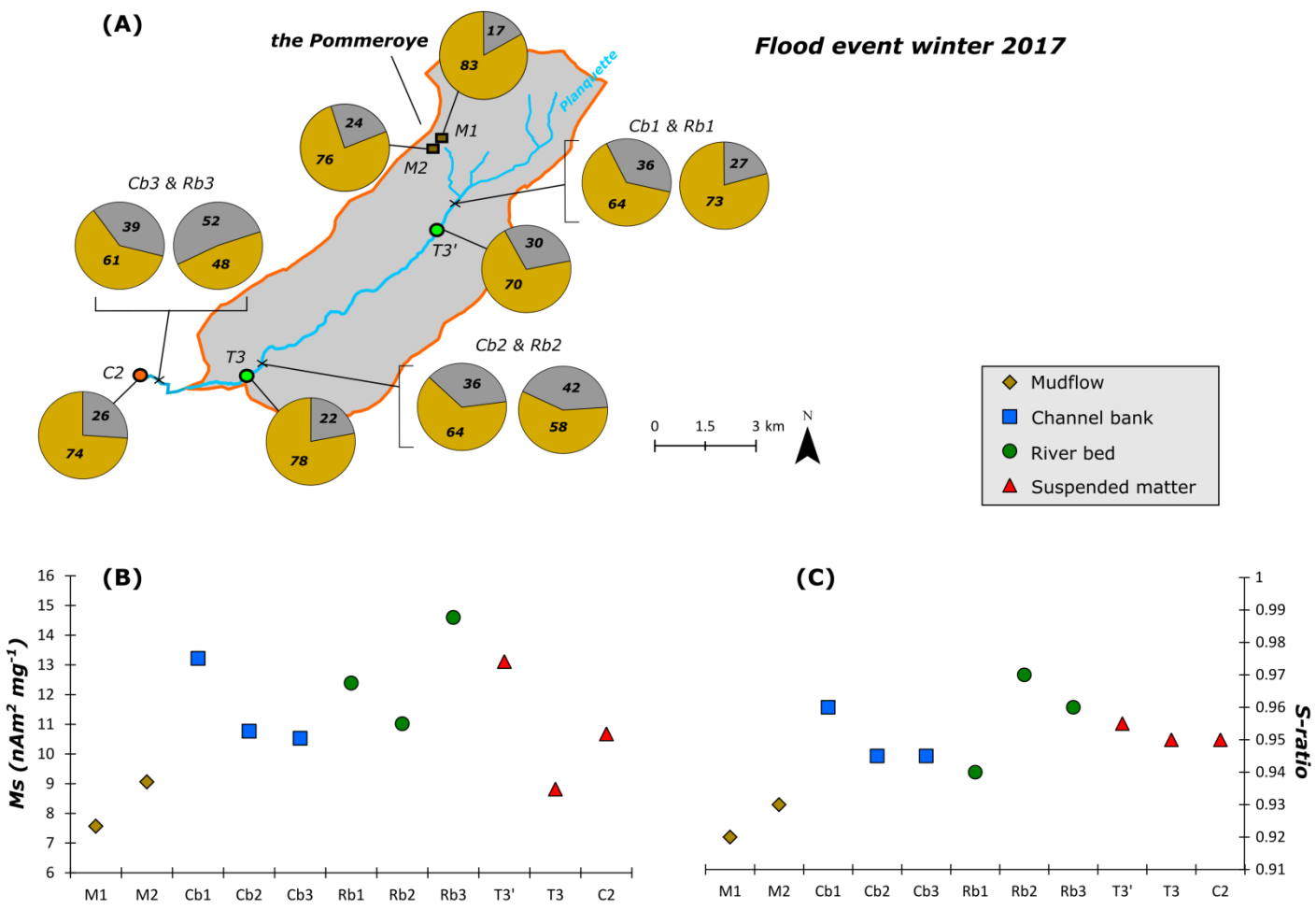

Fig. 70 : (A) Results of the component analysis of IRM acquisition curves of the flood event in winter 2017, and (B, C) Magnetic parameters of the sediment samples of the flood event. Signification of colors: brownish = High Coercivity; grey = Low Coercivity. Signification of acronyms: T = tributary; C= confluence; M = mudflow; Cb = Channel bank; and Rb = River bed. Samples sites T3, T3', M1, M2, Cb1, Rb1, Cb2, Rb2 are in the upper and lower part of the Planquette catchment. Sample sites C2, Cb3, and Rb3 are located downstream of the Canche-Planquette confluence.

4.4 Seasonal mapping of the Canche watershed

The results of the IRM component analysis support our interpretation of the HC fraction as a tracer for soil erosion/sediment flux. But the IRM component unmixing focused on a relatively small area of the studied catchment and still needs some additional sample-to-sample modeling/data processing.

For a bigger data set, that is usually needed to monitor the sediment flux on the scale of an entire catchment, we propose to return now to the already introduced combination of the magnetic concentration (M_s) and the magnetic mineralogy (S-ratio) to compare the five sampled seasons and to obtain a spatio-temporal map of the variations along the linear Canche river profile.

Figure 71 presents the results for both the M_s and S-ratio parameter along the Canche river profile for all five seasonal sampling campaigns. For comparison of the respective seasonal conditions, the blue continuous line shows the mean water discharge along the Canche river for each sampling campaign. In all sampled seasons the magnetic concentration of the Canche river is slightly below or close to an empirical value of 15 $nAm^2 mg^{-1}$, which is highlighted for orientation purposes in all graph M_s panels of Figure 71 as a grey dotted line. Only 25% of all Ms values lie above this line. This observation seams independent of the respective water discharge during the sampling season. Under the hypothesis that this threshold presents the background signal of the magnetic concentration in the Canche river catchment, we may consider that samples that show distinctively higher values, are outliers of this general background trend of the sweet water Canche transect (between Hesdin and Attin: see Fig.61).

Results of sample sites downstream of Attin (points T7, C6, T8, and C7) fall into the area which is strongly influenced by tide activity of the English Channel. In this zone, the M_s values of the downstream tributary rivers Dordogne (T7) and Huîtrepin (T8) are always below the general background line, which is not the case for the sample sites directly in the downstream Canche (C6 and C7) that show strong variations of their magnetic concentration values. In general, the quantity

of the transported suspended material is controlled by the water flow (Williams, 1989; Hickin, 1995; Knighton, 1998). For the Seine river, Estèbe (1996) and Vilmin (2014) state short concentrations peaks in SPM when flooding passes a certain threshold. Estèbe (1996) also state that the total flux of transported iron is proportional to the total SPM, and thus Kayvantash (2016) deduced from it that the concentration in magnetic minerals should not be biased. In fact, Kayvanstash et al. (2017) studied an upstream section of the Seine river which was sampled in the same was as for our study in the Canche river, using 2 l sediment trap bottles. The results for the upstream Seine river section showed that the sampling was representative for the granulometric fraction of the respective low-water and high-water conditions (and thus also for the recovered magnetic fraction). Kayvantash (2016) also state that the variations of the magnetic concentrations Ms at the studied upstream site in the Seine river (Marnay) are between 3.2 and 15.3 $nAm^2\ mg^{-1}$ depending on the respective sample period. Rock magnetic analyses showed a magnetite dominated magnetic assemblage, with a mean S-ratio close to one and thus only very minor contributions of goethite and hematite.

When regarding the S-ratio of the five sampled seasons in the Canche river (Fig.71 – panels F to J), two samples show a pure magnetite composition (points C4 and C7 in summer 2016). From the IRM unmixing results (Fig.69), it has been that the samples at the Planquette-Canche confluence carry a relative high percentage of HC components (between 48-83%). Thus, there is a need to interpret the magnetic concentration parameter M_s in combination with the S-ratio to be able to understand the mixing of the magnetic carriers in the respective SPM sample.

As already employed for the M_s parameter, an empirical marker value of 0.92 was defined for the S-ratio (grey dotted line in Fig.71– panel F to J). All tributary samples from winter 2015 are close to this threshold, whereas the samples from the Canche river are clearly above this value. In winter 2016, this trend seams inversed for most of the samples, despite the very upstream and downstream tributary sites (T1, T3, and T8). In spring 2016, only the Planquette site T3 and the middle part of the Canche samples (C3-C5) show values below the S-ratio < 0.92. In summer 2016, all samples show

values above S-ratio > 0.92, whereas in autumn 2016 all samples show values between 0.96 and 0.92, with exception of T2, C2, C6 and T8.

It can be assume a background magnetic concentration and magnetic mineralogy that corresponds the closest to a no erosive event from the sample set of summer 2016. M_s values and all samples seem to have a mean magnetic mineralogy close to S-ratios ~ 0.96. This corresponds approximatively to an IRM unmixing of 65% HC and 35% LC components (compare e.g. Fig. 70A point C2).

As soon as the runoff conditions change due to rainfall events, a larger contribution of HC components is obtained and the S-ratio values decreases. Depending of the weather conditions in a given season, this might be a very local rainfall event, restricted to a part of the catchment area, such as observed in winter 2016, where S-ratio values are lower (and thus higher runoff) only very upstream (Ternoise and Planquette tributaries) or in spring 2016, in the middle of the Canche catchment. For the latter season, it can be observed that not only the runoff input of HC particles from soil erosion is happening, but at point T5, the magnetic concentration exhibits high values a,d although the S-ratio is around 0.96. So there is a significant input of LC components that originates rather from channel bank or river bed sediments. The situation of winter 2015 or autumn 2016 corresponds rather to global rainfall events, during which runoff from soil erosion attaints all sample sites in the Canche catchment.

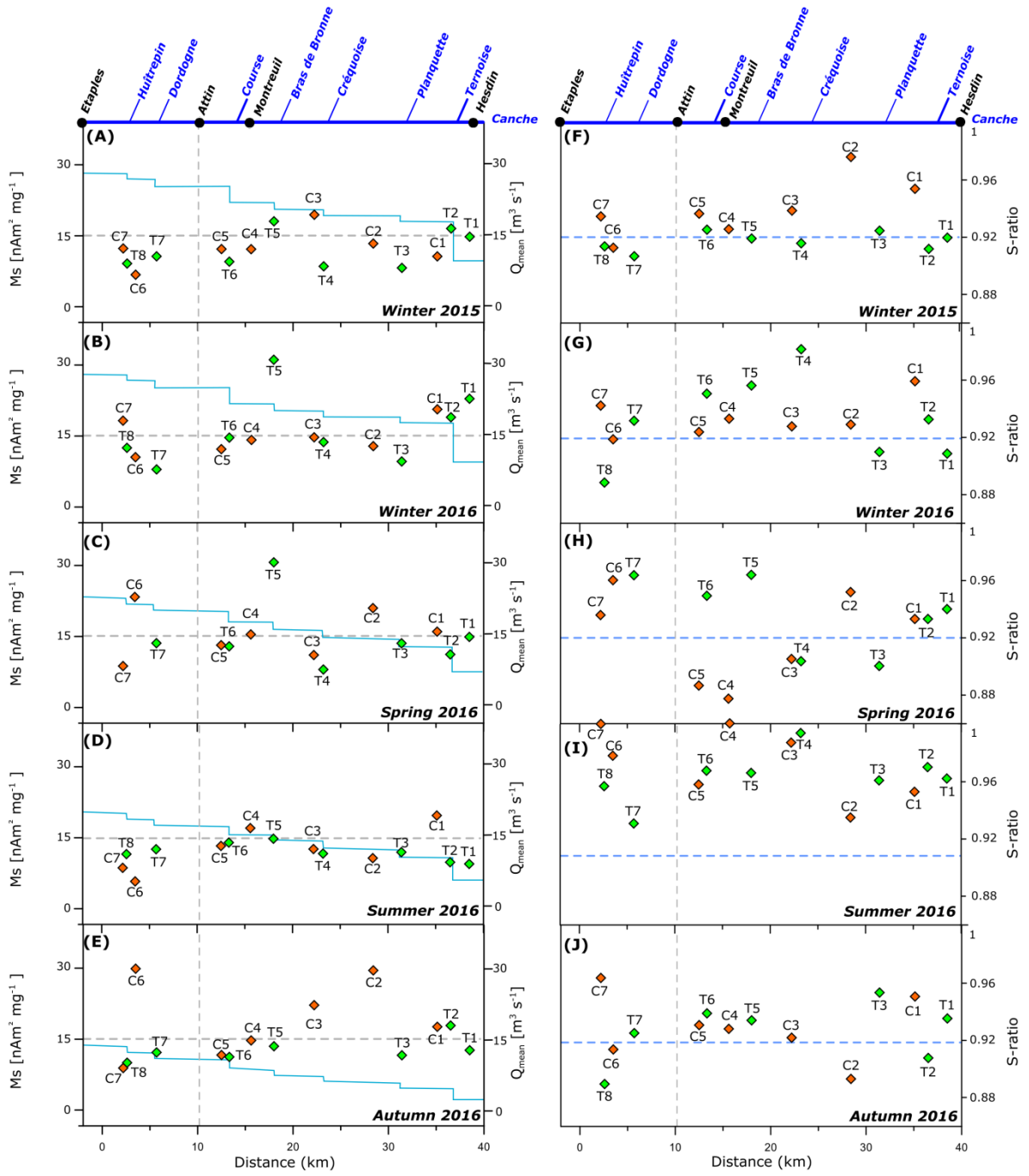

Fig. 71 : Magnetic concentration (Ms) and S-ratio along the Canche river for the five seasonal sampling campaigns.

4.5. Zoom on a specific flood event at Attin

The link between the rain events, the increased runoff/sediment particle transport and the decrease in S-ratio can be highlighted by looking at the high-resolution sampling campaign performed at the automated monitoring station at Attin in June 2016. Figure 72 shows the in-situ

turbidity in the water column compared to the S-ratio of the SPM samples taken during the flooding event.

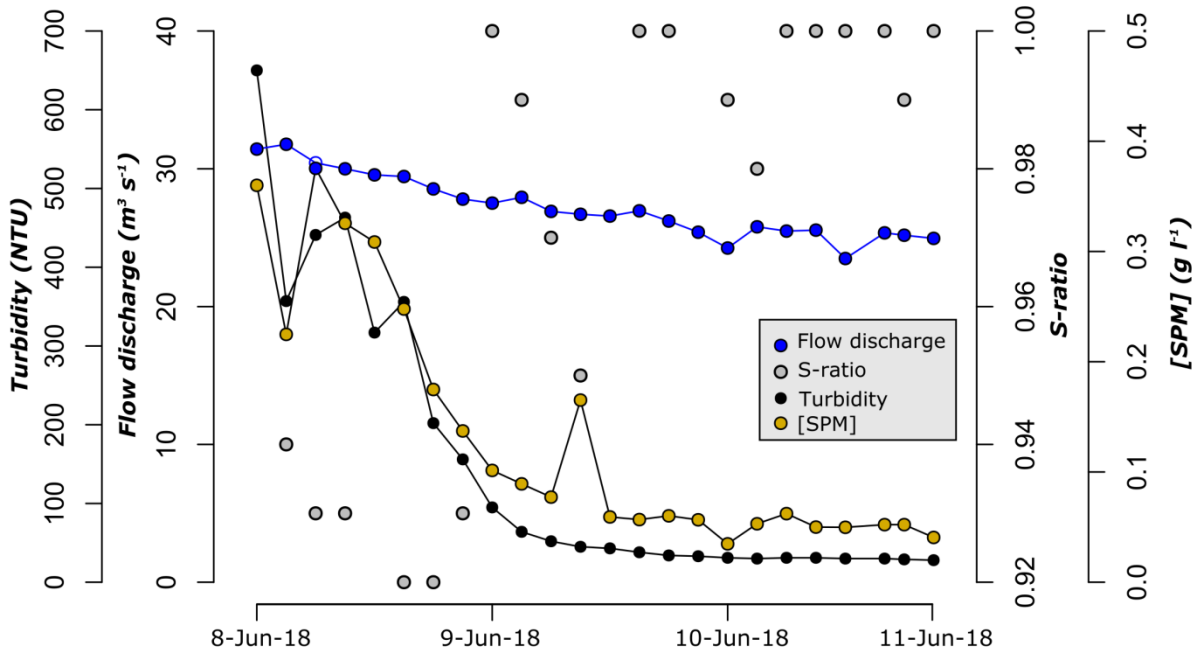

Fig. 72 : Comparison of the turbidity, flow discharge, S-ratio and SPM concentration at the automatic sampling station in the Canche River at Attin.

The beginning of the dataset corresponds to the climax of the rain event (on the 8th of June 2016 at ~12h) and shows high turbidities that correlate to S-ratios with typical high HC fraction values. The turbidity drops until the end of the rain event (early morning of the 10th of June 2016) and at a threshold value below 200 NTU, the S-ratio increases dramatically to values equal or close to one (LC/magnetite dominated). A transition zone can be observed between early morning and mid-day of 10th of June 2016, in which the S-ratio describes another drop to increased proportion of HC component, before going back to values close to one. This second drop in S-ratio, which seems to be uncorrelated to the turbidity, corresponds to the peak of suspended material that flows through the Canche channel after the end of the rain event.

A comparison of our data with results from Walling et al. (1979) and Slattery et al. (1995) confirms the correlation between the amount of suspended particles (SPM), the flow discharge and the evolution of the magnetic material in the water column. Walling et al. (1979) also showed that

the coercivity profiles from the sampled storm material correspond to the cultivated top soil sources. This observation additionally supports our interpretation of the S-ratio parameter as a soil runoff tracer.

5. Discussion and Conclusion

Many studies on suspended sediments in fluvial systems use a multitude of different tracers to identify sources and to quantify the flux in a given catchment. Sediment fingerprinting approaches struggle with the fact that the comparison of source material and suspended load is not always evident (grain size effects or organic matter corrections, diagenetic alterations, conservative behavior, spatial variations, statistical under-representation ; e.g. Pulley et al., 2015; Laceby et al. 2017) and many criterions must be fulfilled to run robust unmixing models. This usually imposes huge logistical and budgetary efforts to the respective study. Therefore, straightforward and easily applied methods offer facilitation to environmental management of catchments.

The presented non-destructive environmental magnetic methods (RT hysteresis analyses in combination with LT MPMS experiments) provide an interesting tool to treat a relatively large number of samples, even in small material quantity without any laborious sample preparation. The achieved parameters may then serve as robust tracers to run un-mixing or confluence-based sediment fingerprinting models to calculate sediment flux budgets. Magnetic tracers are robust under the condition that the ferruginous (iron-bearing) fraction sampled is representative, the spatio-temporal sampling frequency is adapted to the hydro-dynamic regime of the studied catchment some calibration (ground truth) of the magnetic parameters is checked.

This study focuses on the estimation of the sediment from agricultural soil input caused by runoff using variations in magnetic mineralogy in the Canche river catchment. Comparison with M_s and S-ratio values from literature, for example in the rural upstream area of the Seine river watershed (Kayvantash, 2016; Kayvantash et al., 2017) are in the same range of order. Thus the conclusions of Kayvantash et al. (2017) on the grain size dependence between magnetic fraction and

bulk sediment as well as the assumptions on the deconvolution between runoff and base flow in the studied meander bent of the upstream Seine river may be taken into account for comparable fluvial systems, such as the Canche river.

Our results highlights the fact that the S-ratio pictures in first order the state of the sample site due to the weather conditions during the sampling period. Thus, to be able to interpret the local S-ratio values, it is necessary to perform some test samples to identify the spatial background of the studied system corresponding to a no erosion signal. Once this is acquired, positive or negative variations can be interpreted in the respective HC and LC component input, that may be translated to respective sediment sources that have been eroded into the river (soil, channel banks/river bed). This is particularly interesting, when trying to quantify relative sediment flux.

The present study shows the potential and limits of the employed environmental magnetic parameters with respect to the different spatio-temporal scaling. Depending on the size of the studied area, the logistics and resolution must be considered. For example, it is feasible to perform high resolution snap shot sampling during distinct flood events when focusing to a small catchment area, such as the Planquette-Canche confluence, or when disposing an automated sampling station such as at Attin or at the outlet of the Pommeroye catchment. To be able to sample the entire catchment of the Canche river, snap shot sampling becomes impossible and thus regular seasonal sampling campaigns are more adapted. Here, the representative key positions of the sampling sites must be well chosen. If possible, the water flow, the velocity, and precipitation rates must be considered when interpreting the signal of the transported particles stocked in the sediment traps. Ideally, these conditions should be constant during the sampling period to be able to draw conclusions on the sediment flux. The optimum between sampling logistics and spatio-temporal resolution must be adapted with respect to the catchment size and reactivity of the fluvial system.

Comparison with other complementary rapid non-destructive techniques, such as spectrocolorimetry would be interesting, since the latter technique detects the HC magnetic minerals

hematite and goethite (e.g. Balsam et al., 2014; Torrent & Barrón, 2003; Debret et al., 2011) in addition to other sediment components (quartz, carbonates, clay minerals, etc). As observed in Patault et al. (2018 d; *in prep – see chapter 5*), the soil sample color signature in the Canche river catchment is typical of the goethite which comforts our interpretation of the magnetic parameter as a tracer of soil surface erosion.

Acknowledgements

This work was financially supported by the Mines-Telecom Institute of Lille-Douai, with additional funding provided by the Water Agency of Artois-Picardie (QUASPER project) and by the Carnot-MINES institute (FLUVIOMAGTRACK project). We would also like to acknowledge technical support from Emilie Delattre and Jordan Délépine (Syndicat mixte d'aménagement de la Canche) and François Derancourt (regional Chamber of Agriculture Nord-Pas-de-Calais, France). Authors are grateful to the LSCE and the IPGP for the magnetism analysis.

References

Andréassian, V., Lerat, J., Le Moine, N., & Perrin, C. (2012). Neighbors: Nature's own hydrological models. *Journal of Hydrology*, *414–415*, 49–58. http://doi.org/10.1016/j.jhydrol.2011.10.007

Balsam, W., Ji, J., Renock, D., Deaton, B, C., & Williams, E. (2014). Determining hematite content from NUV/Vis/NIR spectra: Limits of detection. *American Mineralogist*, *99*, 2280–2291.

Butler, R.F., Banerjee, S.K., 1975. Theoretical single-domain grain size range in magnetite and titanomagnetite, Journal of Geophysical Research, 80, 4049-4058.

Caitcheon, G. G. (1993). Sediment source tracing using environmental magnetism: A new approach with examples from Australia. *Hydrological Processes*, *7*(4), 349–358. http://doi.org/10.1002/hyp.3360070402

Carter, J., Owens, P., Walling, D., & Leeks, G. (2003). Fingerprinting suspended sediment sources in a large urban river system. *The Science of The Total Environment*, *314–316*(03), 513–534. http://doi.org/10.1016/S0048-9697(03)00071-8

Dearing, J. (1987). *Environmental magnetism*. *Quaternary Science Reviews* (Vol. 6). http://doi.org/10.1016/0277-3791(87)90024-2

Debret, M., Sebag, D., Desmet, M., Balsam, W., Copard, Y., Mourier, B., … Winiarski, T. (2011). Spectrocolorimetric interpretation of sedimentary dynamics: The new "Q7/4 diagram." *Earth-Science Reviews*, *109*, 1–19. http://doi.org/10.1016/j.earscirev.2011.07.002

Dekkers, M. J. (1989). Magnetic properties of natural geothite-II. TRM behavior during thermal and alternating field demagnetization and low-temperature treatment. *Geophys. J. Int.*, *97*(1989),

341–355.

Dunlop , D.J., Özdemir, Ö, 1997. Rock magnetism, fundamentals and frontiers, Cambridge University Press, 573p.

Estèbe, A., 1996, Impact de l'agglomeration parisienne et de ses rejets par temps de pluie sur les co,centrations de métaux de matières en suspension et des sédiments en Seine en période estivale, Ph.D. thesis, Université Paris XII - Val de Marne.

Evrard, O., Némery, J., Gratiot, N., Duvert, C., Ayrault, S., Lefèvre, I., … Esteves, M. (2010). Sediment dynamics during the rainy season in tropical highland catchments of central Mexico using fallout radionuclides. *Geomorphology*, *124*(1–2), 42–54. http://doi.org/10.1016/j.geomorph.2010.08.007

Franke, C., Kissel, C., Robin, E., Bonté, P., & Lagroix, F. (2009). Magnetic particle characterization in the Seine river system: Implications for the determination of natural versus anthropogenic input. *Geochemistry, Geophysics, Geosystems*, *10*(8), n/a-n/a. http://doi.org/10.1029/2009GC002544

Guzmán, G., Quinton, J. N., Nearing, M. A., Mabit, L., & Gómez, J. A. (2013). Sediment tracers in water erosion studies: current approaches and challenges. *Journal of Soils and Sediments*, *13*(4), 816–833. http://doi.org/10.1007/s11368-013-0659-5

Haddadchi, A., Ryder, D. S., Evrard, O., & Olley, J. (2013). Sediment fingerprinting in fluvial systems: review of tracers, sediment sources and mixing models. *International Journal of Sediment Research*, *28*(4), 560–578. http://doi.org/10.1016/S1001-6279(14)60013-5

Hickin, E.J., 1995. River geomorphology, publication International Association of Geomorphologists, Wiley

Kayvantash, D. (2016). *Caractérisation des particules ferrugineuses dans la Seine avec le magnétisme environnemental*. PSL Research University.

Kayvantash, D., Cojan, I., Kissel, C., & Franke, C. (2017). Magnetic fingerprint of the sediment load in a meander bend section of the Seine River (France). *Geomorphology*, *286*, 14–26. http://doi.org/10.1016/j.geomorph.2017.02.020

King, J. W., & Channell, J. E. T. (1991). Sedimentary magnetism, environmental magnetism, and magnetostratigraphy. *Reviews of Geophysics*, *Supplement*(August), 358–370.

Knighton, D., 1998. Fluvial Forms and Processes: a new perspective, Arnold, London.

Kosterov, A. (2003). Low-temperature magnetization and AC susceptibility of magnetite: Effect of thermomagnetic history. *Geophysical Journal International*, *154*(1), 58–71. http://doi.org/10.1046/j.1365-246X.2003.01938.x

Kruiver, P. P., Dekkers, M. J., & Heslop, D. (2001). Quantification of magnetic coercivity components by the analysis of acquisition curves of isothermal remanent magnetisation. *Earth and Planetary Science Letters*, *189*(3–4), 269–276. http://doi.org/10.1016/S0012-821X(01)00367-3

Laceby, J. P., Evrard, O., Smith, H. G., Blake, W. H., Olley, J. M., Minella, J. P. G., & Owens, P. N. (2017). The challenges and opportunities of addressing particle size effects in sediment source fingerprinting: A review. *Earth-Science Reviews*, *169*, 85–103. http://doi.org/10.1016/j.earscirev.2017.04.009

Lagroix, F., Banerjee, S. K., & Jackson, M. J. (2004). Magnetic properties of the Old Crow tephra: Identification of a complex iron titanium oxide mineralogy. *Journal of Geophysical Research B: Solid Earth*, *109*(B01104), doi:10.1029/2003JB002678. http://doi.org/10.1029/2003JB002678

Lagroix, F., & Guyodo, Y. (2017). A New Tool for Separating the Magnetic Mineralogy of Complex Mineral Assemblages from Low Temperature Magnetic Behavior. *Frontiers in Earth Science*, *5*(July), 1–11. http://doi.org/10.3389/feart.2017.00061

Le Gall, M., Evrard, O., Foucher, A., Laceby, J. P., Salvador-Blanes, S., Thil, F., … Ayrault, S. (2016). Quantifying sediment sources in a lowland agricultural catchment pond using 137Cs activities and radiogenic 87Sr/86Sr ratios. *Science of the Total Environment*, *566–567*, 968–980. http://doi.org/10.1016/j.scitotenv.2016.05.093

Lowrie, W., & Heller, F. (1982). Magnetic properties of marine limestones. *Reviews of Geophysics*, *20*(2), 171–192. http://doi.org/10.1029/RG020i002p00171

Maher, B. A. (2007). Environmental magnetism and climate change. *Contemporary Physics*, *48*(5), 247–274. http://doi.org/10.1080/00107510801889726

Maher, B. A., Watkins, S. J., Brunskill, G., Alexander, J., & Fielding, C. R. (2009). Sediment provenance in a tropical fluvial and marine context by magnetic “fingerprinting” of transportable sand fractions. *Sedimentology*, *56*(3), 841–861. http://doi.org/10.1111/j.1365-3091.2008.00999.x

Martínez-Carreras, N., Krein, A., Gallart, F., Iffly, J. F., Pfister, L., Hoffmann, L., & Owens, P. N. (2010). Assessment of different colour parameters for discriminating potential suspended sediment sources and provenance: A multi-scale study in Luxembourg. *Geomorphology*, *118*(1–2), 118–129. http://doi.org/10.1016/j.geomorph.2009.12.013

Motha, J. a., Wallbrink, P. J., Hairsine, P. B., & Grayson, R. B. (2004). Unsealed roads as suspended sediment sources in an agricultural catchment in south-eastern Australia. *Journal of Hydrology*, *286*(1–4), 1–18. http://doi.org/10.1016/j.jhydrol.2003.07.006

Oldfield, F., Rummery, T. A., Thompson, R., & Walling, D. E. (1979). Identification of suspended sediment sources by means of magnetic measurements: some preliminary results. *Water Resour. Res.*, *15*(2).

Ozdemir, O., & Dunlop, D. J. (1996). Thermoremanence and Néel temperature of goethite. *Geophysical Research Letters*, *23*(9), 921–924.

Özdemir, Ö., Dunlop, D. J., & Moskowitz, B. M. (1993). The effect of oxidation on the Verwey transition in magnetite. *Geophysical Research Letters*, *20*(16), 1671–1674. http://doi.org/10.1029/93GL01483

Özdemir, Ö., Dunlop, D. J., & Moskowitz, B. M. (2002). Changes in remanence, coercivity and domain state at low temperature in magnetite. *Earth and Planetary Science Letters*, *194*(3–4), 343–358. http://doi.org/10.1016/S0012-821X(01)00562-3

Poulenard, J., Perrette, Y., Fanget, B., Quetin, P., Trevisan, D., & Dorioz, J. M. (2009). Infrared spectroscopy tracing of sediment sources in a small rural watershed (French Alps). *Science of the Total Environment*, *407*(8), 2808–2819. http://doi.org/10.1016/j.scitotenv.2008.12.049

Pulley, S., Foster, I., & Antunes, P. (2015). The application of sediment fingerprinting to floodplain and lake sediment cores: assumptions and uncertainties evaluated through case studies in the Nene Basin, UK. *Journal of Soils and Sediments*, 1–23. http://doi.org/10.1007/s11368-015-1136-0

Robertson, D. J., & France, D. E. (1994). Discrimination of remanence-carrying minerals in mixtures, using isothermal remanent magnetisation acquisition curves. *Physics of the Earth and Planetary Interiors*, *82*(3–4), 223–234. http://doi.org/10.1016/0031-9201(94)90074-4

Russell, M. ., Walling, D. ., & Hodgkinson, R. . (2001). Suspended sediment sources in two small lowland agricultural catchments in the UK. *Journal of Hydrology*, *252*(1–4), 1–24. http://doi.org/10.1016/S0022-1694(01)00388-2

Shah, V. K., & Wakai, R. T. (2013). A compact, high performance atomic magnetometer for biomedical applications. *Physics in Medicine and Biology*, *58*(22), 8153–8161. http://doi.org/10.1088/0031-9155/58/22/8153

Slattery, M. C., Burt, T. P., & Walden, J. (1995). The application of mineral magnetic measurements to quantify within-storm variations in suspended sediment sources. *Geography*, (229).

Smirnov, A. V., & Tarduno, J. A. (2000). Low-temperature magnetic properties of pelagic sediments (Ocean Drilling Program Site 805C): Tracers of maghemitization and magnetic mineral reduction. *Journal of Geophysical Research*, *105*(B7), 16457–16471. http://doi.org/10.1029/2000JB900140

Tessier, L. (2003). *Transport et caractérisation des matières en suspension dans le bassin versant de la Seine : identification de signatures naturelles et anthropiques*. Ecole des Ponts ParisTech.

Theuring, P., Collins, A. L., & Rode, M. (2015). Source identification of fine-grained suspended sediment in the Kharaa River basin, northern Mongolia. *Science of The Total Environment*, *526*(APRIL), 77–87. http://doi.org/10.1016/j.scitotenv.2015.03.134

Torrent, J., & Barrón, V. (2003). The visible diffuse reflectance spectrum in relation to the color and crystal properties of hematite. *Clays and Clay Minerals*, *51*(3), 309–317. http://doi.org/10.1346/CCMN.2003.0510307

Vale, S. S., Fuller, I. C., Procter, J. N., Basher, L. R., & Smith, I. E. (2016). Characterization and quantification of suspended sediment sources to the Manawatu River, New Zealand. *Science of the Total Environment*, *543*, 171–186. http://doi.org/10.1016/j.scitotenv.2015.11.003

Vilmin, L., 2014. Modélisation du fonctionnenemnt biogéochimique de la Seine de l'agglomeration parisienne à l'éstuaire à differentes échelles temporelles, Ph. D. thesis, Ecole Nationale Superiéure des Mines de Paris.

Walling, D. E., Peart, M. R., Oldfield, F., & Thompson, R. (1979). Suspended sediment sources identified by magnetic measurements. *Nature*, *281*, 110–113. http://doi.org/0028-0836/79/370110-04$01.00

Williams, G.P., 1989. Sediment concentration versus water discharge durng single hydrologic events in rivers, Journal of Hydrology, 111, 89-106.

Conclusion générale

Conclusion générale

Rappel du contexte

L'érosion hydrique des sols est considérable sur le territoire français (~1,5 t ha^{-1} an^{-1}) et peut dépasser les 10 t ha^{-1} an^{-1} dans certaines zones du Nord de la France. Ces transferts sédimentaires peuvent induire des coulées boueuses particulièrement dévastatrices, qui peuvent être à l'origine de préjudices humains (ex. 3 morts en 1997 en Normandie) et matériels (ex. coulées boueuses de 2018 en France : coût estimé 430 M€ selon la Fédération Française des Assurances). Dans ce contexte et depuis l'année 1997, une lutte contre l'érosion et le ruissellement a été entreprise par l'Agence de l'Eau sur le territoire du bassin Artois-Picardie à travers différents programmes. Ces programmes ont été propices au développement d'études et diagnostics du phénomène érosif et à une prise de conscience de la problématique. Ainsi, devant l'introduction de l'objectif du bon état écologique des masses d'eau par la DCE en 2000 et l'augmentation des catastrophes de type coulées boueuses, de nouveaux programmes ont émergé visant à réduire les transferts de matière. Actuellement le 10ème programme de l'Agence de l'Eau Artois-Picardie (2013-2018) vise à lutter contre le phénomène érosif autour de 4 actions : (i) l'approche agronomique, (ii) l'installation d'ouvrages d'hydraulique douce, (iii) l'installation d'ouvrages de régulation, et (iv) l'installation d'ouvrages structurants. Une forte réflexion est donc observée en région Hauts-de-France pour réduire les transferts sédimentaires, mais peu d'études ont cherché à quantifier et caractériser la dynamique sédimentaire sur les bassins versants. Cette réflexion est pourtant indispensable pour orienter les futurs programmes d'actions et proposer des mesures de lutte ciblées et efficaces.

Sur le bassin Artois-Picardie, le bassin versant de la Canche (1274 km²) est particulièrement affecté par les transferts sédimentaires. Chaque année, des quantités importantes de sédiments transitent dans la rivière Canche jusqu'à l'exutoire. Le taux d'érosion spécifique est compris entre 22,5 et 144 t km^{-2} an^{-1} selon les années hydrologiques. Les processus d'érosion diffuse sur les parcelles agricoles, d'érosion concentrée dans les ravines, et de dégradations de berges sont

identifiés comme les processus majoritaires à l'origine du transfert sédimentaire. Si le bilan annuel sédimentaire à l'exutoire de la Canche est bien connu, certaines zones d'ombre subsistent sur le fonctionnement sédimentaire interne de ce bassin versant. La contribution des sous-bassins versant n'est pas quantifiée, et la variabilité des transferts sédimentaires depuis les zones sources est méconnue. De plus, l'efficacité des politiques récentes en matière de réduction des flux sédimentaire n'est pas évaluée. Dans ce contexte, des problématiques importantes existent sur le bassin versant de la Canche. Pour rappel, les problématiques évoquées en introduction de ce manuscrit étaient les suivantes :

i. Quel est le bilan érosif d'un parcellaire agricole ? Quelle est la variabilité spatio-temporelle des flux sédimentaires ? Et quels sont les paramètres forçants ?
ii. Est-il possible de prédire le flux érosif d'un parcellaire agricole ? Quel est l'efficacité d'un schéma d'aménagement anti-érosion à cette même échelle ?
iii. A l'échelle du bassin versant de la Canche, quelle est la variabilité spatio-temporelle des transferts sédimentaires ? Quel est l'efficacité des politiques d'aménagement en matière de lutte contre l'érosion ?
iv. Quelles zones, sources de matières, contribuent à ce transfert et en quelles quantités ?
v. Quels sont les meilleurs traceurs de l'érosion dans le contexte du bassin versant de la Canche ?

Le présent travail de thèse s'inscrit donc dans ce contexte et a été orienté autour de ces problématiques, de façon à acquérir une compréhension globale du bassin versant de la Canche (dynamique des transferts hydro-sédimentaires et origine des sédiments) à travers une démarche systémique à différentes échelles spatio-temporelles.

Orientation méthodologique

L'évaluation du flux sédimentaire d'un parcellaire agricole a été réalisée en instrumentant l'exutoire d'un impluvium de taille limitée. Le site d'étude choisi est le bassin versant de la Pommeroye (0,54 km²), qui présente l'avantage d'avoir une occupation du sol exclusivement composée de terres arables et une taille raisonnable pour réaliser des observations de terrain journalières. A son exutoire, les transferts hydro-sédimentaires s'écoulent au travers d'un organe de mesure (canal venturi à forme exponentielle). Le canal Venturi a été couplé à des appareils de mesure à haute-fréquence (débitmètre – sonde à turbidité – préleveur automatique) et a permis d'observer la variabilité temporelle des transferts hydro-sédimentaires à très haute-résolution (Δt = 6 min). L'utilisation conjointe d'un pluviomètre à augets basculants (0,2 mm) et une analyse statistique approfondie des caractéristiques des hydrogrammes de crue a permis d'évaluer les quantités de sédiments exportées et les paramètres de contrôle liés à ces transferts. Sur ce même bassin versant, des prédictions spatialisées d'érosion et de ruissellement sur le parcellaire agricole ont pu être effectuées à l'aide d'un modèle numérique. Le choix du modèle s'est porté sur *WATERSED* récemment développé par le BRGM, dans le cadre des travaux de Landemaine (2016). C'est un modèle non-dynamique prédisant de manière spatialisée le ruissellement et l'érosion en tout point d'un bassin versant (pixel) pour un évènement de pluie donné. Le modèle permet également d'intégrer des modules d'aménagements d'hydraulique douce sur le bassin versant. Il adopte une approche à base expert qui combine et classifie les paramètres majeurs de l'érosion sur la base d'expérimentations terrain ou en laboratoire. La puissance de ce modèle réside donc dans la précision spatio-temporelle des données injectées et la pertinence des observations liées à l'état du sol. Pour tirer pleinement avantage des possibilités du modèle, des données topographiques issues d'une campagne Lidar en 2015 ont été utilisées. Elles présentent l'avantage d'avoir une résolution très fine, à l'échelle centimétrique (50 cm), et donc une résolution plus importante comparé à d'autres études qui travaillent généralement à l'échelle métrique (scan IGN 25 m). D'autre part, les récentes études liées à l'utilisation du modèle *WATERSED* (e.g. Landemaine, 2016), utilisent un

calendrier cultural pour caractériser l'état de surface du sol à une temporalité donnée (e.g. Evrard et al., 2010). Nos observations ont montré qu'un décalage de croissance, pour une même culture et à un instant t donné, pouvait exister selon les dates de semis. Pour faire face à cette problématique et décrire finement les processus, des observations bi-mensuelles des états de surface des parcelles ont été réalisées. Néanmoins ces relevés parcellaires se sont révélés coûteux en temps d'observations sur le terrain et il est regrettable qu'une faible quantité d'observations soit restée inutilisée. Cette approche a toutefois permis d'injecter des données agro-pédologiques de très haute-qualité en vue de la calibration du modèle. Cette démarche méthodologique permet ainsi d'obtenir, pour un évènement donné, des cartographies extrêmement précises de la dynamique érosive et permet de comparer les évènements au regard de l'arrachement et du cheminement des particules (ex. réactivation de ravines).

Pour évaluer les contributions relatives des affluents au flux sédimentaire de la Canche à différentes échelles temporelles, une approche de type sediment fingerprinting a été utilisée. Cette approche a été largement utilisée par la communauté scientifique ces dernières années pour identifier les contributions des sources de sédiments aux matières en suspension, selon différentes occupations du sol et/ou zones lithologiques. Toutefois, de récentes découvertes suggèrent une utilisation différente de cette méthode et d'orienter les recherches vers une approche par confluence (Smith et al., 2015 ; Nosrati et al., 2018). Ainsi, les sédiments sources deviennent les affluents et les sédiments cibles deviennent les confluences. Cette approche permet ainsi de s'affranchir de certaines problématiques liées aux différences granulométriques et/ou dépôt-remobilisation des sédiments. Cette approche n'ayant jamais été développée sur un bassin versant en France, à notre connaissance, et encore moins dans un contexte aussi lithologiquement homogène que la Canche, il était tout à fait pertinent de saisir cette opportunité de recherche.

Pour fonctionner, les approches de sediment fingerprinting nécessitent l'utilisation d'un nombre important de traceurs environnementaux. Si certains traceurs ont largement été utilisés par

la communauté scientifique (chimie élémentaire, radionucléides, etc.), d'autres traceurs émergents sont développés pour limiter les coûts d'analyse importants liés à l'utilisation de ces méthodes. Parmi ces traceurs, ceux issus de la spectrocolorimétrie et du magnétisme environnemental montrent des avantages certains. Leur faible coût, leur rapidité d'analyse et leur caractère non-destructif les rend traceurs potentiellement intéressants pour évaluer les contributions des sources via une approche de type sediment fingerprinting. D'autre part, les récents travaux de Martinez-Carreras (2010) et Kayvantash (2016) ont respectivement montré le potentiel de ces traceurs pour évaluer les contributions sédimentaires des sols et des berges, et pour caractériser un signal érosif. Le rôle des berges sur le flux de matière en rivière est très mal connu dans le bassin de la Canche. Pourtant, pour une préservation pertinente de ce territoire agricole, la contribution relative des sols agricoles/berges au flux sédimentaire doit être évaluée. Il a donc semblé pertinent de tester la validité des traceurs spectrocolorimétriques et magnétiques dans le contexte du bassin versant de la Canche.

D'autre part, ce n'est que très récemment qu'un outil de modélisation, reprenant l'ensemble des analyses statistiques liées à ces approches pour identifier des traceurs pertinents, a été développé (*Sed-Sat* ; USGS ; Gorman Sanisaca et al., 2017). Cet outil incorpore une procédure statistique robuste (test de normalité – identification des outliers – test de range/Bracket – analyse factorielle discriminante) qui permet l'identification de traceurs discriminants et leur inclusion dans un modèle de mélange afin de quantifier des contributions relatives. La robustesse des sorties du modèle est également évaluée via des simulations Monte-Carlo. Le récent développement de cet outil induit qu'il n'existe pas de retour d'expérience lié à son utilisation. C'est pourquoi, le choix méthodologique s'est porté sur l'utilisation de cet outil pour évaluer les contributions des affluents et des sources sédimentaires de la Canche.

Fonctionnement du bassin versant de la Canche

L'ensemble des méthodologies et outils développés/testés au cours de ce travail ont donc permis de caractériser et de quantifier le fonctionnement global du bassin versant de la Canche. A l'échelle du parcellaire agricole, sur le bassin versant de la Pommeroye (0,54 km²), les flux sédimentaires ont été estimés entre 29 et 70 t km^{-2} an^{-1} selon les années de suivi et montrent de très fortes variabilités temporelles. 40% du flux sédimentaire sont exportés au cours de seulement 6% des évènements érosifs. Les saisons hivernales et automnales sont responsables à elles deux pour 97% du flux sédimentaire. La durée des évènements pluvieux et la quantité de pluie tombée sont les deux paramètres forçants qui expliquent la variabilité de ces flux. Les paramètres liés à l'intensité de pluie et aux quantités de pluie tombées 48h avant un évènement ne semblent pas expliquer la variabilité des flux dans le contexte du bassin versant de la Canche. A cette même échelle d'observation, la modélisation des flux hydro-sédimentaires a montré une forte variabilité spatiale de la remobilisation des particules au cours de différents épisodes érosifs. Les processus d'érosion identifiés sont liés à de l'érosion diffuse dans la partie amont du bassin versant et des processus d'érosion concentrée dans des ravines éphémères à l'aval du bassin versant. L'activité des ravines éphémères est temporellement variable, et leur activité semble rythmée par l'état de dégradation des parcelles. Les flux hydro-sédimentaires prédits sont globalement cohérents avec ceux mesurés à l'exutoire du bassin par la station de mesure haute-fréquence. Les prédictions sur le flux sédimentaire montrent d'excellent résultats avec un coefficient d'efficacité du modèle NSE (Nash & Sutcliffe Efficiency) de 0.92, il est relativement plus faible pour les ruissellements (NSE = 0.53). Les écarts liés à la prédiction des ruissellements s'expliquant par des effets de ré-infiltration de l'eau probablement sous-estimés (Landemaine, 2016). Ces résultats soulignent néanmoins une excellente opérabilité du modèle *WATERSED* dans le contexte du bassin versant de la Canche. La quantification des taux d'érosion parcellaires montre des valeurs pouvant aller jusqu'à 76 t km^{-2} par évènement et de fortes hétérogénéités selon les parcelles. Ces hétérogénéités s'expliquent par une rapide dégradation de l'état fragmentaire du sol sur certaines parcelles induisant une création précoce

d'une croûte de battance. De plus, une très faible croissance de la couverture du sol sur certaines parcelles est identifiée, ainsi qu'une forte diminution de la rugosité au cours d'épisodes pluvieux successifs. Les simulations d'aménagement d'hydraulique douce (haies, fascines, bande enherbée) sur ce bassin versant ont été réalisées via un module complémentaire du modèle *WATERSED.* Elles ont montré qu'une réduction significative (jusqu'à 84%) des transferts sédimentaires pouvait être possible selon les conditions hydro-climatiques.

A l'échelle plus large du bassin versant de la Canche, les flux sédimentaires des sous-bassins versants ont été estimés entre 0,87 et 40,7 kt an^{-1} à partir de traceurs chimiques (éléments majeurs et traces). La Planquette et la Créquoise se sont révélés être, en moyenne, les affluents les plus contributeurs sur cinq périodes d'échantillonnage contrastées. De fortes variabilités temporelles liées aux différentes saisonnalités sont toutefois observées et des processus de stockage/remobilisation des particules ont pu être identifiés sans toutefois pouvoir être quantifiés. En analysant la localisation des aménagements anti-érosion (hydraulique douce et structurants) présents sur le bassin versant de la Canche, on observe une forte corrélation entre la quantité d'aménagements installés sur un territoire et une diminution des quantités de flux sédimentaires exportés. Ces résultats semblent montrer un potentiel impact positif des politiques récentes en matière de lutte contre l'érosion sur le territoire de la Canche.

La quantification de la contribution de la surface des sols cultivés et des berges a également pu être évaluée grâce à l'emploi des traceurs spectrocolorimétriques et ceux liés à la chimie élémentaire des matières en suspension. A travers un modèle de mélange, les contributions ont été évaluées à 70% pour les berges et respectivement 30% pour les terres arables. Cependant ces pourcentages présentent de très fortes variabilités temporelles et ne représente pas une année hydrologique entière. Ainsi, le recueil précis de d'information lors d'évènements pluvieux reste à affiner. Les traceurs qui ont permis de quantifier ces contributions semblent liés à la couleur des oxy-hydroxydes de fer comme la goethite (b*, spectre de dérivée première à 535 nm), mais aussi à

certains composés de fertilisants utilisés sur les terres agricoles (U, Sr). Les analyses en magnétisme environnemental ont révélé un excellent potentiel pour tracer l'érosion des sols à partir des caractéristiques de la minéralogie magnétique de l'échantillon considéré. Selon plusieurs périodes temporelles, il est apparu que lors des périodes de fort transport sédimentaire sur le bassin versant, les matières en suspensions sont caractérisées par une augmentation de la composante de haute-coercivité dominante (i.e. goethite et hématite). A l'inverse, lors des périodes de faible transfert sédimentaire, les particules en suspension sont plutôt caractérisées par une composante de basse coercivité dominante (magnétite).

Références

Evrard, O., Nord, G., Cerdan, O., Souchère, V., Le Bissonnais, Y., & Bonté, P. (2010). Modelling the impact of land use change and rainfall seasonality on sediment export from an agricultural catchment of the northwestern European loess belt. *Agriculture, Ecosystems and Environment*, *138*(1–2), 83–94. https://doi.org/10.1016/j.agee.2010.04.003

Gorman Sanisaca, L. E., Gellis, A. C., & Lorenz, D. L. (2017). Determining the Sources of Fine-Grained Sediment Using the Sediment Source Assessment Tool (Sed _ SAT).

Kayvantash, D. (2016). *Caractérisation des particules ferrugineuses dans la Seine avec le magnétisme environnemental*. PSL Research University.

Landemaine, V. (2016). *Érosion des sols et transferts sédimentaires sur les bassins versants de l'Ouest du Bassin de Paris : analyse, quantification et modélisation à l'échelle pluriannuelle*. Université de Rouen Normandie.

Martínez-Carreras, N., Krein, A., Gallart, F., Iffly, J. F., Pfister, L., Hoffmann, L., & Owens, P. N. (2010). Assessment of different colour parameters for discriminating potential suspended sediment sources and provenance: A multi-scale study in Luxembourg. *Geomorphology*, *118*(1–2), 118–129. https://doi.org/10.1016/j.geomorph.2009.12.013

Nosrati, K., Collins, A. L., & Madankan, M. (2018). Fingerprinting sub-basin spatial sediment sources using different multivariate statistical techniques and the Modified MixSIR model. *Catena*, *164*(January), 32–43. https://doi.org/10.1016/j.catena.2018.01.003

Smith, H. G., Evrard, O., Blake, W. H., & Owens, P. N. (2015). Preface—Addressing challenges to advance sediment fingerprinting research. *Journal of Soils and Sediments*, (OCTOBER). https://doi.org/10.1007/s11368-015-1231-2

Perspectives

Perspectives

Cette étude et les résultats qui en découlent ont permis de faire émerger des perspectives liées à des verrous scientifiques et d'autres plus appliquées à une gestion concrète du bassin versant de la Canche. D'un point de vue recherche fondamentale, il semble particulièrement intéressant de travailler de manière plus approfondie sur la temporalité du transfert sédimentaire selon trois axes principaux. Premièrement, la temporalité des transferts sédimentaires a été étudiée selon un dispositif expérimental précis qui permet de capturer une quantité importante de sédiments pour les différentes analyses mais qui oblige de travailler sur des périodes de temps relativement courtes allant de l'épisode érosif à la semaine d'échantillonnage. Les résultats ne peuvent donc être extrapolés précisément sur des périodes plus longues. Pour répondre à cette rigueur, d'autres dispositifs de capture des matières en suspensions pourraient être testés dans le bassin versant de la Canche. Le dispositif de piégeage des sédiments utilisé dans le cadre des travaux de Le Gall (2016) semble particulièrement adapté, puisqu'il permet de capturer le transfert sédimentaire sur des périodes de 59 à 181 jours. Le couplage des pièges mis en œuvre dans le cadre de la thèse avec d'autres dispositifs semble particulièrement intéressant. D'une part, il permettrait de comparer l'efficacité de piégeage des deux systèmes (quantités récoltées, taille des particules, tri granulométrique), ce qui n'a jamais été réalisé auparavant, et d'autre part, permettrait de travailler sur une gamme d'échelle temporelle plus large (épisode érosif => semaines => mois => saisons).

Deuxièmement, si les transferts sédimentaires ont pu être caractérisés en termes de quantité et de provenance, les informations liées au temps de transfert des particules et donc aux phases de stockages/remobilisation des particules dans le bassin versant de la Canche sont méconnues. Pour cela, il est envisagé de réaliser un bilan massique de l'activité radionucléique des éléments ^{7}Be et $^{210}Pb_{ex}$ sur du matériel sédimentaire (coulées boueuses, berges, et MES) dans le continuum fluvial Pommeroye-Planquette-Canche. A l'instar des travaux de Matisoff (2005) et Evrard et al. (2010), la mesure de l'activité radionucléique de ces éléments permettrait d'évaluer le temps de résidence des particules et d'estimer leur âge. *In-fine*, cette expérience permettrait d'évaluer la part de matière

fraîchement érodée lors d'un épisode érosif sur ce continuum fluvial et d'évaluer les parts de stockage/remobilisation sédimentaire au cours d'un évènement.

Enfin, cette étude porte sur la variabilité spatio-temporelle des flux sédimentaires actuels. Il serait intéressant d'évaluer leur positionnement au regard des flux sédimentaires passés via l'analyse d'archives sédimentaires. Cette perspective a déjà été développée dans le cadre d'un stage de Master 2 au courant de l'année 2017 (Binous, 2017). Les premières prospections avaient permis d'identifier trois zones potentielles de stockage. Deux annexes hydrauliques situées à proximité de l'exutoire de la Ternoise (premier affluent de la Canche) ont ainsi été échantillonnées. L'extrapolation des premiers résultats de datation au ^{137}Cs ont montré un taux d'accumulation sédimentaire relativement faible de 0,48 cm an^{-1}. Néanmoins, il s'avère que des problèmes de datation liés au $^{210}Pb_{ex}$ n'ont pas permis d'affiner le modèle d'âge, en raison d'une trop faible quantité de $^{210}Pb_{ex}$ détectée après les 10 premiers cm de l'archive sédimentaire et de trop fortes incertitudes sur la mesure. En l'absence d'éléments tangibles, le travail n'a pas été reconduit et à l'heure actuelle, ces deux annexes hydrauliques ne sont plus utilisables puisqu'elles ont été curées et remodelées dans le cadre d'un projet de restauration écologique. Dans l'optique de développer à nouveau ce sujet, d'autres zones de dépôt, plus favorables à un stockage sédimentaire non perturbé, devront être identifiées en amont.

Des perspectives plus appliquées et liées à une gestion concrète du bassin versant de la Canche concernent l'efficacité individuelle des aménagements anti-érosion, l'applicabilité du modèle *WATERSED* à l'échelle de la Canche, et enfin l'émergence d'une multidisciplinarité via un site atelier « Pommeroye-Planquette-Canche ».

Premièrement, si cette étude a montré l'efficacité potentielle des aménagements anti-érosion en matière de réduction de transfert sédimentaire à deux échelles d'observation (bassin versant de la Pommeroye et bassin versant de la Canche), l'efficacité individuelle des aménagements n'est, quant à elle, pas quantifiée. Au vu de nos résultats, la capacité de réduction des transferts

sédimentaires des aménagements d'hydraulique douce semble spatialement et temporellement variable. Cette hypothèse de travail est soutenue par les récents résultats de Frankl et al. (2017) sur le bassin versant de l'Aa en France, qui souligne que le bon état des ouvrages assure une meilleure efficacité des ouvrages dans la réduction du transfert sédimentaire. Cette notion sous-entend un suivi et un entretien régulier des aménagements. Compte tenu de l'instrumentation mise en place sur le bassin versant de la Pommeroye et du futur plan d'aménagement d'hydraulique douce prévu sur ce bassin, un suivi précis de l'efficacité des aménagements selon plusieurs paramètres (nature de l'ouvrage, état de l'ouvrage, dimensions, variations de la capacité de stockage sédimentaire, qualité/typologie du matériel sédimentaire stocké) pourrait être mis en place. A travers ce suivi, un modèle d'efficacité des ouvrages pourrait être développé. Une fois ce modèle d'efficacité développé sur le bassin versant de la Pommeroye, son applicabilité à l'échelle du bassin versant de la Canche pourrait être envisagée. Dès lors, il permettrait aux gestionnaires une gestion simplifiée du parc d'aménagements d'hydraulique douce. De plus, il pourrait potentiellement être implémenté dans le modèle *WATERSED* pour une meilleure prise en compte de la capacité réelle de rétention sédimentaire des ouvrages.

Deuxièmement, la présente étude a montré un très fort potentiel du modèle *WATERSED* pour modéliser les flux hydro-sédimentaires lors d'un épisode érosif. Passé cette étape de calibration et de validation du modèle dans le contexte du bassin versant de la Pommeroye, il semble intéressant d'évaluer son applicabilité à une échelle supérieure. Dans la continuité de ces travaux, une application sur le bassin versant de la Planquette semble tout à fait propice. Cela permettrait de répondre à deux objectifs, d'une part évaluer l'efficacité des aménagements sur ce bassin versant et d'autre part, pouvoir tester la pertinence de l'inclusion du critère d'efficacité des aménagements.

L'instrumentation mise en place sur le bassin versant de la Canche, et plus particulièrement sur le bassin versant de la Pommeroye offre de très belles perspectives de travail. Cette synergie des instrumentations pourrait être complétée par l'instrumentation haute-fréquence de l'exutoire de la

Planquette. Cela répondrait à plusieurs objectifs. D'une part, cela permettrait d'évaluer si la calibration du modèle *WATERSED* opérée à l'échelle du bassin versant de la Pommeroye est pertinente à l'échelle du bassin versant de la Planquette, et confirmer/infirmer, la possibilité du transfert d'échelle du modèle selon cette première calibration. D'autre part, les résultats liés à ce travail s'organisent selon deux échelles spatiales (<1 et >1000 km²). Une connaissance plus poussée des processus de transferts sédimentaires à l'échelle des sous-bassins versants de la Canche (~100 km²) semble intéressante.

La quantification des transferts sédimentaires depuis les zones sources de l'érosion, jusqu'à l'exutoire du sous-bassin versant de la Planquette (instrumentation possible) puis à proximité de l'exutoire de la Canche (Attin) offrirait une réelle opportunité scientifique. La combinaison de ces instrumentations permettrait la création d'un site atelier, unique en son genre, avec un très fort potentiel pour travailler sur les notions de temporalité des transferts hydro-sédimentaires. L'intérêt de ce site atelier, ne se limite pas à l'étude des transferts hydro-sédimentaires. L'émergence d'une multidisciplinarité peut être envisagée afin de travailler sur la qualité de l'eau, la persistance des contaminants dans le continuum fluvial et l'efficacité des aménagements d'hydraulique douce (Fig.72).

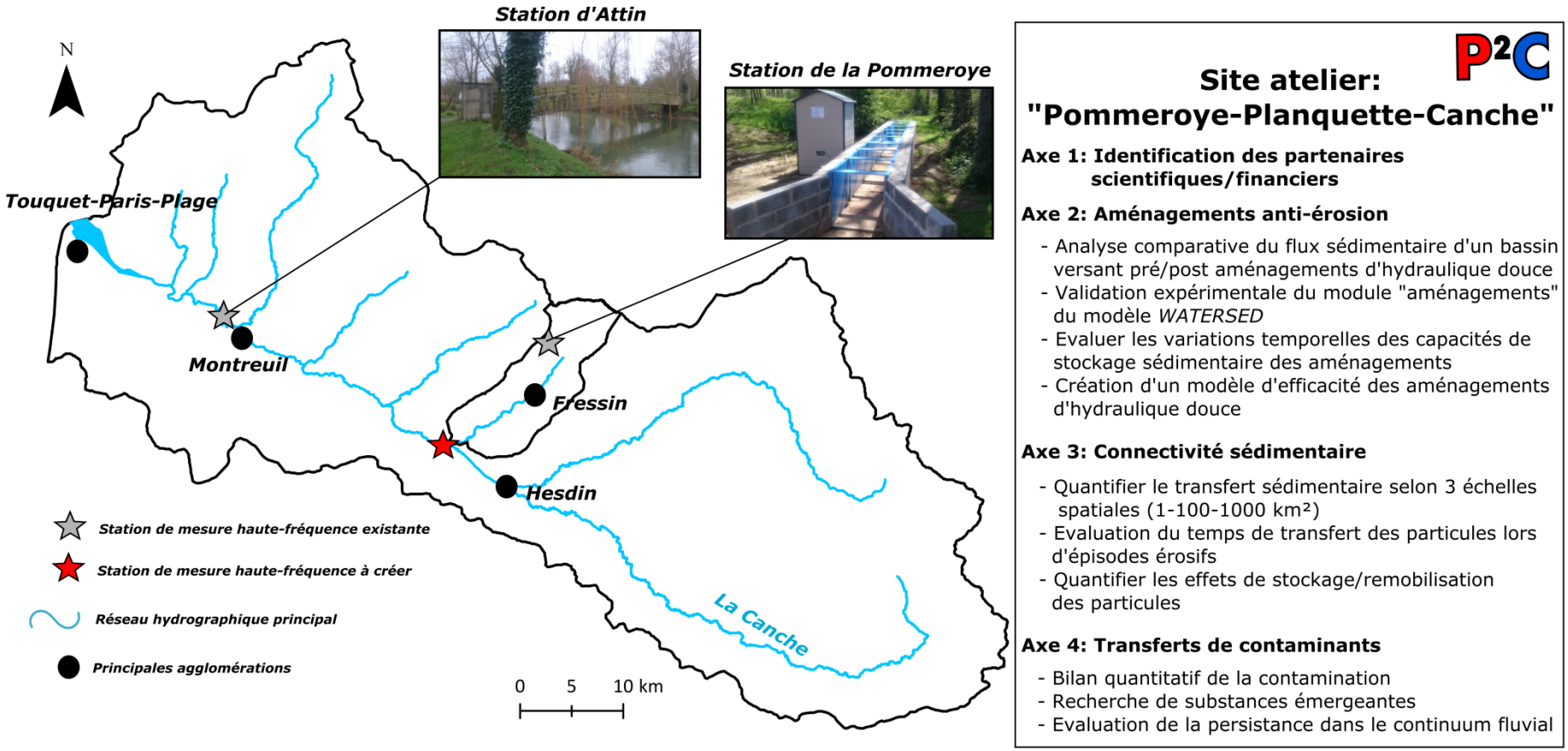

Fig. 73 : Planche explicative du site atelier P2C « Pommeroye-Planquette-Canche ».

Références

Binous, M. (2017). Reconstitution de la dynamique sédimentaire passée d'un hydrosystème en contexte agricole : cas du bassin versant de la Canche. Rapport de stage. Master 2 Géosciences, Planètes, Ressources et Environnement. Université de Nancy. France.

Evrard, O., Némery, J., Gratiot, N., Duvert, C., Ayrault, S., Lefèvre, I., Esteves, M. (2010). Sediment dynamics during the rainy season in tropical highland catchments of central Mexico using fallout radionuclides. *Geomorphology*, *124(1-2)*, 42-55 pp.

Frankl, A., Prêtre, V., Nyssen, J., & Salvador, P.-G. (2017). The success of recent land management efforts to reduce soil erosion in northern France. *Geomorphology*, *303*, 84–93. https://doi.org/10.1016/j.geomorph.2017.11.018

Le Gall, M. (2016). Traçage des sources de sédiments à l'amont des hydrosystèmes agricoles : apport de la géochimie élémentaire, du rapport Sr/Sr et des radionucléides. Géochimie. Université Paris-Saclay. France.

Matisoff, G., Wilson, C. G., & Whiting, P. J. (2005). *The 7Be/210Pbxs ratio as an indicator of suspended sediment age or fraction new sediment in suspension. Earth Surface Processes and Landforms, 30(9),* 1191-1201 pp.

Annexes

Annexe A : Présentation de la station de suivi expérimentale de la Pommeroye

1. Choix méthodologique

Le suivi des flux de MES dans un bassin versant est une opération couramment menée depuis de nombreuses années sur la base de différents protocoles. Le choix de ce dernier est réalisé au regard des contraintes de l'utilisateur, à la fois en termes de temps, de présence sur le terrain, et de post-traitements en laboratoire. Par conséquent, c'est en fonction de la résolution temporelle et de la durée de la période de mesures envisagée qu'est déterminé le mode d'acquisition des données le plus approprié (Vongvixay, 2012). Deux méthodes sont envisageables pour mesures les flux de matières en suspensions. L'une consiste à déterminer directement les concentrations en MES à partir de prélèvements d'eau et la mesure de la concentration multipliée par le débit permet alors de quantifier les flux massiques de sédiments exportés d'un bassin versant (Viel, 2012). Cependant la forte variabilité des transferts de MES implique de devoir réaliser des échantillonnages à haute-fréquence. De plus, pouvoir assurer la filtration des échantillons dans un délai raisonnable s'avère coûteux en temps. Cette méthode n'est pas très adaptée dans notre cas.

Ici, le protocole choisi est d'évaluer les flux de MES basés sur des suivis de turbidité. Ce paramètre, mesuré en NTU (Nephelometric Turbidity Unit) est une propriété optique qui quantifie la diminution de l'intensité de la diffusion de la lumière entre un faisceau incident et un photorécepteur. La quantification des transferts de MES est possible selon le postulat de départ qu'il existe une relation entre la turbidité et la charge solide transportée dans un cours d'eau. Lors de fortes crues, l'eau devient trouble et la turbidité augmente. On peut alors quantifier de manière indirecte la charge en MES et on s'affranchit de réaliser un très grand nombre de filtrations. Néanmoins, cette relation turbidité/charge en MES doit être établie à partir de prélèvements manuels dans différents conditions hydrologiques pour couvrir une large gamme de concentrations. Dans un premier temps, cela ne dispense pas d'un échantillonnage fréquent. Mais une fois la corrélation établie, c'est un gain de temps considérable (Viel, 2012).

2. Matériel

2.1 Canal Venturi à section exponentielle

Le canal Venturi à section exponentielle est un organe en polyester armé destiné à mesurer des débits d'écoulement en canal ouvert rectiligne. Lorsque les conditions d'écoulement fluvial (non turbulent) sont respectées à l'amont de la contraction Venturi, ainsi que le dénoyage assuré à l'aval (écoulement libre sans contraintes de mise en charge), alors la lame d'eau à l'amont de la contraction (charge hydraulique) est directement liée au débit en transit. L'originalité des canaux venturi à section exponentielle est de cumuler les avantages des canaux venturi classiques (libre passage sans seuil) et de pouvoir répondre également aux grandes variations de débits (flancs inclinés). En effet, la contraction latérale est de section parabolique, le col s'évasant de la base au sommet. Cette particularité permet la mesure de faibles débits avec précision, puisque l'écoulement réduit, transite par une section étroite de forme parabolique. De ce fait, ce type de Venturi est le seul à permettre la mesure précise de débits variant dans un rapport extrême de 1 à 100. Pour notre cas, le modèle *ISMA taille VII* (Fig.73 ; dimensions : 10004 x 840 x 855 mm ; L x l x h), la possibilité de mesure continue s'étend de 14,51 $m^3 h^{-1}$ à 1454,87 $m^3 h^{-1}$. Les débits sont calculés selon l'équation suivante :

$$Q = -7{,}223 \times h + 2873{,}2 \times h^2 - 766 \times h^3 + 770 \times h^4$$

Avec Q en $m^3 h^{-1}$ et h en m.

Fig. 74 : Canal Venturi à forme exponentielle, modèle *ISMA taille VII*.

Dès lors, nous obtenons le tableau de conversion suivant (Tab.17) qui est implémenté dans le logiciel de configuration du débitmètre à ultrasons :

Tab. 18 : Table de conversion hauteur/débit du canal venturi *ISMA taille VII*.

mm CE	L s^{-1}	m^3 h^{-1}	mm CE	L s^{-1}	m^3 h^{-1}
73	4,03	14,51	410	124,72	448,99
80	4,85	17,45	425	133,95	482,22
95	6,85	24,65	440	143,52	516,68
110	9,18	33,06	455	153,44	552,39
125	11,86	42,68	470	163,71	589,34
140	14,86	53,50	485	174,32	627,56
155	18,19	65,50	500	185,30	667,06
170	21,86	78,69	515	196,63	707,86
185	25,85	93,05	530	208,33	749,97
200	30,16	108,59	545	220,39	793,41
215	34,80	125,29	560	232,83	838,19
230	39,77	143,17	575	245,65	884,35
245	45,06	162,20	590	258,86	931,88
260	50,67	182,41	605	272,45	980,83
275	56,60	203,77	620	286,44	1031,20
290	62,86	226,31	635	300,84	1083,02
305	69,45	250,01	650	315,64	1136,32
320	76,36	274,88	665	330,87	1191,12
335	83,59	300,92	680	346,51	1247,44
350	91,15	328,15	695	362,59	1305,31
365	99,05	356,56	710	379,10	1364,76
380	107,27	386,17	725	396,06	1425,82

395	115,83	416,97		732	404,13	1454,87

2.2 Débitmètre à ultrasons

En raison de la plage de mesures de débits possible dans le canal venturi, le choix de l'instrument s'est porté sur un débitmètre à ultrasons *LNU300-X* à data logger intégré de la marque *IJINUS* (Fig.74). Ce type d'appareil présente l'avantage d'avoir un système de conversion débit/hauteur d'eau intégré ce qui rend son utilisation facilitée avec un canal venturi. De plus, la gamme de mesure des hauteurs d'eau s'étend de 0 à 3 m avec une résolution de 2 mm ce qui permet de mesurer de nombreuses plages de débits. Cet appareil se démarque également par une puissante autonomie énergétique. Son fonctionnement sur pile lithium 3,6 V 17 Ah permet d'avoir une autonomie de 9 à 12 mois avec une mesure de débits toutes les 6 min dans notre cas. Enfin, l'appareil offre la possibilité de coupler un préleveur automatique d'échantillons d'eau. Le principe de fonctionnement des sondes de mesure des niveaux de liquide à ultrason repose sur l'exploitation du temps de transit d'une impulsion d'ondes ultrasonores entre la surface inférieure de la sonde ultrason et la surface du liquide à mesurer. Cette impulsion d'ondes ultrasons agit sur les constantes piézoélectriques d'un élément sensible interne au capteur de niveau de liquide ultrason, qu'un convertisseur, interne à la sonde de niveau de liquide à ultrason, va exploiter pour en générer un signal analogique de type 4-20 mA. Ce principe permet de paramétrer et re-paramétrer la sonde de niveau de liquide à ultrason, à l'aide d'une simple console. Le capteur est fixé sur le canal venturi, sur une potence rigide, en amont de la contraction latérale. L'angle d'émission du capteur est fixé à la verticale (le défaut de verticalité acceptable étant de ± 2°). Le zéro de la sonde est déterminé par rapport au fond du canal venturi et non par rapport à la sonde. La fréquence des mesures est de Δt = 6 min.

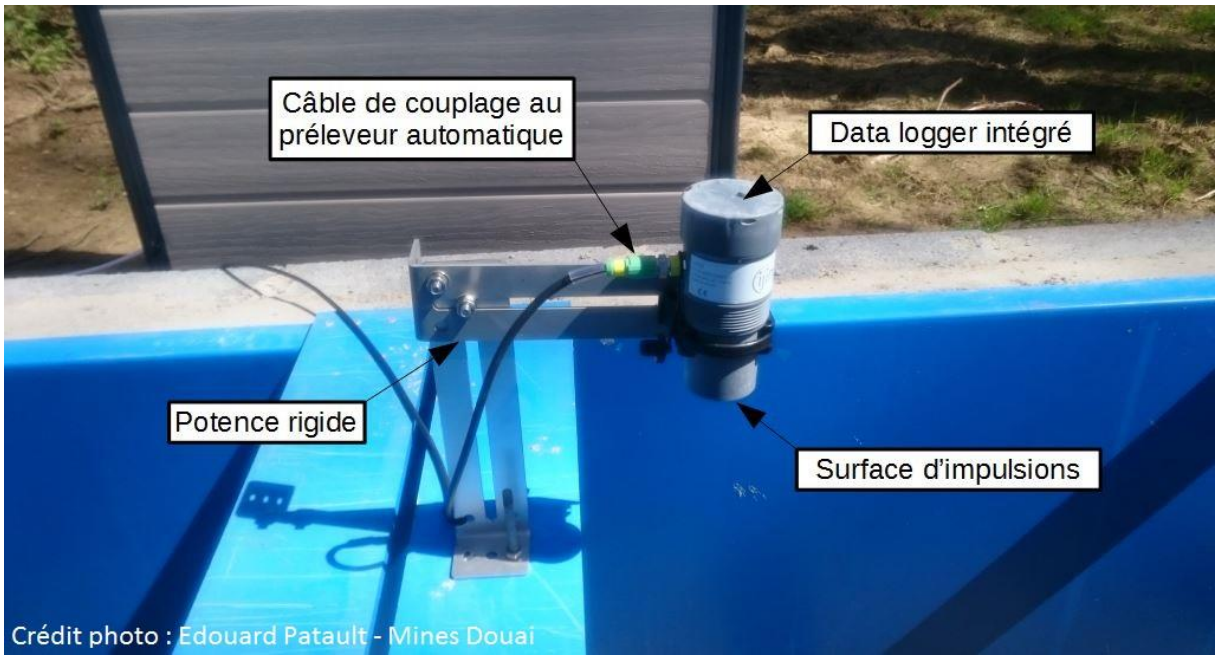

Fig. 75 : Débitmètre à ultrasons *LNU300-X* de la marque *IJINUS*.

2.3 Acquisition des données de turbidité

Les mesures de turbidité sont réalisées à l'aide d'un capteur de turbidité par néphélométrie de la gamme *Odeon/Aqualabo* (Fig.75). Le principe de mesure est basé sur la néphélométrie : une diode émet dans une lumière dans l'infra-rouge (880 nm) et une diode de réception placée à 90° mesure le rayonnement diffusé (mesure normalisée). La sonde de turbidité doit être maintenue propre au niveau de la tête contenant les fibres optiques. Toute trace de biofilm ou d'encrassement pourrait induire un biais dans la mesure. Pour cela, un nettoyage régulier de la tête de la sonde est effectué après chaque crue à l'aide d'une éponge et d'eau déminéralisée. Cela permet également d'éviter toute dérive du signal de la sonde. L'enregistrement des données s'effectue sur un data logger relié à la sonde. La fréquence des mesures est de Δt = 6 min et les plages de mesures sont les suivantes (Tab.19) :

Tab. 19 : Plages de mesures et précision du capteur de turbidité

Gamme de mesure (norme ISO)	0 à 4000 FNU en 4 gammes : 0- 50 FNU ; 0 – 200 FNU ; 0 – 1000 FNU ; 0 – 4000 FNU ; 0 -4500 mg/L
Résolution	De 0,1 à 1 selon la gamme FNU De 0,01 à 1 selon la gamme mg L^{-1}
Précision	+/- 1% de la pleine échelle par gamme

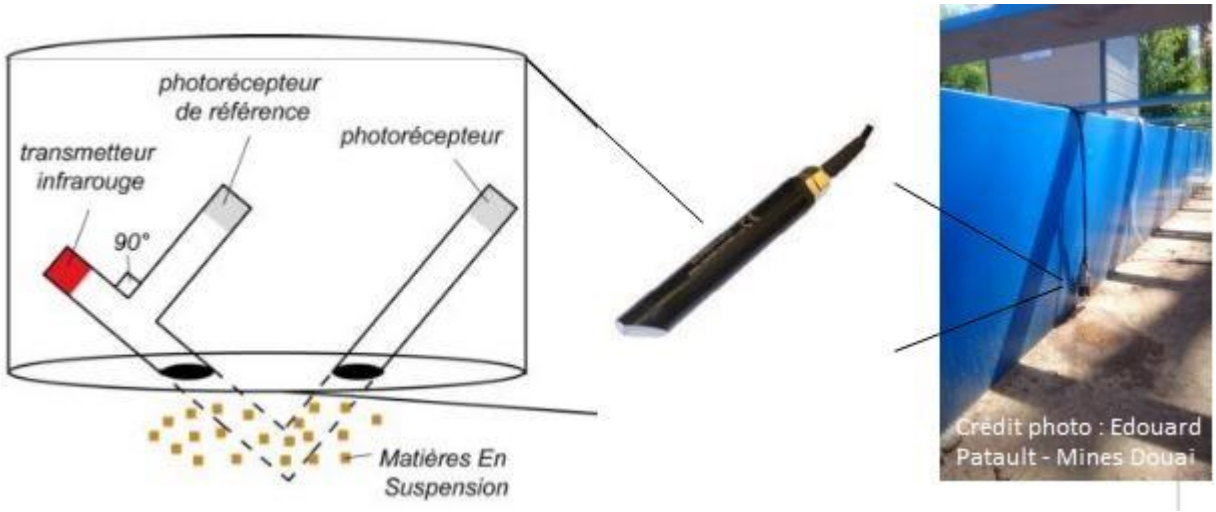

Fig. 76 : Sonde à turbidité (gamme *Odeon/Aqualabo*) et principe de la mesure.

2.4 Echantillonnage de MES à l'exutoire

En parallèle des mesures de turbidité dans le canal venturi, des prélèvements d'échantillons d'eau sont effectués dans le but d'établir une relation entre la turbidité et la concentration en MES équivalente. Pour cela, un échantillonneur automatique d'eau isotherme de type *ISCO 3700* a été installé (Fig.76). Cet appareil constitué d'une pompe et d'un kit de programmation permet d'effectuer des prélèvements à un pas de temps défini par l'utilisateur. Dans notre cas, le couplage au débitmètre à ultrasons permet de le mettre en fonctionnement seulement lorsqu'un flux d'eau est détecté dans le canal venturi (on parle ici « d'impulse »). Les échantillons prélevés sont stockés dans des bidons de 1 l, on en dénombre 24 au total et ils sont situés dans la partie basse de l'appareil. Un système de répartition permet de remplir ces bidons au fur et à mesure. Enfin, le liquide est prélevé dans le canal par le biais d'une crépine, située à proximité de la sonde à turbidité. Chaque prélèvement est réalisé après une purge complète du tuyau. L'appareil se veut autonome en énergie, celui-ci est équipé d'une batterie 12 V 60 Ah.

Fig. 77 : Echantillonneur automatique d'eau *ISCO 3700*.

2.5 Evaluation de la concentration en MES

La concentration en MES des eaux sur le bassin versant de la Pommeroye est évaluée d'après l'analyse des prélèvements automatiques d'eau. Les prélèvements réalisés sur le terrain sont filtrés en laboratoire à l'aide d'un matériel de filtration classique (Fig.77). Les filtres utilisés sont en nitrate de cellulose (Ici, le choix s'est porté sur des filtres magnétiquement neutres dans le but de ne pas créer de biais sur les analyses magnétiques futures) de maille 0,45 µm. Dans un premier temps, les filtres sont mis à l'étuve à 70°C pendant 48 h, refroidis puis pesés. Un volume d'échantillon de 100 mL est ensuite filtré après agitation de celui-ci à l'aide d'une pompe à vide. Une fois l'opération terminée, les filtres sont placés à l'étuve à 30°C pendant 72 h (Ici, la température est volontairement

diminuée pour éviter toute transformation de la magnétite en goethite qui se produit dès 40°C) puis ils sont pesés. La concentration en MES (SSC) est alors évaluée selon la formule suivante :

$$SSC = \frac{M1 - M0}{V}$$

Avec SSC en g l^{-1} ; M_1 la masse du filtre et filtrat en g ; M_0 la masse du filtre en g ; et V le volume filtré en L.

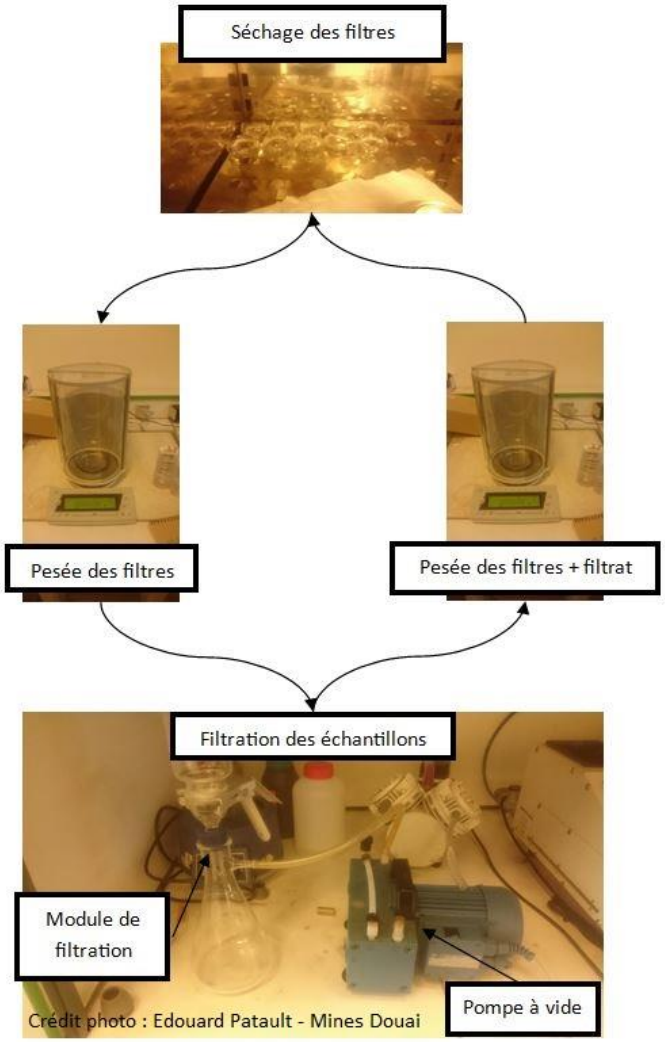

Fig. 78 : Protocole de filtration des MES après prélèvements.

2.6 Relation turbidité/concentration en MES

La relation entre turbidité et concentration en MES est établie d'après la filtration des échantillons et la mise en correspondance avec la valeur de turbidité calculée à un instant t. Ici il est nécessaire d'avoir un nombre important de prélèvements représentatifs des différentes conditions hydrologiques sur l'année. Il est également important que la relation d'étalonnage soit établie pour la plus grande gamme de valeur de turbidité observées in-situ. La relation entre ces deux paramètres a été établie sur 72 échantillons. Nous obtenons une relation très robuste entre turbidité et charge en MES avec un R^2 = 0,9182 (Fig.78) malgré une dispersion du nuage légèrement plus élevée sur les fortes valeurs de turbidité. Des régressions linéaires, polynomiales ou logarithmiques ont été testées et c'est la régression polynomiale qui est retenue car elle présente le plus fort coefficient de détermination. Enfin, on peut noter que notre échantillonnage est conséquent sur l'ensemble des valeurs de turbidité observées au cours des différents évènements.

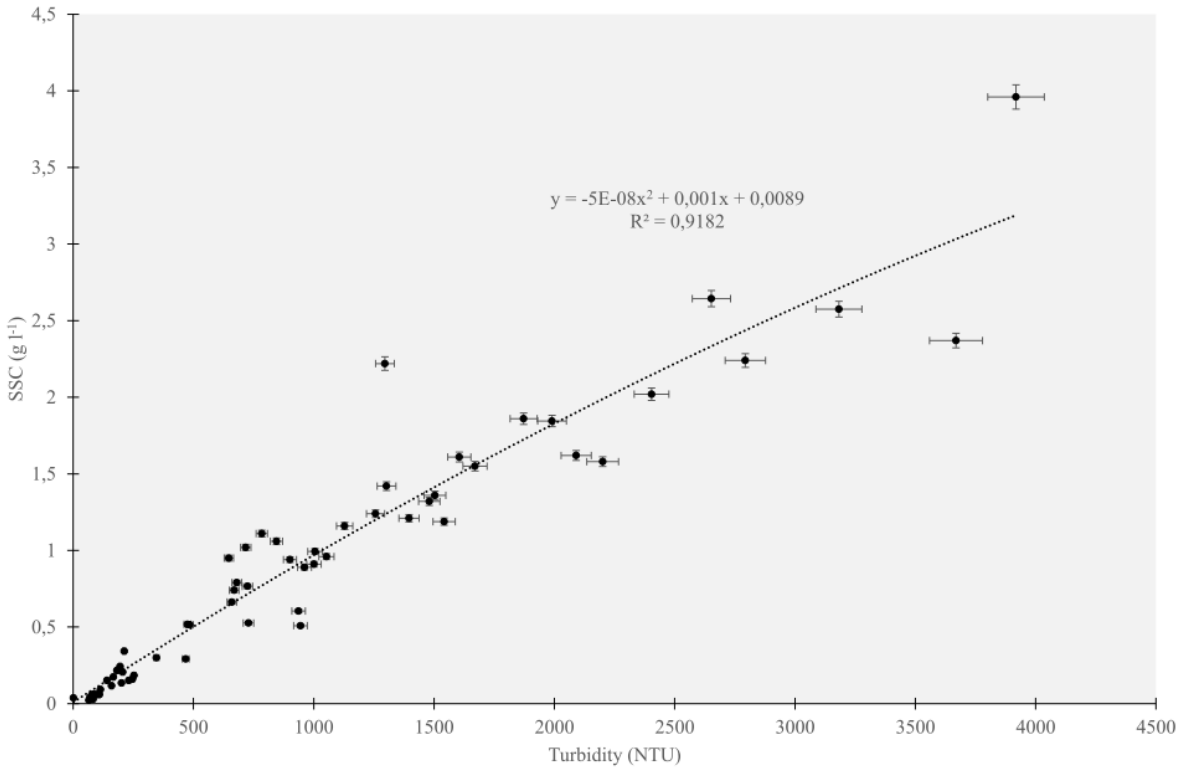

Fig. 79 : Courbe de corrélation entre la concentration en MES (g l^{-1}) et la turbidité (FNU) sur le bassin versant de la Pommeroye.

2.7 Estimation des flux sédimentaires

Une fois l'acquisition des débits et des concentrations en MES réalisée, il est possible d'évaluer les flux sédimentaires qui transitent à l'exutoire du bassin versant. Le flux de matières en suspensions instantané (SSF en kg s^{-1}) est évalué selon l'équation suivante :

$$SSF = Q \times SSC \times 10^3$$

Avec SSF en kg s^{-1}, Q en m^3 s^{-1} et SSC en g l^{-1}.

Le flux de matières en suspensions (SSY en kg) pour chaque évènement est alors évalué de la manière suivante :

$$SSY = \int_{t_0}^{t} SSF \, \Delta t$$

Avec t_0 et t_t qui correspondent au début et à la fin de chaque évènement sur la période de mesures.

2.8 Acquisition des données de pluviométrie

L'acquisition des données pluviométriques est assurée par un pluviomètre à auget basculant 0,2 mm installé en tête du bassin versant de la Pommeroye (Fig.79). Celui-ci est opérationnel depuis le 10 avril 2016. La faible surface de ce bassin permet l'utilisation d'un seul pluviomètre considéré comme représentatif de la zone étudiée. Le principe de mesure est le suivant : l'eau provenant des précipitations est recueillie dans la bague réceptrice et canalisée par le cône de réception. L'eau s'écoule sur le couvercle du transducteur à travers un orifice de 4 mm de diamètre et se déverse dans l'un des deux compartiments de l'auget. Lorsque la contenance d'incrément de l'auget est atteinte, celui-ci bascule brusquement, provoque la fermeture brève d'un circuit électrique et déverse son contenu d'eau à l'extérieur. Le second auget se place en position de remplissage, puis à son tour, bascule lorsque la masse d'eau requise est atteinte. Les impulsions sont enregistrées par

une station d'acquisition automatique. L'enregistrement continu permet de déterminer les cumuls et l'intensité des précipitations. La fréquence d'enregistrement est fixée à Δt = 6 min.

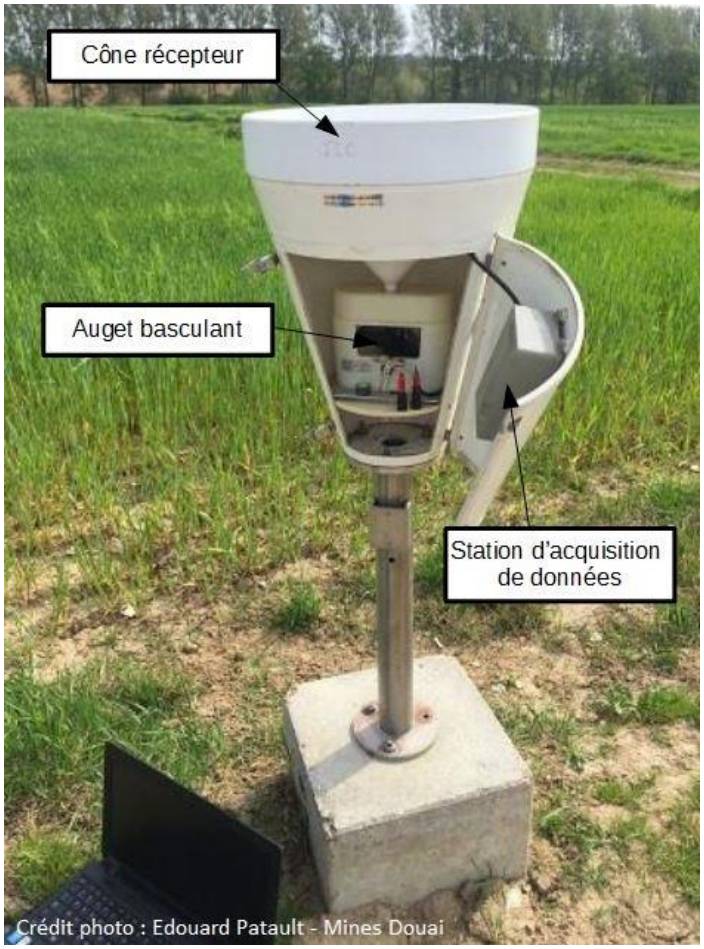

Fig. 80 : Pluviomètre à auget basculant 0,2 mm.

3. Références

Viel, V. (2012). *Analyse spatiale et temporelle des transferts sédimentaires dans les hydrosystèmes normands. Exemple du bassin versant de la Seulles. Geography. Université de Caen. France.*

Vonvixay, A. (2012). *Mesure et analyse de la dynamique temporelle des flux solides dans les petits bassins versants. Cas d'un bassin versant agricole en région d'élevage (Le Moulinet, Basse-Normandie, France). Environmental Engineering. INSA de Rennes. France.*

Annexe B: Supplementary data

Supplementary data – Chapter 3

Tab. 20 : Evaluation of surface crusting according to Le Bissonnais et al. (2005).

Grade	Description
F0	Initial fragmentary structure, all particles are clearly distinguishable
F11	Altered fragmentary state with structural crusts
F12	Transitional: local appearance of depositional crusts
F2	Continuous state with depositional crusts

Tab. 21 : Evaluation of surface roughness: difference in height of the deepest part of micro depressions and the lowest point of their divide adapted from Ludwig et al. (1995).

Soil surface roughness evaluation		
Grade	Roughness index (cm)	Description
R0	0-1	Strongly crusted sown fields, harvested fields with intense compacting
R1	1-2	Sown fields with fine loosened or moderately crusted seedbeds
R2	2-5	Recently sown fields with a cloddy surface, crusted tilled fields without residues
R3	5-10	Stubble-ploughed fields and recently sown fields with a very cloddy surface
R4	>10	Ploughed fields

Tab. 22 : Classification of vegetation cover expressed as a percentage of the area covered by canopy or liter according to Le Bissonnais et al. (2005).

Grade	Soil surface percentage covered by canopy or liter
C1	0-20%
C2	21-60%
C3	61-100%

Tab. 23 : Infiltration capacity rates (mm h^{-1}; according to Cerdan et al. (2001)).

Roughness index (cm)	Crop cover (%)	F0	F11	F12	F2
R0	C1	10	10	5	2
	C2	20	10	5	2
	C3	50	20	10	5
R1	C1	20	10	5	2
	C2	50	20	10	2
	C3	50	20	10	5
R2	C1	50	20	10	5
	C2	50	20	10	5
	C3	50	50	20	10

R3	C1	50	20	10	5
	C2	50	50	20	10
	C3	50	50	50	10
R4	C1	50	20	20	10
	C2	50	50	20	10
	C3	50	50	50	10

Tab. 24 : Potential sediment concentration range (g l^{-1}) in the flow. Values in bold correspond to combination based on field experiment references (Cerdan et al., 2002), the other values are evaluated with a fuzzy logic-based method.

Roughness index (cm)	Crop cover (%)	Max. 6 min intensity (mm h^{-1})	F0	F11	F12	F2
R0-R1	C1	0-10	0-1	1-5	0-1	**1-5**
		10-40	0-1	5-10	1-5	**5-10**
		>40	1-5	10-15	5-10	**10-15**
	C2-C3	0-10	0-1	0-1	0-1	**0-1**
		10-40	0-1	1-5	0-1	**1-5**
		>40	1-5	5-10	1-5	**5-10**
R2	C1	0-10	**0-1**	**0-1**	**0-1**	**0-1**
		10-40	**1-5**	**10-15**	**5-10**	**10-15**
		>40	**5-10**	15-25	10-15	**15-25**
	C2-C3	0-10	0-1	1-5	**0-1**	**1-5**
		10-40	0-1	5-10	**1-5**	**5-10**
		>40	1-5	10-15	**5-10**	**10-15**
R3	C1	0-10	1-5	**5-10**	**5-10**	**10-15**
		10-40	5-10	**10-15**	**10-15**	**15-25**
		>40	10-15	**25-35**	**15-25**	**25-35**
	C2-C3	0-10	0-1	5-10	1-5	**5-10**
		10-40	1-5	**10-15**	5-10	**10-15**
		>40	5-10	**15-25**	10-15	**15-25**
R4	C1	0-10	1-5	10-15	**5-10**	10-15
		10-40	5-10	15-25	**10-15**	**15-25**
		>40	10-15	25-35	**25-35**	25-35
	C2-C3	0-10	1-5	5-10	5-10	10-15
		10-40	5-10	10-15	10-15	15-25
		>40	10-15	25-35	15-25	25-35

Tab. 25 : Manning's roughness coefficient (Gilley et al., 1991).

Roughness index (cm)	Crop cover (%)	Manning
R0	C1	0.039
	C2	0.095
	C3	0.151
R1	C1	0.043
	C2	0.099
	C3	0.155
R2	C1	0.047
	C2	0.103

	C3	0.159
R3	C1	0.056
	C2	0.112
	C3	0.168
R4	C1	0.078
	C2	0.134
	C3	0.190

Tab. 26 : Soil erodibility factor for loamy soils (Souchère et al., 2003).

Crop cover (%)	Erodibility
C1	0.683
C2	0.217
C3	0.047

Tab. 27 : Runoff sensitivity category for the Pays de Caux loamy soils according to Souchère et al. (2003).

Roughness index (cm)	Crop cover (%)	F0	F11	F12	F2
R0	C1	2	2	3	4
	C2	1	2	3	4
	C3	0	1	2	3
R1	C1	1	2	3	4
	C2	0	1	2	3
	C3	0	1	2	3
R2	C1	0	1	2	3
	C2	0	1	2	3
	C3	0	0	1	2
R3	C1	0	1	2	3
	C2	0	0	1	2
	C3	0	0	0	2
R4	C1	0	1	1	2
	C2	0	0	1	2
	C3	0	0	0	2

Tab. 28 : Evaluation of the imbibition rainfall height (mm) as a function of antecedent rainfall and runoff sensitivity category.

Category	48-h antecedent rainfall height (mm)			
	0	1-15	16-40	>40
0	20	15	12	8
1	15	12	8	5
2	12	8	5	2
3	8	5	2	1
4	5	2	1	0

Tab. 29 : Average grain size in µm and element concentrations in µg g^{-1}, at the sub-basin outlet in the Canche river catchment for all five sampling campaigns.

Catchment	Canche	Ternoise	Planquette	Créquoise	Bras de Bronne	Course	Dordogne	Huîtrepin
Sample point	T1	T2	T3	T4	T5	T6	T7	T8
D50	59.8	52.9	54.9	62.1	72.3	67.6	55.7	57.1
As	3.1	4.0	4.2	2.8	4.0	3.9	4.5	4.6
Cd	0.2	0.2	0.4	0.2	0.3	0.3	0.3	0.3
Co	3.7	5.0	4.9	4.0	4.8	4.8	5.4	5.3
Cs	1.1	1.4	1.2	0.9	1.4	1.1	1.4	1.8
Cu	22.9	16.6	20.7	14.8	22.0	25.4	20.8	26.5
La	23.5	30.7	19.7	16.6	22.4	22.2	24.4	23.8
Li	7.6	10.2	9.0	7.3	10.2	8.5	10.4	12.0
Mo	0.2	0.2	0.2	0.2	0.3	0.2	0.2	0.3
Ni	10.0	12.3	11.4	9.4	11.9	11.8	12.4	13.5
Pb	14.0	15.5	14.0	11.2	12.9	13.5	12.3	14.6
Rb	12.0	18.1	16.7	12.3	18.8	13.8	18.6	21.2
Sb	0.3	0.3	0.3	0.2	0.3	0.2	0.3	0.3
Se	0.8	0.9	0.9	0.9	0.9	1.3	0.8	0.8
Sn	1.4	1.5	1.9	1.7	2.3	0.8	0.9	2.2
Th	5.7	7.4	4.6	3.3	5.1	4.4	5.9	5.6
Tl	0.1	0.1	0.1	0.1	0.1	0.1	0.1	0.1
U	0.8	1.0	0.6	0.5	0.7	0.7	0.8	0.7
Bi	0.1	0.2	0.2	0.1	0.1	0.1	0.2	0.2
Cr	17.2	22.0	19.3	14.7	22.1	19.0	22.2	24.6
Sc	1.8	2.7	2.2	1.8	2.8	2.3	2.9	3.1
V	15.9	22.8	20.9	15.0	24.0	19.5	25.3	27.2
Ba	32.3	41.3	42.2	30.0	42.3	46.7	43.5	42.9
Ce	41.1	55.0	33.1	29.4	34.6	36.8	39.7	38.8
Al	6589.7	9920.3	8964.7	6819.7	10118.4	7812.8	10170.3	11078.2
Ca	24622.1	23597.8	31998.4	29287.4	33794.2	42341.0	24393.7	22054.9
Fe	9347.6	11997.4	11073.0	8032.1	10480.7	10333.2	11501.8	11745.6
K	633.5	990.2	858.7	751.8	1075.0	844.8	1162.9	688.0
Mg	1366.9	1863.3	1638.4	1304.9	1712.3	1494.1	1736.3	1895.5
Mn	354.7	346.5	424.0	235.8	369.4	353.1	372.6	394.9
Na	167.1	254.8	234.5	140.2	255.2	132.1	193.5	226.4
P	1262.3	1347.6	1269.3	955.9	916.7	1869.3	1053.6	786.1
S	2057.9	2066.6	2173.0	2580.1	1850.6	4723.3	2056.2	1013.4
Si	473.9	474.1	552.4	342.3	452.5	574.6	400.8	384.0
Sr	47.5	57.4	64.2	54.1	72.7	64.9	42.7	65.4
Ti	480.7	613.7	474.8	280.0	549.9	385.6	611.6	603.2
Zn	77.8	93.3	75.1	61.7	83.3	82.1	63.1	75.8

Tab. 30 : Average grain size in µm and element concentration in µg g^{-1}, at the confluences in the Canche river catchment for all five sampling campaigns.

Sample point	C1	C2	C3	C4	C5	C6	C7
D50	61.9	63.0	68.3	59.2	59.3	78.4	85.8
As	3.7	5.2	4.0	3.7	5.1	4.4	4.8
Cd	0.2	0.3	0.2	0.2	0.3	0.3	0.3
Co	4.4	6.0	4.0	4.6	6.0	4.3	4.6
Cs	1.3	1.8	0.9	1.3	1.9	1.3	1.4
Cu	33.1	26.6	14.8	25.1	29.7	19.2	89.2
La	21.4	23.8	24.8	22.1	24.0	16.0	20.0
Li	9.2	13.0	6.9	9.4	13.5	8.7	9.8
Mo	0.2	0.3	0.2	0.2	0.3	0.2	0.2
Ni	12.2	15.7	9.2	11.7	15.7	10.5	11.6
Pb	15.6	18.9	13.5	15.8	19.1	13.8	15.8
Rb	16.6	23.4	11.8	17.0	24.6	16.7	18.3
Sb	0.3	0.4	0.3	0.3	0.4	0.3	0.3
Se	0.9	1.1	0.9	1.0	1.4	0.8	1.0
Sn	1.6	1.8	2.1	1.5	2.7	1.4	1.3
Th	5.2	5.1	6.1	5.6	5.6	3.4	4.9
Tl	0.1	0.1	0.1	0.1	0.2	0.1	0.1
U	0.7	0.7	0.8	0.7	0.7	0.5	0.7
Bi	0.2	0.4	0.1	0.2	0.3	0.1	0.2
Cr	19.9	27.8	17.0	20.8	28.5	19.2	21.7
Sc	2.4	3.1	1.9	2.5	3.5	2.2	2.4
V	19.5	28.0	16.1	20.3	29.0	19.4	21.5
Ba	44.9	60.7	35.4	40.5	51.5	40.5	43.0
Ce	39.5	43.3	44.9	36.4	35.3	27.5	35.8
Al	8669.5	12592.1	6365.3	9029.9	13408.1	7600.2	8771.8
Ca	29558.7	41767.1	47620.6	34589.2	31870.4	63461.3	62523.0
Fe	10620.5	14154.2	9020.9	10794.9	14435.8	10623.1	11591.4
K	820.6	1616.6	642.2	712.8	1632.9	787.6	1112.9
Mg	1678.2	2249.9	1393.6	1694.8	2266.6	2252.9	2553.5
Mn	373.0	544.5	423.0	414.3	493.2	434.9	415.3
Na	236.2	281.9	190.6	178.4	218.4	629.8	784.2
P	1330.2	1586.0	1572.2	1241.8	1576.2	1541.9	1601.4
S	2155.3	3462.2	3362.7	2372.1	2549.6	3768.8	3743.5
Si	522.7	616.4	466.2	407.0	473.3	417.4	430.2
Sr	61.3	82.0	72.3	64.0	72.2	177.8	195.1
Ti	484.9	537.3	483.3	532.9	604.6	329.3	365.2
Zn	100.5	112.7	75.9	86.1	105.1	71.6	74.8

Tab. 31 : Results from rock magnetic analyses for the high-resolution sampling campaign of SPM during flooding event (8-11 June 2016) at the automatic sampling station at Attin (downstream Canche).

Sample	Date-Hour	Turbidty	Mass (mg)	Field (T)	Hc (mT)	Mr (nAm²)	Ms (nAm²)	Hcr (mT)	Mrs (nAm²)	Mr/mass	Ms/mass	Mrs/mass	Mr/Ms	Mrs/Ms	Hcr/Hc	S-ratio
1	6/8/16 19:30	650	0.3	0.3	9.976	2.68	13.66	29.86	2.552	8.93	45.53	8.51	0.20	0.19	2.99	0.91
				1	10.6	2.995	16.85	30.52	2.802	9.98	56.17	9.34	0.18	0.17	2.88	
2	6/8/16 22:30	357	0.1	0.3	7.925	2.655	17.34	26.01	2.576	26.55	173.40	25.76	0.15	0.15	3.28	0.94
				1	8.438	2.898	21.9	27.1	2.732	28.98	219.00	27.32	0.13	0.12	3.21	
3	6/9/16 1:30	441	0.4	0.3	9.272	1.81	2.972	26.71	1.661	4.53	7.43	4.15	0.61	0.56	2.88	0.93
				1	9.963	1.926	4.002	32.29	1.789	4.82	10.01	4.47	0.48	0.45	3.24	
4	6/9/16 4:30	463	0.2	0.3	9.583	1.86	9.34	27.2	1.718	9.30	46.70	8.59	0.20	0.18	2.84	0.93
				1	10.3	1.946	11.58	31.5	1.846	9.73	57.90	9.23	0.17	0.16	3.06	
5	6/9/16 7:30	317	0.4	0.3	9.364	2.228	10.59	27.41	2.084	5.57	26.48	5.21	0.21	0.20	2.93	0.91
				1	10.46	2.217	13.47	32.05	2.294	5.54	33.68	5.74	0.16	0.17	3.06	
6	6/9/16 10:30	356	0.2	0.3	9.308	1.686	11.25	27.69	1.611	8.43	56.25	8.06	0.15	0.14	2.97	0.92
				1	9.497	1.827	14.92	34.92	1.753	9.14	74.60	8.77	0.12	0.12	3.68	
7	6/9/16 13:30	202	0.6	0.3	9.506	2.697	16.32	29.68	2.511	4.50	27.20	4.19	0.17	0.15	3.12	0.92
				1	9.787	2.831	22.14	32.39	2.74	4.72	36.90	4.57	0.13	0.12	3.31	
8	6/9/16 16:30	156	0.2	0.3	7.905	1.299	8.795	18.26	1.198	6.50	43.98	5.99	0.15	0.14	2.31	0.93
				1	8.498	1.317	11.56	33.43	1.293	6.59	57.80	6.47	0.11	0.11	3.93	
9	6/9/16 19:30	95	0.3	0.3	7.714	1.181	6.98	25.9	1.028	3.94	23.27	3.43	0.17	0.15	3.36	1.10
				1	13.11	1.06	10.68	22.78	0.936	3.53	35.60	3.12	0.10	0.09	1.74	
10	6/9/16 22:30	64	1.8	0.3	9.739	1.044	6	28.98	0.861	0.58	3.33	0.48	0.17	0.14	2.98	0.99
				1	12.99	8.48	41.5	41.95	0.866	4.71	23.06	0.48	0.20	0.02	3.23	
11	6/10/16 1:30	52	0.9	0.3	10.31	3.187	23.06	31.57	3.139	3.54	25.62	3.49	0.14	0.14	3.06	0.97
				1	9.972	3.387	32.3	32.84	3.239	3.76	35.89	3.60	0.10	0.10	3.29	
12	6/10/16 4:30	45	1	0.3	9.593	2.369	18.5	29.23	2.16	2.37	18.50	2.16	0.13	0.12	3.05	0.95
				1	10.11	2.525	19.45	30.93	2.264	2.53	19.45	2.26	0.13	0.12	3.06	
13	6/10/16 7:30	43	0.3	0.3	6.926	1.1	9.137	29	0.751	3.67	30.46	2.50	0.12	0.08	4.19	0.91
				1	16.07	0.968	11.16	36.21	0.827	3.23	37.20	2.76	0.09	0.07	2.25	
14	6/10/16 10:30	38	0.3	0.3	9.524	0.947	7.657	29.76	0.927	3.16	25.52	3.09	0.12	0.12	3.12	1
				1	8.493	0.915	8.495	28.87	0.923	3.05	28.32	3.08	0.11	0.11	3.40	
15	6/10/16 13:30	34	0.1	0.3	8.597	1.323	10.9	34.45	1.219	13.23	109.00	12.19	0.12	0.11	4.01	1.04
				1	8.39	1.113	15.97	36.7	1.171	11.13	159.70	11.71	0.07	0.07	4.37	
16	6/10/16 16:30	33	0.7	0.3	8.054	3.019	26.5	18.9	6.598	4.31	37.86	9.43	0.11	0.25	2.35	2.49
				1	1.143	1.556	18.15	47.41	2.648	2.22	25.93	3.78	0.09	0.15	41.48	
17	6/10/16 19:30	31	0.5	0.3	7.88	0.79	7.833	37.29	0.799	1.58	15.67	1.60	0.10	0.10	4.73	0.99
				1	8.844	0.862	11.4	33.73	0.807	1.72	22.80	1.61	0.08	0.07	3.81	
18	6/10/16 22:30	30	0.4	0.3	7.75	1.902	18.52	31.48	1.754	4.76	46.30	4.39	0.10	0.09	4.06	0.98
				1	7.699	1.932	28.16	31.75	1.783	4.83	70.40	4.46	0.07	0.06	4.12	
19	6/11/16 1:30	31	0.7	0.3	6.478	2.012	19.82	25.3	1.939	2.87	28.31	2.77	0.10	0.10	3.91	1.01
				1	6.286	2.079	27.2	26.26	1.912	2.97	38.86	2.73	0.08	0.07	4.18	
20	6/11/16 4:30	31	0.5	0.3	6.391	0.736	7.67	31.59	0.712	1.47	15.34	1.42	0.10	0.09	4.94	1

				1	6.651	0.741	11.05	31.75	0.71	1.48	22.10	1.42	0.07	0.06	4.77	
21	6/11/16 7:30	30	0.2	0.3	6.199	1.379	15.37	14.72	1.291	6.90	76.85	6.46	0.09	0.08	2.37	1.09
				1	6.777	1.338	16.31	27.01	1.187	6.69	81.55	5.94	0.08	0.07	3.99	
22	6/11/16 11:30	30	0.4	0.3	8.683	3.181	32.71	32.01	3.233	7.95	81.78	8.08	0.10	0.10	3.69	1.01
				1	8.304	3.588	47.7	32.63	3.21	8.97	119.25	8.03	0.08	0.07	3.93	
23	6/11/16 13:30	29	0.3	0.3	7.501	1.954	23.28	29.88	1.931	6.51	77.60	6.44	0.08	0.08	3.98	0.99
				1	6.496	2.063	33.8	31.84	1.944	6.88	112.67	6.48	0.06	0.06	4.90	
24	6/11/16 16:30	28	0.3	0.3	9.88	0.638	4.013	11.06	0.395	2.13	13.38	1.32	0.16	0.10	1.12	1.11
				1	3.821	0.129	9.431	33.61	0.357	0.43	31.44	1.19	0.01	0.04	8.80	

Tab. 32 : Results from rock magnetic analyses for the sediment trap sampling campaign of winter 2015 on the Canche watershed.

Sample	Mass (mg)	Field (T)	Hc (mT)	Mr (nAm²)	Ms (nAm²)	Hcr (mT)	Mrs (nAm²)	Mr/mass	Ms/mass	Mr/Ms	Mrs/Ms	Hcr/Hc	S-ratio
T1	20.73	0.3	9.83	33.73	230.57	32.53	35.56	1.61	11.04	0.15	0.16	3.34	0.92
		1	10.29	36.94	302.13	30.57	34.98	1.76	14.45	0.13	0.12	3.00	
T2	20.53	0.3	9.60	34.05	266.30	42.04	36.95	1.64	12.67	0.13	0.14	4.39	0.91
		1	10.17	37.52	344.27	38.62	36.14	1.80	16.28	0.11	0.11	3.80	
T3	16.97	0.3	10.49	16.85	96.85	37.01	16.73	1.02	5.79	0.17	0.17	3.54	0.92
		1	11.46	18.29	123.70	37.59	17.26	1.10	7.39	0.15	0.14	3.28	
T4	11.80	0.3	10.77	12.05	72.25	36.91	12.37	1.03	6.11	0.17	0.17	3.42	0.92
		1	11.38	13.00	94.93	38.06	12.64	1.12	8.09	0.14	0.13	3.37	
T5	23.00	0.3	8.84	42.47	317.13	34.36	42.61	1.79	13.25	0.14	0.14	3.88	0.92
		1	9.37	46.07	411.73	33.96	43.67	1.94	17.14	0.12	0.11	3.63	
T6	15.67	0.3	10.55	19.02	117.00	31.10	18.46	1.21	7.40	0.17	0.16	2.96	0.93
		1	11.02	20.74	146.23	35.19	19.33	1.31	9.24	0.14	0.13	3.20	
T7	27.80	0.3	10.51	32.87	232.50	35.61	31.45	1.22	8.53	0.14	0.14	3.43	0.91
		1	10.92	36.09	303.80	41.66	34.23	1.33	11.11	0.12	0.11	3.86	
T8	28.13	0.3	11.18	38.36	202.89	30.89	38.07	1.32	6.92	0.19	0.19	2.79	0.91
		1	11.44	42.44	275.80	31.50	39.80	1.46	9.41	0.15	0.14	2.83	
C1	17.83	0.3	7.99	22.98	165.35	25.27	22.82	1.29	9.21	0.14	0.14	3.20	0.95
		1	8.33	24.05	206.35	24.56	22.85	1.35	11.48	0.12	0.12	3.00	
C2	9.47	0.3	9.69	17.39	105.82	29.61	17.77	1.90	11.48	0.17	0.17	3.06	0.98
		1	10.06	17.75	127.65	28.77	16.74	1.95	13.89	0.14	0.13	2.86	
C3	24.00	0.3	8.93	46.51	366.23	34.43	47.05	1.95	15.29	0.13	0.13	3.85	0.94
		1	9.32	49.88	481.73	35.11	48.20	2.08	19.94	0.10	0.10	3.77	
C4	14.10	0.3	10.41	21.19	153.76	31.99	21.49	1.48	10.11	0.16	0.16	3.16	0.93
		1	11.03	22.80	194.27	33.94	22.00	1.60	12.83	0.13	0.13	3.12	
C5	25.34	0.3	10.28	34.00	236.14	33.48	34.56	1.37	9.17	0.15	0.15	3.26	0.94
		1	10.66	38.37	325.50	36.13	38.82	1.53	12.37	0.13	0.12	3.38	
C6	16.30	0.3	11.05	17.61	98.57	32.38	18.31	1.08	6.05	0.18	0.19	2.93	0.91

		1	11.65	19.31	124.75	36.54	18.19	1.18	7.65	0.15	0.15	3.14	
C7	7.87	0.3	10.85	11.30	71.51	35.84	10.87	1.44	8.93	0.17	0.16	3.31	0.93
		1	11.30	12.09	106.83	38.62	11.41	1.54	13.12	0.14	0.13	3.44	

Tab. 33 : Results from rock magnetic analyses for the sediment trap sampling campaign of winter 2016 on the Canche watershed.

Sample	Mass (mg)	Field (T)	Hc (mT)	Mr (nAm²)	Ms (nAm²)	Hcr (mT)	Mrs (nAm²)	Mr/mass	Ms/mass	Mr/Ms	Mrs/Ms	Hcr/Hc	S-ratio
T1	4.27	0.3	7.82	7.23	63.33	28.59	7.07	1.71	17.13	0.14	0.13	4.30	0.91
		1	8.31	7.84	85.06	31.68	7.55	1.87	23.22	0.11	0.11	4.43	
T2	5.07	0.3	8.74	9.65	65.36	25.49	9.27	1.95	13.46	0.16	0.15	2.91	0.93
		1	9.50	10.33	84.27	28.58	9.86	2.09	17.36	0.13	0.13	3.01	
T3	3.73	0.3	11.29	4.70	27.06	32.53	4.63	1.26	7.05	0.18	0.18	2.90	0.91
		1	12.16	5.20	34.26	39.39	5.15	1.39	8.96	0.16	0.15	3.26	
T4	4.30	0.3	11.34	7.38	39.16	34.92	6.57	1.71	9.02	0.19	0.17	3.09	0.98
		1	11.43	7.13	56.83	38.19	6.82	1.66	13.00	0.13	0.13	3.34	
T5	3.43	0.3	10.37	11.81	65.85	30.68	11.22	4.15	22.12	0.18	0.17	2.92	0.96
		1	10.91	12.27	87.64	34.79	11.77	4.39	30.42	0.14	0.13	3.10	
T6	3.43	0.3	10.51	7.48	38.19	28.68	7.11	2.21	11.28	0.20	0.19	2.72	0.95
		1	10.75	7.96	49.35	31.52	7.33	2.35	14.44	0.16	0.15	2.90	
T7	6.70	0.3	10.29	5.94	39.72	30.36	5.35	0.89	5.90	0.15	0.14	2.95	0.93
		1	10.85	6.37	51.28	34.61	6.23	0.95	7.62	0.13	0.12	3.20	
T8	3.30	0.3	8.01	4.39	34.42	27.55	4.19	1.36	10.82	0.13	0.12	3.45	0.89
		1	8.31	4.94	41.66	30.75	4.48	1.54	13.06	0.12	0.11	3.70	
C1	6.53	0.3	8.86	17.41	98.61	21.63	16.73	2.60	14.55	0.18	0.18	2.42	0.96
		1	9.29	17.98	125.83	23.74	17.61	2.68	18.59	0.15	0.15	2.53	
C2	7.67	0.3	10.29	17.11	75.79	26.31	16.54	2.09	9.43	0.22	0.22	2.57	0.93
		1	11.00	18.52	105.56	30.81	17.84	2.25	12.57	0.18	0.18	2.81	
C3	4.60	0.3	10.81	12.38	53.20	30.30	11.93	2.50	10.98	0.22	0.21	3.00	0.93
		1	11.80	13.01	70.51	33.89	12.71	2.64	14.54	0.18	0.17	3.02	
C4	8.90	0.3	12.09	18.40	94.91	34.13	17.75	2.11	10.88	0.19	0.19	2.87	0.93
		1	12.64	19.71	119.43	37.27	18.85	2.26	13.65	0.16	0.16	2.99	
C5	4.90	0.3	11.66	8.88	48.81	31.28	8.57	1.79	9.62	0.19	0.18	2.69	0.92
		1	12.40	9.62	65.07	34.96	9.16	1.94	12.88	0.15	0.14	2.83	
C6	4.90	0.3	10.72	8.16	39.62	27.57	7.84	1.70	8.46	0.20	0.20	2.57	0.92
		1	11.51	8.85	50.77	30.68	8.37	1.85	10.89	0.17	0.16	2.66	
C7	4.30	0.3	8.37	9.75	62.18	26.37	9.04	2.09	13.60	0.15	0.14	3.30	0.94
		1	8.79	10.26	82.46	28.98	9.69	2.18	18.02	0.12	0.12	3.39	

Tab. 34 : Results from rock magnetic analyses for the sediment trap sampling campaign of spring 2016 on the Canche watershed.

Sample	Mass (mg)	Field (T)	Hc (mT)	Mr (nAm²)	Ms (nAm²)	Hcr (mT)	Mrs (nAm²)	Mr/mass	Ms/mass	Mr/Ms	Mrs/Ms	Hcr/Hc	S-ratio

T1	4.10	0.3	11.13	8.39	45.00	31.02	8.06	2.11	11.41	0.19	0.18	2.78	0.94
		1	12.05	8.95	56.15	36.58	8.55	2.26	14.23	0.16	0.15	3.02	
T2	3.95	0.3	9.80	6.12	33.98	27.71	5.94	1.57	8.88	0.18	0.17	2.83	0.93
		1	10.41	6.34	40.86	31.62	6.32	1.63	10.68	0.15	0.15	3.04	
T3	2.47	0.3	9.59	3.83	24.84	32.35	3.59	1.68	11.06	0.15	0.14	3.41	0.90
		1	10.13	3.88	31.50	36.53	3.96	1.71	13.92	0.13	0.13	3.62	
T4	5.60	0.3	11.60	5.84	36.63	34.53	5.63	1.02	6.25	0.16	0.16	2.99	0.90
		1	12.37	6.48	48.45	38.75	6.20	1.14	8.30	0.14	0.13	3.13	
T5	4.63	0.3	8.05	16.13	96.37	20.58	15.51	3.78	22.69	0.17	0.16	2.61	0.96
		1	8.28	16.97	125.57	22.03	16.09	3.99	29.62	0.14	0.13	2.70	
T6	4.38	0.3	10.65	7.88	43.70	30.28	7.54	1.81	10.17	0.18	0.18	2.86	0.95
		1	11.10	8.38	56.18	33.89	8.01	1.92	13.05	0.15	0.14	3.08	
T7	5.95	0.3	10.81	10.50	65.48	33.69	10.09	1.76	10.91	0.16	0.16	3.11	0.92
		1	11.24	11.31	84.88	39.55	11.02	1.89	14.16	0.13	0.13	3.52	
T8		0.3											
		1											
C1	3.77	0.3	10.34	6.48	42.46	29.99	6.50	1.73	11.43	0.15	0.15	2.89	0.93
		1	10.40	7.29	57.87	31.39	6.97	1.95	15.62	0.13	0.12	3.04	
C2	2.93	0.3	11.35	7.51	42.25	30.49	7.33	2.61	14.79	0.17	0.17	2.79	0.95
		1	11.62	7.96	59.71	33.35	7.72	2.75	20.82	0.13	0.13	2.93	
C3	4.00	0.3	10.09	6.36	33.36	27.63	6.07	1.58	8.48	0.19	0.18	2.82	0.91
		1	11.19	6.92	44.24	34.26	6.71	1.72	11.18	0.16	0.15	3.12	
C4	2.80	0.3	9.99	5.47	35.09	30.33	5.13	1.96	12.80	0.16	0.15	3.05	0.88
		1	10.79	5.96	41.65	34.96	5.83	2.12	15.12	0.14	0.14	3.26	
C5	3.75	0.3	9.84	5.67	38.32	30.85	5.42	1.51	10.22	0.15	0.14	3.13	0.89
		1	10.53	6.21	49.02	34.53	6.11	1.66	13.06	0.13	0.13	3.28	
C6	3.82	0.3	10.03	10.66	69.69	27.06	9.85	2.70	17.29	0.18	0.17	2.74	0.96
		1	10.57	11.46	86.65	31.15	10.21	2.90	21.52	0.15	0.14	2.96	
C7	5.47	0.3	10.33	8.38	47.04	30.64	7.84	1.54	8.60	0.18	0.17	2.98	0.94
		1	10.68	8.65	58.69	33.93	8.37	1.59	10.68	0.15	0.14	3.19	

Tab. 35 : Results from rock magnetic analyses for the sediment trap sampling campaign of summer 2016 on the Canche watershed.

Sample	Mass (mg)	Field (T)	Hc (mT)	Mr (nAm²)	Ms (nAm²)	Hcr (mT)	Mrs (nAm²)	Mr/mass	Ms/mass	Mr/Ms	Mrs/Ms	Hcr/Hc	S-ratio
T1	2.20	0.3	11.14	2.89	18.54	31.38	2.91	1.31	8.43	0.19	0.18	3.00	1
		1	10.96	2.87	19.94	32.52	2.83	1.30	9.07	0.17	0.17	3.02	
T2	4.50	0.3	9.84	6.71	37.66	28.79	6.32	1.49	8.37	0.18	0.17	2.94	0.97
		1	10.53	6.89	44.16	33.56	6.48	1.53	9.81	0.16	0.15	3.20	
T3	3.60	0.3	9.41	5.03	35.13	29.15	4.76	1.40	9.76	0.14	0.14	3.10	0.99
		1	9.81	5.07	41.58	34.72	4.95	1.41	11.55	0.12	0.12	3.54	
T4	3.70	0.3	10.26	5.03	31.07	31.45	4.82	1.36	8.40	0.16	0.15	3.06	1.00
		1	10.86	5.05	37.61	34.15	4.94	1.36	10.16	0.13	0.13	3.14	
T5	4.70	0.3	9.43	8.22	55.16	29.98	7.92	1.75	11.74	0.15	0.14	3.19	0.97

		1	9.81	8.53	66.89	32.98	8.21	1.81	14.23	0.13	0.12	3.36	
T6	3.30	0.3	8.27	4.60	38.93	28.02	4.47	1.40	11.80	0.12	0.12	3.41	0.97
		1	8.66	4.75	45.00	30.70	4.49	1.44	13.64	0.11	0.10	3.57	
T7	4.00	0.3	10.16	5.84	39.52	31.72	5.65	1.46	9.88	0.15	0.14	3.12	0.93
		1	10.82	6.26	48.83	36.90	6.02	1.57	12.21	0.13	0.12	3.41	
T8	3.50	0.3	10.87	5.54	33.27	31.90	5.34	1.58	9.51	0.17	0.16	2.94	0.96
		1	11.40	5.82	41.05	38.83	5.54	1.66	11.73	0.14	0.13	3.41	
C1	2.40	0.3	9.55	5.06	33.75	28.77	4.90	2.11	14.06	0.15	0.15	3.03	0.95
		1	9.89	5.33	42.97	33.15	4.98	2.22	17.90	0.13	0.12	3.35	
C2	3.90	0.3	10.47	5.32	31.30	30.66	5.33	1.36	8.02	0.17	0.17	2.94	0.94
		1	11.02	5.68	38.06	34.77	5.49	1.46	9.76	0.15	0.15	3.16	
C3	3.60	0.3	7.91	5.24	38.58	25.96	5.07	1.46	10.72	0.13	0.13	3.29	1
		1	8.54	5.19	42.92	33.32	5.03	1.44	11.92	0.12	0.12	3.90	
C4	2.90	0.3	11.97	7.13	39.93	37.04	6.76	2.46	13.77	0.18	0.17	3.12	1
		1	12.12	6.97	48.05	40.83	6.73	2.40	16.57	0.14	0.14	3.41	
C5	4.10	0.3	10.07	7.42	44.94	29.15	7.60	1.81	10.96	0.16	0.17	2.90	0.96
		1	10.45	7.76	53.60	31.66	7.70	1.89	13.07	0.14	0.14	3.04	
C6	4.20	0.3	11.20	4.67	23.48	32.71	4.55	1.11	5.59	0.20	0.19	2.92	0.98
		1	12.59	4.77	28.17	39.40	4.68	1.14	6.71	0.17	0.17	3.12	
C7	3.90	0.3	10.62	5.05	29.79	30.72	4.76	1.29	7.64	0.18	0.17	2.92	1
		1	10.87	4.82	35.64	34.02	4.71	1.24	9.14	0.15	0.14	3.13	

Tab. 36 : Results from rock magnetic analyses for the sediment trap sampling campaign of autumn 2016 on the Canche watershed.

Sample	Mass (mg)	Field (T)	Hc (mT)	Mr (nAm²)	Ms (nAm²)	Hcr (mT)	Mrs (nAm²)	Mr/mass	Ms/mass	Mr/Ms	Mrs/Ms	Hcr/Hc	S-ratio
T1	3.45	0.3	9.98	5.36	33.73	26.70	5.39	1.56	9.87	0.16	0.16	2.67	0.94
		1	10.43	5.75	42.43	31.06	5.80	1.67	12.39	0.14	0.14	2.99	
T2	3.70	0.3	10.20	7.92	43.03	27.81	7.76	2.37	13.22	0.18	0.18	2.73	0.91
		1	10.93	8.82	54.39	29.53	8.38	2.60	16.80	0.16	0.15	2.70	
T3	3.15	0.3	11.01	5.35	27.63	30.39	4.72	1.70	8.83	0.19	0.17	2.77	0.95
		1	10.46	5.35	35.43	38.04	5.25	1.70	11.31	0.15	0.15	3.63	
T4		0.3											
		1											
T5	2.10	0.3	9.19	2.91	21.01	30.37	2.66	1.41	10.08	0.14	0.12	3.32	0.93
		1	9.36	3.11	27.38	34.58	2.95	1.51	13.15	0.11	0.10	3.71	
T6	2.60	0.3	9.41	3.02	18.54	30.63	2.85	1.32	7.70	0.16	0.15	3.30	0.93
		1	10.05	3.27	24.02	28.34	3.09	1.44	10.03	0.13	0.13	2.86	
T7	4.15	0.3	10.57	6.35	35.51	38.64	6.00	1.54	8.75	0.18	0.17	3.68	0.93
		1	11.42	6.87	46.09	45.79	6.56	1.67	11.34	0.15	0.15	4.06	
T8	4.30	0.3	11.65	6.20	35.67	34.18	6.22	1.44	8.31	0.17	0.17	2.93	0.89
		1	12.30	6.97	46.50	38.73	6.64	1.62	10.84	0.15	0.14	3.15	
C1	2.30	0.3	7.62	3.98	27.63	23.40	3.79	2.10	12.90	0.16	0.15	3.25	0.95
		1	8.40	4.18	34.98	24.54	4.03	2.22	16.64	0.13	0.13	3.15	

C2	3.60	0.3	11.92	11.41	57.00	31.88	11.77	3.33	16.33	0.20	0.21	2.69	0.89
		1	12.12	13.91	112.32	33.97	13.34	3.93	29.62	0.14	0.14	2.82	
C3	3.45	0.3	8.37	8.07	56.11	27.49	7.73	2.41	16.17	0.15	0.14	3.29	0.92
		1	8.89	8.75	70.65	28.82	8.32	2.62	20.28	0.13	0.12	3.25	
C4	3.80	0.3	10.62	5.96	33.97	31.43	5.66	1.59	9.14	0.17	0.17	2.96	0.93
		1	11.00	6.42	55.44	33.64	6.31	1.71	14.42	0.12	0.12	3.06	
C5	3.20	0.3	9.06	4.35	27.65	29.57	4.26	1.30	8.35	0.15	0.14	3.32	0.93
		1	9.19	4.56	33.34	32.43	4.58	1.35	10.07	0.12	0.13	3.64	
C6	4.30	0.3	10.29	8.91	77.09	25.66	9.08	2.56	23.89	0.16	0.16	2.62	0.91
		1	9.93	9.82	100.58	27.59	9.62	2.83	30.08	0.11	0.11	2.84	
C7	5.20	0.3	12.50	7.24	38.80	38.41	6.85	1.39	7.46	0.19	0.18	3.07	0.76
		1	12.47	7.52	51.27	39.63	7.31	1.45	9.86	0.15	0.14	3.18	

Tab. 37 : Results from VSM analyses in the Planquette catchment.

Sample	Type	Mass (mg)	Field (T)	Hc (mT)	Mr (nAm²)	Ms (nAm²)	Hcr (mT)	Mrs (nAm²)	Mr/mass	Ms/mass	Mrs/mass	Mr/Ms	Mrs/Ms	Hcr/Hc
M1	Mudflow	366.8	1	10.67	298.14	2778.30	65.16	326.46	0.81	7.57	0.11	0.12	6.11	0.89
			1.5	10.27	302.90	2952.50	66.71	393.59	0.83	8.05	0.10	0.13	6.50	1.07
			1.8	10.77	305.60	3359.80	66.40	416.27	0.83	9.16	0.09	0.12	6.17	1.13
M2	Mudflow	331.9	1	8.71	344.41	3007.50	62.43	410.07	1.04	9.06	0.11	0.14	7.17	1.24
			1.5	8.59	330.39	3182.70	62.72	419.16	1.00	9.59	0.10	0.13	7.30	1.26
			1.8	9.66	326.22	3653.80	64.38	452.60	0.98	11.01	0.09	0.12	6.66	1.36
Cb1a	Channel bank	312.3	1	7.79	440.74	4557.90	55.29	680.57	1.41	14.59	0.10	0.15	7.10	2.18
			1.5	7.77	465.98	4563.10	60.00	609.50	1.49	14.61	0.10	0.13	7.72	1.95
			1.8	7.75	433.09	5085.90	56.86	560.99	1.39	16.29	0.09	0.11	7.34	1.80
Cb1b	Channel bank	322.3	1	7.60	439.56	3820.70	59.02	539.95	1.36	11.85	0.12	0.14	7.77	1.68
			1.5	7.68	456.97	3925.10	60.07	465.08	1.42	12.18	0.12	0.12	7.82	1.44
			1.8	8.78	445.60	4362.50	60.28	544.80	1.38	13.54	0.10	0.12	6.87	1.69
Cb2a	Channel bank	340	1	8.95	510.23	3816.70	61.18	462.37	1.50	11.23	0.13	0.12	6.84	1.36
			1.5	10.09	520.46	3979.50	61.97	528.93	1.53	11.70	0.13	0.13	6.14	1.56
			1.8	9.93	524.49	4475.80	62.53	459.07	1.54	13.16	0.12	0.10	6.30	1.35
Cb2b	Channel bank	338.8	1	9.90	465.45	3497.00	59.41	592.27	1.37	10.32	0.13	0.17	6.00	1.75
			1.5	10.19	481.90	3706.90	60.27	561.14	1.42	10.94	0.13	0.15	5.91	1.66
			1.8	9.87	485.10	4094.40	60.23	549.10	1.43	12.09	0.12	0.13	6.10	1.62
Cb3a	Channel bank	324.8	1	10.60	509.90	3492.30	61.70	523.81	1.57	10.75	0.15	0.15	5.82	1.61
			1.5	10.46	519.07	3628.00	62.64	503.68	1.60	11.17	0.14	0.14	5.99	1.55
			1.8	11.13	524.16	4107.20	63.15	537.42	1.61	12.65	0.13	0.13	5.67	1.65
Cb3b	Channel bank	333.2	1	8.41	471.13	3437.80	60.37	443.90	1.41	10.32	0.14	0.13	7.18	1.33
			1.5	9.62	469.02	3639.90	60.60	533.64	1.41	10.92	0.13	0.15	6.30	1.60
			1.8	9.76	460.37	4117.10	59.68	574.35	1.38	12.36	0.11	0.14	6.11	1.72
Rb1	River bed	236.8	1	17.80	713.90	2933.90	55.20	717.50	3.01	12.39	0.24	0.24	3.10	3.03
			1.5	18.11	606.88	3061.80	48.76	705.73	2.56	12.93	0.20	0.23	2.69	2.98
			1.8	17.02	692.97	3300.40	55.57	696.50	2.93	13.94	0.21	0.21	3.26	2.94

Rb2	River bed	297.5	1	8.93	373.78	3278.90	59.36	438.90	1.26	11.02	0.11	0.13	6.65	1.48
			1.5	8.81	362.10	3432.10	57.78	459.32	1.22	11.54	0.11	0.13	6.56	1.54
			1.8	8.52	383.50	3937.10	57.58	423.11	1.29	13.23	0.10	0.11	6.76	1.42
Rb3	River bed	290.6	1	8.88	584.90	4241.90	59.04	580.10	2.01	14.60	0.14	0.14	6.65	2.00
			1.5	9.01	602.86	4517.40	59.19	527.61	2.07	15.55	0.13	0.12	6.57	1.82
			1.8	9.47	604.33	5145.10	59.09	592.67	2.08	17.71	0.12	0.12	6.24	2.04
C2	Suspended matter	314.7	1	8.86	469.42	3361.70	58.44	494.95	1.49	10.68	0.14	0.15	6.60	1.57
			1.5	8.89	471.63	3609.40	60.73	443.23	1.50	11.47	0.13	0.12	6.83	1.41
			1.8	8.76	473.20	4033.50	58.90	439.41	1.50	12.82	0.12	0.11	6.72	1.40
T3a	Suspended matter	273.4	1	10.07	343.78	2320.20	61.51	340.74	1.26	8.49	0.15	0.15	6.11	1.25
			1.5	12.38	349.41	2437.00	62.78	341.46	1.28	8.91	0.14	0.14	5.07	1.25
			1.8	11.63	351.80	2846.50	63.30	405.03	1.29	10.41	0.12	0.14	5.44	1.48
T3b	Suspended matter	292.2	1	9.92	303.08	2604.20	59.81	429.10	1.04	8.91	0.12	0.16	6.03	1.47
			1.5	9.76	310.15	2753.00	60.04	377.46	1.06	9.42	0.11	0.14	6.15	1.29
			1.8	10.22	309.05	3068.30	59.90	372.50	1.06	10.50	0.10	0.12	5.86	1.27
T3c	Suspended matter	320.2	1	8.68	386.03	2840.70	61.90	376.54	1.21	8.87	0.14	0.13	7.13	1.18
			1.5	9.13	397.20	3107.50	62.84	302.04	1.24	9.70	0.13	0.10	6.88	0.94
			1.8	12.06	404.70	3541.20	63.45	396.01	1.26	11.06	0.11	0.11	5.26	1.24
T3d	Suspended matter	334.8	1	10.44	407.06	3017.10	61.54	415.12	1.22	9.01	0.13	0.14	5.89	1.24
			1.5	11.65	415.12	3152.30	62.80	363.88	1.24	9.42	0.13	0.12	5.39	1.09
			1.8	10.18	417.80	3603.50	63.15	412.85	1.25	10.76	0.12	0.11	6.20	1.23
T3'a	Suspended matter	297.3	1	8.56	490.49	3756.60	57.63	524.78	1.65	12.64	0.13	0.14	6.73	1.77
			1.5	10.07	490.22	4062.90	58.09	569.78	1.65	13.67	0.12	0.14	5.77	1.92
			1.8	9.47	511.27	4462.30	58.22	568.15	1.72	15.01	0.11	0.13	6.15	1.91
T3'b	Suspended matter	288.2	1	9.54	443.88	3405.40	59.65	427.07	1.54	11.82	0.13	0.13	6.25	1.48
			1.5	9.01	453.90	3547.40	58.66	472.10	1.57	12.31	0.13	0.13	6.51	1.64
			1.8	9.84	442.30	3975.30	59.37	488.49	1.53	13.79	0.11	0.12	6.03	1.69
T3'c	Suspended matter	303.8	1	8.10	602.94	4685.20	57.92	699.86	1.98	15.42	0.13	0.15	7.15	2.30
			1.5	9.96	633.74	4850.00	56.26	704.23	2.09	15.96	0.13	0.15	5.65	2.32
			1.8	9.45	633.57	5343.20	56.46	684.47	2.09	17.59	0.12	0.13	5.97	2.25
T3'd	Suspended matter	315.7	1	10.12	574.41	3972.30	59.02	551.30	1.82	12.58	0.14	0.14	5.83	1.75
			1.5	10.58	594.57	4163.10	59.57	568.46	1.88	13.19	0.14	0.14	5.63	1.80
			1.8	10.39	606.54	4634.60	60.53	595.68	1.92	14.68	0.13	0.13	5.83	1.89

Tab. 38 : Results of deconvolution of IRM components.

			Comp1	Comp2	Comp3	Comp4
Sample	Nature	Season	%	%	%	%
C1	Suspended matter	Winter 2015	45	26.75	25.75	2.5
		Winter 2016	40	27	29	4
		Spring 2016	33	24	38	5
		Summer 2016	17	41.5	41.5	

		Autumn 2016	26	37	37	
T3	Suspended matter	Winter 2015	22	33	35	10
		Winter 2016	23	37	37	3
		Spring 2016	17	44	39	
		Summer 2016	24	38	38	
		Autumn 2016	15	42.5	42.5	
T3	Suspended matter	Winter 2015	33	32	35	
		Winter 2016	36	32	32	
		Spring 2016	33	28	27	12
		Summer 2016	22	42	36	
		Autumn 2016	22	39	39	
Rb1	Riverbed	Winter 2017	19	33	40	8
Rb2	Riverbed	Winter 2017	24	29	29	18
Rb3	Riverbed	Winter 2017	20	24	24	32
Cb1	Channel bank	Winter 2017	28.5	31	33	7.5
Cb2	Channel bank	Winter 2017	23	32	32	13
Cb3	Channel bank	Winter 2017	29	28	33	10
M1	Mudflow	Winter 2017	17	45	38	
M2	Mudflow	Winter 2017	19	38	38	5
T3	Suspended matter	Winter 2017	22	39	39	
T3’	Suspended matter	Winter 2017	22	35	35	8
C2	Suspended matter	Winter 2017	26	37	37	

Annexe C: Communications internationales

AGU 2017

Assessing the seasonal variability of ephemeral gully erosion using high-frequency monitoring: case study in a fully cultivated catchment (The Pommeroye, Northern France)

Edouard Patault[a],[b],*, Claire Alary[a], Christine Franke[b], Arnaud Gauthier[a], Nor-Edine Abriak[a]

[a]IMT Lille Douai, Univ. Lille, EA 4515 – LGCgE – Civil Engineering and Environmental department, F-59000 Lille, France
[b]MINES ParisTech, PSL Research University, Centre de Géosciences, 35 rue Saint-Honoré, 77305 Fontainebleau Cedex, France

Gully erosion results in on-site and off-site problems including the loss of cultivated soils, the silting of riverbeds and dams as well as infrastructure and property damage by muddy floods. Regions of intensive agricultural production situated on the European loess belt are particularly affected. Recently a growing interest has focused on ephemeral gullies since there have been recognized as a major contributor to the sediment yield in small agricultural catchment in this area. The aims of this case study are (i) to quantify the sediment yield transported by ephemeral gullies, (ii) to identify parameters that control the function of the hydro-sedimentary response and (iii) to evaluate the influence of seasonal variability on the ephemeral gully erosion. For this study a high-frequency monitoring station was implemented. For each flood event, 8 variables related to hydro-sedimentary and rainfall dynamics are calculated and the relationships between these variables are analyzed using the Pearson correlation matrix and Principal Component Analysis. During the first year of monitoring (03/2016-03/2017), 22 flood events were recorded of which 75% occurred in spring and winter. The specific sediment yield was evaluated to 30 t km^{-2} yr^{-1} which is conventional for the study region, but the results show a highly variable seasonal distribution; 90% of the sedimentary transfer occurred in winter and autumn. The main reasons were a high cumulative rainfall and a long duration for the events. The maximum suspended sediment concentration at the catchment outlet was observed in spring, likely due to maximum rainfall intensities in that season. Also, a huge variability between the events is observed; e.g. one exceptional rain storm in 11/2016 represents 45% of the total sediment yield of the study period. For the monitored 22 events, 2 different types of hysteresis behavior were observed: (i) clockwise and (ii) complex. In winter, only clockwise hysteresis was observed. These results suggest that other factors must be considered to better explain the variability of gully erosion, such as the soil surface characteristics (crop cover, crusting stage, roughness). A monitoring of these parameters on experimental plots is in progress.

EGU 2016

Source tracing of fluvial suspended sediments by magnetic and geochemical particle characterization: example of the Canche watershed (Nord-Pas-de-Calais, France)

Edouard PATAULT [1,2,*], Claire ALARY [1], Christine FRANKE [2], Arnaud GAUTHIER [1], Nor-Edine ABRIAK [1]

[1]LGCgE, Ecole des Mines de Douai, Département Génie Civil & Environnemental, 764 boulevard Lahure, 59508 Douai Cedex, France.
[2]MINES Paris Tech, Centre de Géosciences, 35 rue Saint-Honoré, 77305 Fontainebleau Cedex, France.

In France, erosion by water runoff is estimated to 1.5 t ha^{-1} yr^{-1} and can exceed 10 t ha^{-1} yr^{-1} in large growing areas, such as the North of France (Nord-Pas-de-Calais). In this region, the Canche watershed (1294 km²) sustains heavy loss of fertile soils. The land use is mainly dominated by arable lands (80%) and in 2013, 104 kt of suspended sediment transited to the estuary. As demonstrated in literature, agricultural soil erosion leads to the gradual disappearance and depletion of fertile soil, which constitute a non-renewable resource at human time scale. Additionally, water erosion can significantly damage the aquatic habitat and can be responsible for the input of nutrients, bacteria, pesticides, heavy metals and radionuclides into surface waters. Conscious of these effects, many programs have emerged in the Nord-Pas-de-Calais to reduce erosion. This study presents a combination of environmental magnetic proxy parameters and geochemical analyses on sediments and suspended particulate matter. The aim is to develop effective tools to trace erosion by water runoff and quantify this process. To identify the respective sediment sources in the Canche watershed, sediment trap samples of suspended particulate matter were recovered at key positions along the Canche watershed. The preliminary results show that magnetic concentration (Mrs) shows typical values for the agricultural soils in the region, but these variations in magnetic concentrations and total irons concentrations are not always correlated, which may be explained by the iron speciation. In calculating the so-called S-ratio for each sample we can distinguish changes in magneto-mineralogy (and thus iron speciation) from magnetite-dominated assemblages in the mainstream Canche (naturel background signal) to high-coercivity-dominated assemblages in the tributaries, typical for soil erosion material rich in hematite/goethite. In combination with the element concentrations from ICP analyses, this proxy parameter may give valuable insight into the tracing of the suspended sediment sources. In perspective, the seasonal variability and the discharge in the Canche watershed must be considered.

ICRM 2017

"Magnetic fingerprinting" of fluvial suspended particles in the context of fertile soil erosion: example of the Canche River watershed (Nord-Pas-de-Calais, France)

Christine Franke (1), Edouard Patault (1, 2), Claire Alary (2), France Lagroix (3), Arnaud Gauthier (2), Nor-Edine Abriak (2)

(1) MINES ParisTech, PSL Research University, Centre de Géosciences, 35 rue Saint-Honoré, 77305 Fontainebleau Cedex, France
(2) LGCgE, IMT Lille-Douai, Département Génie Civil & Environnemental, 764 boulevard Lahure, 59508 Douai Cedex, France
(3) IPGP, Équipe de Paléomagnétisme, 1 rue Jussieu, 75238 Paris Cedex 05

In the North of France, where land use is mainly dominated by agricultural activity, erosion by water runoff results in heavy loss of fertile soil and leads to the gradual disappearance and depletion of this non-renewable resource at human time scales. Additionally, water erosion can significantly damage the aquatic habitat and can be responsible for the input of nutrients, bacteria, pesticides or heavy metals into surface water. This study combines environmental magnetic characterisation (RT hysteresis parameters, LT remanence cycles) with other sediment-physical (grain size analyses, XRD, color spectroscopy) and geochemical analyses (ICP) on suspended particulate matter. The objective is to develop effective tools to trace erosion by water runoff. In 2015 and 2016, spatio-temporal sampling campaigns of suspended particulate matter (SPM) were conducted at key positions along the Canche River and its tributaries using bottle sediment traps. RT hysteresis curves of the recovered dry bulk SPM were obtained using at the AGM 2900 of the LSCE. Magnetic concentration of the SPM evaluated by M_{rs} or M_s values are typical of values for agricultural soils in the region. However, magnetic concentration and total iron from geochemical analyses are not always correlated. S-ratio data indicate that during low water conditions ("natural fluvial background signal") the Canche River SPM is dominated by a soft ferrimagnetic mineral assemblage while during high water stages (local rain events) the magnetic mineral assemblage is dominated by high coercivity phases. Increased soil erosion, especially via water runoff, is expected during rain events. The observed temporal (seasonal) variations in the magnetic mineral assemblage would be expected if the agricultural soils were enriched in goethite and/or hematite with respect to ferrimagnetic pedogenic minerals. Additional LT remanence experiments are being conducted on selected samples using the MPMS housed at IPGP providing greater insight into the mineralogy of the magnetic phases of the SPM and surrounding agricultural soils. We also attempt to determine whether magnetic grain size varies between low and high water conditions and how it compares to sedimentary grain size variations.

Annexe D: Collaborations

ICCE 2017

Long-term accumulation of metals and persistent pollutants (PAHs, PCBs, organochlorine pesticides) from Eure river watershed (France) in sediments: possible consequences of a dam removal.

THOMAS GARDES[1,2], YAN LABERDESQUE[1,2], EDOUARD PATAULT[2], MAXIME DEBRET[2], YOANN COPARD[2], JULIEN DELOFFRE[2], STÉPHANE MARCOTTE[3], ANNE-LISE DEVELLE[4], PIERRE SABATIER[4], ERIC CHAUMILLON[5], FLORENCE PORTET-KOLTALO[1]

[1]University of Rouen-Normandy, Laboratory COBRA UMR CNRS 6014, 55 rue Saint Germain, 27000 Evreux, France.
[2]University of Rouen-Normandy, Laboratory M2C UMR CNRS 6143, Place Emile Blondel, 76821 Mont-Saint-Aignan, Cedex, France.
[3]INSA of Rouen, Normandy University, Laboratory COBRA UMR CNRS 6014, avenue de l'Université, 76800 Saint-Etienne-du-Rouvray, France.
[4]University of Savoie Mont Blanc, EDYTEM, CNRS, 73370 Le Bourget du Lac, France.
[5]University of La Rochelle, LIENSS UMR CNRS UMR 7266, 2 rue Olympe de Gouges, 17000 La Rochelle, France.

The Dam of Martot in Eure (France) will be destroyed in order to restore the ecological continuity but removal impacts of such small structures remain poorly studied. The aim of this study is (i) to characterize the variability and the origin of the hydro-sedimentary transfers, (ii) to determine the history, at a decadal scale, of the pollution emitted in the watershed of the Eure River, by analyzing the sediment stored in the Martot's pond upstream the dam and (iii) to predict the hazards of the dam removal. Present day sedimentary transfers were assessed from high frequency measurements from two sampling sites while past transfers were reconstructed by analyzing sediment archives taken from the Martot's pond (hydraulic annex). The analysis of present day hydro-sedimentary transfers showed a strong variability of water and sediment discharges where main forcing are rainfall, water depth and tidal cycles from the Seine estuary. On sedimentary archives, sedimentological analysis (macroscopic description, spectrophotometry, magnetic susceptibility…) identified two heterogeneous facies. The use of radionuclides for dating the sediment suggests that this transition date of 1942. This change is related to river management policy that led the annex first to trap sediments from the Seine River, and then those from the Eure River. High resolution analysis of the metal composition of the sediments by X-ray fluorescence showed two origins of the sedimentary transfers: one component is linked to soil erosion and a second highlight an anthropic contribution. It appeared that the sedimentation rate remains unchanged since the 40's suggesting a simple relationship between the sediment depth and the year of contamination. XRF core scanning is not quantitative; it allowed to compare different levels of metal contamination, but not to determine accurate quantification. So other methods were developed to quantify some metallic and persistent organic pollutants accumulated in the sedimentary archive before and after 1942. Extractions or wet digestion were carried out in a micro-wave extractor. The analyses of organic pollutants (PAH, PCB and organochlorine pesticides) were performed with GC-MS, and heavy metals with ICP-OES. Our results showed that the most polluted fractions in the sediment core correspond to the Eure signal, with however a different timing according to the pollutant: a majority of them were particularly

concentrated in the fractions accumulated in the 50's (economic development after the World War II), whereas the lead was more concentrated on the top of the sediment core. Some other pollutants, such as PCB or Lindane, presented unusual high punctual pollution peaks around their prohibition of sale. In conclusion, this archive can track the human impact on the watershed since 1942. However, it is strongly expected that the dam removal would provoke some significant changes in the hydro-sedimentary characteristics of the Eure River. So the pollutants stored in sediments could be remobilized in the river. As a consequence, it will be necessary to evaluate the overall pollutants stock in the Martot's pond, as well as the sediments dynamics and the risk of contamination of the Eure River after the dam removal.

Transfer pathway and fluxes of water-soluble pesticides in different compartments of the agricultural catchment of the Canche River (northern France).

Angel BELLES [a]*, Claire ALARY [b], Nicolas FLIPO [a], Sophie GUILLON[a], Edouard PATAULT[a,b], Agnès RIVIERE [a], Christine FRANKE [a]

[a]MINES ParisTech, PSL Research University, GEOSCIENCES - Centre for geosciences and geoengineering, 35 rue St. Honoré, F-77305 Fontainebleau Cedex, France
[b]IMT Lille Douai, Univ. Lille, EA 4515 - LGCgE - Civil & Environmental Engineering Department, F-59000 Lille, France

Abstract

Five frequently used pesticides were monitored in the surface water and the groundwater of an agricultural catchment for examining the edge-of-field pathway of substances and their characteristic time of transport. Study of surface water contamination was conducted through two time scales: continuously over 1 year at a single point of the catchment and punctually during 4 seasons at 15 sampling points of the watershed. In addition, groundwater contamination measured in winter and summer periods shows low and relatively constant contamination level. The outflow of pesticides from groundwater results in a background contamination of surface water. In addition a contamination peak above the baseline level is observed in surface water during the period of substance spreading. Our results show that pesticides were essentially transported to the surface water by fast flow components (runoff water). Losses of pesticides during the contamination peak period and long-term monitoring were compared showing that transport of substances within weeks after pesticides spreading dominates the annual flux of pesticides excepted for atrazine which shows a pattern of background contamination. Short-term or low frequency monitoring scheme provide only a partial picture of contamination state and are not enough to evaluate the contamination state of such rivers in regard of the fact that ¾ of the annual load of pesticides are transported in stream during only 2-3 months of the annual monitoring.

Article in preparation for submission.

Liste des figures

Liste des tableaux

Analyse multi-échelle des processus d'érosion hydrique et de transferts sédimentaires en territoire agricole : exemple du bassin versant de la Canche (France).

Résumé : L'érosion hydrique est un processus majeur de dégradation des sols dans le monde avec des conséquences multiples : perte de terres agricoles, envasement des cours d'eau, coulées boueuses. En France, la région Hauts-de-France est la zone la plus touchée par ces pertes en terres qui peuvent dépasser les 10 t ha^{-1} an^{-1}. Si les processus à l'origine de ces transferts sédimentaires ont été largement étudiés par la communauté scientifique ces dernières années, il reste néanmoins des verrous liés aux variabilités spatio-temporelles. De plus, l'efficacité des politiques récentes de lutte contre l'érosion n'est pas quantifiée. Cette étude propose une analyse de la variabilité spatio-temporelle des transferts sédimentaires selon plusieurs échelles (1-1000 km²), et une première évaluation de l'efficacité des politiques d'aménagement au sein d'un bassin du Nord de la France (la Canche ; 1274 km²). Une station de mesure haute-fréquence, a été implémentée à l'exutoire d'un sous-bassin versant de la Canche (la Pommeroye ; 0,54 km²) pour quantifier les transferts hydro-sédimentaires sur deux années hydrologiques contrastées. Selon nos résultats, les transferts varient de 29,4 à 70 t km^{-2} an^{-1}. 40% du flux est exporté au cours de 3 épisodes érosifs majeurs (sur 48 enregistrés) et les paramètres forçants sont liés à la durée d'un épisode pluvieux et la quantité de précipitations. Sur ce même bassin, la prédiction spatiale à l'échelle centimétrique des transferts hydro-sédimentaires a pu être effectuée via le nouveau modèle d'érosion des sols *WATERSED* (BRGM) et l'efficacité d'un plan d'aménagement de lutte contre l'érosion a été quantifiée. Nos résultats permettent de valider l'opérabilité du modèle sur ce territoire. Les transferts sédimentaires à l'échelle du parcellaire agricole peuvent atteindre les 76 t km^{-2} pour un évènement donné et sont influencés par l'état de surface du parcellaire agricole. Une réduction significative (jusqu'à 84%) des transferts par les aménagements d'hydraulique douce est également observée. A l'échelle du bassin de la Canche, l'utilisation de traceurs chimiques et spectrocolorimétriques dans un modèle de mélange (*Sed_Sat* ; USGS) a permis d'évaluer d'une part les contributions des affluents de la Canche et d'autre part les contributions des sols et des berges (respectivement 30-70%). Des variations spatio-temporelles significatives ont pu être observées et les résultats tendent à montrer un potentiel impact positif des politiques récentes d'aménagement du territoire. Cette étude montre également que de nouveaux traceurs liés à la signature spécifique des particules magnétiques sont particulièrement prometteurs dans ce contexte pour tracer un signal d'érosion des sols. A terme, ces données pourraient être incluses dans des approches sediment fingerprinting. L'analyse selon plusieurs modalités spatio-temporelles et le couplage expérimentation/modélisation améliore donc notre compréhension de la dynamique des transferts sédimentaires sur le bassin versant de la Canche. Cela fournit des résultats essentiels pour orienter les futures politiques de lutte contre l'érosion des sols.

Mots clés : érosion des sols, sediment fingerprinting, suivi haute-fréquence, modélisation, traceurs environnementaux, bassin versant

Multi-scale analysis of water erosion processes and sedimentary transfer in agricultural territory: example of the Canche river catchment (France).

Abstract: Water erosion is a serious concern in global land degradation leading to multiple consequences: loss of arable lands, siltation of streams, mudflows. In France, the Hauts-de-France region is the most affected area, and soil loss can exceed 10 t ha^{-1} yr^{-1}. Although hydro-sedimentary processes have been widely studied by the scientific community, there is still a lack of knowledge in the understanding of the spatio-temporal variabilities. Additionally, the effectiveness of recent erosion control policies so far cannot be quantified. This study proposes an analysis of the spatio-temporal variability of sedimentary transfer at different scaling (1-1000 km²), and an initial assessment of the effectiveness of management policies within a northern France catchment (the Canche river, 1274 km²). A high-frequency monitoring station was implemented at the outlet of a Canche sub-catchment (the Pommeroye, 0.54 km²) to quantify the hydro-sedimentary transfer over two contrasted hydrologic years. According to our results, sediment yield varies from 29.4 to 70 t km^{-2} yr^{-1}. 40% of the flux is exported during 3 major erosive events (out of 48 recorded) and the forcing parameters are related to the duration and the amount of rainfall. In this sub-catchment, the centimeter-scale spatial prediction of the hydro-sedimentary transfer was carried out using the new soil erosion model *WATERSED* (BRGM) and the effectiveness of an anti-erosion management plan was quantified. Our results validate the operability of the model in this context. For a given event, sediment transfer can reach 76 t km^{-2} yr^{-1} in agricultural plots and are strongly depending on the soil surface state. A significant reduction (up to 84%) of sedimentary transfer by the anti-erosion plan was also observed. At the scale of the Canche catchment, the use of chemical and spectrocolorimetric tracers in a mixing model (*Sed_Sat tool*; USGS) evaluated the contributions of the Canche tributaries and sediment sources contributions (i.e. channel banks and soils; 30-70% respectively). Significant spatio-temporal variations have been observed and the results show a potential positive impact of the recent management policies. This study also shows that new tracers related to the specific signature of magnetic particles are promising in the context to trace soil erosion. For further analyses, this data could be included in sediment fingerprinting approaches. Thus, this study based on several spatio-temporal modalities and the coupling of experimentation and modelling improves our understanding of the Canche hydro-sedimentary dynamics. It provides essential results to guide the future erosion control policies.

Keywords: soil erosion, sediment fingerprinting, high-frequency monitoring, modelling, environmental tracers, catchment